Évolution Topographique, Tectonique et Sédimentaire Syn- à Post-rift de la Marge Transformante Ouest Africaine

Jing Ye

Université Fédérale
Toulouse Midi-Pyrénées

THÈSE

En vue de l'obtention du

DOCTORAT DE L'UNIVERSITÉ DE TOULOUSE

Délivré par :

Université Toulouse 3 Paul Sabatier (UT3 Paul Sabatier)

Présentée et soutenue par :
Jing YE
le lundi 7 novembre 2016

Titre :

Évolution Topographique, Tectonique et Sédimentaire Syn- à Post-rift de la Marge Transformante Ouest Africaine

---

École doctorale et discipline ou spécialité :
ED SDU2E : Sciences de la Terre et des Planètes Solides

Unité de recherche :
UMR 5563

Directeur/trice(s) de Thèse :

Delphine ROUBY
Dominique CHARDON

Jury :
Sébastien CARRETIER (président du jury)
Gianreto MANATSCHAL (rapporteur)
Dominique FRIZON DE LAMOTTE (rapporteur)
Sébastien CASTELLTORT (rapporteur)
Mary FORD (examinatrice)

Résumé

Cette thèse présente la première étude *Source-to-Sink* de la marge Atlantique Equatoriale africaine au Méso-Cénozoïque. Nous avons dans un premier temps produit, à partir d'une nouvelle méthode intégrant les limites d'érosion des dépôts préservés dans les bassins et leur extension initiale minimum, une nouvelle reconstruction paléogéographique et structurale couplant pour la première fois le continent ouest africain et l'Atlantique Equatoriale au cours du Méso-Cénozoïque. Ceci nous permet de suivre l'évolution depuis 200 Ma des domaines en érosion (sources) et en sédimentation (puits) à l'échelle continentale. Nous montrons en particulier qu'au Crétacé supérieur la zone correspondait à un grand bassin intracratonique Saharien qui exportaient ses sédiments à la fois vers la Téthys et vers l'Atlantique Equatoriale. La fragmentation de ce bassin a eu lieu à l'Oligocène par le soulèvement du bouclier du Hoggar qui a isolé les petits dépôt-centres résiduels actuels. Le développement de cette topographie particulière est issu de la superposition de différentes longueurs d'onde de déformation à l'échelle continentale combinant les bourrelets marginaux longeant la marge équatoriale et un bombement de type « point chaud ».

Nous avons ensuite caractérisé, à partir de l'interprétation des données sismiques et des puits, la segmentation de la marge continentale équatoriale en segments transformants et divergents et l'architecture stratigraphique post-rift du prisme stratigraphique associée au Crétacé Supérieur. Nous montrons que les parties proximales (dépôts de plateforme et pente continentale) des prismes stratigraphiques du Crétacé Supérieur ne sont préservés que le long des segments divergents de la marge, et pas le long des segments transformants. Nous interprétons cette différence de préservation comme résultant de mouvements verticaux post-rift plus importants dans les domaines proximaux des segments transformants empêchant la préservation des termes proximaux des systèmes sédimentaires.

La caractérisation des architectures stratigraphiques post-rifts a ensuite permis la quantification des volumes sédimentaires préservés dans ces bassins de marges passives. En parallèle, de nouvelles données de thermochronologie basse-température (AFTA et (U-Th-Sm/He sur apatite) acquises à l'Université de Glasgow sur les échantillons de trois profils perpendiculaires à la marge équatoriale ont permis de quantifier l'histoire de l'érosion et les volumes dénudés sur le domaine continental au cours du Méso-Cénozoïque. Ces données montrent que le seul événement thermique majeur enregistré correspond au refroidissement lié à la dénudation d'une topographie syn-rift le long de la marge. Le bilan d'érosion et d'accumulation montre que les ordres de grandeur des volumes dénudés et accumulés sont comparables à l'échelle de la marge équatoriale au cours du Méso-Cénozoïque. Certaines périodes (Crétacé Supérieur et depuis le Miocène Supérieur), montrent cependant un excès d'accumulation qui pourrait être associé à la remobilisation de sédiments précédemment stockés dans des bassins intracontinentaux ou sur la plateforme de la marge.

Mots clés : marge passive, bassin intracratonique, rifting, source-to-sink, paléogéographie, l'Océan Atlantique Equatoriale, Afrique, bilan d'érosion, bilan d'accumulation

Abstract

This PhD thesis presents the first source-to-sink study of the African Atlantic Equatorial margin. We established new Meso-Cenozoic paleogeographic and structural reconstructions, integrating the West African sub-continent and the Equatorial Atlantic Ocean, based on a new mapping method defining both erosion limits of preserved deposits and their minimum original extension. We show the evolution over 200 Myrs of the eroding (sources) and accumulating domains (sinks) at continental scale. We demonstrate in particular that during the Cretaceous, a large Saharan intracratonic basin was exporting sediments toward both the Tethys and the future Atlantic Equatorial Ocean. The fragmentation of this basin occurred in the Oligocene, by the growth of the Hoggar swell that isolated the present-day small residual depot-centers. The development of this specific "basin and swell" topography results from the superimposition of various deformation wavelength at continental scale combining a marginal upwarp along the equatorial margin and a hot spot swell.

We then characterized, from the interpretation of seismic data and well logs, the segmentation of the Equatorial Atlantic passive margin and the stratigraphic architecture of the post-rift Upper Cretaceous sedimentary wedge. We show that the proximal parts of the Late Cretaceous sedimentary wedge are only preserved along divergent segments of the margin and not along transform segments. We interpret this differential preservation as the result of a greater uplift, during the early post-rift, in the proximal parts of the transform segments preventing the preservation of the proximal terms of the sedimentary systems. The transform segments are associated with narrow necking zone, resulting in greater flexural uplift than divergent segments showing wider necking zones, in particular during the early post-rift.

The characterization of the stratigraphic architecture of the post-rift sedimentary wedge then allowed for the quantification of accumulation history in the passive margin basins. New low-temperature thermochronological data (AFTA and Apatite (U-Th-Sm)/He) acquired at the University of Glasgow on the samples of three regional transects perpendicular to the margin allowed for the quantification of the denudation history and eroded volume on the continental domain. These data shows that the major thermal event recorded by those samples is the cooling phase related to the erosion of a rift-related topography along the margin. Erosion and accumulation budgets fall within the same order of magnitude. During some given periods (Late Cretaceous and since the Late Miocene), excess in accumulation may be associated with the reworking of sediments previously stored within intracontinental basins or on the shelf of the margin.

Key words: passive margin, intracratonic basin, rifting, source-to-sink, paleogeography, Atlantic Equatorial Ocean, Africa, erosion budget, accumulation budget

Table of Contents

Table of Contents

Remerciements

D'abord, je tiens à remercier mes directeurs de thèse, Delphine Rouby et Dominique Chardon, pour cet excellent sujet de recherche original et multidisciplinaire qu'ils m'ont proposé. Pendant trois ans, ils m'ont fait confiance et m'ont guidé dans mon développement vers une jeune chercheuse. Ils ont été toujours disponibles pour mes questions et les discussions scientifiques. Leur exigence m'a aidé à aller plus loin dans ma recherche. Le travail avec eux était une expérience précieuse et enrichissante.

Je remercie également Massimo D'allasta qui a consacré beaucoup temps à me préparer des données de subsurface et à m'aider dans l'interprétation sismique. Je le remercie pour sa disponibilité et son expertise dans la sédimentologie et la stratigraphie sismique.

Ensuite, je remercie François Guillocheau pour son encadrement dans l'interprétation sismique et son expertise dans la stratigraphie séquentielle. Je remercie aussi Olivier Broucke qui m'a encadré au début de ma thèse et m'a aidé à bien démarrer mon travail de recherche.

Merci à l'équipe de Glasgow, Rod Brown, Mark Wildman et David Webster, qui m'ont beaucoup appris dans la thermochronologie basse-température. Je les remercie non seulement pour les discussions scientifiques, mais aussi leur accueil chaleureux pendant mon séjour à Glasgow.

Merci à Damien Huyghe avec qui j'ai travaillé ensemble sur le même projet pendant 2 ans. Je le remercie pour son accompagnement durant de nombreuses missions chez Total, et pour de super moments qu'on a passé ensemble à la fois au boulot et dans des bars.

Merci à mes collègues du bureau F162 (le meilleur pour moi), Antonin, Bryan et Thomas, qui m'ont supporté et soutenu pendant 3 ans et qui m'ont fait à manger pendant ma grossesse! Merci à tous les jeunes du GET et aussi leur compagnon avec qui j'ai passé de super moments depuis 2013, accompagné des bières, du fromage et des plats français bien sûr: Laetitia, Alexandre, Baptiste, Léandre, Juliette, Jessy, Nicolas, Hannah, Jean, Adrien, Claire, Sylvain, Caroline, Romain, Fanny, Gilles, Arnaud, Martin, Chris, Andria, Aridane, Ha, Chi, Alice, Pierre, Juliette, Maxime, Melody, Manon…

Merci aux jeunes chercheurs chinois au labo, grâce à qui j'ai pu garder un lien directe avec mon pays natal et régaler de la cuisine chinoise de temps en temps: Xiaojun, Yu, Bing, Yi, Xu, Hongmei, Biyun, Chuxian, Yaole, Xin…

Merci à mon chéri Long qui m'a soutenu et encouragé ces dernières années. La rencontre avec toi pendant la thèse, c'est la meilleure surprise de ma vie. Merci à notre bébé qui va arriver dans trois mois...

List of Figures

List of Figures

List of Figures

List of Figures

List of Figures

List of Tables

INTRODUCTION

Les reliefs continentaux évoluent aux échelles de temps géologiques sous l'influence de l'érosion et la déformation de la lithosphère. La dynamique d'érosion des domaines orogéniques est largement étudiée dans la littérature, ainsi que ses interactions et rétroactions avec la convergence et le climat. Cependant, la dynamique de l'érosion dans les domaines non-orogéniques (ou cratoniques) reste très peu étudiée, en particulier aux échelles de temps géologiques. En effet, ces domaines sont caractérisés par un relief beaucoup plus modéré et des taux d'érosion beaucoup moins élevés que dans les chaînes de montages. Leurs contributions aux bilans sédimentaires globaux sont pourtant non négligeables, étant données les surfaces très importantes impliquées sur des durées de temps longues. Les variations de relief dans ces domaines semblent à être contrôlées par des déformations épirogéniques, de faible amplitude et de grande longueur d'onde ainsi que par les variations climatiques. La dynamique de l'érosion des domaines non-orogéniques et les volumes exportés restent à cependant encore analyser afin de comprendre la dynamique de ces surfaces continentales, et ce, à grand échelle et à long terme (x 10 Ma).

Les domaines non-orogéniques sont souvent bordés par des bassins de marges passives ou intracratoniques, dans lesquels le matériel exporté est préservé. Dans des cas simples où l'histoire des aires drainées (source area) peut être contrainte, l'histoire de l'accumulation (sink) peut être directement comparée à celle des volumes exportés (source). Les changements dans la distribution des sédiments dans les bassins et leur architecture stratigraphique peuvent donc révéler des évènements tectoniques ou climatiques affectant le domaine continental. Cette approche *Source-to-Sink* a été appliquée principalement dans des contextes de marges passives (Galloway et al., 2011; Guillocheau et al., 2012; Somme et al., 2013; Braun et al., 2014; Liu Zhifei et al., 2016), et dans des chaines de montagne et leurs bassins d'avant-pays (Kuhlemann et al., 2002; Matenco and Andriessen, 2013; Zattin et al., 2014; Wittmann et al., 2016). La plupart de ces études se sont focalisées sur l'étude de l'accumulation dans les bassins afin d'en déduire des évènements affectant le domaine en érosion (e.g., soulèvements, changement de drainage ou climat). Quelques études ont analysé à la fois la dénudation et l'accumulation (Galloway et al., 2011; Simon, 2015) mais dans un seul basin. Les analyses *source-to-sink* sont rarement réalisées dans les domaines non-orogéniques en couplant les aires drainées et les bassins avoisinants.

INTRODUCTION

L'Afrique de l'Ouest est une région d'étude pertinente pour contraindre l'histoire *'Source-to-Sink'* terre-mer en contexte non-orogénique. Elle est en effet constituée d'un craton Archéan-Protérozoïque bordé par la marge Atlantique Equatoriale où une quantité importante de sédiments clastiques ont été préservés depuis le Crétacé Inférieur. La déformation orogénique y est absente depuis 500 Ma. Cette stabilité géodynamique facilite l'interprétation de la dynamique du domaine en érosion en lien avec les déformations épeirogéniques et l'évolution de ces marges. Son contexte climatique, de type essentiellement intertropicale depuis 140 Ma, facilite l'altération et, ainsi, la production de surfaces d'altération (régolithe). Des études récentes ont montré que la corrélation des reliques de surfaces d'altération cénozoïques permet la reconstitution des paleo-drainages et la quantification des volumes érodés à l'échelle sous-continentale (Grimaud, 2014; Grimaud et al., 2015; Chardon et al., 2016). L'histoire de la dénudation cénozoïque associée est, au premier ordre, en accord avec l'histoire d'accumulation offshore (Grimaud, 2014; Grimaud et al., in prep.; Huyghe, 2016). Cependant, seules de très rares reliques de régolithes plus anciennes que le Cénozoïque ont été préservées. A ce jour, l'histoire du relief du craton au Mésozoïque demeure inconnue, ainsi que l'histoire de la dénudation et les quantités de volumes érodés et exportés par le craton. De nouvelles données de la thermochronologie basse-température ont été acquises sur le craton Leo-Man dans le cadre de ce projet afin de révéler l'histoire de la dénudation anté-Cénozoïque.

La marge Atlantique Equatoriale est la zone principale d'accumulation du matériel érodé en Afrique de l'Ouest depuis le Crétacé Inférieur (ca. 140 Ma). L'histoire géodynamique et cinématique de cette marge a été largement discutée dans la littérature (Mascle and Blarez, 1987; Basile et al., 1998; Basile and Allemand, 2002; Antobreh et al., 2009; Moulin et al., 2010; Heine et al., 2013). Elle est découpée en segments par de grandes failles transformantes et a subi une histoire d'extension polyphasée. On s'attend ainsi à une histoire des mouvements verticaux complexe selon le type de segment considéré, chacun ayant une histoire de subsidence et de soulèvement propre. Afin de comprendre l'histoire Mésozoïque du remplissage des bassins Atlantiques Equatoriales, une nouvelle étude de l'architecture stratigraphique a été réalisée en prenant en compte les structures syn-rift et les mouvements verticaux post-rift au Crétacé Supérieur. La quantification des volumes déposés dans ces bassins au Crétacé Supérieur a été réalisée pour chaque période clé, dans chaque bassin correspondant à un segment de la marge.

L'objectif de ce travail est d'étudier, d'une part, l'évolution de la marge Atlantique Equatoriale, notamment l'architecture stratigraphique et les volumes préservés pendant la phase post-rift du Crétacé Supérieur, et d'autre part, l'histoire de la dénudation de l'Afrique de l'Ouest depuis le début du Mésozoïque. Ces résultats permettront de répondre à deux questions majeures: quels sont, d'un point de vue des transferts sédimentaires, les liens terre-mer au Mésozoïque le long de la marge Atlantique Equatoriale et, quels types de mouvements verticaux au niveau de la marge peuvent être associés à ces transferts sédimentaires. Pour répondre à ces questions, ce mémoire de thèse présente les résultats de 5 tâches principales :

(1) La reconstruction paléogéographique onshore-offshore de l'Afrique de l'Ouest en intégrant les bassins intracratoniques afin de comprendre l'évolution des domaines en érosion (source) et en sédimentation (sink) depuis le début du Mésozoïque.
(2) La caractérisation de l'architecture stratigraphique syn- à post-rift des différents segments de la marge à partir de données de sub-surface (sismiques et puits).
(3) La quantification des volumes et des taux d'accumulation des sédiments silicoclastiques dans chaque basin en intégrant les incertitudes associées à la méthode de quantification. Cette tâche a été conduite en collaboration avec Artiom LOPAREV dans le cadre de son stage de Master 2 à l'Université de Toulouse.
(4) La répartition des volumes dénudés à terre estimée d'après l'histoire thermique issue d'une étude de thermochronologie basse-température (traces de fission et (U-Th-Sm)/He sur apatite) en collaboration avec l'Université de Glasgow. Les données AHe ont été acquises par David WEBSTER dans le cadre de sa thèse de doctorat à l'Université de Glasgow. L'analyse des traces de fission et la modélisation des chemins Temps/Température ont été réalisées par Mark WILDMAN, post-doctorant à l'Université de Glasgow.
(5) La modélisation numérique de la réponse en isostasie flexurale de la marge passive aux transferts de sédiments de la source au puits.

La compréhension des mécanismes de déformation et de structuration de la lithosphère durant le rifting de la marge équatorial n'est pas un objectif de ce travail.

Le manuscrit est organisé en sept chapitres suivant l'ordre des tâches exposées ci-dessus. Les chapitres 1 et 2 font un bref état des connaissances sur la dynamique des marges passives (notamment les marges transformantes) et de la géologie de l'Afrique de L'Ouest. Le chapitre 3 présente la nouvelle série de reconstructions paléogéographiques et structurales terre-mer de l'Afrique de l'Ouest depuis le début de Mésozoïque. Le chapitre 4 synthétise l'évolution structurale et stratigraphique syn- à post-rift de la marge Atlantique Equatoriale et le chapitre 5 l'histoire de l'accummulation dans ces bassins. L'histoire de la dénudation et l'estimation des volumes érodés sont présentées dans le chapitre 6. Enfin, le chapitre 7 est consacré à la comparaison volumétrique des matériaux érodés et déposés et aux mouvements verticaux associés à ces transferts de matière.

Ce travail a été financé par le groupe pétrolier TOTAL dans le cadre du projet de collaboration avec le CNRS « TS2P » (Transform Source-to-Sink Project). Total R&D *Frontier Exploration* a également permis l'accès aux données de subsurface.

CHAPTER 1 : TRANSFORM MARGINS: A SHORT REVIEW

1.1. Passive Margin Classification: Rifted Vs Transform Margins

Atlantic-types passive margins were commonly classified into two categories, (1) rifted and (2) transform or sheared (Mascle, 1976; Scrutton and Dingle, 1976). Rifted margins, also called divergent margins, are characterized by an initial opening motion perpendicular to the continental crust. Transform margins are, as a difference, opened by transcurrent movements parallel to the continental crust.

Kinematic models of rifted margins evolved from pure shear (uniform extension, McKenzie, 1978), simple shear (Wernicke, 1985), to recent compound depth-dependent extension models (Huismans and Beaumont, 2008, 2014). Depth-dependent extension with different lithospheric rheological properties accounts for various geometries of rifted margins observed around the world (e.g. narrow Newfoundland-Iberia and ultra-wide South Atlantic margins, Huismans and Beaumont, 2008, 2014, Figure 1-1). Narrow margin can be modelled via rheologically coupled lithospheric crust and mantle, generating a narrow necking zone and exhuming mantle after the breakup of the crust (Figure 1-1A). Whereas wide margin can be reproduced with a weak lower crust, resulting a wide necking zone and the breakup of the mantle before that of the curst (Figure 1-1B, Huismans and Beaumont, 2014). Some authors defined rifted margins resulting from ‘passive’ and ‘active’ rifting (Sengör and Burke, 1978; Bott and Kusznir, 1979; Spohn and Schubert, 1982). Passive rifting results from a lithospheric extension due to horizontal movements of divergent plates, generating a passive upwelling of underlying asthenosphere. Whereas, active rifting is related to the presence of an active mantle plume head, doming up and cracking the overlaying lithosphere. Uplifted areas usually form by isostatic compensation bordering the active rift center (e.g. East African dome).

Transform/sheared margins were first defined by Mascle (1976) (Figure 1-2A). They were relatively poorly investigated, although they represent 16% of continental margins in cumulative length (Mercier de Lépinay et al., 2016). Transform faults, first identified by Wilson (1965) as one of three major plate boundary types (mid-oceanic ridge and subduction zone), play a major role in transform margin formation, controlling the continental crust stretching during rifting and oceanic

crust formation. The resulting continent-ocean transition is often relatively sharp (Keen et al., 1990; Sage et al., 2000). Marginal ridges parallel to transform faults have been locally identified although their origin is still debated (Mascle, 1976; Wagner and Pletsch, 2001; Basile and Allemand, 2002; Basile, 2015).

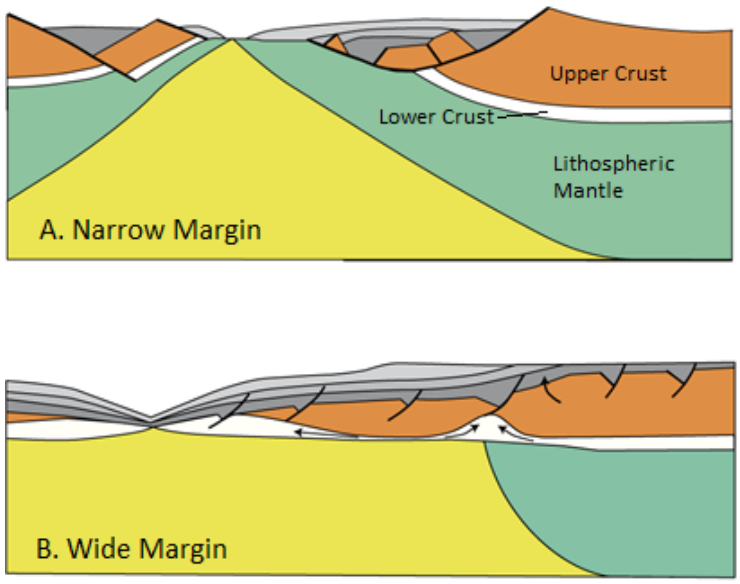

Figure 1-1 : Conceptual model of narrow (A) and wide (B) margins resulting from depth-dependent extension. (A) Narrow margin can be modelled via rheologically coupled lithospheric crust and mantle, in which the crust breakup occurs while the mantle is still necking. (B) Wide margin can be modelled via rheologically decoupled lithospheric crust and mantle. The breakup of lithospheric mantle precedes that of the crust (Huismans and Beaumont, 2014).

Oblique or oblique-shear margins are intermediate case sharing characteristics of both rifted and transform margins. They formed by obliquity between plate motion and margin direction and undergo oblique-shearing. The major difference between transform/oblique margins and rifted margins is the differential timing between breakup and oceanic spreading (Turner et al., 2003; Guiraud et al., 2010, Figure 1-2B). Rifted margins experience immediate oceanic opening after breakup, whereas transform and oblique margins may undergo separately the breakup and the oceanic drift as evidenced by discrete breakup and drift unconformities (Turner et al., 2003). The duration between these two depends on the length of the transform/oblique margin segment and the spreading rate (Turner et al., 2003).

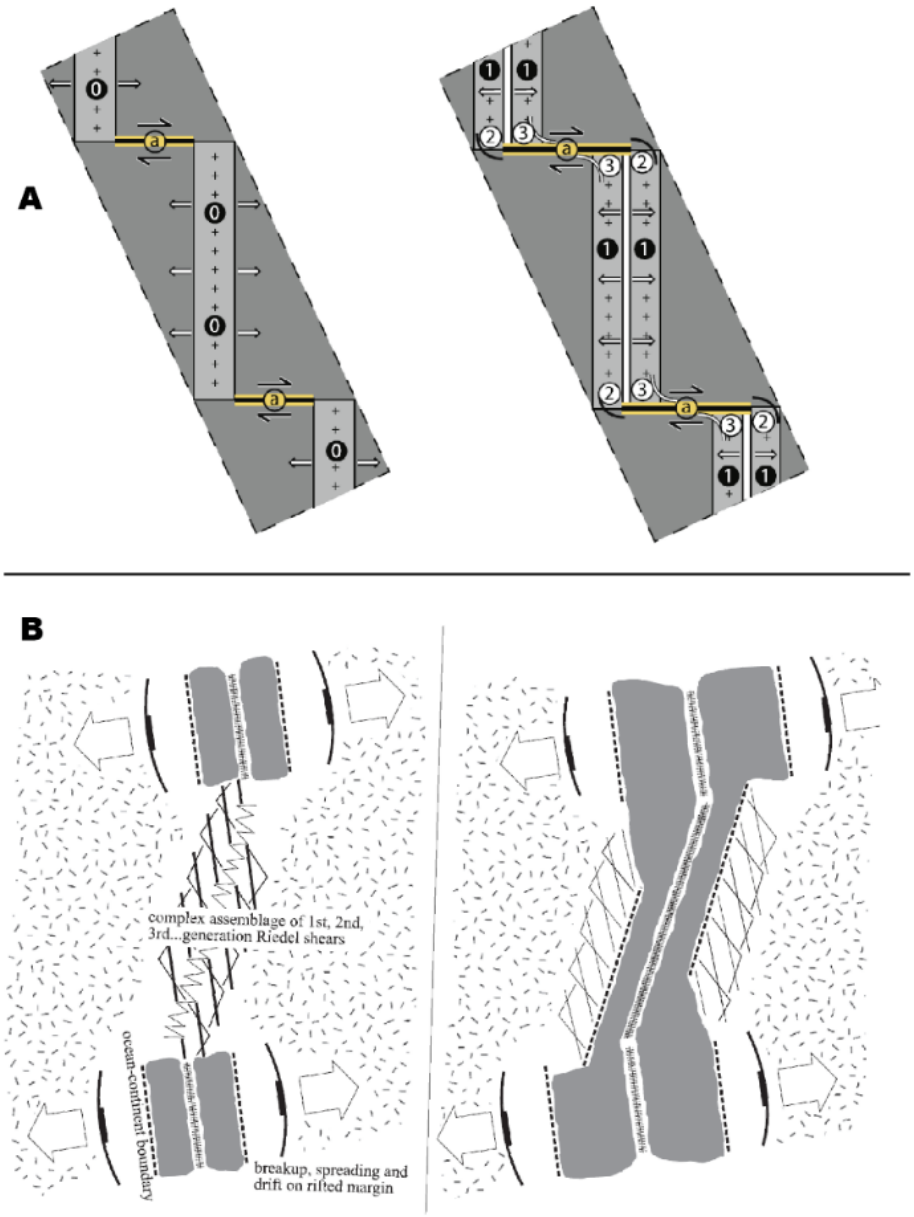

Figure 1-2 (A) Formation model of transform margins with margin strike parallel to opening direction, contrasting with rifted margins opening perpendicularly to margin strike (Basile, 2015). (B) Model illustrating the development of oblique margins by oblique shearing associated to oblique-slip faults (Turner et al., 2003).

1.2. Geodynamic Model of Transform Margins

The geodynamic evolution of transform margins were first illustrated in the model of Mascle and Blarez (1987), based on geometries and opening kinematics. The model suggests three major stages during the development of transform margin, which differs from the two-stage (syn-rift and post-rift) evolution of rifted margins (Figure 1-3).

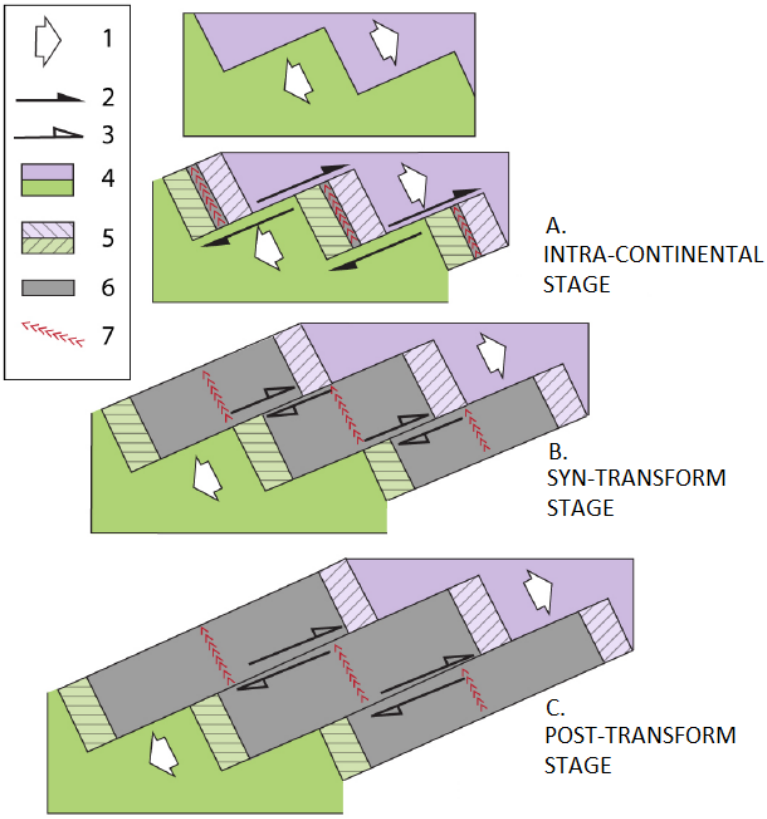

Figure 1-3 A simplified model for the evolution of transform margins. A. Intracontinental stage with active continent to continent contact. B. Syn-transform stage with progressive migration of oceanic spreading ridge along transform margin. C. Post-transform stage with transform faults only active between two oceanic crusts (Mercier de Lépinay, 2016, modified from Mascle and Blarez, 1987).

During the **first intra-continental stage** (Figure 1-3A), small segments of rifted/divergent margin form by continental crust stretching and tilted rotated blocks form on both sides of the main shear zone. Active transcurrent deformation occurs along future transform margins between

stretched and unstretched continental crusts. The sedimentation and the subsidence are probably high (Mascle and Blarez, 1987).

The **second syn-transform stage** begins when the oceanic crust forms along divergent margins (Mascle and Blarez,1987, Figure 1-3B). Syn-rift continental sedimentation ends, as a post-rift breakup unconformity forms along divergent margins. The hot oceanic spreading ridges migrate progressively towards active transform faults. The evolving contact between a hot center and a continental crust could induce thermal exchanges along future transform margins.

The **third post-transform stage** starts when the oceanic ridges is beyond the transform margin tip and the two plates are no longer connected (Mascle and Blarez, 1987, Figure 1-3C). Transform faults are then only active between two oceanic crusts. Transform margins are no longer sheared and undergo mainly thermal subsidence.

A specificity of transform margins is the diachronism of margin connection to a stable oceanic crust during the syn-transform stage. In fact, various locations (blue, purple and red stars in Figure 1-4) experience active transform faulting at different times (Basile, 2015). The purple star ends its active transform faulting, before the blue and the red stars (Figure 1-4). The red star location experience active transform faulting during the longest duration until the beginning of post-transform stage. A post-transform unconformity may form, due to an uplift following the progressive passage of oceanic ridge, which should be diachronous along transform margins.

Transform margin are usually bordered at their two extremities by divergent margins. Two types of transfer zones (inner and outer corners) can be identified with distinct characteristics (Basile, 2015, Figure 1-4). The inner corner is not affected by active transform faulting, but by transfer structures (e.g. horsetail system). It records only the post-rift breakup unconformity, as the divergent margins. As a difference, the outer corner experiences the longest transform faulting, ending only at the beginning of post-transform stage. Both post-rift and post-transform unconformities could be recorded with a considerable time interval (x 10 myrs). Marginal ridges can be found at outer corner of transform margins.

The model of Mascle and Blarez (1987) remains the most popular scenario. It accounts for certain features observed on transform margins, such as narrow continent-ocean transition and

different morphologies between inner and outer corner. However, the diachronism of the active transform faulting is rarely confirmed along transform margins, as precise dating is absent.

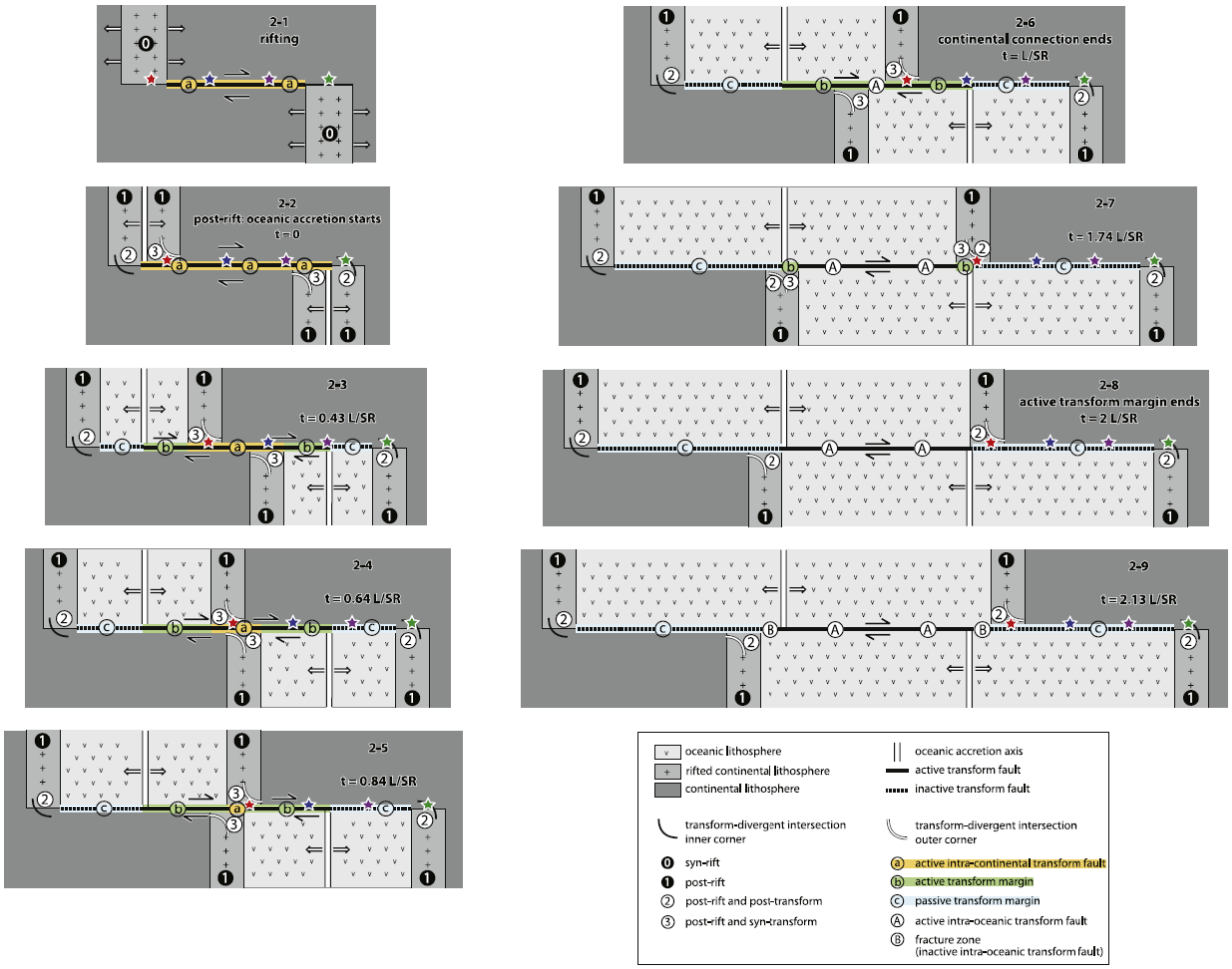

Figure 1-4 Schematic evolution of a transform margin and adjacent divergent margins (Basile, 2015).

1.3. Equatorial Atlantic Transform Margins of West Africa

1.3.1. Margin Segmentation

Transform margins have been studied in the Equatorial Atlantic domain, that results from the transform rifting in the Lower Cretaceous (MacGregor et al., 2003; Basile et al., 2005; Antobreh et al., 2009). The West African and Brazilian margins are segmented into both rifted and sheared

margins (Figure 1-5). Conjugate transform margin segments can be identified by tracing major oceanic fracture zones, whereas rifted margins are located at the terminations of two major fracture zones.

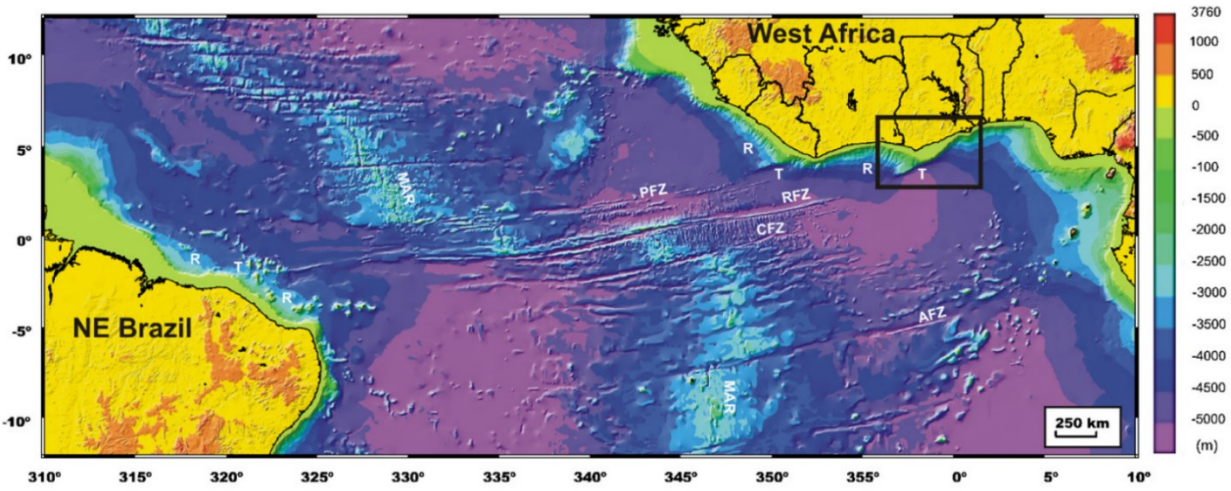

Figure 1-5 Bathymetric map of the Equatorial Atlantic. R= rifted (or divergent) margin, T= Transform (or sheared) margin, MAR= Mid-Atlantic Ridge, PFZ= Saint Paul Fracture Zone, RFZ= Romanche Fracture Zone, CFZ= Chain Fracture Zone, AFZ= Ascension Fracture Zone. Location of Ivory Coast- Ghana transform margin is shown in box (after Antobreh et al., 2009).

West African Equatorial Atlantic margin may be divided into 6 margin segments limited by three major fracture zones (Romanche, Saint Paul and Grand Cess fracture zones, Figure 1-5). Three long transform segments are located at the prolongation of each fracture zones (Saint Paul, Liberia-Ivory Coast and Ivory Coast-Ghana transform margins). Shorter divergent segments are present between two transform segments, such as the Ivorian and Cape Palmas divergent margins (Basile, 2015, Figure 1-6). Marginal plateaus are found at the outer corners of the Saint Paul and Ivory Coast-Ghana transform margins.

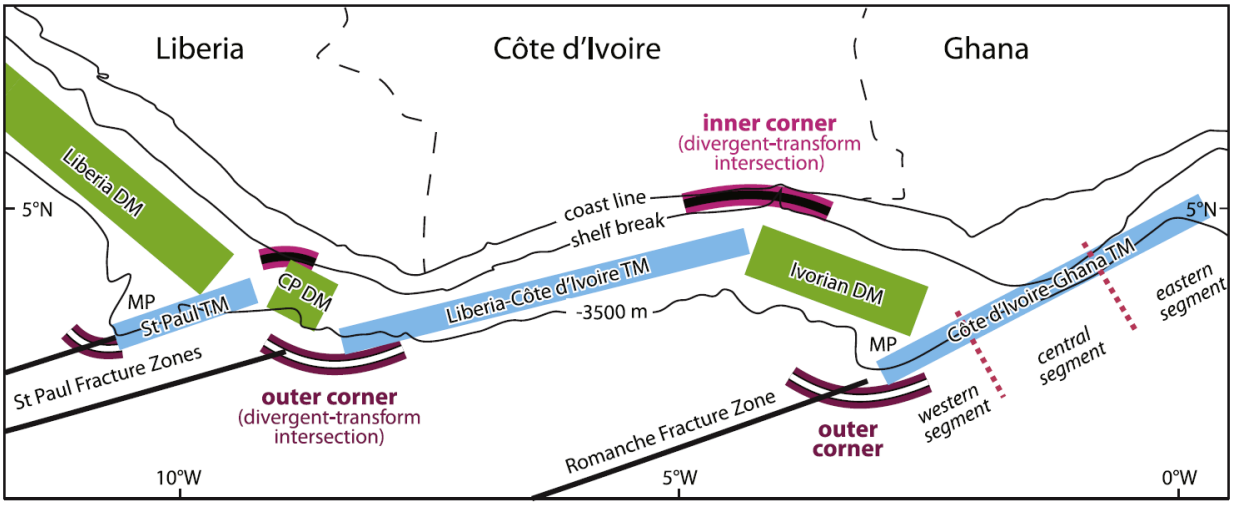

Figure 1-6 Map showing different margin segments of the western side of the Gulf of Guinea. MP: Marginal Plateau; TM: Transform Margin; DM: Divergent Margin; CPDM: Cape Palmas Divergent Margin (after Basile, 2015).

1.3.2. Ivory Coast-Ghana Transform Margin

The Ivory Coast-Ghana transform margin is the most studied part of the West African margin, partially because of its spectacular marginal plateau and sharp continent-oceanic transition (Figure 1-7 and Figure 1-8). The Ivory Coast-Ghana (IC-GH) marginal ridge forms as an elevated and elongated structural high located in the outer corner of the margin, from the Ghanaian shelf to the Southern border of the adjacent Deep Ivorian Basin (Figure 1-7). It is now partly buried under sediments and lines up with the Romanche fracture zone, as well as the continent-ocean transition (Figure 1-7). Marine geophysical cruises, scientific dives and drilling (ODP Leg 159) were carried out during 90s for investigating its evolution and associated vertical movements (Basile et al., 1996; Benkhelil et al., 1997; Guiraud et al., 1997; Lamarche et al., 1997; Mascle et al., 1997; Pletsch et al., 2001; Basile et al., 1998).

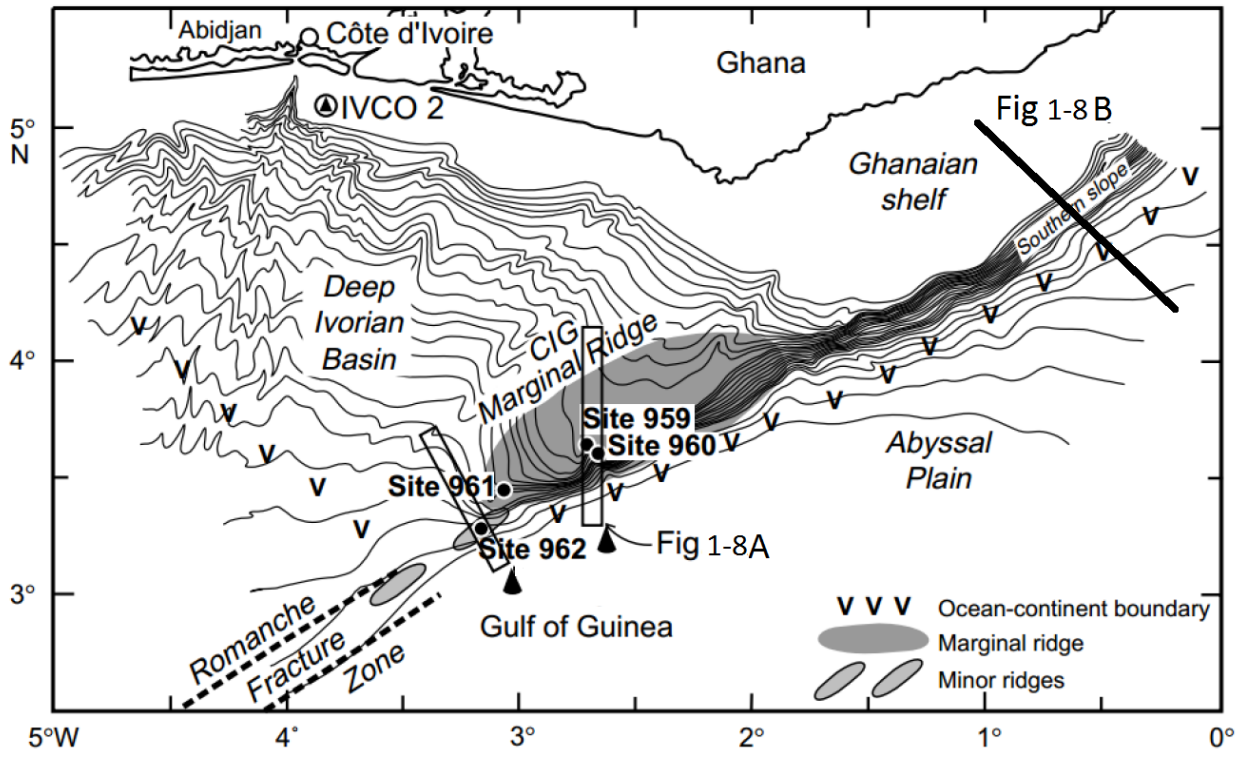

Figure 1-7 Bathymetric framework of the Ivory Coast-Ghana transform margin. Leg 159 sites are indicated by solid circles. Its location is shown in Figure 1-4. The rectangles show the location of the seismic reflection lines shown in Figure 1-78B (Basile et al., 1998).

They showed a thick sedimentary piles was discovered on the northern slope of the Marginal Ridge connecting to the Deep Ivorian Basin (Figure 1-8). A basal Unit A was identified to be the syn-rifting siliciclastic sequence filling half-grabens of probably Early Aptian-Late Albian age (Figure 1-8A, Basile et al., 1996, 1998). The associated sedimentary environments vary from intracontinental lacustrine to open marine from Site 960 to Site 962 (Basile et al., 1998). An ubiquitous erosional unconformity (well dated to be Late Albian in Site 926) tops Unit A. It is interpreted as the post-rift breakup unconformity for the IC-GH transform margin and the adjacent divergent Ivorian margin (Figure 1-8A). Overlying Unit B, is the first post-rift sediments on the divergent segment, but is a 'syn-transform' unit along the IC-GH transform margin. The post-transform units (D-F) showing very little deformation, onlap by a 'post-transform' unconformity the unit B (Basile et al., 1996).

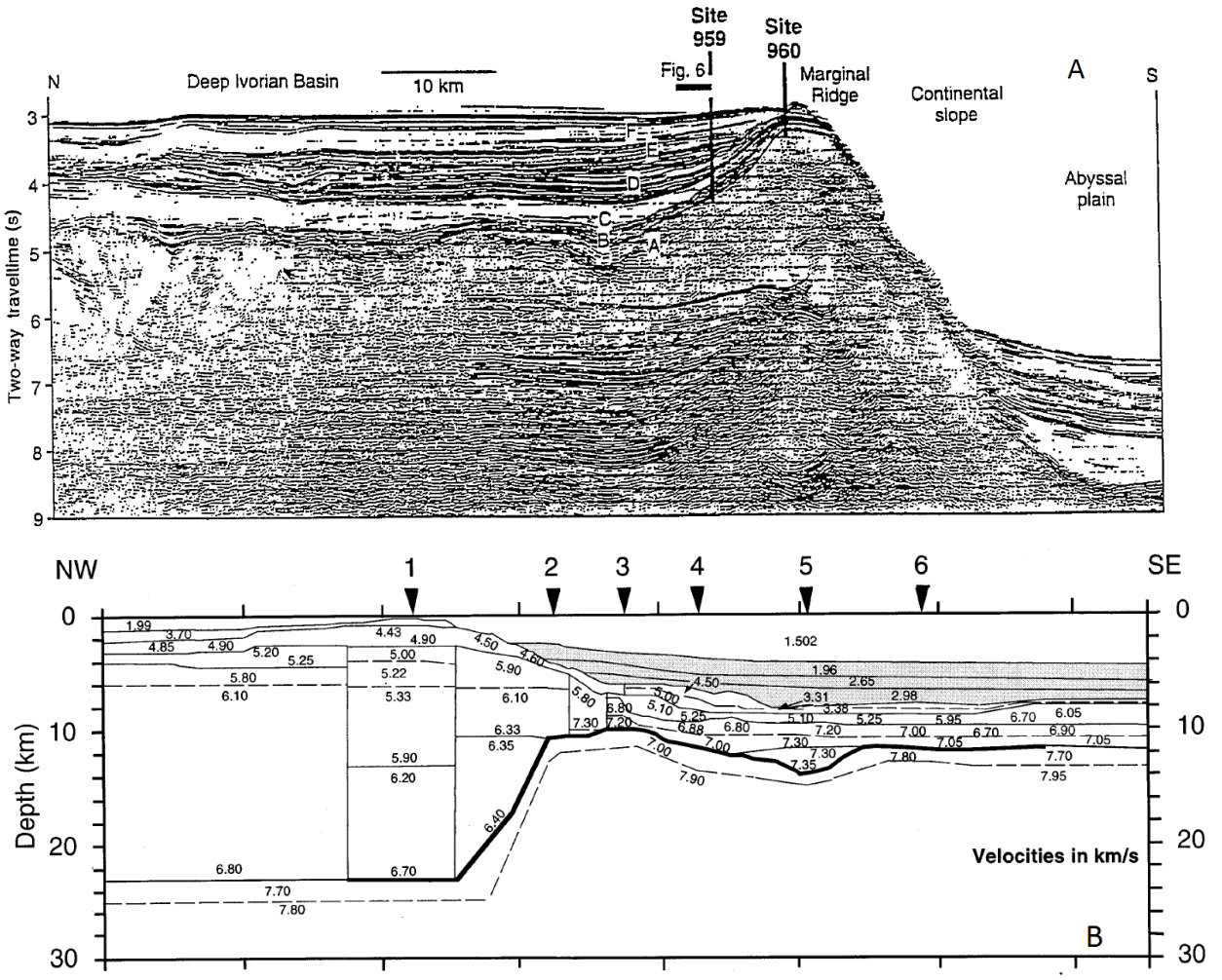

Figure 1-8 Structural and sedimentary characteristics of the Ivory Coast-Ghana marginal ridge. (A) Seismic reflection line across the marginal ridge, the Ivorian Basin and the abyssal plain (Basile et al., 1996). Its location is in Figure 1-67. (B) Seismic velocity model based on a refraction line, see location in Figure 1-7. The Moho is indicated by the bold line (Edwards et al., 1997).

The formation of the Marginal Ridge has been extensively debated since the 1970s (Scrutton, 1979; Mascle and Blarez, 1987; Lorenzo et al., 1991; Vagnes, 1997; Basile et al., 1998; Sage et al., 2000; Wagner and Pletsch, 2001; Basile and Allemand, 2002; Attoh et al., 2004; Bigot-Cormier et al., 2005). Various hypotheses were proposed, including crustal thickening by transpression (Figure 1-9A, Attoh et al. 2004), thick continental sliver transported laterally by transform fault (Figure 1-9B, Le Pichon and Hayes, 1971) and flexural uplift related to erosion discharges of more elevated continental crust (Figure 1-9C, Basile and Allemand, 2002). However,

these models are inconsistent with the flat and horizontal Moho below the Marginal Ridge (Edwards et al., 1997; Sage et al., 2000). Another discussed model explains the development of the Marginal Ridge by thermal uplift, in which uplift is triggered by heat transfer from the hot oceanic to the continental lithosphere (Figure 1-9E, Scrutton, 1979; Mascle and Blarez, 1987; Vagnes, 1997). It cannot, however, account for the maintenance of the Marginal Ridge long time after the passage of the oceanic ridge. Moreover, the timing of the uplift was revealed to start during the intra-continental stage (Basile et al., 1998).

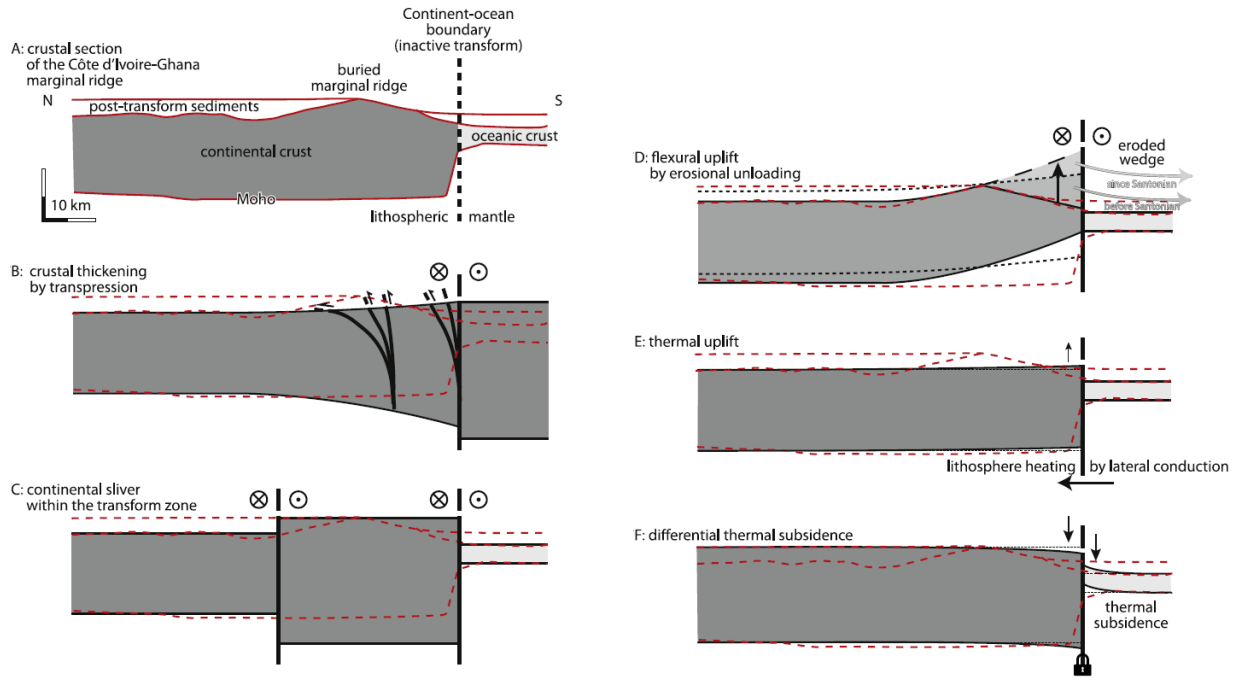

Figure 1-9 Different existing models for explaining the development of the marginal ridge and its associated vertical displacements (Basile, 2015).

Most of studies were concentrated at the Marginal Ridge alone which represents a local feature of the IC-GH transform margin. The most part of the Equatorial Atlantic margin from Guinea to Benin was not systematically investigated. The segmentation of this margin is only based on the present-day geometries of the fracture zones and the bathymetry map and profiles (Le Pichon and Hayes, 1971; Gorini and Asmus, 1981; Mercier de Lépinay, 2016). The evolution of the margin geometry from the syn- to post-rift needs to be further investigated. The post- rift stratigraphic architectures along different margin segments remain unexplored, neither their implication for the margin segmentation.

CHAPTER 2 : CONTEXTE GEOLOGIQUE DE L'AFRIQUE DE L'OUEST

2.1. Topographie et Bathymétrie

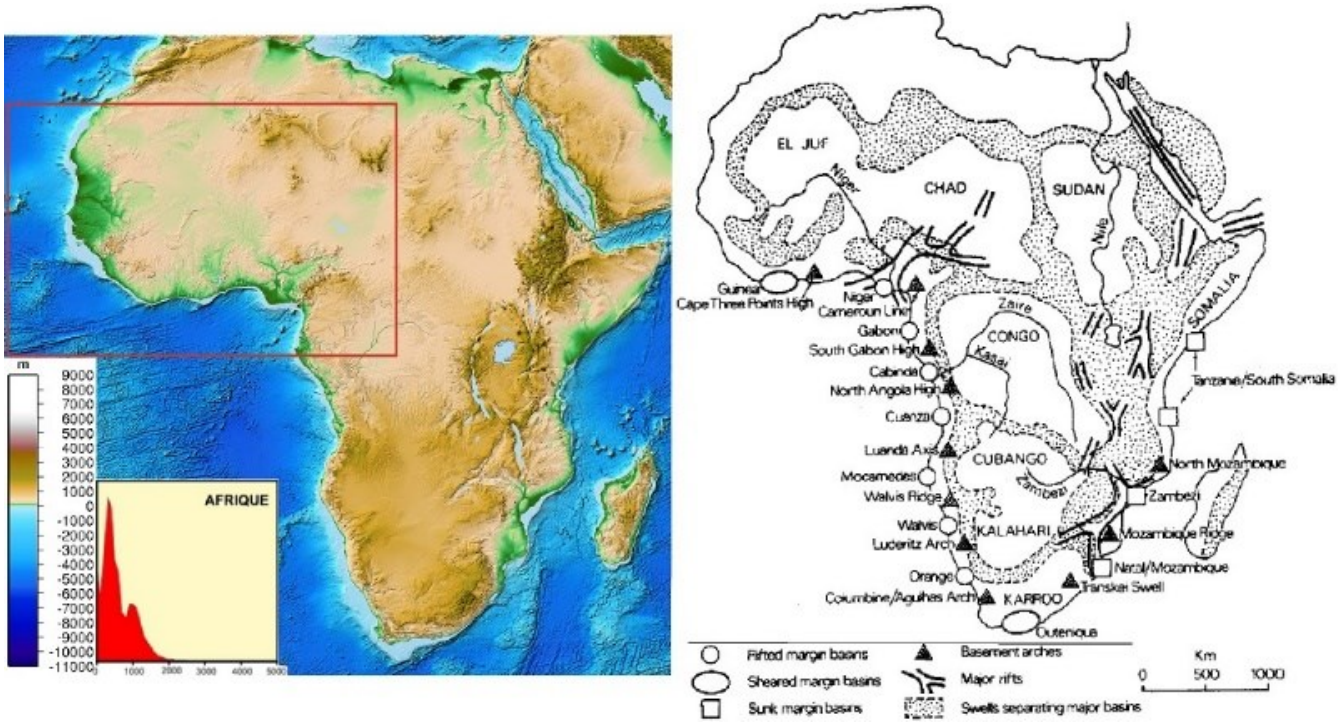

Figure 2-1 Carte topographique du continent africain (gauche), diagramme de la distribution des altitudes du continent africain (en bas à gauche) (Dauteuil et al., 2008) et carte morphologique et structurale schématique de l'Afrique (droite) (Summerfield, 1985).

A la différence des autres continents, l'Afrique possède une hyopsométrie bimodale au premier ordre qui existerait déjà au pré-Crétacé (Figure 2-1): l'altitude moyenne est plus élevée au Sud (Plateau Sud-Africain) et à l'Est (Rift Est Africain) (>1000m) qu'au centre et à l'Ouest (< 500 m) (Summerfield, 1996; Doucouré et de Wit, 2003).

Des structures topographiques sont superposées: les rides et les bassins (« *basins and swells* ») et les rifts (Figure 2-1). Le plateau sud-africain et le rift est-africain qui culminent à plus de 1000m forment un *Superswell* (Summerfield, 1996). Il correspond au système de rifts est-africain se prolongeant par la haute topographie du plateau sud-africain (Figure 2-1). Certains hauts topographiques occupent les sommets culminants des rides sont des ponits chauds volcaniques post-Eocène tels que le Hoggar, le Tibesti et l'Adamaoua. Les rides topographiques se longeant la marge atlantique sont appelées bourrelets marginaux (marginal upwarp).

A part les chaînes de l'Atlas au Nord, les hauts topographiques en Afrique ne sont pas liés à la tectonique compressive. En effet, le *Superswell* est expliqué par un support dynamique du manteau (Summerfield, 1996; Doucouré et de Wit, 2003). L'alternance de bassins et de rides serait liée aux mouvements épeirogéniques dûs à la dynamique mantellique sous la plaque (Figure 2-1) (Sahagian, 1988; Fairhead, 1988; Burke, 1996; Doucouré et de Wit, 2003). La formation des massifs de point chaud du Nord et du centre de l'Afrique seraient liée à un grand épisode de volcanisme ayant démarré à l'échelle de la plaque vers 35 Ma (Rougier, 2012).

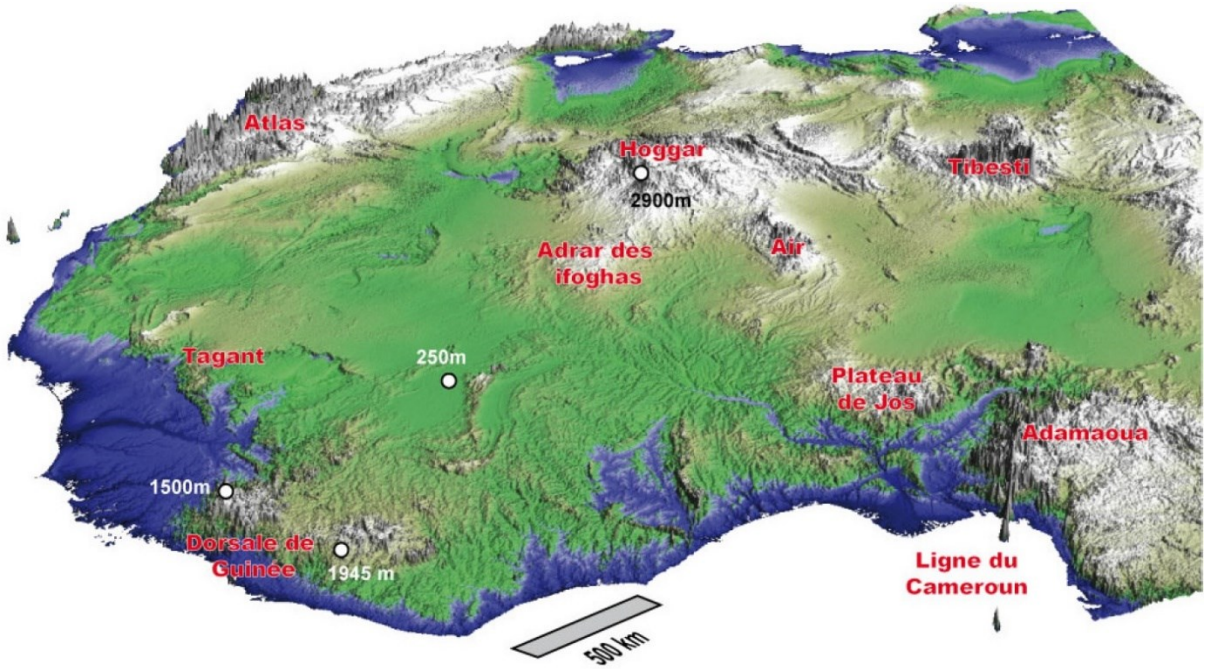

Figure 2-2 Vue oblique vers le NE de la topographie NW de l'Afrique (Grimaud, 2014).

La zone d'étude de cette thèse est située en Afrique de l'Ouest. Elle est limitée au Nord par le massif du Hoggar, à l'Est par le bassin du Chad et le massif de l'Aïr, et au Sud-Est par le massif de l'Adamaoua et la ligne du Cameroun (Figure 2-2).

Le relief de l'Afrique de l'Ouest est en général faible et se caractérise par de vastes dépressions (bassin de Taoudenni, bassin du Chad, bassin côtier Sénégalais, Figure 2-2). Il est accidenté par les massifs orientaux à l'Est: le Hoggar et ses dépendances (Adrar des Ifoghas et Aïr,

plateau de Jos, Adamaoua) et d'un bourrelet marginal au niveau de la dorsale guinéenne. Le bombement topographique du Hoggar serait lié à un point chaud (Burke, 1996; Rougier, 2012).

L'hypsométrie de l'Afrique de l'Ouest est aussi bimodale avec un pic proche de zéro et un autre à 300 m (Grimaud, 2014). Le fait que l'altitude de 300 m soit plus dominante que le niveau de base actuel (0 m) suggère un soulèvement de l'Afrique de l'Ouest de 300 m qui s'est produit durant le Cénozoïque et qui serait encore en cours (Bond, 1978; Burke, 1996). Le mécanisme du soulèvement serait lié à des processus mantelliques profonds consécutifs à un ralentissement de la dérive de la plaque à partir de l'Oligocène (modèle défendu par Burke, 1996).

2.2. Géologie Continentale et Géodynamique

2.2.1. Aperçu des Grands Ensembles Structuraux

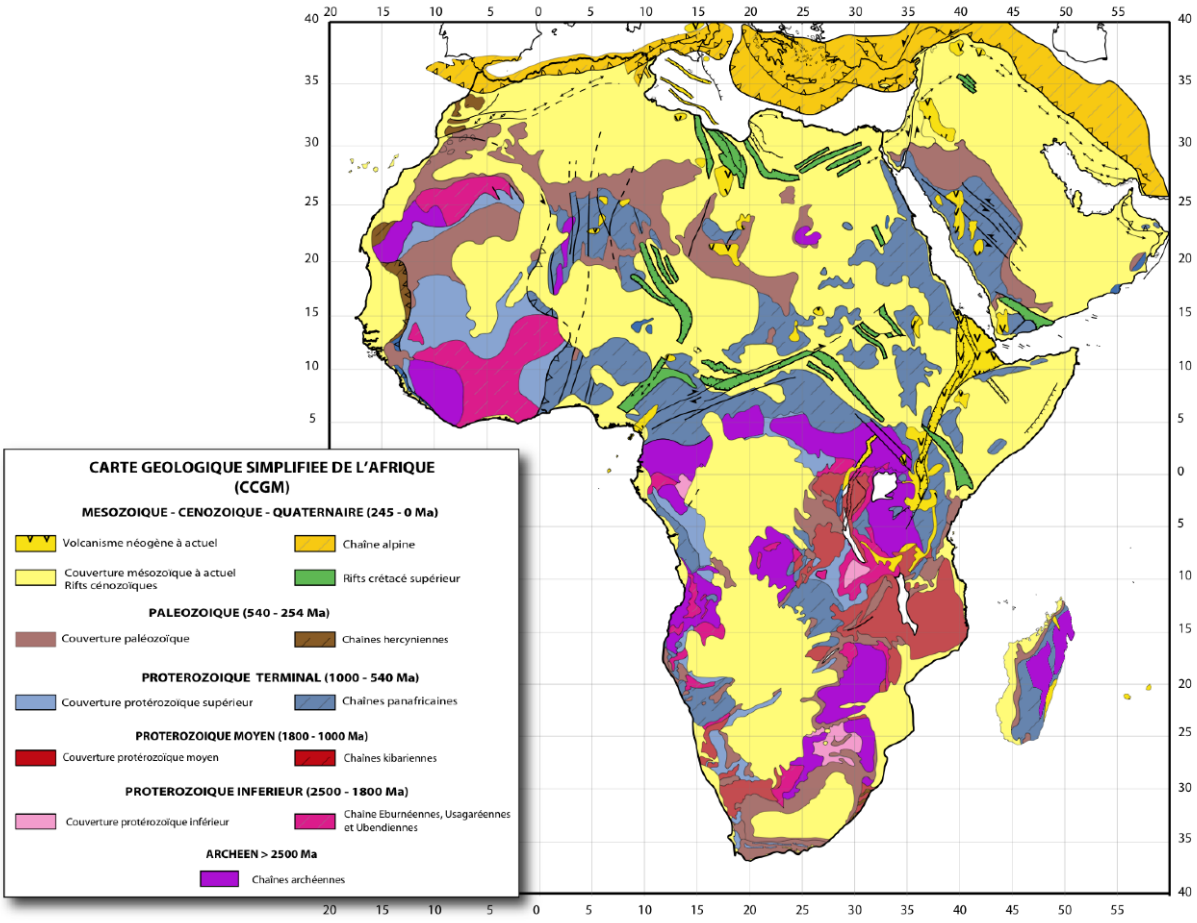

Figure 2-3 Carte géologique simplifiée de l'Afrique (Dauteuil et al., 2008).

CHAPTER 2 :CONTEXTE GEOLOGIQUE DE L'AFRIQUE DE L'OUEST

Le continent africain offre l'opportunité d'étudier l'histoire de la Terre depuis l'Archéen. Les affleurements Archéen et Paléoprotérozoïque (4600-1800Ma) à l'Ouest et au Sud de l'Afrique appartiennent aux cratons de l'Afrique de l'Ouest, du Congo et de l'Afrique australe (craton tanzanien, craton du Zimbabwe, craton du Kaapvaal, Figure 2-3, Begg et al., 2009). Les terrains néoprotérozoïques sont représentés par les orogènes (dits « ceintures mobiles ») panafricains formés au cours de l'assemblage ultime des cratons et forment ainsi leurs pourtours (Figure 2-3). Des séries silicoclastiques néoprotérozoïques non déformées sont également présevées dans divers bassins intracratoniques. Des séries Paléozoïques silicoclastiques sont présentes en Afrique septentrionale et dans la dépression du Congo. Il s'agit de grands bassins intracratoniques qui comprennent, notamment des dépôts fluvio-glaciaires et des tillites d'âge Ordovicien-Silurien (Le Heron et al., 2009). Les formations mésozoïques sont présentes principalement dans les bassins de rift continentaux et sur les marges de l'Océan Atlantique (Figure 2-3). Une large surface du continent est couverte par de sédiments continentaux et marins méso-cénozoïques. Les chaînes de l'Atlas se sont formées également à partir de l'Eocène.

Les terrains archéens et paléoprotérozoïques d'Afrique de l'Ouest appartiennent au craton Ouest Africain et affleurent dans le Nord du Sahara dans la dorsale Reguibat et au Sud dans la dorsale de Leo-Man (Figure 2-4 and 2-5). Des chaînes néoprotérozoïques et paléozoïques ceinturent le craton. Il s'agit principalement des Mauritanides à l'Ouest et de la chaîne des Dahomeyides et du Hoggar à l'Est. Au centre du craton, s'est formé le grand bassin intracratonique de Taoudeni présentant majoritairement des sédiments néoprotérozoïque-paléozoïques couverts par des formations méso-cénozoïques Figure 2-4 et Figure *2-7*). Des rifts crétacés se sont développés essentiellement dans la partie orientale de la zone d'étude. En dehors du bassin sénégalais et du bassin des Iullemmedens (Figure 2-7), les dépôts cénozoïques sont très peu représentés en Afrique de l'Ouest.

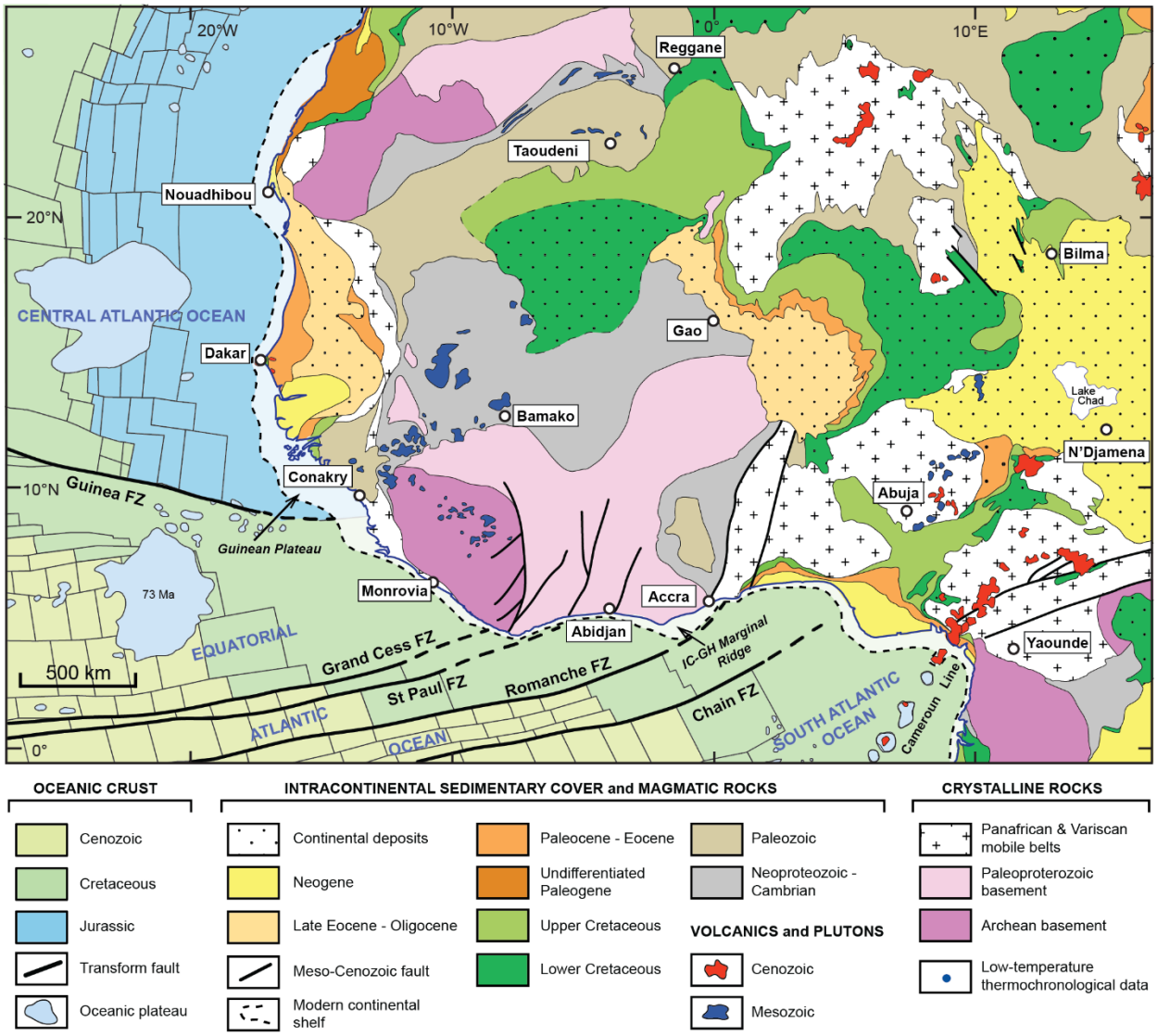

Figure 2-4 Carte géologique simplifiée de l'Afrique de l'Ouest d'après Choubert and Faure-Muret, 1988; Fabre et al., 1996; Milesi et al., 2010. Les sables quaternaires sont enlevés, et les affleurements trais-jurassique au sud-ouest du Hoggar sont incorporés dans le Crétacé Inférieur. Les failles potentiellement réactivées au Méso-Cénozoïque sont présentées.

2.2.1.1. Craton Ouest Africain et les Chaînes Bordières

L'Afrique de l'Ouest est occupée en grande partie par le craton Ouest Africain qui affleure sur la dorsale de Léo-Mann au Sud et la dorsale Réguibat au Nord (Figure 2-5). Les données géophysiques, notamment gravimétriques montrent qu'il s'agit d'un seul craton dont la partie centrale est couverte de sédiments protérozoïque supérieur à cénozoïque (Roussel et Lesquer, 1991).

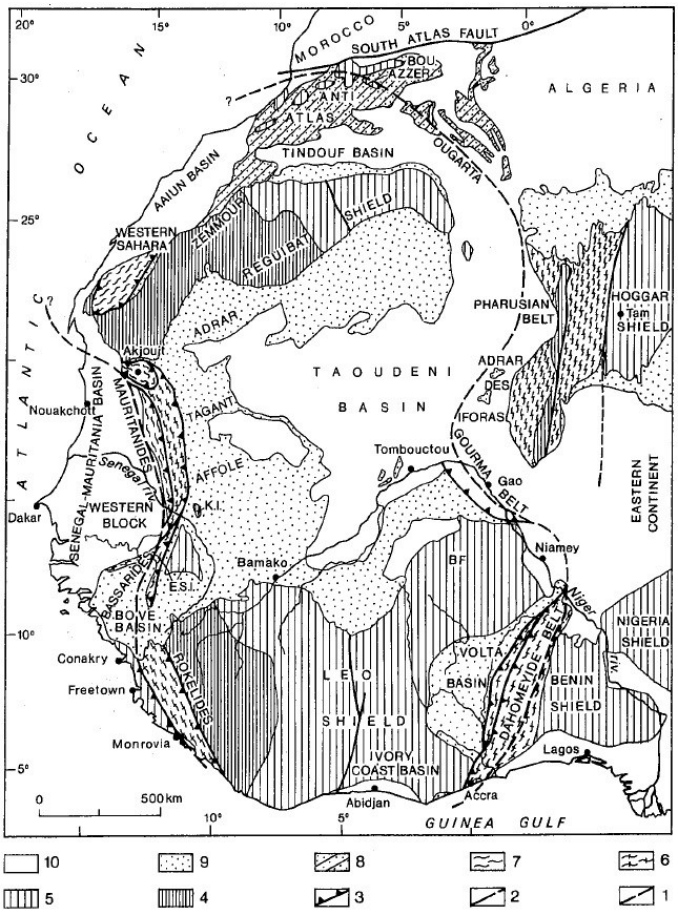

Figure 2-5 Eléments structuraux majeurs précambriens et paléozoïques de l'Afrique de l'Ouest. (1) limite du craton Ouest Africain, (2) Faille, (3) Chevauchement, (4) Socle Archéen Supérieur, (5) Socle Protérozoïque Inférieur, (6) Orogenèse Panafricaine, (7) Orogenèse Paléozoïque Supérieur, (8) Couverture Protérozoïque Supérieur-Paléozoïque Supérieur plissée, (9) Couverture Protérozoïque Supérieur-Paléozoïque Supérieur, (10) Couverture Post-Paléozoïque. ESI : Eastern Senegal inlier, KI : Kayes inlier, BF : Burkina Faso, Tam : Tamanrasset (Roussel et Lesquer, 1991).

On distingue deux grands ensembles précambriens au sein du craton:

- L'Archéen sur la partie Ouest de la dorsale de Léo-Mann et la partie Sud-Ouest de la dorsale Réguibat composées de séries gneissiques et migmatitiques appelées TTG (tonalites, trondhjemites, granodiorites) séparées par des ceintures de roches vertes et intrudées par des plutons (Dauteuil et al., 2008).
- Le Paléoprotérozoïque occupe la partie Est de la dorsale de Léo-Man et la partie Nord-Est de la dorsale Réguibat. Il est constitué de terrains à granites et ceintures des roches vertes mis en place à partir de ~2000 Ma et affectés par l'orogenèse éburnéenne jusqu'à ~1800 Ma. A la fin de cette orogenèse, le craton est stabilisé.

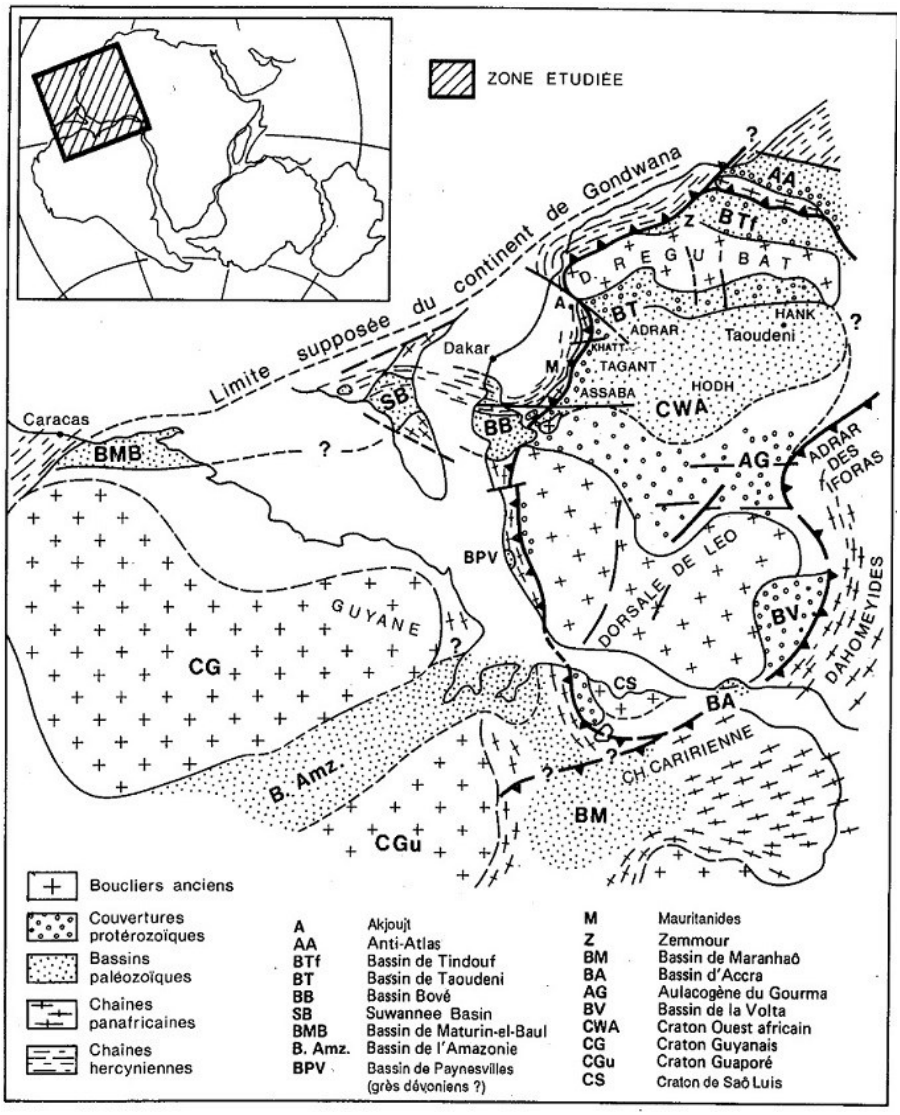

Figure 2-6 Reconstitution de la bordure NW du continent de Gondwana à la fin du Paléozoïque (Villeneuve, 1988).

Le craton Ouest Africain était connecté avec le craton de Sao Luis au NE du Brésil, selon leur position voisine pré-ouverture de l'Atlantique Equatorial (Figure 2-6, Bertrand et Jardim de Sa, 1990; Villeneuve et Cornée, 1994; De Castro et al., 2014). Des chaînes Panafricaines et Hercyniennes entourent le craton Ouest Africain et se prolongent autour du craton de Sao Luis. Ces orogenèses induisent un fort héritage sur l'évolution Phanérozoïque de l'Afrique de l'Ouest.

2.2.1.2. Bassins Continentaux de l'Afrique de l'Ouest

Paléozoïque :

Le bassin intracratonique de Taoudeni a accumulé plus de 3 km de dépôts néoprotérozoïque-paléozoïques (Figure 2-7). Ils sont couverts au centre par une fine couche de sédiments méso-cénozoïques de moins d'1 km qui contiennent des conglomérats et une série d'alternances argilo-gréso-carbonatées du 'Continental Intercalaire' représentant le Crétacé Inférieur (Bellion, 1987).

Les terrains sédimentaires paléozoïques se retrouvent tout autour du Hoggar et sont préservés dans les bassins des Iullemedens, de Murzuk et du Sahara septentrional/Sud Algérien (Figure 2-7). Ces terrains ont été cintrés et exhumés au cours du bombement du Hoggar au Cénozoïque (Rougier, 2012; Rougier et al., 2013).

Le bassin de Volta à l'Est de la dorsale de Léo-Man est considéré comme étant un bassin d'avant-pays de la chaîne des Dahomeyides (Figure 2-5 à Figure *2-7*, Deynoux et al., 2006; Roussel et Lesquer, 1991). Le bassin de Kandi, situé au Sud du bassin des Iullemedens, est découpé par divers accidents panafricains orientés N15-20°E dont la faille principale de Kandi sur la bordure ouest du bassin est réactivée à la fin du Crétacé (Figure 2-7, Guiraud et Alidou, 1981). Un autre bassin Paléozoïque, le bassin Bové (Cambro-Dévonien Supérieur), est localisé sur la connexion entre la chaîne des Rokelides et la chaîne des Bassarides (Figure 2-5 à Figure *2-7*).

La formation de ces bassins est associée à la plateforme d'âge Cambrien moyen–Dévonien couvrant l'Afrique septentrionale. Elle est affectée par les cycles de transgression-regression paléozoïques. L'orogenèse hercynienne au Carbonifère-Permien a fait émerger les bassins en

formant des chaînes sur la bordure Est de l'Afrique de l'Ouest (Guiraud et al., 2005). L'environnement de dépôt devient continental au Trias-Crétacé Inférieur ('Continental Intercalaire') dans le bassin de Taoudeni et dans les bassins autour du Hoggar.

Mésozoïque :

Un important réseau de rifts s'est développé dans la partie orientale de l'Afrique de l'Ouest à partir du Crétacé Inférieur. Ce système, en forme de 'U', est constitué de plusieurs branches (Figure 2-7):

- La branche SE-NW passant par la Bénoué jusqu'à la Centrafrique;
- La première branche NW-SE dans le bassin du Chad couverte par-dessus des sédiments Tertiaires. Sa structure est dévoilée à l'aide des données sismiques (Genik, 1993);
- La seconde branche NW-SE parallèle à l'Ouest comprend le bassin de Bida et le fossé de Gao. A l'Ouest du fossé de Gao et dans le centre du bassin de Taoudeni, se trouve un rift E-W d'âge discutable (Jurassique ou Crétacé), appelé le fossé de Nara (Bellion, 1987, Figure 2-7).

Des bassins côtiers se trouvent le long de la marge ouest-africain. Le bassin Sénégalo-Mauritanien est le plus grand d'entre eux avec plus de 10 km de dépôts méso-cénozoïques (Figure 2-7). Les bassins côtiers situés en Côte d'Ivoire et au Golfe de Guinée ont une subsidence plus modérée dont la structure et la géométrie seraient associées aux mouvements des grandes failles transformante de l'Atlantique Equatorial (Choubert et al., 1971).

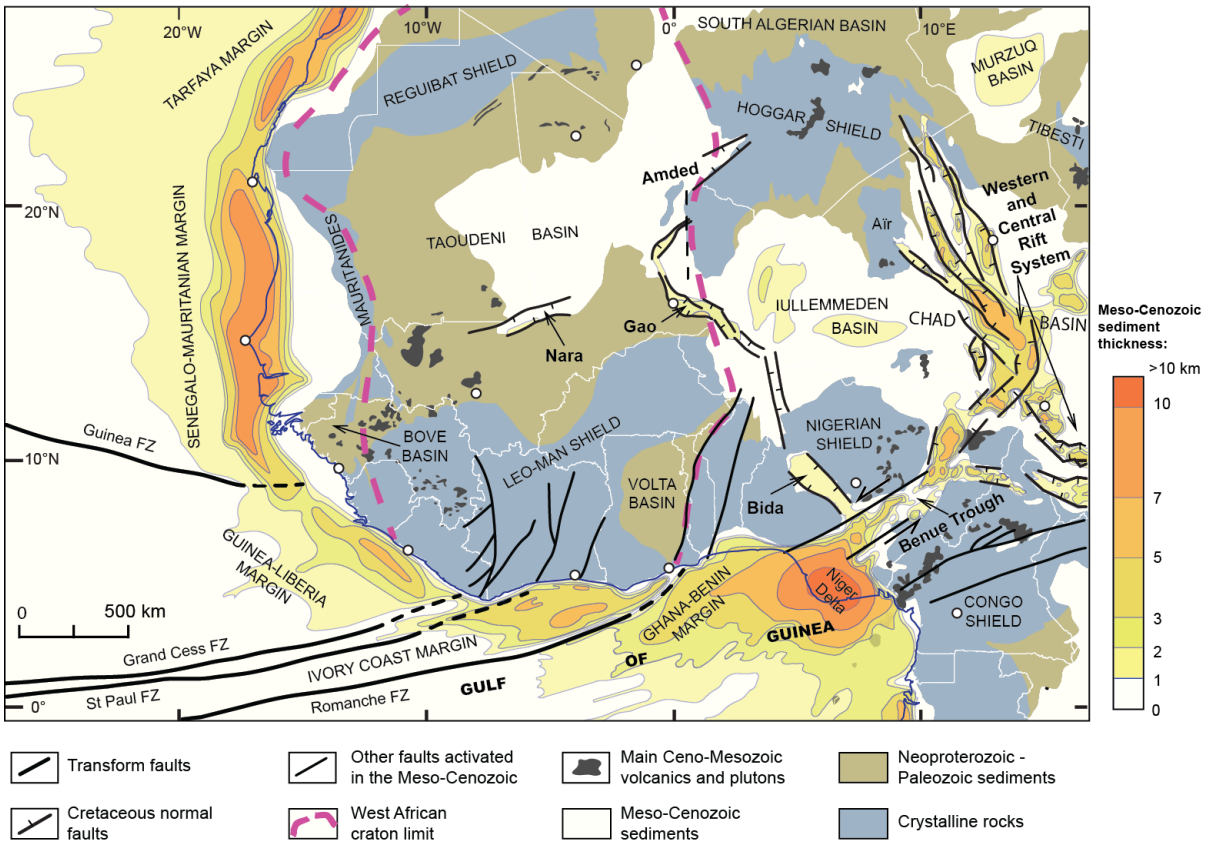

Figure 2-7 Carte simplifiée des bassins ouest africains basée sur la carte tectonique de l'Afrique (Milesi et al., 2010). Noter que la couverture Méso-Cénozoïque ou Cénozoïque de moins d'1 km d'épaisseur est enlevée de la carte.

2.2.2. Evolution Géodynamique Méso-Cenozoïque de l'Afrique de l'Ouest

2.2.2.1. Riftings Mésozoïques

Trias-Jurassique :

La dislocation de la Pangée commence au Trias Supérieur (vers 225 Ma) par le rifting de l'Atlantique Central (Davison, 2005). De nombreux bassins de rift apparaissent le long de la côte Est de l'Amérique du Nord et la côte Ouest de l'Afrique septentrionale (Figure 2-8). L'axe du rifting est parallèle à la ceinture orogénique hercynienne et contrôlé par des structures préexistantes.

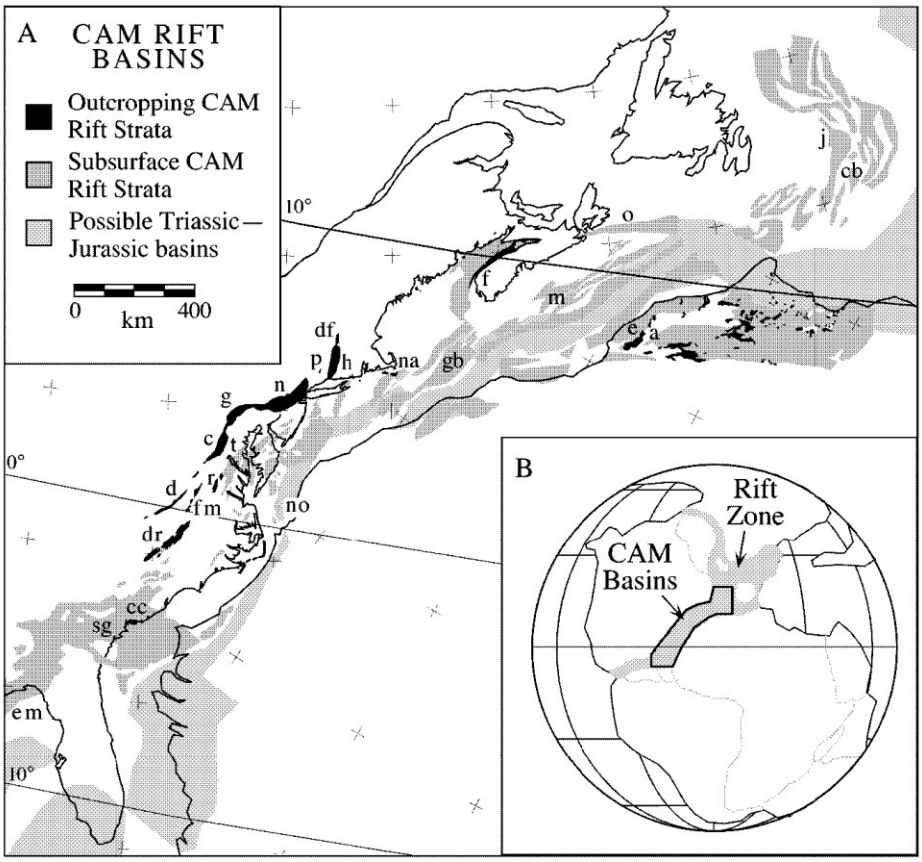

Figure 2-8 Les bassins de rift de la marge de l'Atlantique Centrale (CAM) en position paléogéographique au Carnien (225 Ma). (A) bassins de CAM: a, bassin d'Argana; c, bassin de Culpeper; cb, bassin de Carson; cc, region de Clubhouse Crossroads dans le bassin de South Georgia; d, bassins de Dan River–Danville; df, bassin de Deerfield; dr, bassin de Deep River; e, bassin de Essaouira; em, bassins les plus à l'est avec la formation d'Eagle Mills; f, bassin de Fundy; fm, Farmville et des bassins associés; g, bassin de Gettysburg; gb, bassin de Georges Bank; h, bassin de Hartford; j, bassin de Jeanne d'Arc; m, bassin de Mohican; n, bassin de Newark; na, bassin de Nantucket; no, bassin de Norfolk; o, bassin d'Orpheus; p, bassin de Pomperaug; t, bassin de Taylorsville. (B) Reconstruction de la Pangée au Carnien (225 Ma), montrant la zone de rifting (gris) et les bassins de CAM (Olsen, 1997).

Selon des données sismiques, de puits et de dykes, l'évolution de l'Atlantique Central est polyphasée (Withjack et al., 1998) :

- Le rifting a commencé au Trias Supérieur avec une direction d'extension NW-SE en formant des grabens/demi-grabens (Figure 2-9A). Des chevauchements d'âge Paléozoique de direction NE-SW ont été réactivés en failles normales en Amérique du Nord. Ceux qui sont orientés E-NE ou NNE ont rejoué en failles normales avec une composante décrochante sénestre ou dextre.

- L'inversion avec une direction de compression NW-SE a eu lieu durant la transition rift-drift ou au début de l'expansion océanique au Tiras Supérieur-Crétacé Inférieur (Figure 2-9B et C). Des failles inverses de direction NE-SW se forment, en partie par la réactivation des failles normales. L'origine de cette inversion est expliquée par la force de poussée à la ride liée à la remontée asthénosphère et à la résistance initiale du continent contre le déplacement (Figure 2-9B et C).
- L'expansion de la croûte océanique migre du sud au nord jusqu'à l'actuel (Figure 2-9C).

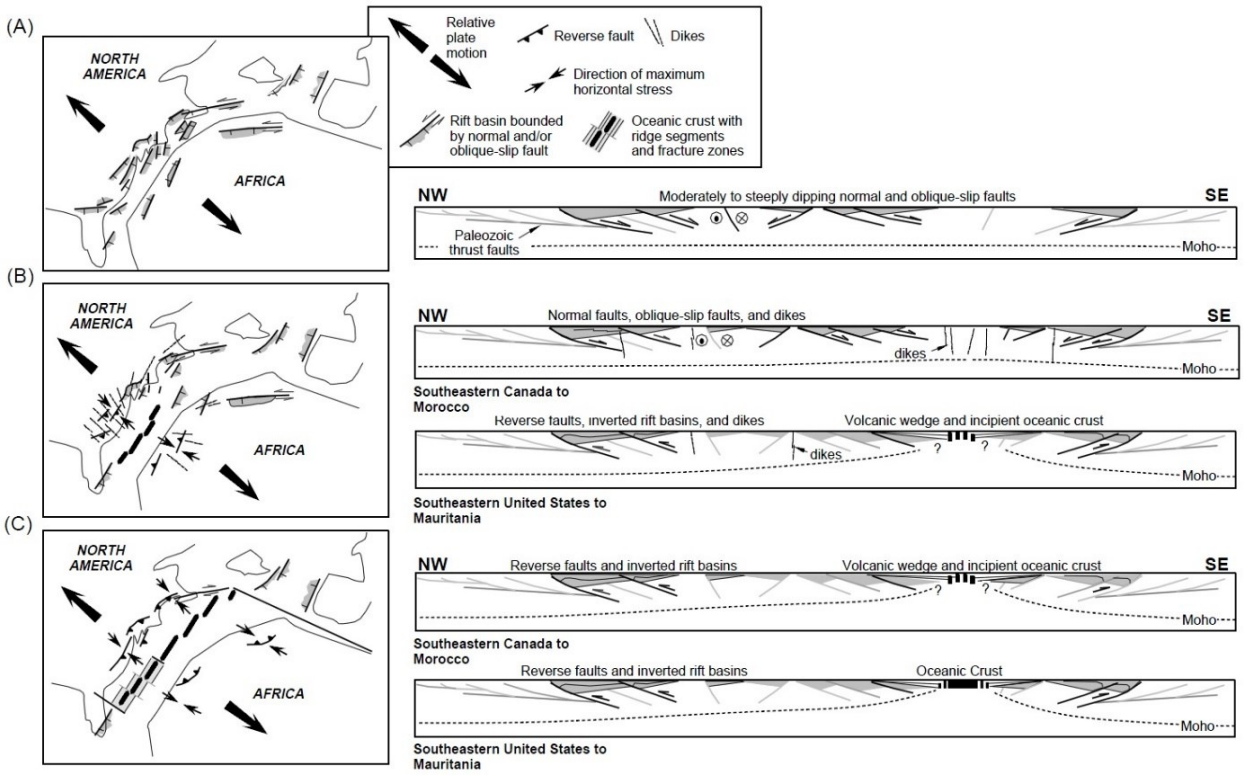

Figure 2-9 Schéma de l'évolution tectonique et géodynamique de l'Atlantique Central en carte et en coupes. (A) Trias Moyen et Supérieur, (B) Trias Supérieur et Jurassique Inférieur, plus ou moins pendant la CAMP qui met en place des dykes. Le rifting se termine au Sud et l'inversion a lieu en formant des failles inverses et des plis. (C) Jurassique Inférieur-Crétacé Inférieur, après la CAMP. L'expansion de la croûte océanique commence au Sud et en Afrique de l'Ouest. Le rifting au Nord se termine avant la fin du Jurassique Inférieur- début du Jurassique Moyen. L'inversion se met en place au Nord avant ou pendant le Crétacé Inférieur (Withjack et al., 1998).

La transition rift-drift est en effet diachrone et commence d'abord au sud au Trias Supérieur avant la mise en place de la *Central Atlantic Magmatic Province* (CAMP) (vers 200 Ma). Elle migre ensuite vers le nord après la CAMP, plus précisément avant le dépôt synrift Jurassique Inférieur ou durant le Crétacé Supérieur (Figure 2-9, Withjack et al., 1998).

Des dépôts de sel de plus de 1.5 km d'épaisseur initiale sont observés dans des strates syn-rift au Trias Supérieur-Jurassique Inférieur. Des basaltes de la CAMP sont intercalés dans le sel ou déposés sur le sel dans des bassins marocains, ce qui confirme qu'il n'y a pas eu de soulèvement ou d'inversion avant ou durant le volcanisme au NW de l'Afrique (Davison, 2005). L'influence de l'inversion sur la marge ouest africaine reste à élucider avec des données sismiques et thermochronologiques.

Crétacé :

Au moment de l'ouverture de l'Atlantique Sud et Equatoriale au Crétacé Inférieur, l'Afrique subit un *rifting* continental. L'Afrique se scinde en trois parties (le bloc Ouest, le bloc Arabien-Nubien et le bloc Austral) suite à la formation d'un grand système de rift appelé *Western Central African Rift System* (WCARS) (Figure 2-10 et Figure *2-11*, Genik, 1992 ; Guiraud et al., 2005).

Il s'agit en effet d'un *rifting* Crétacé polyphasé à l'échelle continentale sur des zones de faiblesse panafricaines. La direction des failles normales est contrôlée par des structures préexistantes panafricaines. Selon Guiraud et al. (2005), il existerait deux phases:

- La première phase serait liée à une direction d'extension N160E à N-S (Figure 2-11A). Elle aurait eu lieu au Néocomien-début Aptien (140-120 Ma), en même temps que le *rifting* de l'Atlantique Sud. Le bloc Arabo-Nubien se déplaçait vers le Nord. Le décrochement N-S délimitant le bloc Ouest et Arabo-Nubien était actif en sénestre au contraire du décrochement dextre E-W situé dans le futur Atlantique Equatorial;
- La deuxième phase opère à l'Aptien Inférieur-Albien Supérieur (119-101 Ma) avec une direction d'extension NE-SW qui déplace le bloc Arabo-Nubien vers le NE (Figure Figure 2-9B). L'Atlantique Equatorial s'ouvrait à cette époque par une zone de cisaillement dextre dans les bassins de rift offshore et un cisaillement sénestre dans le fossé de la Bénoué (Figure 2-7 et Figure *2-12*).

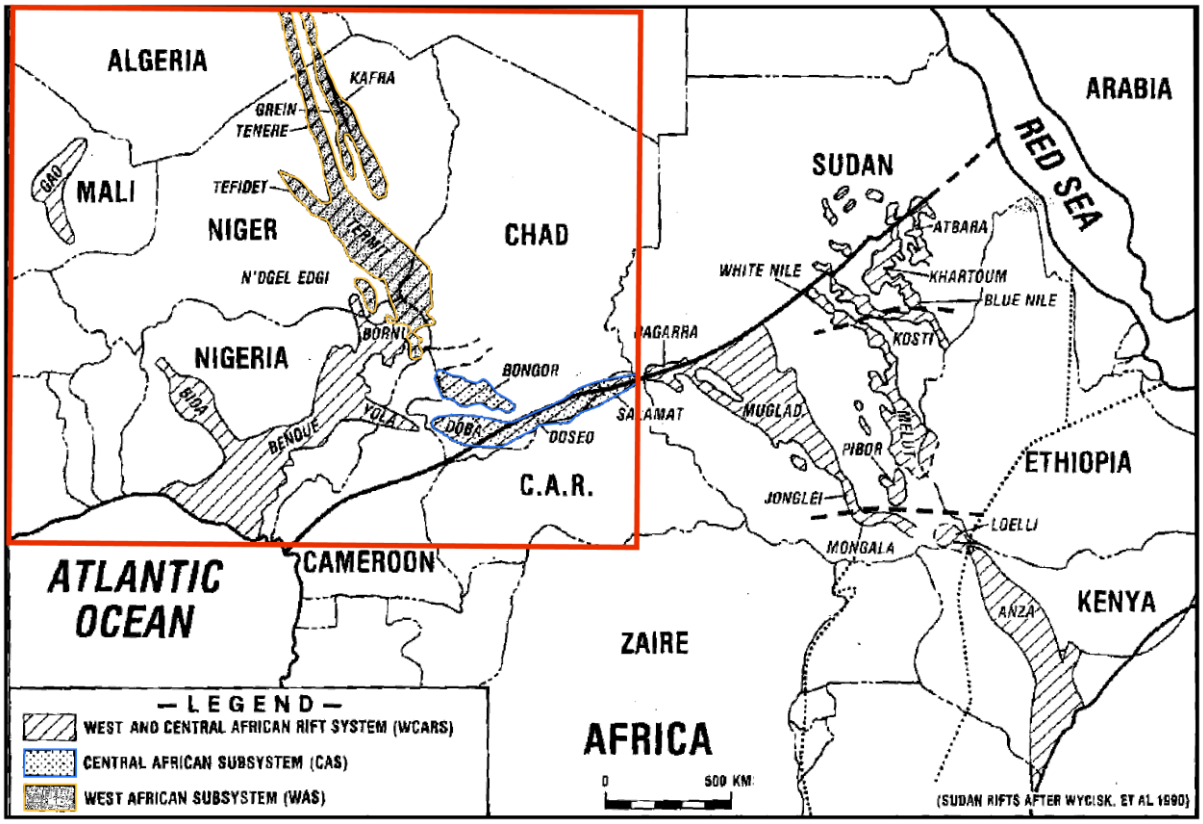

Figure 2-10 Le Western Central Africain Rift System (WCRS) avec localisation du sous-système occidental (WAS) et central (CAS). Lignes continues : failles majeures, lignes tiretées : failles supposées, lignes pointillées : Axe du futur rift Est-Africain. Le rectangle rouge délimite les bassins d'interêt pour l'Afrique de l'Ouest (Genik, 1993).

La zone d'étude ne comprend que la partie Ouest et Centrale du WCARS qui est divisée en trois sous-systèmes (Figure 2-7, Figure *2-10*0 et Figure *2-12*2) :

- les rifts orientés NW-SE au Niger et au Chad (le bassin de Termit, Tefidet, Ténéré, Grein, Kfra et N'Dgel Edgi ; *West Africain Subsystem* (WAS) de Genik, 1993),
- les rifts orientés E-W en Centrafrique (bassins de Bongor, Doba, Doseo et Salamat ; *Central Africain Subsystem* (CAS) de Genik, 1993),
- les rifts au Nigéria et au Mali (fossés de la Bénoué, de Gao, bassin de Bida et probable fossé de Nara).

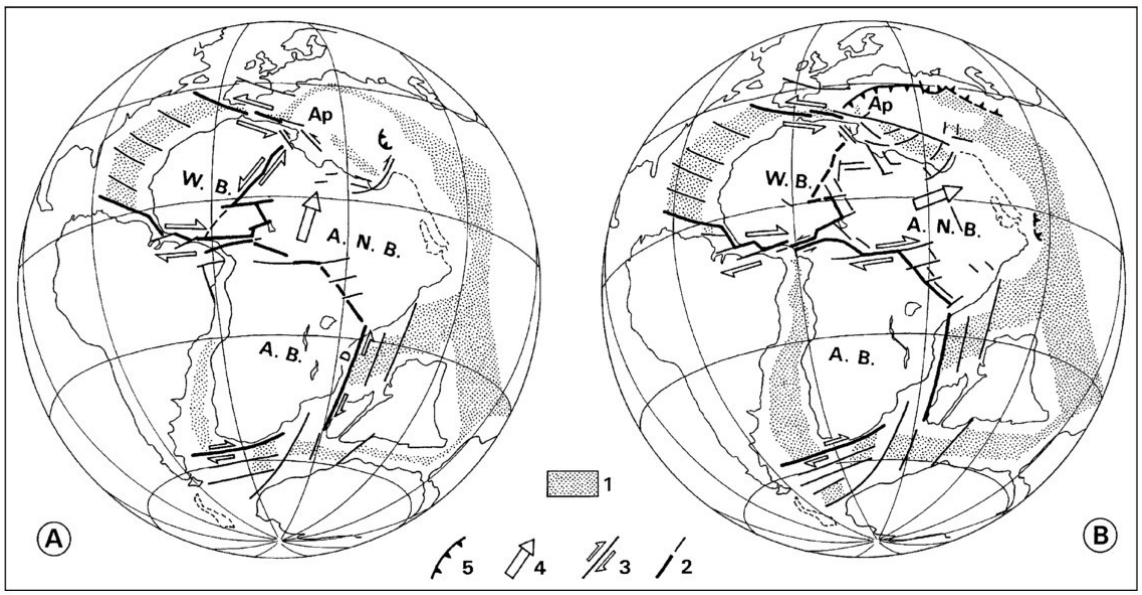

Figure 2-11 Dynamique du rifting crétacé en Afrique (modèle de Guiraud et al. (2005)). (A) Barrémien Supérieur (122 Ma). (B) Albien Inférieur (110 Ma). A.B.= bloc austral, A.N.B.= bloc Arabo-Nubien, W.B.= bloc Ouest, Ap= plaque apulienne. 1 : Croûte océanique, 2 : Faille ou décrochement, 3 : Décrochement majeur ou faille de transfert. 4 : Mouvement relatif du bloc Arabo-Nubien au Crétacé Inférieur, 5 : Chevauchement.

Les bassins des deux premiers sous-systèmes (WAS et CAS) sont couverts actuellement par des sédiments cénozoïques. Des études détaillées de ces bassins ont été effectuées à l'aide de données de forage et de sismique par Genik (1993). Des blocs basculés et des failles normales sont observables dans les bassins du WAS, alors que des structures en fleur dans les bassins du CAS suggèrent une déformation transtensive (Genik, 1992 ; Genik, 1993). La phase majeure d'extension dans ces bassins datée du Néocomien-Aptien est suivie par une phase de subsidence thermique (*Sag basin*) à l'Albien (Figure 2-13). Une réactivation en extension est observée dans le WAS et CAS au moment de la transgression marine cénomanienne suivie par une autre longue phase de subsidence tectono-termique au Turonien-Mid-Maastritchiten. Une inversion tectonique, associée à une direction de raccourcissement NNW-SSE a eu lieu au Santonien (84 Ma). Cette inversion est due au changement de direction et de vitesse de mouvement de plaque Africaine associé à la convergence entre l'Europe et l'Afrique (Guiraud and Bosworth, 1997). Cette inversion se manifeste par des structures réactivées en compression et en transpression observées dans le WAS et CAS, notamment dans le fossé de la Bénoué, le bassin de Bongor, Doseo et Doba (Genik, 1993; Cooper and Warren, 2014). Des plis et des structures en fleur en transpression dextre sont également observés dans le fossé de la Bénoué et les bassins soudanais (Figure 2-10, Guiraud et

Bosworth, 1997). Une dernière réactivation en extension a eu lieu au Mid-Maastrichtien-Paléogène dans le WAS. Elle s'est terminée par de nouveau une phase de subsidence thermique (Figure 2-13) (Genik, 1993).

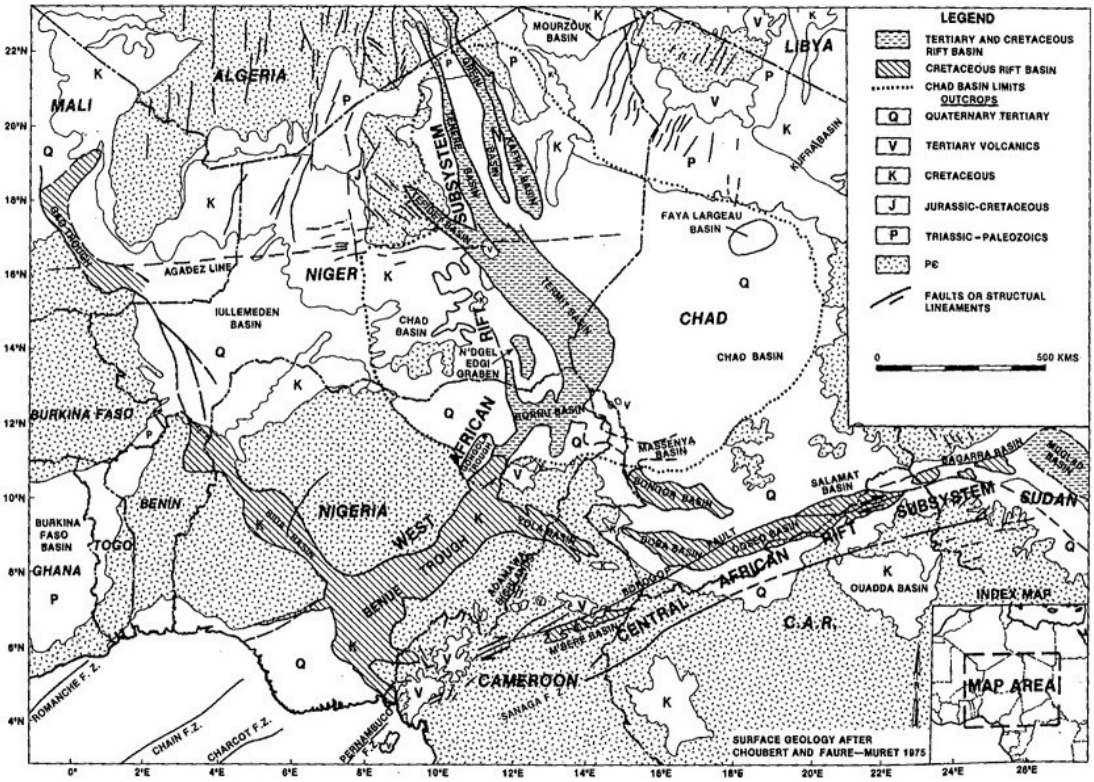

Figure 2-12 Schéma structural de la partie occidentale des WCARS (Genik,1992).

En comparant les résultats de Genik (1993) avec le modèle de Guiraud et al. (2005), on constate des désaccords notamment sur les âges de syn-rift. En effet, selon Genik (1993), il y n'a pas eu de déformation extensive à l'Albien dans les bassins de WAS et CAS contrairement à ce que suggère le modèke de Guiraud et al., (2005). La deuxième phase de syn-rift de Guraud et al. (2005) correspondrait à la réactivation au Cénomanien dans le modèle de Genik (1993). La troisième phase d'extension au Mid-Maastrichtien-Paléogène dans des rifts du WAS n'a pas été prise en compte par Guiraud et al. (2005). Afin de mieux comprendre l'évolution du WCARS, l'étude tectono-sédimentaire des bassins de rift au Nigéria et au Mali (fossé de la Bénoué, bassin de Bida, etc., Figure 2-12) sera nécessaire.

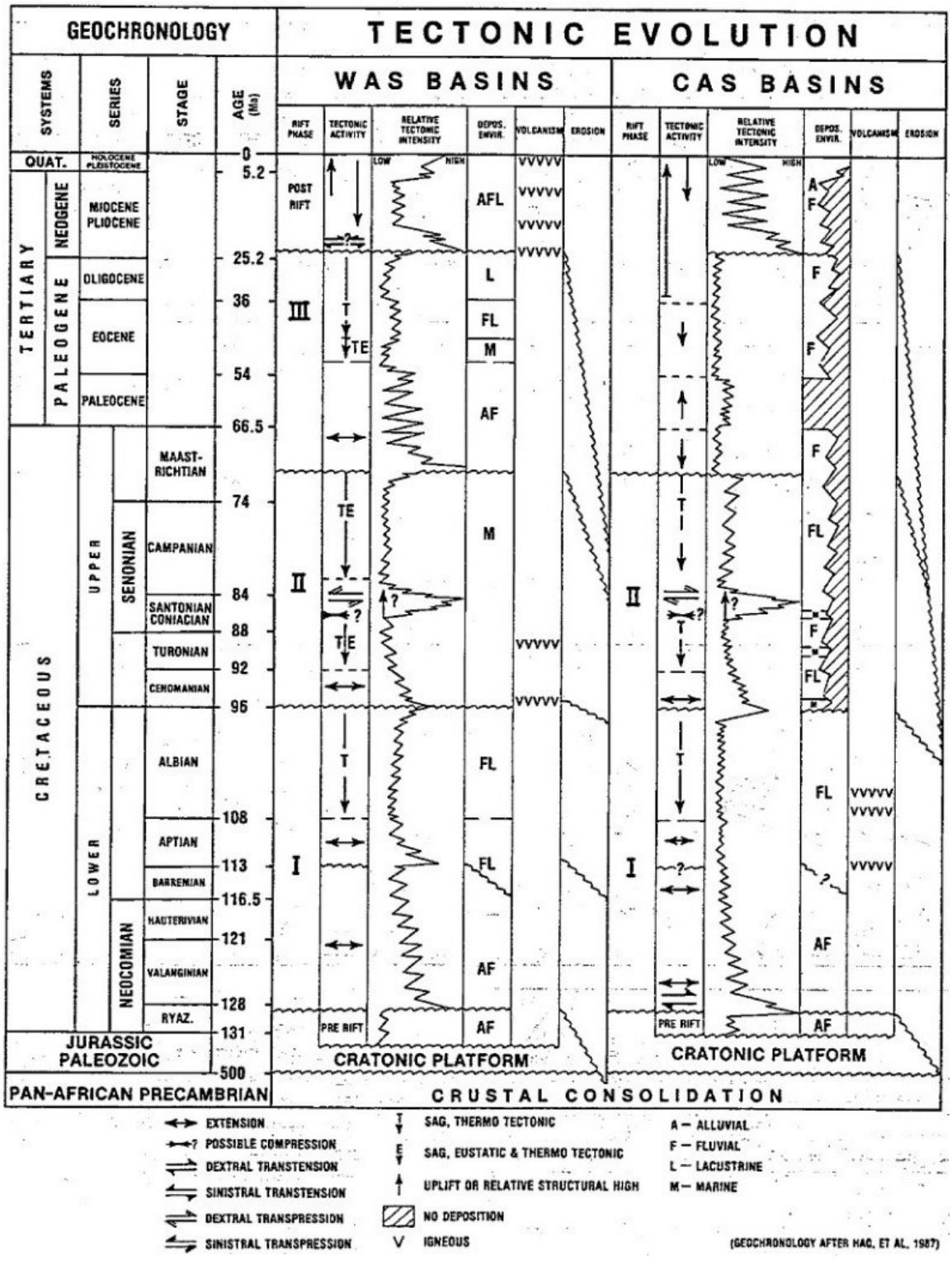

Figure 2-13 Evolution paléotectonique des bassins de rift de la partie occidentale du WCARS. A noter que les âges absolus sont à réactualiser (Genik, 1993).

2.2.2.2. Evolution Cénozoïque

Le WCARS continue d'évoluer au Cénozoïque. Une phase de rifting est enregistrée dans les bassins du WAS au Maastrichtien Supérieur-Eocène Inférieur qui est suivie par une période de subsidence thermique (Sag) et de chute eustatique à l'Eocène-Oligocène (Figure 2-13, Genik, 1993). Cependant, les bassins du CAS présentent des alternances de subsidence et soulèvement au Cénozoïque.

A l'Est, un grand épisode de *rifting* a commencé à l'Oligocène Supérieur (30 Ma) en Afrique de l'Est, dans la mer Rouge et dans le golfe d'Aden (Figure 2-14). Le processus est considéré comme étant l'origine du futur rift est-africain.

La collision entre l'Afrique et l'Europe a débuté à l'Eocène Supérieur (37 Ma) avec une direction de compression N160, au même moment que le ralentissement de la plaque africaine (Burke, 1996 ; Guiraud et al., 2005). Elle a ensuite été intensifiée au Miocène (22 Ma) en formant la chaîne Atlas-Alpine au Nord-Ouest de l'Afrique. La répercussion de la collision alpine sur l'Afrique de l'Ouest reste très mal contrainte. Des linéaments seraient réactivés, y compris le linéament guinéo-nubien E-W, panafricain N-S, etc. (Figure 2-14, Guiraud et al., 1985; Guiraud, 1986). Cependant, on observe rarement sur ces linéaments une déformation ou des décallages contemporains qui soient clairement démontrés.

Des bombements topographiques (le Hoggar, l'Aïr, l'Iforas, le Tibesti, etc.) se sont formés en association avec un grand épisode de volcanisme en Afrique depuis 35 Ma (Figure 2-1 et Figure *2-14*, Rougier, 2012). Des bourrelets marginaux le long l'Océan Altantique (guinéen, namibien, etc) se sont développés (Figure 2-14). Le taux de dénudation le plus élevé a été localisé sur le bourrelet marginal guinéen au cours du Cénozoïque (Grimaud, 2014). Il s'agit en effet de mouvements verticaux de grandes longueurs d'onde et d'amplitudes variables à l'échelle continentale qui ne sont pas encore bien caractérisés en terme de quantité de soulèvement, d'origines (mouvement mantellique, collision alphine, etc), et quant aux effets de l'héritage des anciennes structures. Selon Burke (1996), les mouvements verticaux sont dus aux processus mantelliques associés au ralentissement du mouvement de la plaque africaine depuis l'Oligocène.

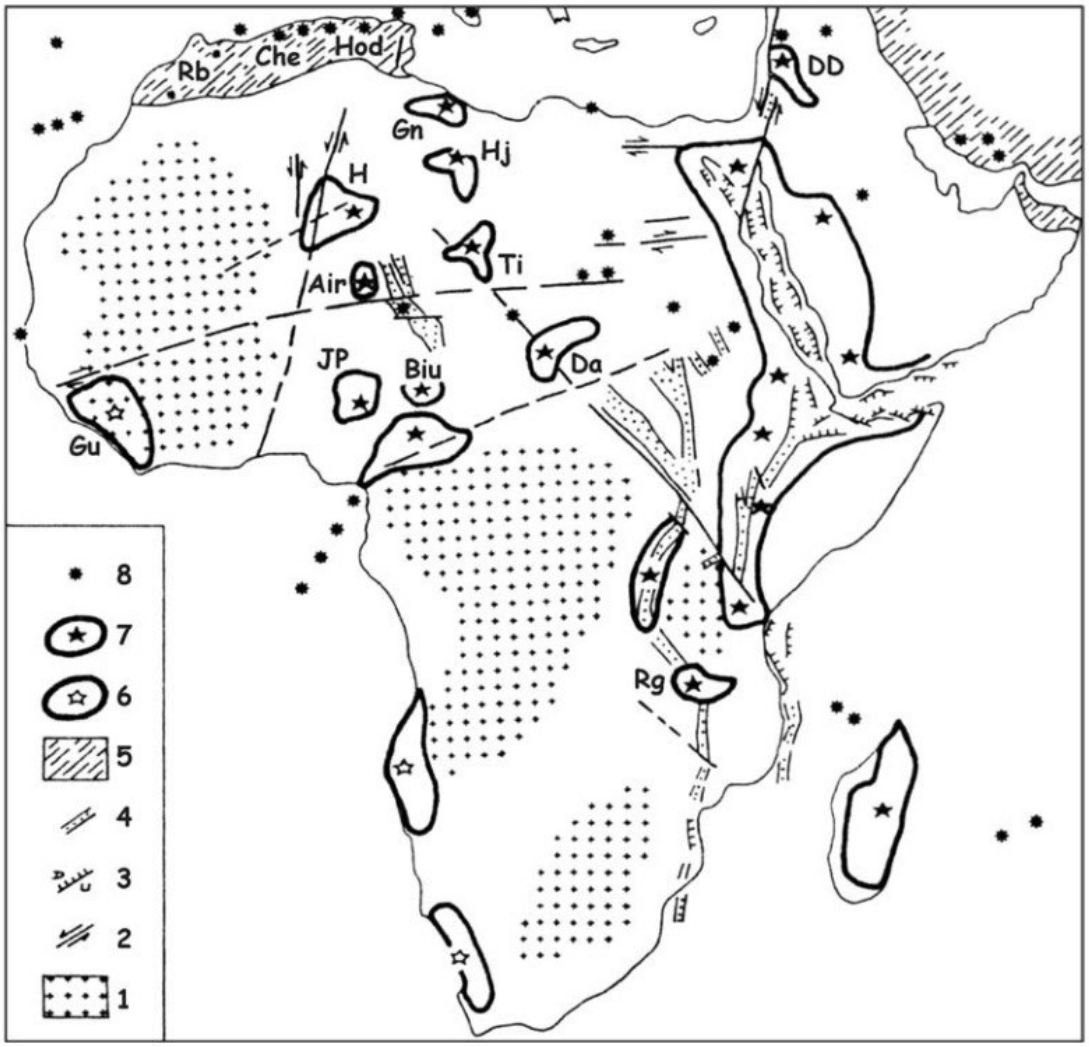

Figure 2-14 Modèle néotectonique du continent africain depuis l'Eocène, selon Guiraud et al. (2005). (1) région cratonique, (2) décrochement, (3) failles, (4) rift, (5) chaîne Alpine, (6) zone soulevée, (7) zone soulevée avec magmatisme, (8) volcans. Che : Cheliff, Da : Darfur, DD : Dj.Druze, Gn : Garian High, Gu : Guinea, H : Hoggar, Hj : Haruj, Hod : Hodna, JP : Jos Plateau, Rb : Rharb, Rg :Rungwe, Ti : Tibesti.

2.3. Magmatisme Post-Paléozoïque

Même si la région est considérée comme 'stable' depuis la fin du Paléozoïque, une activité magmatique non négligeable est documentée en Afrique de l'Ouest. Ses relations avec la tectonique et/ou les mouvements verticaux de la sous-région sont encore mal définies.

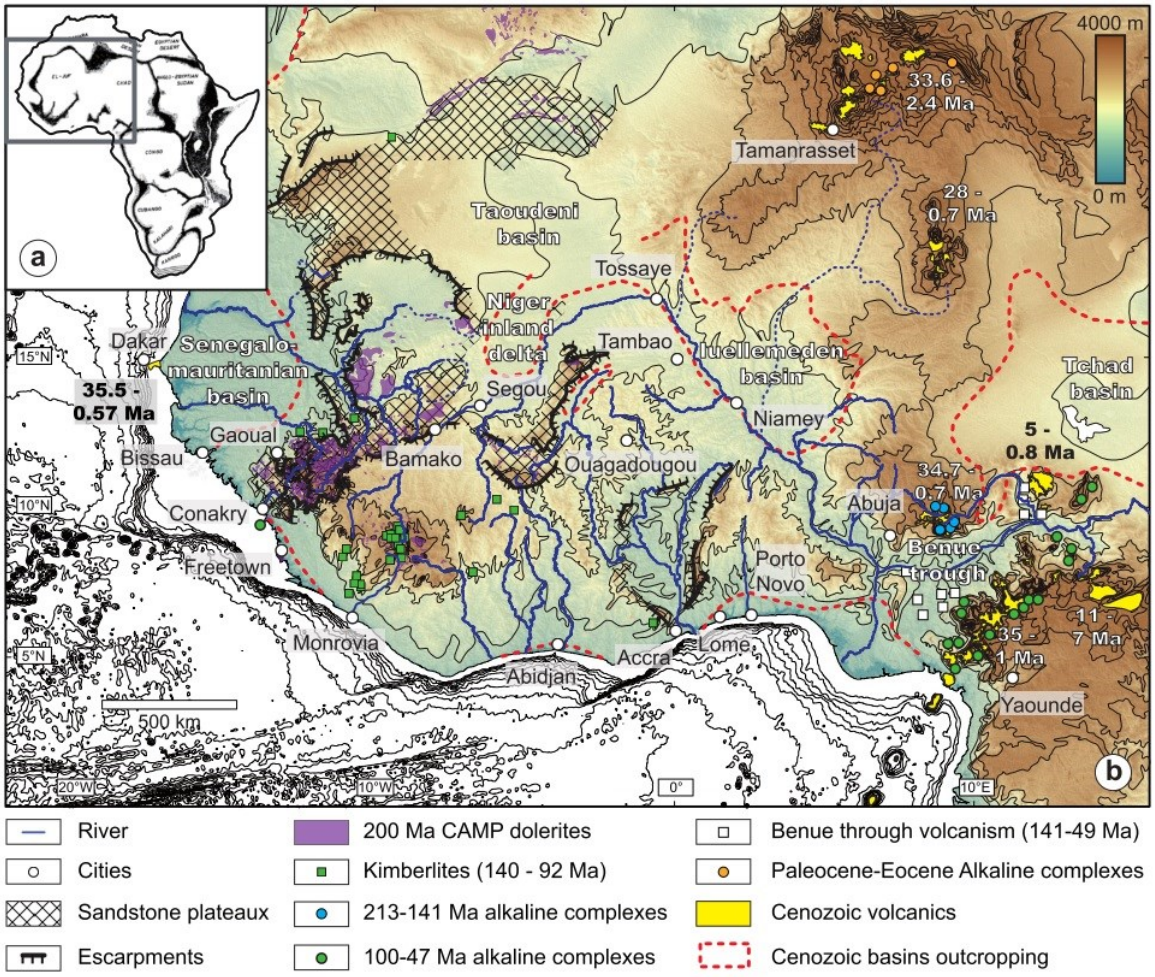

Figure 2-15 La distribution du magmatisme en Afrique de l'Ouest depuis le depuis du Mésozoïque (Grimaud, 2014).

La Figure 2-15 montre la répartition du magmatisme en Afrique de l'Ouest depuis le Trias :

- Les coulées, dykes et sills doléritiques de la province magmatique de l'Atlantique Central (*Central Atlantic Magmatic Province* (CAMP), 200 Ma) sur la partie occidentale du craton et dans le bassin de Taoudenni.
- Des kimberlites du Crétacé Inférieur, réparties sur la partie occidentale du craton,
- Des complexes granitiques alcalins jurassiques (213-140 Ma) sur le plateau de Jos (*Younger Granites*, Figure 2-2),
- Le magmatisme Crétacé-Eocène Inférieur dans le fossé de la Bénoué,
- Des complexes granitiques alcalins plus récents le long de la ligne volcanique du Cameroun et dans le Hoggar,

- Des épanchements basaltiques cénozoïques sur le socle panafricain du bombement du Hoggar (Hoggar proprement dit et Aïr, Figure 2-2),
- La chaîne volcanique du Cameroun au SE du bassin de la Bénoué.

2.4. Cinématique de l'Atlantique

L'Océan Atlantique s'est mis en place progressivement durant le démantèlement de la Pangée depuis le Trias Supérieur, en formant les marges passives Africaines et Américaines. La reconstitution cinématique de l'ouverture de l'Atlantique, surtout l'Atlantique Central et Equatoriale est nécessaire pour comprendre l'évolution de la marge Ouest Africaine. Il existe de nombreux modèles de reconstitution cinématique dont les plus récents montrent qu'en effet, l'ouverture de l'Atlantique s'est fait en plusieurs stades successifs associés souvent avec des événements magmatiques.

2.4.1. Ouverture de l'Atlantique Central

L'Atlantique Central est limité au Nord par la zone de fracture de Pico et Gloria et au Sud par la zone de fracture de 15°20' et Guinéenne (Figure 2-16). De nombreux modèles proposés par différents auteurs tentent de reconstruire l'évolution cinématique depuis son ouverture. En effet, la phase initiale de l'ouverture de l'Atlantique Central reste débattue. Son histoire depuis 120Ma (Chron M0) est relativement mieux contrainte grâce à la présence des linéaments des anomalies magnétiques remarquables et des zones de fracture océaniques. Il existe de différents modèles désignant l'ouverture avec ou sans saut de ride océanique (*Ridge jump*). Le modèle le plus récent de Labails et al. (2010) suggère que l'ouverture de l'Atlantique Central, sans saut de ride océanique, débute au Jurassique Supérieur (190 Ma). Il est basé sur l'analyse des données géophysiques récentes (magnétiques, gravimétriques et sismique) et la géologie continentale.

Quatre linéaments des anomalies magnétiques conjugués ont été identifiés (Figure 2-16, Labails et al., 2010) :

- ECMA (*East Coast Magnetic Anomaly*) et WACMA(*West African Coast Magnetic Anomaly*) premièrement défini par Sahabi et al. (2004) sont considérés étant la limite océan/continent. Son âge Sinémurien Inférieur (190 Ma) représente le moment de la création de la première croûte océanique (*Breakup*) qui est basé sur l'âge des dépôts salifères synrifts (Formation d'Eurydice/Argo en Nouvelle Ecosse et d'Argana au Maroc, Figure 2-17).
- BSMA (*Blake Spur Magnetic Anomaly*) et ABSMA (*African Blake Spur Magnetic Anomaly*) datés Bajocien Inférieur (170 Ma) identifiable seulement dans la partie Sud de la côte Atlantique Central coïncident avec le changement de la topographie du socle lié à la vitesse de l'expansion.
- Anomalies M0 conjugués daté 120,6 Ma (Gaina et al., 2013).
- Anomalies M25 conjugués daté 154 M.

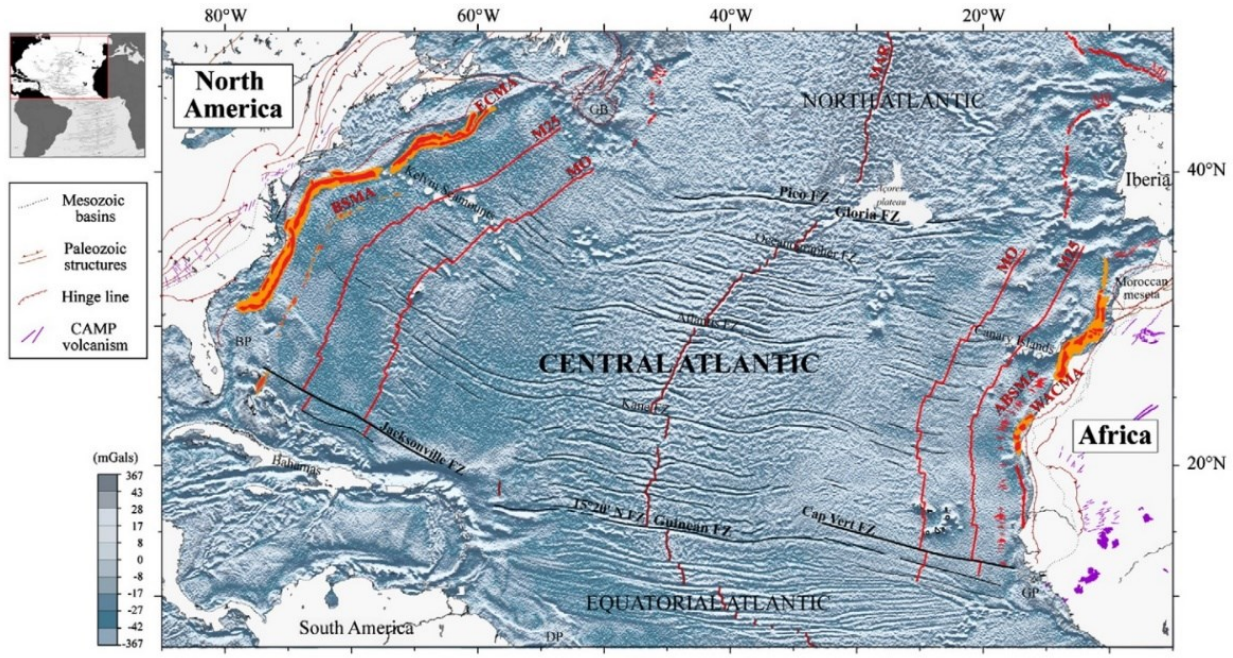

Figure 2-16 Limites générales des zonations de l'expansion de la croûte océanique dans l'Océan Atlantique sur les deux côtés, superposées sur un fond des données gravimétriques dérivant du satellite (free-air, one arc-minute grid of uniform coverage). Les anomalies magnétiques sont indiquées en rouge : ECMA : Côte Est de l'Amérique du Nord, WACMA : Côte de l'Afrique de l'Ouest, BSMA : Blake Spur, ABSMW : Blake Spur Africain. ECMA est présenté en deux couleurs (rouge et orange) selon son amplitude. Les zones de fracture océaniques et les structures tectoniques majeurs sont indiquées. Les provinces de l'anomalie magnétique entre ECMA/WACMA et Chron M25, et entre Chron M25 et M0, constituent Jurassic Magnetic Quiet Zone (JMQZ). MAR, Mid-Atlantic Ridge; GB, Grand Banks of

Newfoundland; CAMP, Central Atlantic Magmatic Province; BP, Blake Plateau; DP, Demerara Plateau; GP, Guinean Plateau (Labails et al.,2010).

Même si l'incertitude sur l'identification et l'âge de ces linéaments des anomalies magnétiques conjugués persiste, ils permettent de reconstituer l'ouverture de l'Atlantique Central en plusieurs phases à l'aide des zones de fracture océanique visibles sur les données gravimétriques et des données sismiques.

Le *rifting* dans l'Atlantique Central a eu lieu au Tiras-Jurassique Inférieur accompagné par la CAMP et une épaisse séquence d'évaporites (Figure 2-17). Il s'est terminé par l'ouverture de l'Océan Atlantique Central au Sinémurien Supérieur (190 Ma) déduit par l'âge de la fin du dépôt du sel. L'âge de la création de la première croûte océanique serait diachrone et plus tard dans la zone plus au Nord entre le Maroc et la Nouvelle Ecosse vers 185-175 Ma (Schettino and Turco, 2009; Labails et al., 2010; Withjack et al., 1998).

Au Sinémurien Supérieur-Bajocien Inférieur (190-170 Ma), l'accrétion de la croûte océanique était lente (0,8 cm/an) avec probablement une direction d'expansion NNW-SSE oblique par rapport à l'axe (Figure 2-18). Au Bajocien Inférieur-Oxfordien (170-154 Ma), la direction d'expansion a évolué vers NW-SE avec une augmentation de taux d'expansion à 1,7 cm/an. Il s'agit en effet d'une réorganisation des plaques et d'un changement de sédimentation de grés-argile (Mahican/Ameskhoud formation) au calcaire (Abenali/Imouzzer formation) sur les marges (Figure 2-17, Labails et al., 2010).

A partir de 154 Ma, le mouvement de plaque est devenu relativement stable, excepté de quelques changements de taux d'expansion. En effet, le taux d'expansion a augmenté jusqu'à 2,8 cm/an au Kimméridgien (154-150 Ma), et puis diminué à 1,3 cm/an au Thitonien Inférieur (150 Ma). Enfin, il restait constant jusqu'à l'Aptien Supérieur (120 Ma) (Figure 2-17). A cette époque, l'Atlantique Sud s'est mise à s'ouvrir, en même temps que l'Océan Atlantique Nord (Labail et al., 2010).

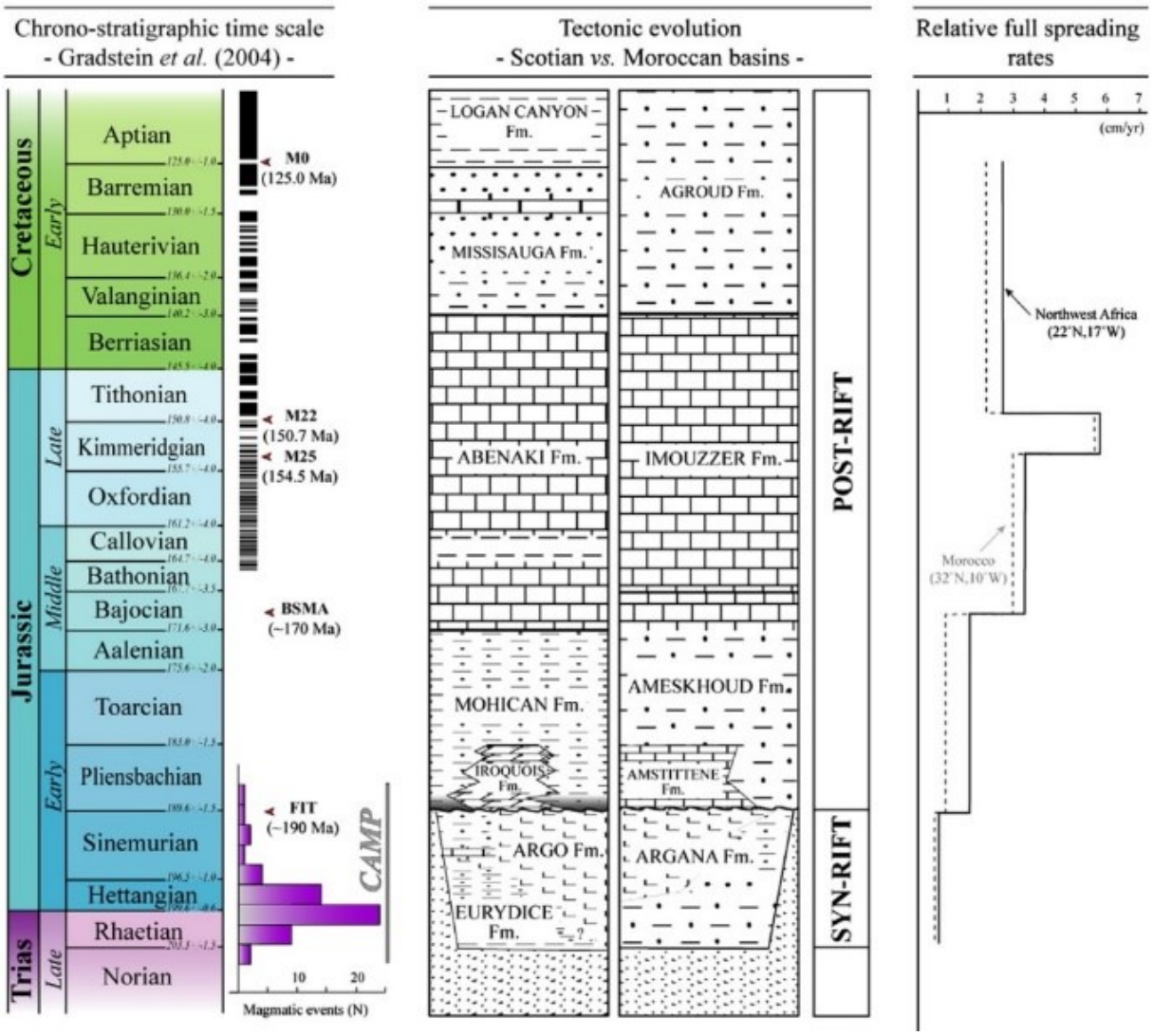

Figure 2-17 Chronologie simplifiée du Trias au Crétacé de l'accrétion de la croûte océanique, de l'événement magmatique, des formations sédimentaires principales de l'Atlantique Central et des taux d'expansion calculés pour deux endroits au Maroc et NW de l'Afrique (Labail et al.,2010). M0 a été redaté plus récemment à 120.6 Ma (Gaina et al., 2013).

Dans ce modèle cinématique de l'ouverture de l'Atlantique Central, l'accrétion est en fait asymétrique, avec un taux d'accrétion plus grand à l'Ouest qu'à l'Est (Figure 2-18). Cette asymétrie peut-être liée à l'anomalie thermique situé préférentiellement sous la plaque africaine durant la CAMP dont l'éruption violente dans les rifts triasiques se serait propagée très loin vers l'ouest (Labails et al.,2010). D'autres modèles de la cinématique proposent une accrétion symétrique impliquant des sauts de ride océanique (Schettino et Turo, 2009).

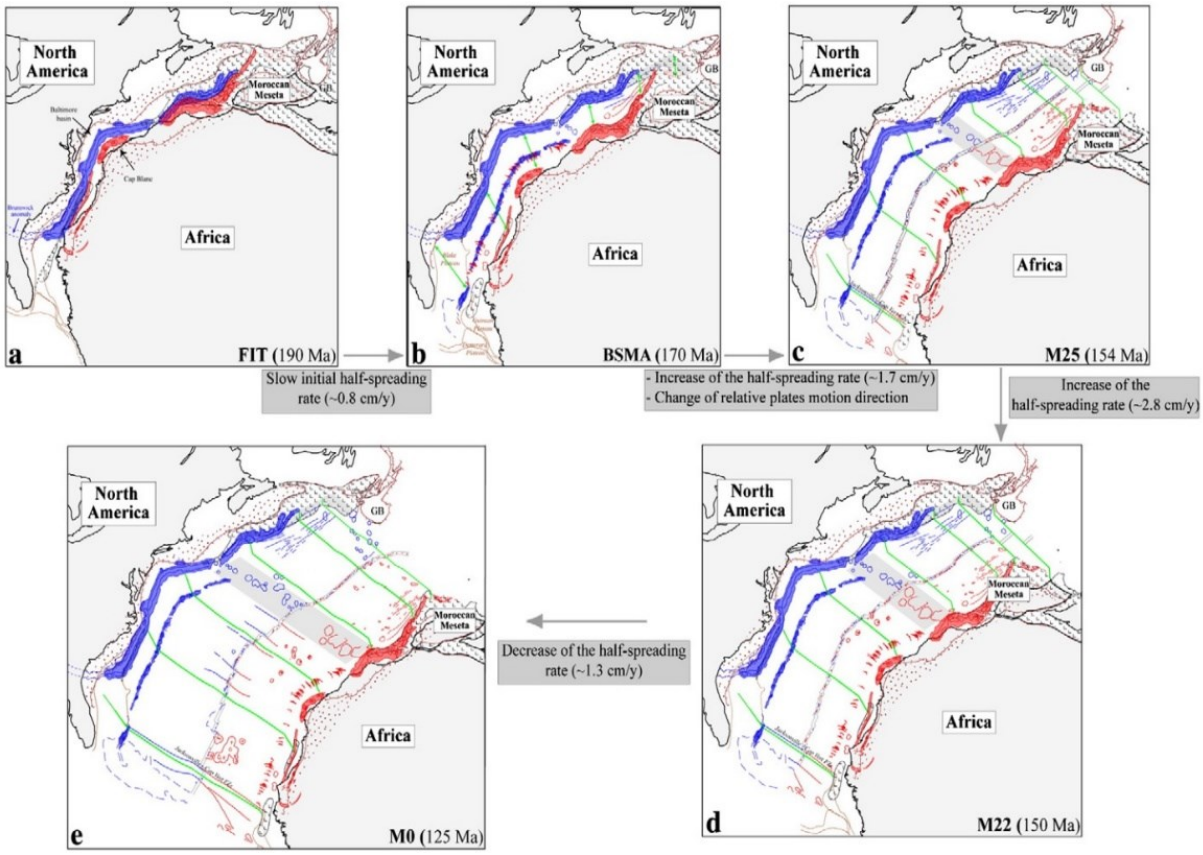

Figure 2-18 Ouverture de l'Atlantique Central proposé par Labail et al., 2010. L'Amérique du Nord est fixée. M0 est daté plus récemment 120.6 Ma (Gaina et al., 2013).

2.4.2. Ouverture de l'Atlantique Sud

Le démantèlement de la Pangée continue au Crétacé Inférieur (120 Ma) dans l'Atlantique Sud, l'Atlantique Nord et autour du continent Antarctique. L'Atlantique Sud s'est ouverte en effet sur la zone de suture Panafricaine entre les continents Sud-Américain et Africain.

L'Atlantique Sud peut être divisé en trois segments : le segment central, le segment austral et le segment des Falklands (Figure 2-19). On différencie ici le segment équatorial des autres segments comme étant l'Atlantique Equatorial. Le segment central est séparé du segment équatorial par la zone de fracture d'Ascension au Nord et du segment austral par la zone de fracture de Rio Grande au Sud. Le long du segment central, se localise un grand bassin Aptien d'évaporites

sur les deux côtés. Le segment austral est séparé du segment de Falklands par la zone de fracture d'Agulhas-Falkland. On trouve des SDRs (*Seaward Dipping Reflectors*) sur les marges du segment austral qui indiquent qu'elles seraient volcaniques de ces marges (Figure 2-19). Le segment de Falklands sert de jonction entre la ride Atlantique et la ride de l'Inde SW (Moulin et al., 2010).

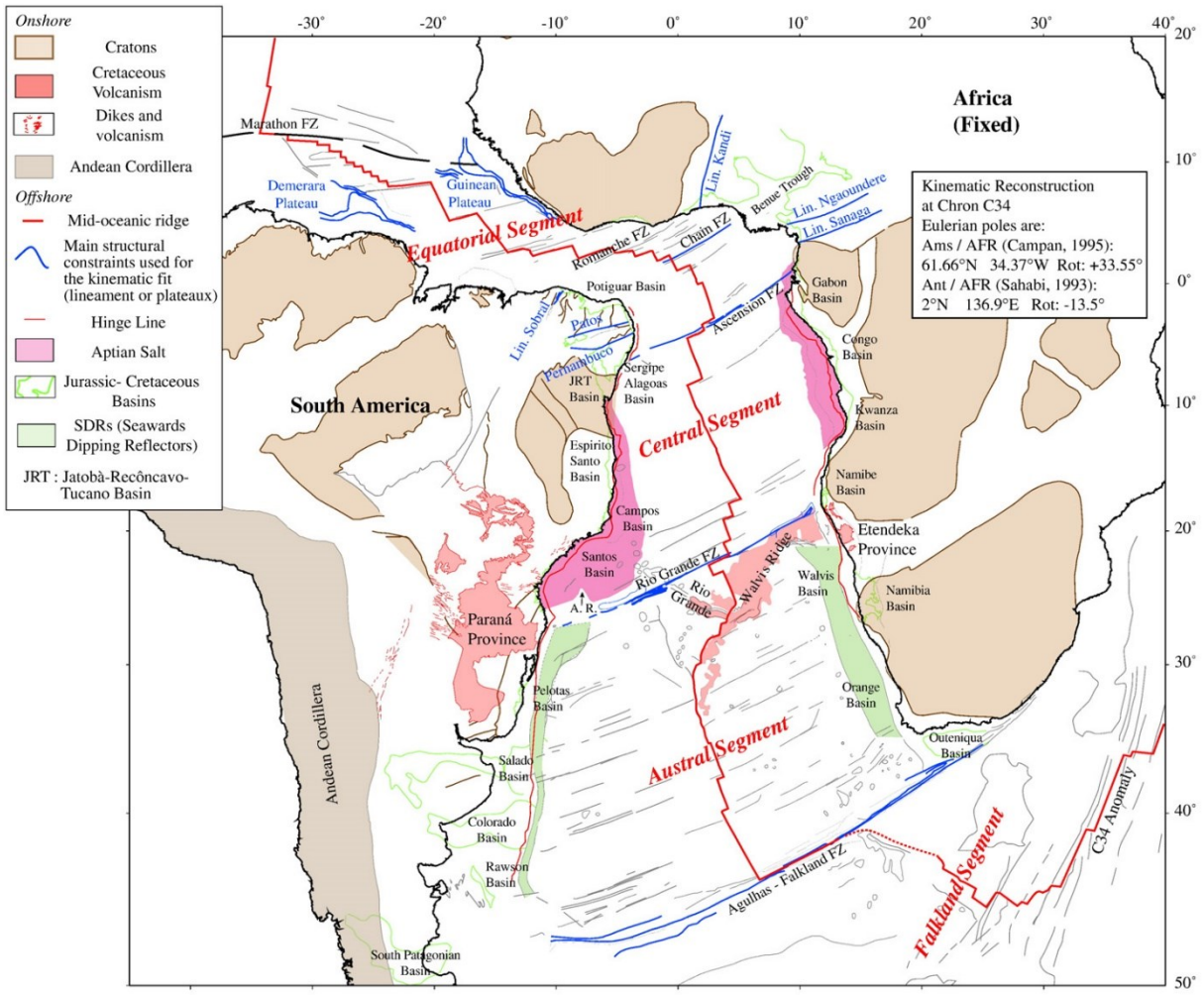

Figure 2-19 Schéma tectono-structurale de l'Atlantique Sud à 84 Ma. A.R. : Ride d'Abimael (ancienne ride avortée) FZ, Zone de Fracture (Moulin et al., 2010).

Bien que de nombreux modèles cinématiques de l'ouverture de l'Atlantique Sud existent, leurs configurations initiales pré-breakup sont souvent mal contraintes du fait de la complexité des déformations intraplaques associées. De plus, la période non-magnétique au Crétacé Inférieur (120 Ma) (*Cretaceous magnetic quiet zone*) du segment central rend la reconstitution difficile.

Moulin et al. (2010) propose un modèle contraint par des données géophysiques récentes et la géologie des deux plaques, y compris les anomalies magnétiques, les zones de fracture et les systèmes de linéaments conjugués observés sur les deux continents. Ils ont pris en compte également les limites du dépôt salifère et celles des SDRs. Les déformations intraplaques impliquées dans le modèle, comme le *rifting* avorté sont en effet nécessaires pour établir une configuration pré-ouverture plus fiable.

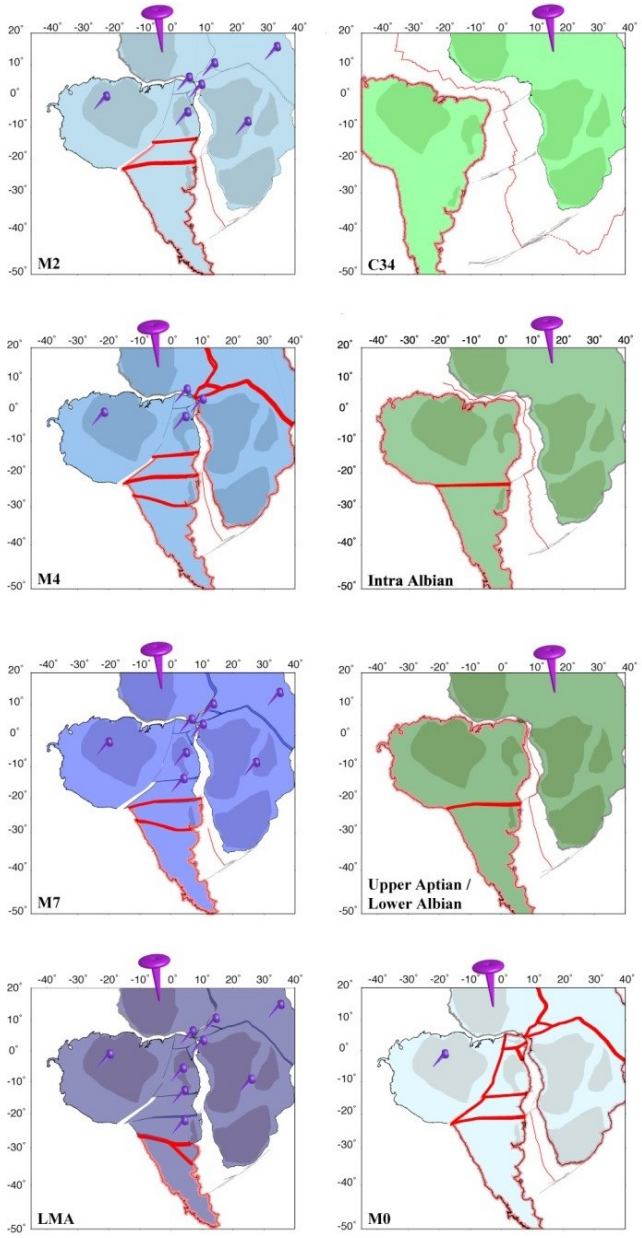

Figure 2-20 Reconstitution de l'évolution de l'océan Atlantique Sud et Equatoriale par Moulin et al., 2010. Le bloc Ouest Africain est fixé. La localisation de la déformation intraplaque entre deux chrons est marquée par des lignes

rouges. La côte des plaques en déplacement est indiquée en orange. Les punaises violettes marquent des blocs qui ne bougent pas. LMA : 133 Ma, M7 : 127,5 Ma, M4 : 125,7 Ma, M2 :123,5 Ma, M0 : 121 Ma, C34: 84 Ma. La datation de M7, M4 et M2 sont d'après Gaina et al., (2013). Voir Table 2 dans l'Annexe pour les pôles Eulériens utilisés.

Modèle de l'ouverture de l'Atlantique Sud (Figure 2-20, Moulin et al., 2010):

Hautérivien-Barrémien (LMA-M4) (133 Ma -125,7 Ma) :

L'ouverture de l'Atlantique Sud commence par le segment austral à la suite d'un événement magmatique de Parana-Etendeka en Angola et Namibie. En même temps, des blocs Sud de l'Amérique du Sud se déplacent à l'Ouest.

Aptien Inférieur (M4-M0) (125.7-121 Ma) :

Le segment austral continue à s'ouvrir du Sud au Nord. Des blocs Sud de l'Amérique du Sud continuent à se déplacer à l'Ouest. Le bloc austral Africain (voir 1 se met à se déplacer vers le NE et le bloc Nubien vers le Nord durant principalement 125.7-123 Ma (M4-M2).

Aptien Supérieur(M0)- Albien Inférieur (121-112 Ma) :

Le segment central se met à s'ouvrir par un saut de ride océanique vers l'Est à la limite Aptien-Albien en même temps que la déposition du sel se termine.

En conclusion, l'Atlantique Sud s'est ouverte du Sud au Nord du segment austral au segment central à partir de Hauterivien (133 Ma). Les déformations intra-plaques étaient impliquées sur le continent Africain et Sud- Américain au cours de l'ouverture. La connexion entre l'Atlantique Sud et Centrale s'est faite ensuite par l'ouverture de l'Atlantique Equatorial.

2.4.3. Ouverture de l'Atlantique Equatorial

L'Atlantique Equatorial est limitée au Nord par la zone de fracture de Marathon, au Sud par la zone de fracture d'Ascension (Figure 2-19). Elle forme un étroit passage orienté NW-SE avec une dorsale océanique fortement segmentée. L'étude de l'évolution tectono-sédimentaire de l'Atlantique Equatorial et ses marges passives constituent une partie majeure de la thèse.

Le *rifting* dans l'Atlantique Equatorial est contrôlé par des zones de faiblesse Panafricaines. Il a eu lieu au Néocomien-Aptien, comme le montre par le développement des bassins offshores au NE du Brésil (De Matos, 1992). Le *rifting* dans le segment central s'est fait en deux phases, du Nord au Sud et du Berriasien Supérieur jusqu'au début de l'Aptien. Il s'est terminé par une phase de subsidence (Sag bassin) au Mid-Aptien-Aptien Supérieur (Chaboureau et al., 2013). Au même moment, le *rifting* avorté s'est développé dans le continent Africain avec une phase majeure au Valanginien-Aptien (Genik, 1993). Il s'agit en effet d'un point triple RRR (fossé de la Bénoué) dont les deux bras atlantiques ont atteint la rupture lithosphérique. A noter que l'ouverture de l'Atlantique Equatorial a entrainé la séparation du craton ouest africain avec le craton de Sao Luis brésilien.

L'évolution cinématique de l'Atlantique Equatorial est difficile à interpréter par manque de linéament d'anomalie magnétique. Moulin et al. (2010) propose une configuration pré-ouverture (vers 112 Ma) basée sur la corrélation des structures géologiques et les mouvements relatifs déduits des zones de facture (Figure 2-21). En effet, le plateau guinéen est considéré comme le conjugué du plateau de Démérara. Des systèmes conjugués identifiables sur les continents sont utilisés (les linéaments de Saboral et Kandi, de Patos et Ngaoundere et de Pernambuco et Sananga).

Le modèle de Moulin et al. (2010) montre que l'ouverture de l'Atlantique Equatorial est presque contemporaine de l'ouverture du segment central à la limite Aptien-Albien (112 Ma) (Figure 2-20 et Figure *2-21*1). La connexion entre l'Océan Atlantique Central et Sud s'est fait vers 105 Ma. Il n'y a plus eu de déformation intra-plaque majeur sur les deux continents depuis son ouverture.

En Conclusion, d'après le modèle de Labails et al., (2010) et Moulin et la. (2010), l'ouverture de l'Atlantique a commencé dans l'Atlantique Central vers 190 Ma dans une zone de suture Hercynienne précédée par le magmatisme de la CAMP. Ensuite, l'Atlantique Sud s'ouvrait du Sud au Nord au Barrémien (vers 130 Ma) le long des zones Panafricaines, au moment du magmatisme de Parana-Etendeka. A la limite Aptien-Albien (112 Ma), l'Atlantique Equatorial s'est ouverte en même temps que le segment central de l'Atlantique Sud, ce qui permet la connexion entre l'Atlantique Sud et Centrale plus tard vers 105 Ma (Moulin et al., 2010).

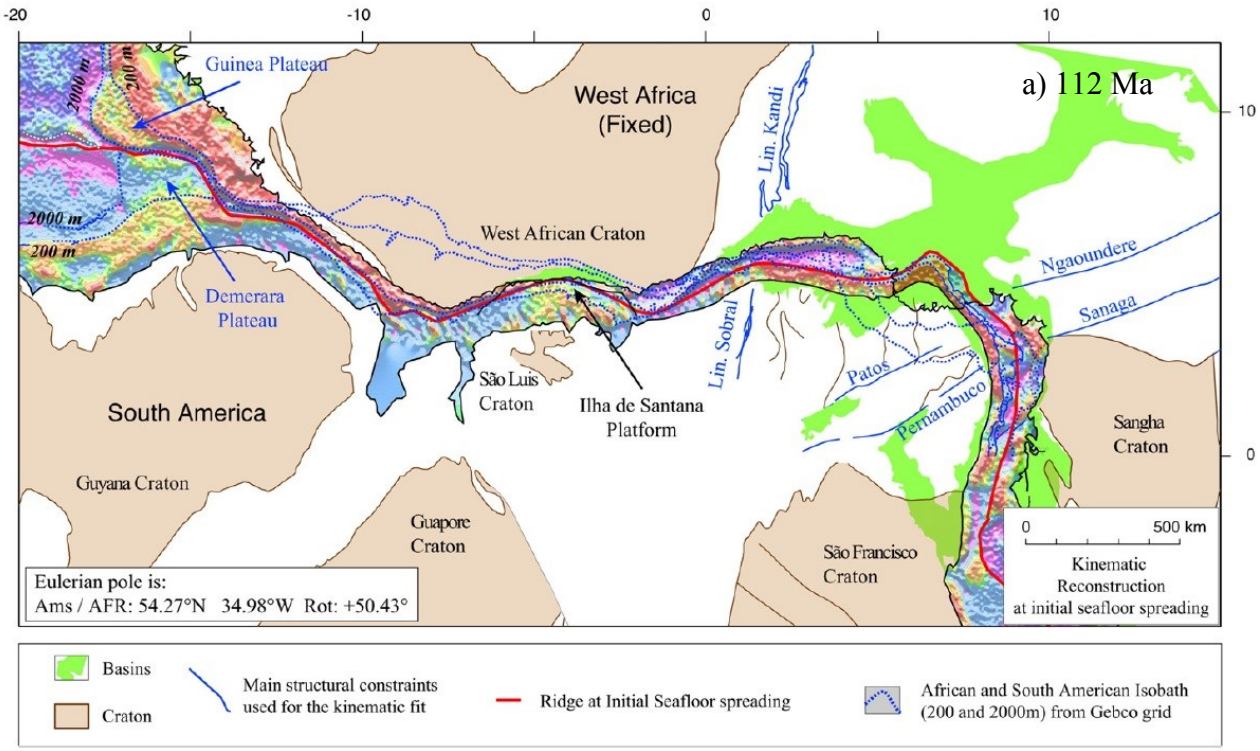
a) 112 Ma
Guinea Plateau
West Africa
(Fixed)
Lin. Kandi
West African Craton
Ngaoundere
Sanaga
Demerara
Plateau
São Luis
Craton
Ilha de Santana
Platform
Lin. Sobral
Patos
Pernambuco
South America
Sangha
Craton
Guyana Craton
Guapore
Craton
São Francisco
Craton
2000 m
200 m
Eulerian pole is:
Ams / AFR: 54.27°N 34.98°W Rot: +50.43°
0 500 km
Kinematic
Reconstruction
at initial seafloor spreading
Basins
Craton
Main structural constraints
used for the kinematic fit
Ridge at Initial Seafloor spreading
African and South American Isobath
(200 and 2000m) from Gebco grid

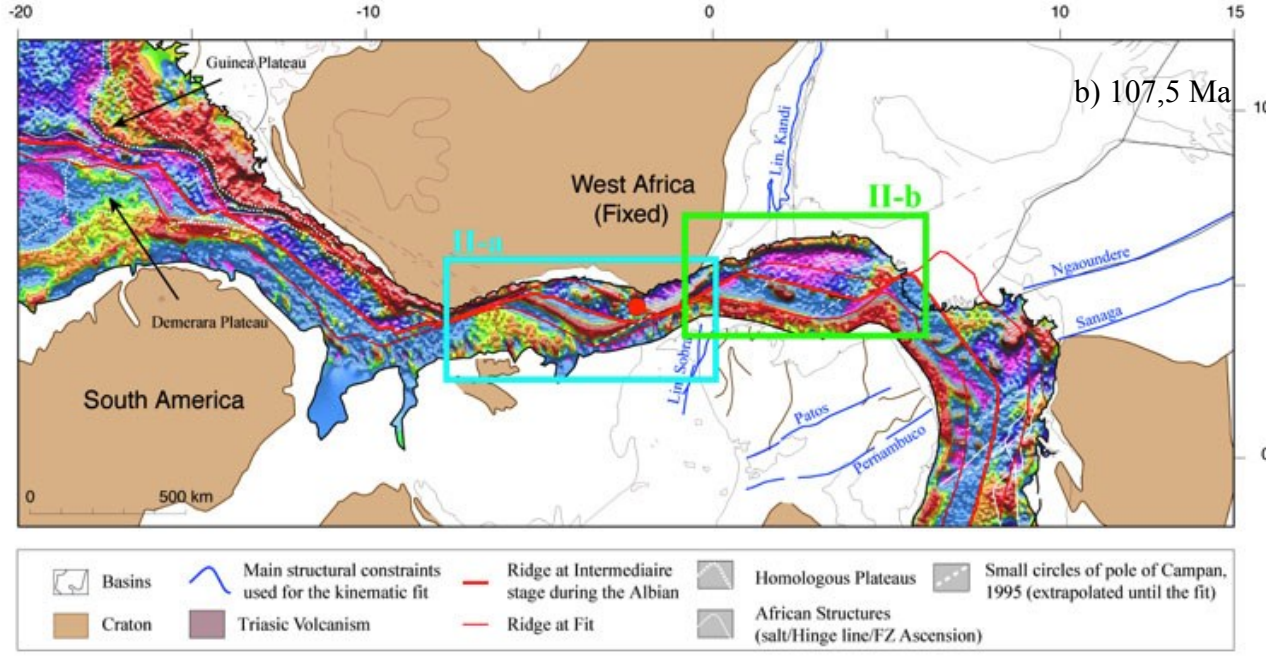
b) 107,5 Ma
Guinea Plateau
West Africa
(Fixed)
Lin. Kandi
II-a
II-b
Ngaoundere
Sanaga
Demerara Plateau
Lin. Sobral
Patos
Pernambuco
South America
0 500 km
Basins
Craton
Main structural constraints
used for the kinematic fit
Triasic Volcanism
Ridge at Intermediaire
stage during the Albian
Ridge at Fit
Homologous Plateaus
African Structures
(salt/Hinge line/FZ Ascension)
Small circles of pole of Campan,
1995 (extrapolated until the fit)

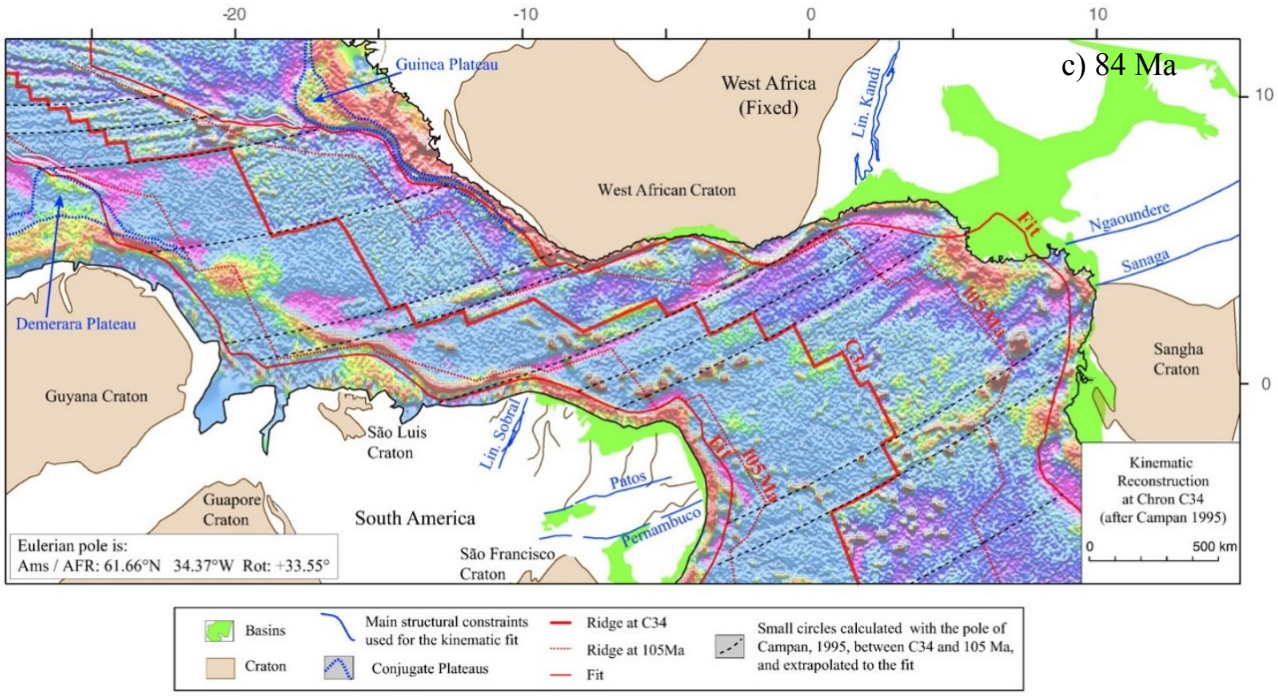

Figure 2-21 a) Reconstruction pré-ouverture de l'Atlantique Equatorial à 112 Ma. Les données gravimétriques sont montrées dans la partie océanique. L'Afrique est fixée. L'Amérique du Sud et les grilles gravimétriques sont tournées suivant les petits cercles. b) Reconstruction de l'Atlantique Equatorial à Mid-Albien (vers 107.5 Ma) (Moulin et Labail, Communication personnelle) c) Reconstruction à 84 Ma (C34) (Moulin et al., 2010).

Cependant, dans ces modèles, les limites océan/continent sont déterminées à partir les anomalies magnétiques qui sont parfois absentes, sans tenir compte de la zone de transition O/C qui peut parfois atteindre quelques centaines de km de large (25-700 km). La variation de la position de la ligne de rivage contrôlée par le flux de sédiments au cours du temps géologique peut avoir une influence sur la reconstruction. Les déformations intra-plaques ne sont pas vérifiées quantitativement avec des observations géologiques. Ces points doivent être améliorés dans le futur.

CHAPTER 3 : PALEOGEOGRAPHIC AND STRUCTURAL RECONSTRUCTION

PAPER 1 - Paleogeographic and structural evolution of northwestern Africa and its Atlantic margins since the Early Mesozoic

Jing Ye[1,2], Dominique Chardon[1], Delphine Rouby[1], François Guillocheau[3], Massimo Dall'asta[2], Jean-Noel Ferry[2], Olivier Broucke[4]

[1] Géosciences Environnement Toulouse, Université de Toulouse, CNRS, IRD, UPS, CNES, F-31400, France

[2]TOTAL R&D, Frontier Exploration, CSTJF, Avenue Larribau, F-64018 Pau Cedex, France

[3]Géosciences Rennes, Université de Rennes 1, CNRS, CS 74205, 35042 Rennes Cedex, France

[4]TOTAL E&P, Middle East and North Africa – Technical Excellence, La Defense, Paris, France

Manuscript submitted to **Geosphere**

08 September 2016

Abstract

The tectonic, magmatic, sedimentary and erosional histories of Northwestern Africa and its adjoining continental margins are investigated in the light of nine successive Meso-Cenozoic paleo-geological maps. Mapping is based on a compilation of original data on the stratigraphy, depositional environments, structures and magmatic occurrences, as well as extensive integration of industrial seismic and borehole data. Maps integrate original minimal extent of sedimentary deposits beyond their present-day erosional limits and published thermochronological data are used to further constrain areas under burial or erosion.

Rifting propagated eastward from the Central Atlantic between the Valanginian (ca. 140 Ma) and the Aptian (ca. 112 Ma) as an en-échelon transform-rift system connected to an inland rift network, defining a 6-microplate syn-rift pattern for the African continental domain. The pre-opening fit between Africa and South America is refined. Persistent / renewed eroding upwarps along the continental margin are documented. They fed both the margin basins and a very large, persistent intracratonic basin, which acted as a transient sediment reservoir because the products of its erosion were transferred both to the Tethys (to the north) and to the Equatorial Atlantic Ocean by south-flowing rivers crossing the marginal upwarp. The morpho-sedimentary scheme is further complicated by Late Paleogene upheaval of the intracratonic basin by hot-spot swell growth, which fragmented the basin into smaller residual depocenters. By linking the evolution of the continental margins to that of their African hinterland, this study has implications for the interplay of long-wavelength deformation and sediment transfers over paired shield area-continental margin systems.

Résumé

L’histoire tectonique, magmatique, sédimentaire et d’érosion de l’Afrique Nord-Ouest et ces marges continentales a été étudiée à l’aide de neuf cartes paléo-géologique successives méso-cénozoïques. La reconstruction est basée sur une compilation des données originales concernant la stratigraphie les environnements de dépôts, les structures et le magmatisme, ainsi que l’intégration des données sismiques et des forages industrielles. Les cartes intègrent l’extension originale minimum des dépôts sédimentaires au-delà de leur limite actuelle qui sont presque exclusivement des limites érosives. Les données thermochronologiques publiées sont utilisées pour préciser, le cas échéant, l’étendue relative des zones en érosion ou en sédimentation dans le passé.

Le rifting de l'Atlantique Equatoriale s'est propagé d'Ouest en Est depuis l'Atlantique Centrale, et du Valanginien (140 Ma) à l'Aptien (112 Ma), sous la forme d'un système en-échelon « rift-transformante ». Sa connexion au système de rift continental permet de définir un nouveau modèle cinématique syn-rift constitué de six microplaques impliquant le nord-ouest du continent africain. La reconstruction des structures syn-rift a également permis d'affiner la configuration pré-ouverture entre l'Afrique et l'Amérique du Sud. Les cartes révèlent la présence et le maintien des bourrelets topographiques le long de la marge continentale. L'érosion de ces bourrelets a alimenté non seulement les bassins des marges équatoriales, mais aussi un grand bassin intracratonique qui a fonctionné comme une zone de stockage temporaire de sédiments. Ces sédiments méso-cénozoïques ont en effet pu être transférés vers la Téthys (au Nord) ou vers l'Océan Atlantique Equatoriale (au Sud). Le schéma morpho-sédimentaire est de plus compliqué par le bombement topographique du point chaud du Hoggar qui a mené à la fragmentation tardive du bassin intracratonique en petits dépôt-centres résiduels. En liant l'évolution à grande échelle de l'Afrique nord-occidentale à celle de ces marges continentales, notre travail ouvre de nouvelles perspectives sur les l'interférence entre déformation à grande longueur d'onde et transferts de sédiments, notamment pour les systèmes *source-to-sink* de type craton-marges.

3.1. Introduction

The Equatorial Atlantic Ocean opened as a consequence of oblique divergence along what were to become the best-known examples of transform / oblique continental margins of Northern South America and West Africa (Emery et al., 1975; Mascle and Blarez, 1987; Basile et al., 2005; Figure 3-1 and Figure 3-2). Those margins belonged to a large-scale network of rifts that led to the final dispersion of the Gondwana supercontinent by break-up between South America and Africa during the Early Cretaceous (Figure 3-2A). Counterclockwise rotation of the African plate produced a northward rift propagation leading to the formation of the South Atlantic Ocean under dominantly normal divergence, whereas the future Equatorial Atlantic domain underwent dextral-oblique divergence (e.g., Moulin et al., 2010; Frizon de Lamotte et al., 2015). The intracontinental African rifts, which were connected to the South and Equatorial Atlantic rift systems by a triple point, aborted before the African continent could split into three sub-plates along the Western and Central Rift System (Burke and Whiteman, 1973; Guiraud and Maurin, 1992, Figure 3-1).

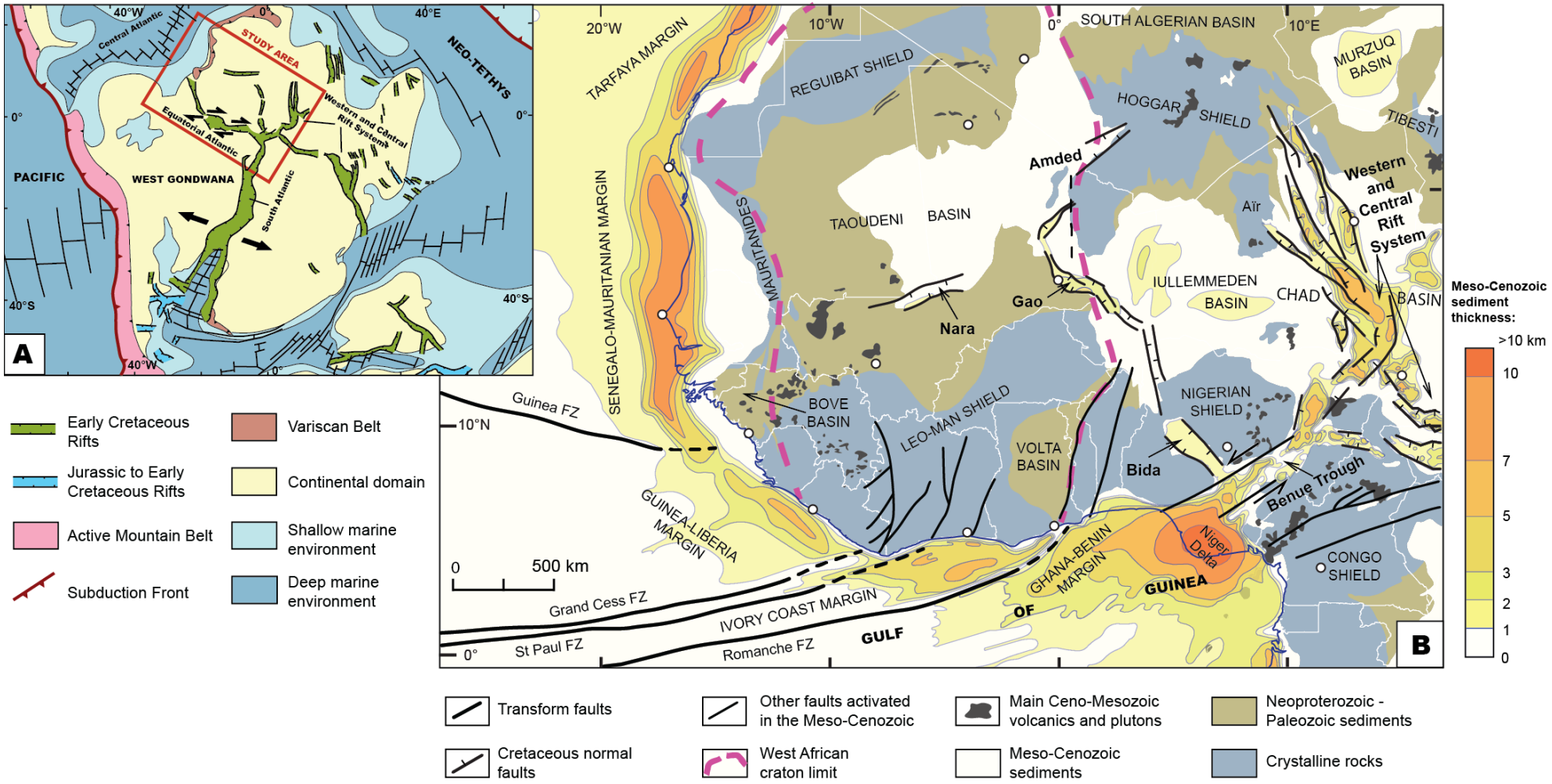

Figure 3-1 (A) Map showing the African and South American rift systems at ~120 Ma during dispersal of Gondwanaland (modified after Frizon de Lamotte et al., 2015). (B) Structural map of northwestern Africa showing Meso-Cenozoic faults and sedimentary basins (after Kogbe, 1981 and Milesi et al., 2010). Geological contours are simplified from Figure 3-2. The names of the main Early Cretaceous intracontinental rifts are indicated (bold font). The frame of Figure 3-1B is shown in red on Figure 3-1A.

Given their transform character, the margins of the Equatorial Atlantic Ocean were mainly investigated through the kinematics of Ocean opening (e.g., Basile et al., 2005; Heine et al., 2013; Heine and Brune, 2014; Moulin et al., 2010) with an emphasis on the fracture zones and the vertical movements induced along the margins (Clift et al., 1998; Bouillin et al., 1998; Bigot-Cormier et al., 2005; Mercier de Lépinay, 2016). The abruptness of the Equatorial margins of Africa results from the strong control of transforms during rifting. These steep margins have specific thermal and subsidence histories that are not yet well understood, but they are crucial in controlling - and for unraveling - their high hydrocarbon potential (Burke et al., 2003; MacGregor et al., 2003). Published exploration studies have provided insights (Delteil et al., 1974; Kjemperud et al., 1992; Bennett and Rusk, 2002; MacGregor et al., 2003), but only at the scale of individual sub-basins and/or along cross sections that do not allow apprehending the fully three-dimensional nature of the tectonostratigraphic evolution of the margins.

Integrated regional studies allowing for linking the stratigraphic history of the margins to their deformation since pre-rift configuration are still lacking. Such studies require structural and paleogeographic reconstitutions (i.e., maps showing depositional environments) of their adjoining continental domain in order to address the coupling between margins evolution and the erosional and deformation history of their hinterland in a "source-to-sink" perspective. So far, paleogeographic reconstitutions for Northwestern Africa did not include the Equatorial margin domain (e.g., Guiraud et al., 2005). Furthermore, those paleogeographic reconstitutions were biased from a methodological viewpoint. Indeed, they consider the preservation limits of sedimentary deposits of a given age as the limits of the sedimentation area of that age. But it is never the case, because the edges of coastal and intracratonic basins undergo erosion that leads to significant reduction of the basins' original extent (e.g., Sloss and Scherer, 1975; Watts, 2001).

In this contribution, we reassess the Meso-Cenozoic structural, stratigraphic, magmatic and geomorphic evolution of the Equatorial margins of northwestern Africa and their hinterland (south of 28°N, West of 17°E) as well as the conjugate Equatorial margins of Northern South America (Figure 3-1). Our work is based on a series of large-scale offshore – onshore geological cross-sections and nine maps showing successive geological configurations since 200 Ma, taking into account (1) restoration of the position of Northern South America relative to Northwestern Africa, (2) fault patterns and magmatic occurrences, (3) extent of sedimentation / erosion areas and

associated depositional environment of sediments, and (4) constraints provided by low-temperature thermochronology data on the burial / erosion of specific areas. Our work is based on a compilation of original geological source data from the literature, as well as seismic and well data along the continental margins. A specificity of our approach is that we evaluated the potential original minimal extent of sedimentary deposits for coastal and intracratonic basins beyond the present-day erosional limit of those basins. In addition to provide a new evolving integrated structural / sedimentary offshore – onshore scheme at a sub-continental scale, we proposed a new pre-rift fit between South America and Northwestern Africa to account for our observations. Our study opens new perspective for linking margins' evolution to intracontinental long-wavelength deformation and erosion / deposition patterns, with implication for shield-margin source-to-sink systems.

3.2. Geological Outline and Earlier Works

The West African lithosphere mainly consists in an Archean-Proterozoic craton, (i.e., the West African craton), fringed by Panafrican (Late Neoproterozoic) and Variscan mobile belts (Figure 3-1 and Figure 3-2). Panafrican crystalline rocks of the Saharan craton, outcropping as the Nigerian and Hoggar shields and the Tibesti massif, form the basement of the sedimentary basins located East of the West African craton (Figure 3-1). Meso-Cenozoic sediments are preserved in several intracratonic basins around the Hoggar shield. The Taoudeni, South Algerian, Murzuc, Chad and Iullemmeden basins developed either on Neoproterozoic-Paleozoic platform sequences or directly on the basements (Radier, 1959; Greigert, 1966; Busson and Cornée, 1991; Davidson et al., 1998; See also Choubert and Faure-Muret, 1988; Fabre et al., 1996). Jurassic and - mostly - Lower Cretaceous intracratonic sediments have been grouped as the "Continental Intercalaire", which is dated only by sparse vertebrates and fossil woods (Dars, 1960; Lefranc, 1983a; Lefranc and Guiraud, 1990; Mateer et al., 1992, Figure 3-1). A Cretaceous rift system is preserved inland West Africa, most of which is now buried under Upper Cretaceous and Cenozoic series: the Western Central Rift System in the Chad basin, which extends up to East Africa, the Gao and Bida rifts in the Iullemmeden basin, and the Nara and Amded rifts in the Taoudeni basin (Radier, 1959; Dars, 1960; Bellion et al., 1984; Fabre et al., 1996; Genik, 1992, 1993; Zanguina et al., 1998; Figure

3-2). The Upper Cretaceous sequences recorded mostly transgressions far inland that ultimately formed the "Trans-Saharan Seaway", connecting the Equatorial Atlantic Ocean to the Tethys Ocean (Reyment, 1980; Dufaure et al., 1984). Marine sedimentation is recorded repeatedly until the Late Paleocene-Early Eocene, particularly in the Iullemmeden and Chad basins by limestone and phosphate deposits (e.g., Radier, 1959; Kogbe, 1980; Reyment, 1980; Moody and Sutcliffe, 1991). Those series are overlain by fluvial sediments of the late Eocene - Oligocene 'Continental Terminal' (Lang et al., 1986, 1990; Chardon et al., 2016; Figure 3-2). Intense weathering has affected West Africa since the Late Cretaceous and left relicts of lateritic paleo-landscapes, which have been used for reconstructing denudation histories and drainage evolution of West Africa (Beauvais and Chardon, 2013; Chardon et al., 2016). The present-day West African drainage system has stabilized since the Early Oligocene, following the onset of hot spot-related growth of intraplate basin-and-swell topography (Chardon et al., 2016).

The inland rift system is temporally and kinematically linked to the development of the Equatorial Atlantic margin of Africa (Moulin et al., 2010; Heine and Brune, 2014), which may be divided into three segments separated by transforms (the NW trending Guinea-Liberia margin, the E-W trending Ivory Coast and Ghana-Benin margins, Figure 3-1). The current views on the opening of the Equatorial Atlantic Ocean are summarized as follows (Popoff, 1988; MacGregor et al., 2003; Brownfield and Charpentier, 2006). The syn-rift stage begins during the Neocomian by transcurrent and extensional faulting (MacGregor et al., 2003; Brownfield and Charpentier, 2006, Figure 3-1). Grabens and half-grabens of the Ghana-Benin margin are filled by Barremian -Aptian continental conglomerates, sandstones and siltstones (Kjemperud et al., 1992; Chierici, 1996), which are overlain by Albian marine sandstones, black shales and minor limestones (Chierici, 1996). The end of syn-rift deformation is marked by a major regional unconformity underlying Latest Albian-Cenomanian marine series, 'the Breakup unconformity', also observed on the conjugate Brazilian margins (Zalan and Matsuda, 2007; Trosdtorf Junior et al., 2007; Soares Júnior et al., 2011). The kinematic model for the opening of the Equatorial Atlantic Ocean is still debated, because of the 'Cretaceous Magnetic Quiet' period and a lack of strong constraints on syn-rift structures restoration (Moulin et al., 2010; Heine et al., 2013). Regression and transgression cycles and tectonic reactivation affected the African Equatorial Atlantic margin during the post-rift stage. Two major regional unconformities whose origin is debated are identified on the Ivory Coast and Ghana-Benin margins in the Senonian and the Oligocene (Simon and Amakou, 1984; Grillot et al.,

1985; Chierici, 1996). Lateral variations in syn-rift deformation patterns and the correlations within the post-rift stratigraphy along the whole margin are also not well established. Despite some large-scale first-order kinematic syntheses such as those of Fairhead, (1988), Binks and Fairhead (1992) or Guiraud and Maurin (1992), no study has integrated the tectonostratigraphic evolution of the margin and that of its hinterland.

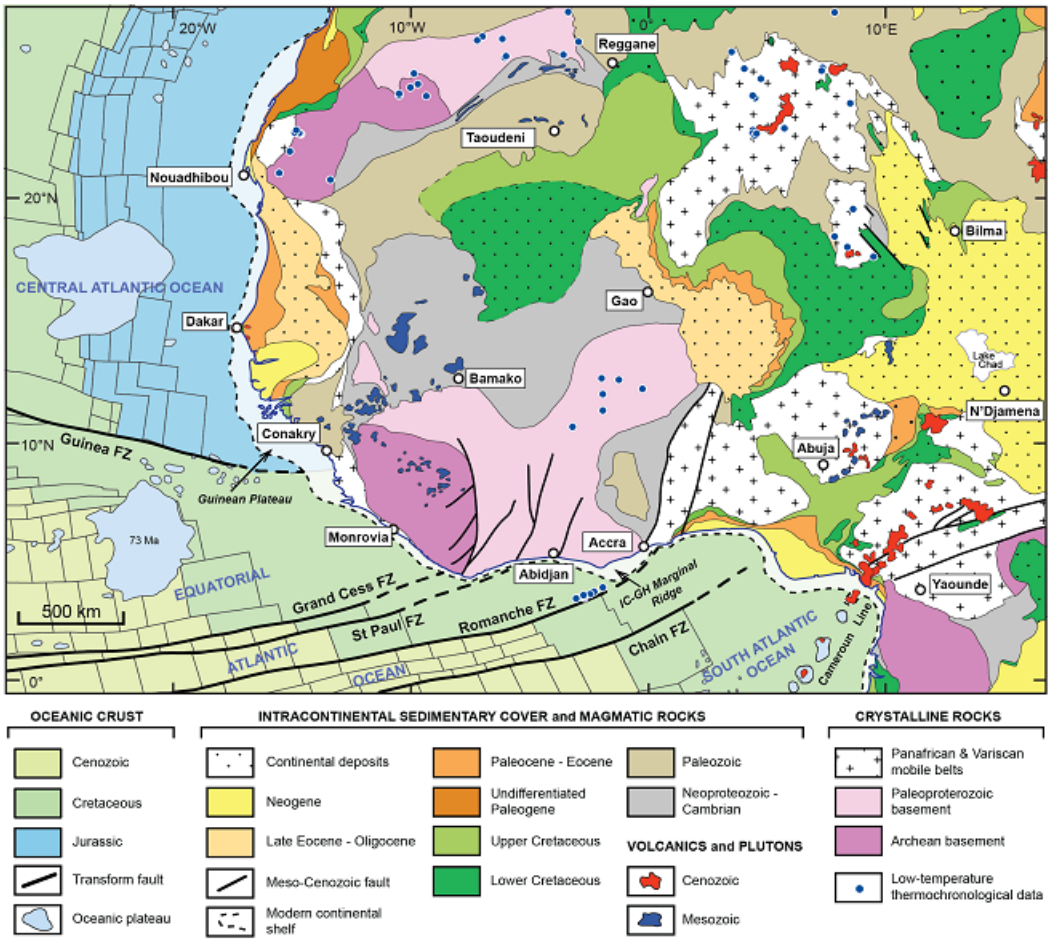

Figure 3-2 Simplified geological map of West Africa compiled from Choubert and Faure-Muret (1988), Fabre et al. (1996), Milesi et al. (2010) and this work. Quaternary sand cover has been omitted, and small Triassic-Jurassic sedimentary outcrops in the Tim Mersoi basin were included in Lower Cretaceous sediment map units. Lower Cretaceous and Paleogene continental sediments are grouped as the "Continental Intercalaire" and "Continental Terminal", respectively. Only outcropping faults that were potentially activated during the Meso-Cenozoic are shown. Sources for low-temperature thermochronological data shown on the map are listed in Table 3-1. The Equatorial Atlantic Ocean is classically the oceanic lithosphere between the Guinea Fracture Zone to the North (boundary with the Central Atlantic Ocean) and the Chain Fracture Zone in the South (boundary with the South Atlantic Ocean). FZ: Fracture Zone.

3.3. Materials and Method

We established four large-scale onshore-offshore cross-sections across the study area in order to visualize the spatial relationships among inland sedimentary basins and continental margins, and particularly the marginal upwarp separating these two domains (Figure 3-3). These cross-sections complement the paleo-maps, which were established for specific periods matching known geodynamic episodes such as the emplacement of magmatic provinces, the continental rifting or global transgression/regression. Paleo-maps represent time increments usually less than 10 Myr. In this study, we refer to the time scale of Walker et al. (2012).

3.3.1. Integration of the Sedimentary Record

The paleo-maps display the depositional environments and potential extent of intracontinental and marginal basins. We first mapped the boundaries of the preserved sediments deposited during each time step. Stratigraphy, lithology and paleoenvironment of these deposits (both at the surface and subsurface) have been compiled from published literature reporting first-hand data, observations and maps (Table 3-1). Additional information was obtained along the African Equatorial Atlantic margins and in the Gao rift on the basis of seismic and well data. For South American basins, we used essentially published sedimentological studies and detailed stratigraphic charts of Petrobras (Figueiredo et al., 2007; Zalan, 2007; Zalan and Matsuda, 2007; Trosdtorf Junior et al., 2007; Pessoa Neto et al., 2007; Conde et al., 2007). Depositional environments of sediments are grouped in four categories: non-marine/continental, transitional, shallow marine and deep marine. Transitional environment are coastal, lagoonal, estuary and/or deltaic sedimentary environments with near sea level elevation. Available paleocurrent measurements are also indicated. The present-day extent of preserved sedimentary deposits is hypothetical when strata are covered by younger deposits and are only revealed by seismic and well data. For non-marine deposits, in particular, the ‘Continental Intercalaire’ that are usually poorly dated, only uncertain (dashed) boundaries have been represented.

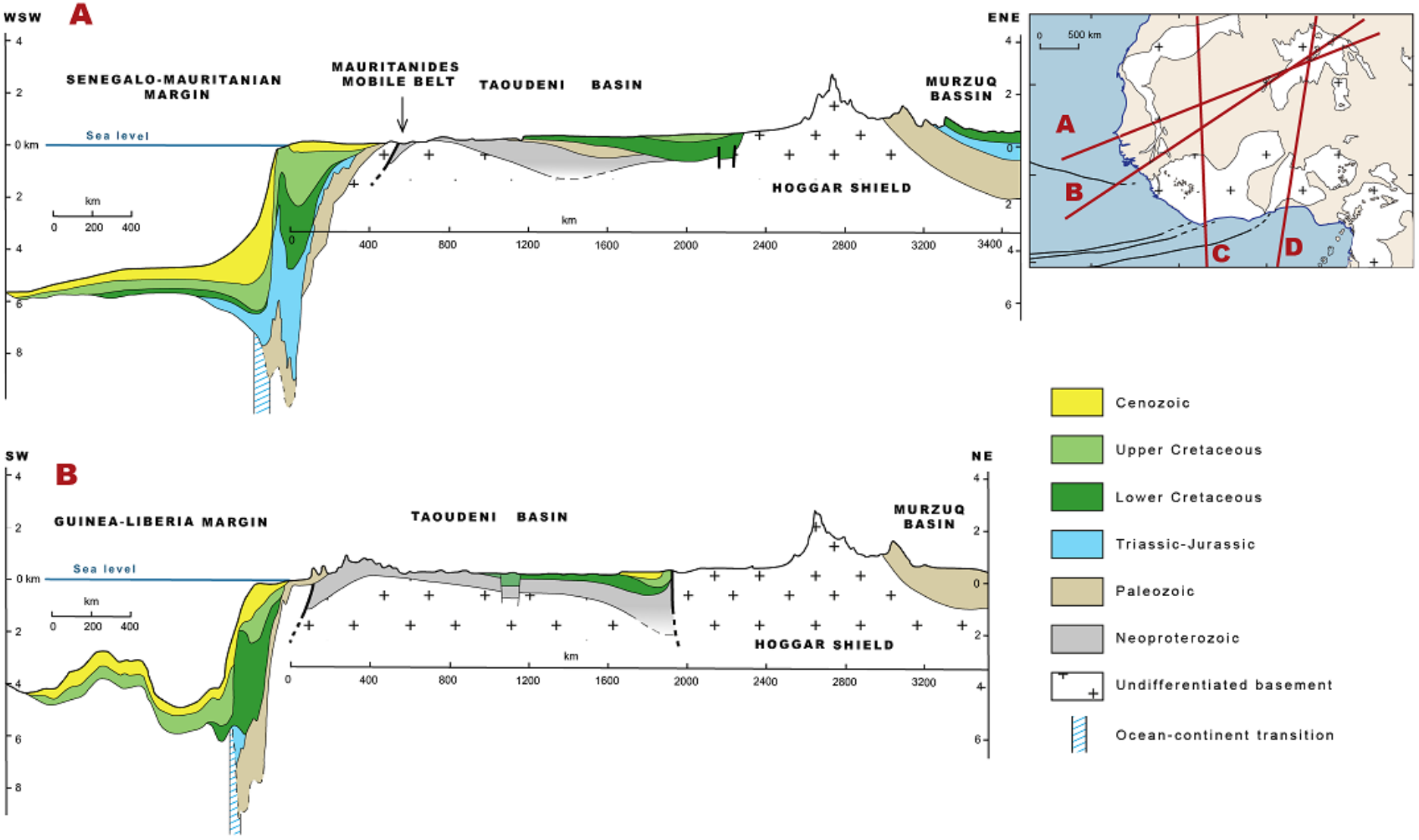
WSW
A
SENEGALO-MAURITANIAN MARGIN
MAURITANIDES MOBILE BELT
TAOUDENI BASIN
MURZUQ BASSIN
ENE
Sea level
0 km
km
0 200 400
HOGGAR SHIELD
0 400 800 1200 1600 2000 2400 2800 3200 3400
0 500 km
A
B
C
D
SW
B
GUINEA-LIBERIA MARGIN
TAOUDENI BASIN
MURZUQ BASIN
NE
Sea level
0 km
km
0 200 400
HOGGAR SHIELD
0 400 800 1200 1600 2000 2400 2800 3200
Cenozoic
Upper Cretaceous
Lower Cretaceous
Triassic-Jurassic
Paleozoic
Neoproterozoic
Undifferentiated basement
Ocean-continent transition

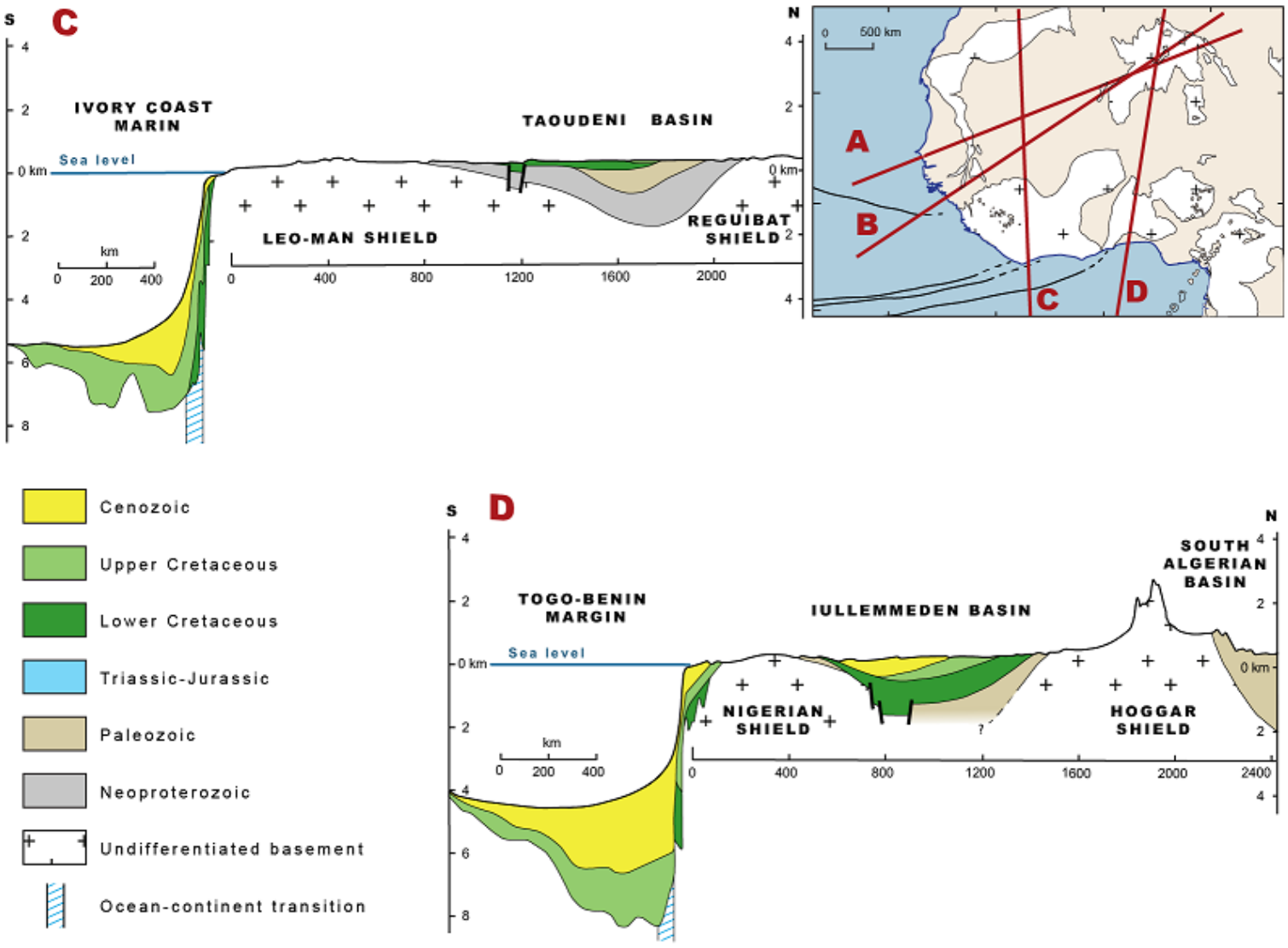

Figure 3-3 Large-scale onshore – offshore geological cross-sections across northwestern Africa based on various sources, among which Helm (2009) for the offshore sections, Choubert and Faure-Muret (1988) and Milesi et al., (2010) for the intracontinental domains. See section locations on the inset map. Syn-rift fault on passive margins are omitted for clarity.

Table 3-1 Original sources compiled for reconstructing the geological configurations shown in Figure 3-5 to Figure 3-13.

REFERENCES USED FOR THE GEOLOGICAL RECONSTRUCTIONS

Thematic geological items	References	Paleogeographic maps								
		235-190 Ma	140-133 Ma	120-115 Ma	107-100 Ma	97-93 Ma	86-84 Ma	72-66 Ma	61-56 Ma	34-23 Ma
		Fig 3-5	Fig 3-6	Fig 3-7	Fig 3-8	Fig 3-9	Fig 3-10	Fig 3-11	Fig 3-12	Fig 3-13
SEDIMENTARY RECORD										
Intracontinental Africa										
Taoudenni Basin	Fabre et al., 1996		x	x	x	x	x			
(including the Nara and Amded rifts)	Fabre, 2005		x	x	x	x	x			
	Bellion et al., 1984		x							
	Cornet, 1943		x	x	x			x	x	x
	Busson, 1971			x	x	x	x	x	x	
	Dars, 1960		x	x	x			x	x	x
	Choubert and Faure-Muret, 1988		x	x	x					
Iullemmeden Basin	Greigert, 1966		x	x	x	x		x	x	x
(including the Gao and Kandi rifts)	Greigert and Pougnet, 1967		x	x	x	x		x	x	x
	Chardon et al., 2016								x	x
	Kogbe, 1981		x	x	x			x	x	x
	Valsardieu, 1971	x	x	x	x					
	Radier, 1959							x	x	x
	Mateer et al., 1992			x	x					
	Zanguina et al., 1998	x	x	x	x	x	x	x	x	
	Moody et Sutcliffe, 1991		x	x	x	x		x		
	Alidou and Lang, 1983		x	x	x					x

	Alidou et al., 1991		x	x	x					x
Chad Basin (including the Western Central African Rift System)	Genik, 1992, 1993	x	x	x	x	x	x	x	x	x
	Choubert and Faure-Muret, 1988		x	x	x	x	x	x	x	x
	Greigert and Pougnet, 1967		x	x	x	x	x	x	x	x
	Zanguina et al., 1998		x	x	x	x	x	x	x	x
	Avbovbo et al., 1986				x	x	x	x	x	x
Murzuq Basin	Davidson et al., 2000	x	x	x	x					
	Klitzsch, 2000	x	x	x	x					
	Dufaure, 1984					x				
Benue Trough	Benkhelil et al., 1988			x	x	x		x	x	
	Benkhelil, 1989			x	x	x		x	x	
	Allix, 1983			x	x	x		x	x	
	Allix and Popoff, 1983			x						
	Allix et al., 1981			x						
	Jermannaud, 2010									x
	Petters, 1980, 1983			x	x	x		x	x	
	Popoff, 1988		x	x	x					
	Sokari, 1992			x	x					
Bida Rift	Akande et al., 2005							x		
	Ojo and Akande, 2009							x		
	Agyingi, 1993							x		
Leo-Man Shield (Weathering record)	Grimaud et al., 2015								x	x
	Chardon et al., 2016								x	x
	Beauvais et al., 2008								x	x
	Beauvais and Chardon, 2013								x	x
Atlantic Margins										
Tarfaya Basin	Leprêtre, 2015		x	x	x	x	x	x	x	x
	Davison, 2005	x	x	x	x	x	x	x	x	x
	Baby et al., 2014		x					x		
Senegalo-Mauritanian Basin	Baby, 2012	x	x	x	x	x	x	x	x	x
	Baby et al., 2014	x	x	x	x	x	x	x	x	x
	Davison, 2005	x	x	x	x	x	x	x	x	x
	Tari et al., 2003	x	x	x	x	x	x	x	x	x

	Brownfield and Charpentier, 2003	x	x	x	x	x	x	x	x	x
Eastern North America	Olsen, 1997	x								
Guinea & Demerara Plateau	Dumestre and Carvalho, 1985	x	x	x	x	x	x	x	x	x
	Stoecklin, 1987		x	x	x	x	x	x	x	x
	De Oliveria Marinho et al., 1985	x	x	x	x	x	x	x	x	x
	Benkhelil et al., 1995		x	x	x					
Equatorial Atlantic margins	*This study*			x	x	x	x	x	x	x
	Gouyet, 1988		x	x	x					
	Benkhelil et al., 1995		x	x	x					
	Da Costa et al., 2009							x	x	x
	Yang and Escalona, 2011		x	x	x					
	Figueiredo et al., 2007	x	x	x	x	x	x			
	Zalan and Matcuda, 2007		x	x	x	x				
	Soares et al., 2007			x	x	x	x			
	Zalan, 2007			x	x	x	x			
	Trosdtorf Junior et al., 2007			x	x	x	x			
	Condé et al., 2007			x	x	x	x			
	Pessoa Neto et al., 2007		x	x	x	x	x			
	Soares Junior et al., 2011	x	x	x	x	x				
South Atlantic margins	Chaboureau, 2012		x	x						
	Chaboureau et al., 2013		x	x						
	Seranne and Anka, 2005				x	x	x	x	x	x
Intracontinental Northern South America	Cunha et al., 2007			x	x	x				
	Costa et al., 2001			x	x	x				
	Vaz et al., 2007a	x		x	x	x				
	Vaz et al., 2007b	x	x	x						
	Assine, 2007		x		x					
	De Matos et al., 1992		x		x					
FAULT PATTERNS and KINEMATICS										
Intracontinental Africa										
Amded rift	Fabre et al., 1996		x	x	x					
	Dars, 1960		x	x	x					

Nara rift	Dars, 1957; Dars, 1960		x	x	x					
	Bellion et al., 1984		x	x	x					
Gao rift	*This study*			x	x					
Western Central African Rift System	Genik, 1992, 1993		x	x		x	x	x		
	Zanguina et al., 1998		x	x		x	x	x		x
	Guiraud and Bosworth, 1997					x				
	Loule and Pospisil, 2013			x	x	x	x			
	Guiraud et Maurin, 1992						x			
	Le Marechal and Vincent, 1972		x	x	x					
	Ngangom, 1983		x	x	x					
Bida rift	Kogbe et al., 1983							x		
	Ojo and Ajakaiye, 1976							x		
Benue Trough	Benkhelil, 1988			x	x		x	x		
	Benkhelil et al., 1989			x	x		x	x		
	Allix, 1984			x	x		x	x		
	Benkhelil et Guiraud, 1980			x	x		x	x		
	Guiraud, 1993		x	x	x			x		
Atlantic Margins										
Central Atlantic margins	Withjack et al., 1998	x								
	Le Roy and Pique, 2001	x								
	Labails, 2007	x								
Guinea & Demerara Plateau	Benkhelil et al., 1995		x	x	x					
	Sapin et al., 2016		x	x	x					
	Marinho et al., 1988		x	x	x					
Equatorial Atlantic margins	*This study*			x	x	x	x	x		
	Basile et al., 2013		x	x	x					
	Benkhelil et al., 1995		x	x	x					
	Sapin et al., 2016		x	x	x					
	Soares Junior et al., 2008		x	x	x					
	Soares Junior et al., 2011	x	x	x	x					
South Atlantic margins	Chaboureau, 2012		x	x						
	Chaboureau et al., 2013		x	x						
	Turner et al., 2003		x	x						

Inland Northern South America	Vaz et al., 2007b	x	x	x						
	Assine, 2007		x		x					
	De Matos et al., 1992		x		x					
LOW-TEMPERATURE THERMOCHRONOLOGICAL CONSTRAINTS										
Northwestern Africa	Leprêtre et al., 2014	x	x	x	x	x	x	x	x	x
	Leprêtre, 2015	x	x	x	x	x	x	x	x	x
	Gunnell, 2003		x	x	x	x	x	x	x	x
	Rougier, 2012					x	x	x	x	x
	Rougier et al., 2013					x	x	x	x	x
	Cavelle,2006					x	x	x	x	x
	English et al., 2016		x	x	x	x	x	x	x	x
	Bigot-Cormier et al., 2005				x	x	x			
	Clift et al., 1997, 1998				x	x	x	x	x	x
	Bouillin et al., 1997, 1998				x	x	x	x	x	x
Northern South America	Harman et al., 1998	x	x	x						
	Morais Neto et al., 2006	x	x	x	x					
	Morais Neto et al., 2008	x	x	x	x					
	Turner et al., 2008			x						

At the edges of intracratonic and coastal basins, the present-day map sedimentary limits of a given age are usually erosional limits. Indeed, erosion generally removes deposits along basin's fringes as a consequence of flexural uplift of basins' edges accompanying subsidence and sediment accumulation (Sloss, 1963; Sloss and Scherer, 1975; Watts, 2001, Figure 3-4A). The preserved deposits therefore only represent the minimum extent of the deposits at the time they emplaced. This has led to major methodological limitation of paleogeographic studies, which usually mistake the extent of preserved sediments for their depositional area. In this study, we have assessed the potential minimum areal extent of sedimentary basins by estimating the map width of the subsequent erosion they have undergone at their margins. Let us consider ΔZ as the denudation due to a drop in base level consecutive to an uplift and/or a sea level change from time T1 to T2. E is the resulting inward (i.e., towards the basins' main depocenter) retreat of basins' edges and S the topographic slope of a basin's margin (Figure 3-4B). Ei and Si and Es and Ss are defined for the inlandward slope of intracratonic basins and the seaward slope of coastal basins, respectively (Figure 3-4B). Assuming a negligible short-wavelength relief, which is reasonable for cratonic surfaces and their marginal upwarps, we have $E = \Delta Z/S$.

For non-marine deposits, ΔZ may be constrained from basement denudation estimates derived from geomorphology and low-temperature thermochronology. For instance, denudation of the Leo-Man Shield (Figure 3-1 and Figure 3-2) is estimated to be in the range of 2 to15 m/Ma for the Cenozoic, based on incision of dated lateritic relict landscapes (Beauvais and Chardon, 2013; Grimaud et al., 2014 2015) and 6 - 13 m/Ma for the Mesozoic based on low-temperature thermochronological analysis (Gunnell, 2003). Assuming an average denudation rate of 9 m/Ma in the past over a 10 Myr period (typical time-slice of successive paleo-maps), the value of E would be 300 to 900 km for intracratonic basins (considering Si = 0.1 to 0.3 ‰) and 45 to 90 km for coastal basins (Ss = 1 to 2 ‰) (Figure 3-4C). For marine deposits, ΔZ is controlled by both substrate uplift and base level changes. Paleobathymetry of preserved marine sediments may be a rough gauge of relative sea-level change over geological time scales. As such, shallow marine sediments ($\Delta Z \leq 200$m) may be used to define the minimum value of E less than 660 km for inland slope of an upwarp and 100 km for its seaward slope.

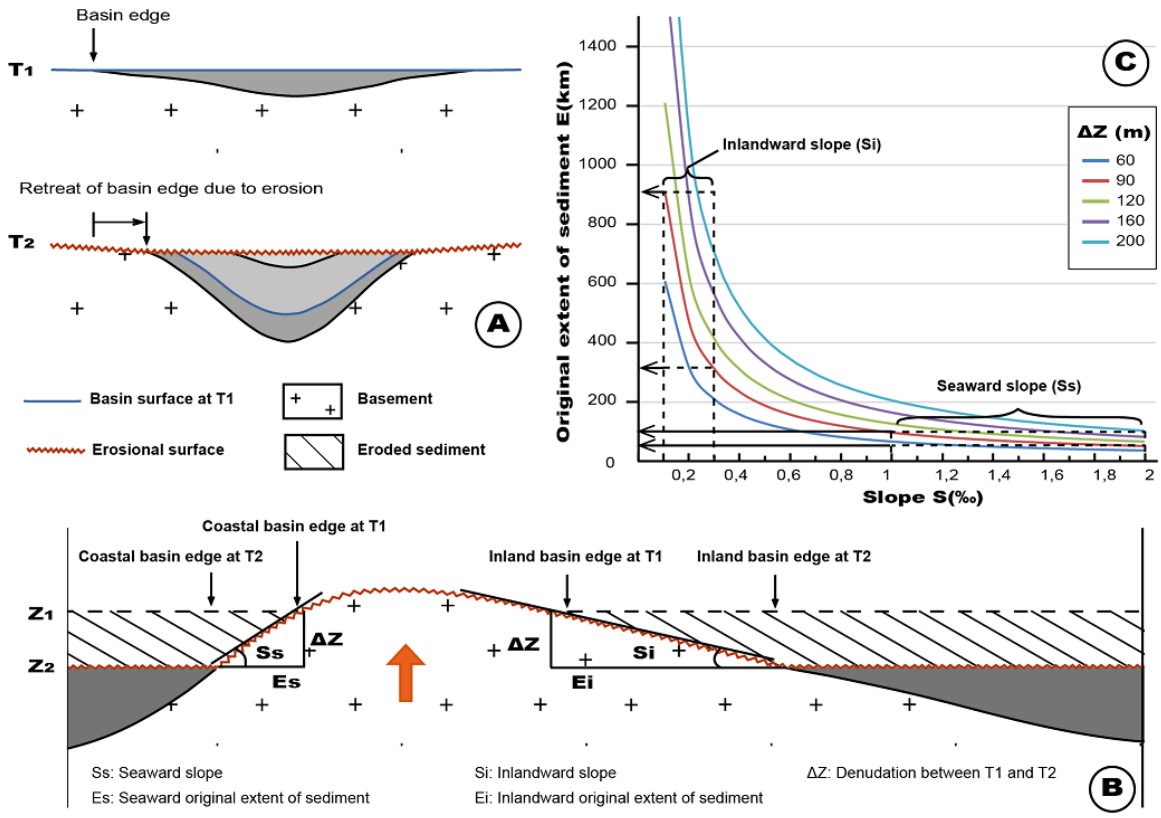

Figure 3-4 Estimation of the original minimum extent of sedimentary deposits at the edges of coastal and intracratonic basins. (A) Schematic illustration of the retreat (E) of an intracratonic basin edges between time T1 to T2 (modified after Sloss and Scherer, 1975). (B) Cross-section of a marginal upwarp showing the influence of topographic slopes (S) on the original horizontal extent of sedimentary deposits and their erosion at basin edges. (C) Curves showing the relationships among the regional slope (S), the original extent of sediments (E) and denudation (ΔZ). See text for further explanations.

To summarize, the potential miminum original horizontal extent of sedimentary basins' edges in the past is of the order of 100 km (typically 300 km) greater than that of preserved deposits in intracratonic contexts. This value would be of the order of tens of kilometers (typically 50 km) for coastal basins. On must point out that this approach does not apply to active rifts sedimentation, which is mostly controlled by active faults bounding the deposits (Magnavita et al., 1994). Paleocurrent data have locally been used to further constrain the potential minimum original extent of sedimentation areas, because they help reconstructing paleo-alluvial plains later fragmented by uneven erosion. If paleocurrents indicate flow towards a present-day exposed basement, the basement had to be flooded by the considered alluvial plain when the plain was active.

Published apatite fission track analysis (AFTA) and apatite (U-Th-Sm)/He dating have also been used to further constrain the extent of past depositional areas, as they constrain thermal histories of samples residing in the first 3-4 km of the crust (e.g., Gallagher et al., 1998; Ehlers and Farley, 2003). Considering the non-orogenic context of West Africa and its margins, and in the cases where the samples were not affected by thermal events such as magmatism, heating periods reflect burial under sediments, whereas cooling periods indicate dominant erosion-driven exhumation and therefore an eroding landsurface above. Published temperature-time paths obtained by data inversion have been used (Appendix 2, Figure 3-2). For the time step corresponding to each paleo-map, heating or cooling sample locations are reported and used to semi-quantitatively enlarge or restrain the potential original extent of sedimentation areas, respectively. Samples undergoing rapid cooling/heating (cooling/heating rate higher than 1°C/Ma) were distinguished from those undergoing slow cooling/heating. Samples with similar thermal histories in the same region were gathered and displayed under a single symbol. All the constraints used above allow mapping the original minimum extent of sedimentation areas (in lighter colors than those of the preserved deposits; Figure 3-5 to Figure *3-13*). Conversely, continental areas mapped as exposed to erosion or sediment by-passing therefore correspond to their maximum potential extent.

3.3.2. Fault Patterns

Intracontinental active faults were mainly established from literature sources (Table 3-1). For the Equatorial Atlantic margins, we also integrated results of our interpretation of unpublished seismic profiles calibrated by boreholes on the African side, and used published fault patterns for the South American side (Table 3-1). Only structures active during the considered time step are displayed (e.g., normal faults bounding rifted basins, strike-slip faults and anticlines/arches). The onset of rifting is not well constrained because only a few wells reached pre-rift strata. Moreover, rifting generally led to the accumulation of non-marine sediments, which are not well dated. Therefore, uncertain faults are indicated as dashed lines on the maps in those cases (Figure 3-5 to Figure *3-13*).

3.3.3. Magmatism

We compiled and mapped the location, emplacement mode, age and dating method of Meso-Cenozoic magmatic occurrences in West Africa and along its margins from literature (Figure 3-5 to Figure *3-13*; Appendix 1). For northern South America, we used the synthesis of Mizusaki et al. (2002). Magmatic occurrences are categorized in lava flow, dyke/sill, ring complex, kimberlite clusters and kimberlite occurrences (Figure 3-5 to Figure *3-13*).

3.3.4. Palinspastic and Kinematic Reconstruction

We adopted the kinematic models of the Atlantic Ocean opening proposed by Moulin et al. (2010) and Heine et al. (2013) for relatively positioning the current coastlines for each time slice. The pre-rift and pre-opening fits between West Africa and northern South America proposed by Heine et al. (2013) are based on a reconstruction of the stretching and subsidence due to rifting from the Berriasian (145 Ma) to the Late Albian (104 Ma) before continental breakup. Moulin et al. (2010) suggest another pre-opening fit at 112 Ma, based mainly on correlations of structures across the Equatorial Atlantic domain (magnetic lineaments, conjugate plateaus, fracture zones), without considering syn-rift fault patterns and deformation. The pre-opening fit of Heine et al., (2013) appears to be more consistent with our syn-rift fault patterns on conjugate margins (see below), which must develop within stretched and thinned continental crusts, assuming no major post-rift reactivation occurred. It also appears to better match what is known from the timing of the lithospheric breakup (Dumestre and Carvalho, 1985; Kjemperud et al., 1992; Chierici, 1996). We therefore used the kinematic model of Heine et al. (2013) from the Valanginian to the Late Albian, and adjusted it based on our mapping of fault patterns. As for the post-rift period, we adopted the model of Moulin et al., (2010) because the magnetic anomalies they used are well constrained from 84 Ma onward (Chron 34).

We produced nine paleo-maps for Late Triassic-Early Jurassic (235-190 Ma, Figure 3-5), Vanlanginian (140-133 Ma, Figure 3-6), Middle Aptian (120-115 Ma, Figure 3-7), Late Albian (107-100 Ma, Figure 3-8), Late Cenomanian (97-93 Ma, Figure 3-9), Santonian (86-84 Ma, Figure 3-10), Maastrichtian (72-66 Ma, Figure 3-11), Late Paleocene (61-56 Ma, Figure 3-12) and

Oligocene (34-23 Ma, Figure 3-13). For specific localities, structures or sedimentary basins' locations, the reader may refer to Figure 3-1 and Figure 3-2.

3.4. Results and Interpretation

3.4.1. Cross-sections Linking the Marginal and Intracontinental Domain

The cross-sections display the present-day configurations of onshore and offshore basins, basement highs and their typical wavelengths (Figure 3-3). The geometry is spatially consistent across the Central and Equatorial margins, with continental margin basins separated from intracratonic basins by a marginal upwarp (or bulge). The inland basal unconformities of intracratonic basins coincide with the slope of basement highs such as the Hoggar and Reguibat shields. The marginal upwarps are long-wavelength positive topographic features that are believed to form at the time of rifting and are sustained and/or reactivated afterwards (Gilchrist and Summerfield, 1990; Gallagher et al., 1995). Considering only the Meso-Cenozoic sediments (that recorded continental surface evolution of northwestern Africa since the rifting of the Central Atlantic), the edges of intracratonic basins are erosional limits, resulting from the truncation of the strata on the inland slopes of the marginal upwarps. Similar truncations are expected, though on a shorter wavelength, at the coastal fringes of marginal basins (see also Figure 3-3B) and along the edges of intracratonic basins on the slopes of intracratonic highs.

Our cross-sections show that the preservation patterns of sediments in intracratonic basins at a sub-continental scale is controlled by an interference in time and space, between intracontinental basement highs and marginal upwarps that have contrasted wavelengths, notwithstanding intracratonic basins subsidence histories. Furthermore, Meso-Cenozoic basins display uneven spatial relationships with preserved Neoproterozoic and Paleozoic depocenters. This suggests a complex migration of depocenters through time potentially driven by the interference of vertical movement of basement highs and marginal upwarps at contrasted wavelengths. The width of the present-day erosional marginal upwarp is consistent along the

Central Atlantic margin (ca. 800 km; Figure 3-3A and B). It varies greatly along the Equatorial margins, from ca. 800 km in Ivory Coast-Ghana to less than 400 km in Benin-Togo (Figure 3-3C and D).

Meso-Cenozoic series are thinner in the intracratonic basins (less than 2 km thick) than in the marginal basins (up to 5 km thick). Triassic and Jurassic sediments are mainly preserved along the Central Atlantic margin (Figure 3-3A and B) due to Latest Triassic rifting. Lower Cretaceous post-rift deposits are much thicker along the Central Atlantic margin than the Equatorial margins (Figure 3-3C and D). Cenozoic sediments are thinner but emplaced over larger widths on the Central Atlantic margin, suggesting comparable volumes on both types of margins (Figure 3-4A and B). Cenozoic sediments are well preserved along the Equatorial Atlantic margins (up to 3 km thick), especially along the Ghana-Benin margin that has been partly fed by the Niger Delta located to the East (e.g., Figure 3-1B).

3.4.2. Paleo-maps

3.4.2.1. Late Triassic-Earlier Jurassic (235-190 Ma): The CAMP and the Opening of the Central Atlantic Ocean (Figure 3-5)

During the Late Triassic – Earliest Jurassic, multiple rifts form from North to South along the future Central Atlantic margins and inland North America (e.g., Labail et al., 2010). Non-marine sediments and massive salt deposits accumulate and are preserved today in these rift basins (Olsen, 1997; Brownfield and Charpentier, 2003; Davison, 2005). The extent of these deposits may have been much wider originally given the pervasive unconformity truncating the upper syn-rift sediments (Olsen, 1997; Withjack et al., 1998). The Guinea-Liberia margin seems to experience crustal stretching at this time, given the accumulations of aeolian sediments interbedded with basaltic lava flows reported in South America (Figueiredo et al., 2007; Soares Júnior et al., 2011). This, together with our observations on unpublished seismic lines, suggests the occurrence of an aborted Central Atlantic rift along the future Guinea-Liberia margins of the Equatorial Atlantic. In the continent, non-marine sediments (mainly siltstones) are deposited in the north-easternmost part of the study area (future Iullemmeden, Murzuk and Chad basins) with currents to the N or NW

(Valsardieu, 1971; Genik, 1993). The rest of the continental domain is potentially subjected to erosion. The Central Atlantic Magmatic Province (CAMP, dated at 235-185 Ma with a peak activity at 200 Ma, Jourdan et al., 2009, Appendix 1), affects most of the exposed domain in the form of extensive lava flows, sills and dykes. Large sills may still be buried within the Taoudeni basin, as well as onshore South American basins. Given the very limited number of lava flow occurrences compared to sills and dikes, significant (several kilometers) post-CAMP surface erosion must have taken place. Outside the CAMP, ring complexes emplaced in the Nigeria Shield (Younger Granites, dated at 213-141 Ma), and near the Hoggar Shield (dated at 215-166 Ma). Most of the continental domains outside the Central Atlantic rift system may have been subject to massive erosion, forming a "CAMP superswell" fringed by a drainage network feeding a proto-Saharan basin.

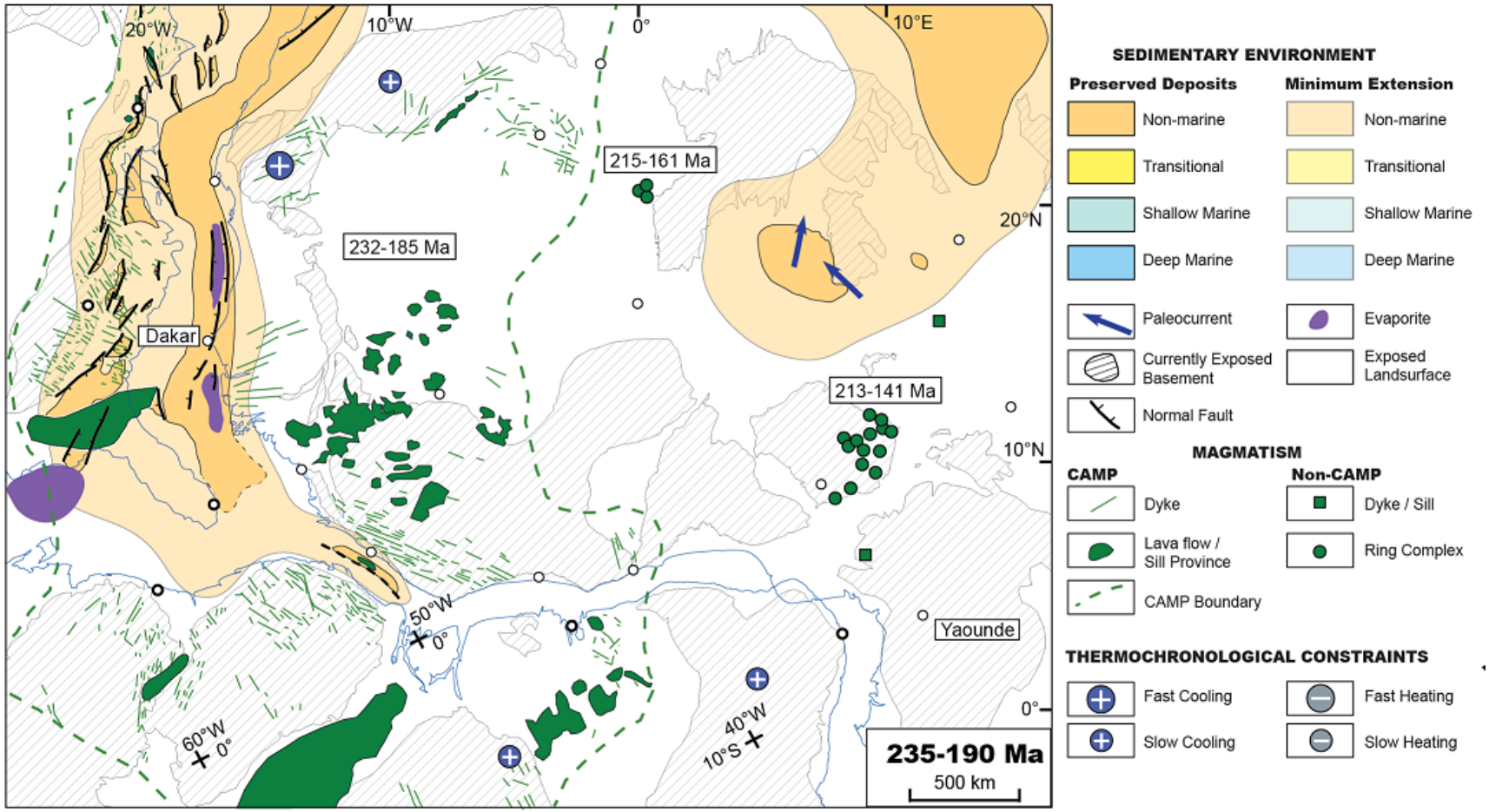

Figure 3-5 Geological configuration of Northwestern Africa and adjoining North and South America during Late Triassic-Early Jurassic (235-190 Ma). Magmatic features of the Central Atlantic Magmatic Province (CAMP) come from Jourdan et al. (2009). The range in age of the magmatic clusters is indicated. The present-day shorelines of North America and Northern South America (thin blue lines) are restored to their position relative to fixed Africa at the end of the considered time interval. Magmatic occurrences emplaced during the considered time interval for the map, unless if specified otherwise on the map or in the explanation. Open circles are the localities from Figure 3-1B and Figure 3-2.

3.4.2.2. Valanginian (140-133 Ma): Pre-rift Configuration (Figure 3-6)

As North America has been drifting away from West Africa since the Early Jurassic, the Central Atlantic margin of Africa had long reached its post-rift stage and builds a continental shelf (Dillon et al., 1988; Davison, 2005; Baby et al., 2014). Rifting takes place along the future Guinea Plateau (Figure 3-2) and its South American counterpart (the Demerara plateau), where Valanginian syn-rift sediments have been reported (Gouyet, 1988). That rifting probably propagated along the future Guinea-Liberia margin into the interior of South America (Cassipore and Marajo graben; Figueiredo et al., 2007; Zalan and Matsuda, 2007). The NE-SW trending Tacutu rift (onshore Suriname, further to the West) continues to be filled after its initiation in the Late Jurassic (Vaz et al., 2007b). The future South Atlantic domain consists in a wide rift system receiving non-marine sediments (De Matos, 1992; Chaboureau et al., 2013). It is mostly located in intracontinental South America and interacts with ENE-trending transfer faults (future transforms) reactivating Panafrican shear zones (e.g., Popoff, 1988).

In intracontinental Africa, a large alluvial basin (named hereafter the ‘Saharan basin’) has installed. It is separated from the margins of the Central and future Equatorial Atlantic margins by a wide erosional domain suggestive of a marginal upwarp. Thermochronological data (Gunnell, 2003; Leprêtre, 2015) as well as widespread kimberlitic magmatism are consistent with uplifts in this domain. Given paleocurrent data, erosion of the upwarp must have fed the Saharan basin, which is connected to the Tethys Ocean located further to the North (e.g., Guiraud et al., 2005; Frizon de Lamotte et al., 2015). Within the Saharan basin, the low resolution of biostratigraphic data does not allow deciding whether the Nara and Amded rifts or the Western and Central Rift System are active (Figure 3-1). Magmatic activity is widespread over Northern South America since the Latest Jurassic, inside and mostly outside the rifts. River systems crossing the future Equatorial Atlantic domain may still exist at the time.

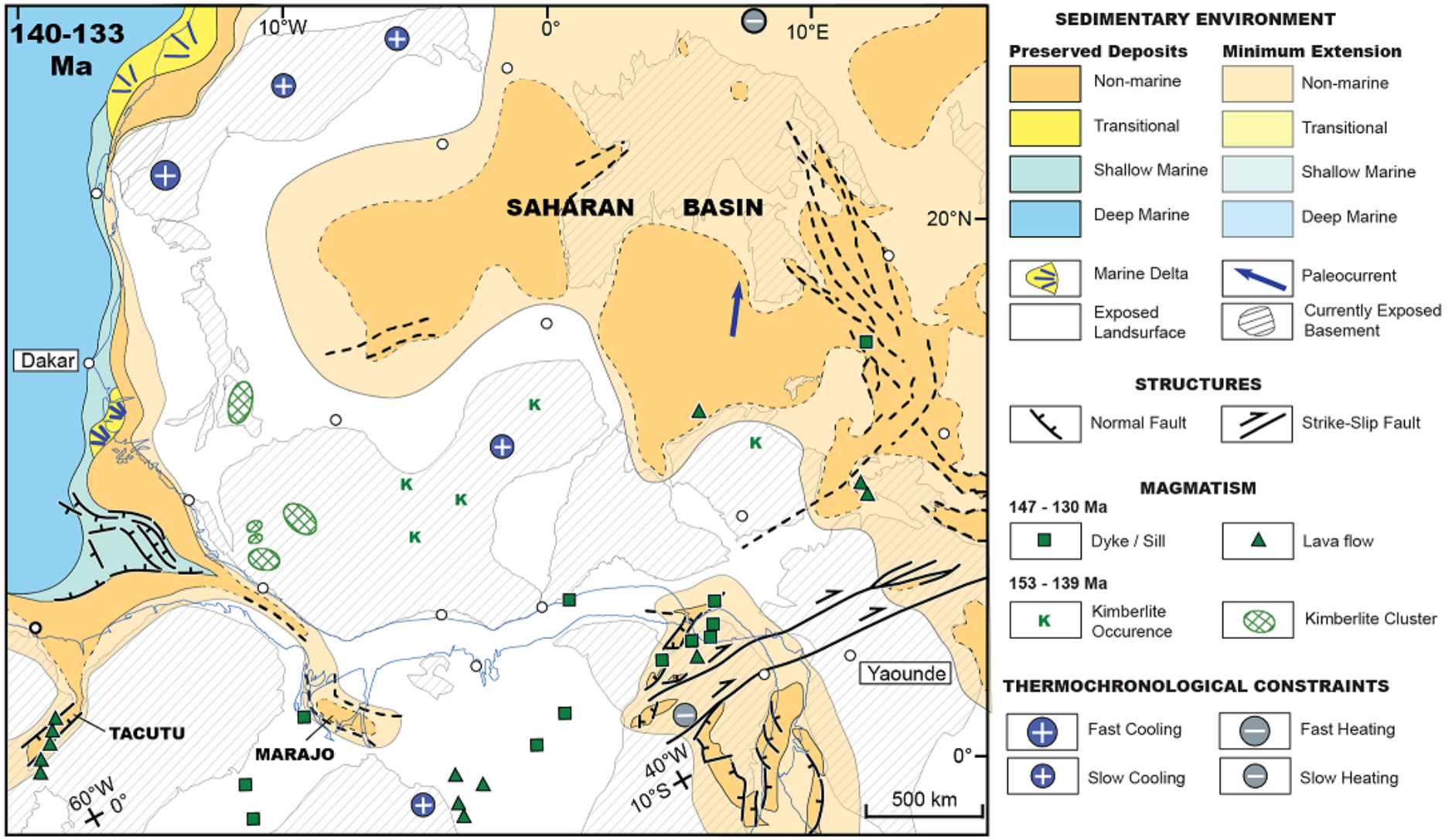

Figure 3-6 Geological configuration of Northwestern Africa, adjoining South America and the Eastern Central Atlantic Ocean during the Valanginian (140-133 Ma). Same conventions as in Figure 3-5.

3.4.2.3. Middle Aptian (120-115): Main Rift Phase (Figure 3-7)

By the Middle Aptian, rifting affects the entire Equatorial domain with ENE- trending dextral strike-slip faults (future transforms) and NW- to W- trending normal faults, forming an en-échelon rift system. Mafic lava flows emplace in this rift system, as well as over intracontinental South America, attesting to a link between rifting and magmatism. If seawater may have invaded the Guinea-Liberia margin from the NW, the Ivory-Ghana and Ghana-Benin marginal basins remain under fluvial-lacustrine sedimentation environment. In the Saharan basin, the Western and Central Rift System and the Gao rift are active and receive Barremian (?) to Albian continental clastic sediments (Figure 3-1). Interestingly, the Saharan basin appears to be connected to the Equatorial Atlantic rift system basin. A non-marine alluvial plain forms in the Benue Trough fed from the NE by probable tapping of sediments from the Saharan basin, feeding the Equatorial rift basins system (Figure 3-1B). A 300 to 1500 km wide erosional upwarp separates the Saharan basin from the Central Atlantic margin and the Equatorial rift system, probably feeding those basins with clastic sediments. Aptian sediments filling up the Equatorial rift system may also come from the denudation of the exposed South American surface.

Large-scale transpressional inversion structures (folds and oblique-reverse faults) affect the southern margin of the Guinea plateau (Benkhelil et al., 1995) and that of its South American counterpart in Guiana (the Demerara plateau; e.g., Sapin et al., 2016, Figure 3-1B and Figure 3-2). This inversion takes place in the vicinity of the future Guinea fracture zone that separated the two plateaus, at the junction between the Central and future Equatorial Atlantic Oceans. Shortening also affects intracontinental South America, forming several major arches along sedimentary basins' margins. These features indicate that transform/oblique rifting of the Equatorial Atlantic domain responded to plate reorganization (e.g., Benkhelil et al., 1995). The southern jump of the rotation pole of the African plate led to the abandonment of part of the South American rifts, stopping South- to Southeastward propagation of the Central Atlantic Ocean into South America and enhancing transform rifting along a new small circle. Aptian plate reorganization that caused the opening of the Central Atlantic Ocean and induced major inversion along the Guinea fracture zone is also attested by the telescoping pattern of transforms of the Southern Central Atlantic Ocean towards that transform (Bouysse and coll., 2014).

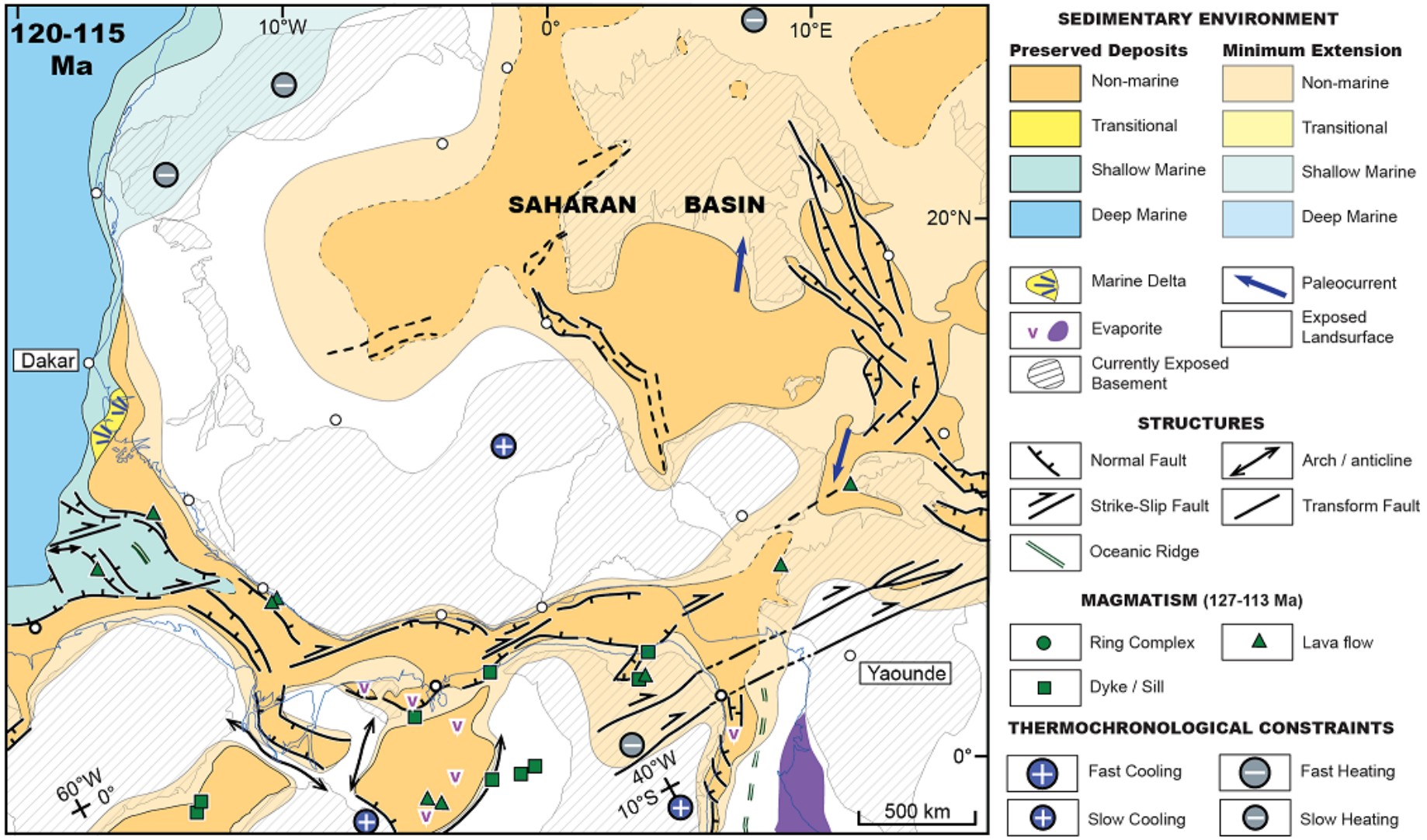

Figure 3-7 Geological configuration of Northwestern Africa, adjoining South America and the Eastern Central Atlantic Ocean during the Middle Aptian (120-115 Ma). Same conventions as in Figure 3-5.

3.4.2.4. Late Albian (107-100 Ma): Lithospheric Breakup and Onset of Seafloor Spreading (Figure 3-8)

In the Late Albian, new WNW-trending rifts form along the South American margin between the Romanche and the Saint Paul fracture zones (Soares Júnior et al., 2008, 2011). The main normal faults of the Equatorial rift system remain active at least at the beginning of that period. Inversion continues to affect the African margin at the junction between the Central and Equatorial domains. Magmatism is reported locally along the Equatorial Atlantic margins. Intracontinental African rifts ceased their activity (except the Gao rift) and a corridor of shallow marine anoxic seawater invades the narrow Equatorial Atlantic Oceans, connecting the Central and South Atlantic Ocean (at c.104 Ma, MacGregor et al., 2003; Brownfield and Charpentier, 2006). Strike-slip and normal faulting along the Equatorial margins ends during the Late Albian, as shown by the ubiquitous “break-up” unconformity. The Ivory Coast-Ghana marginal ridge (offshore Accra, Figure 3-2) is considered as the last connection between the two continents before the ultimate breakup, which leads to seafloor spreading all along the Equatorial domain. The Saharan alluvial basin is still functional and drained northward and westward. Sinistral transtensional faulting is documented in the Benue Trough (Benkhelil, 1988; Benkhelil et al., 1998). A delta forms in the middle of the Trough, forming a transition between the Sahara basin and the Equatorial Atlantic Ocean. That delta appears to be fed from the southernmost Saharan basin and by longitudinal drains of the South Atlantic marginal upwarp of Africa. A coastal plain develops in a very large embayment on South America, attesting to the very low regional continental slopes. The surface of exposed land has not evolved significantly since the Aptian in West Africa. The northwestern African marginal upwarp feeds both the Saharan basin and the margins. From this time on, no river systems will connect Africa to South America.

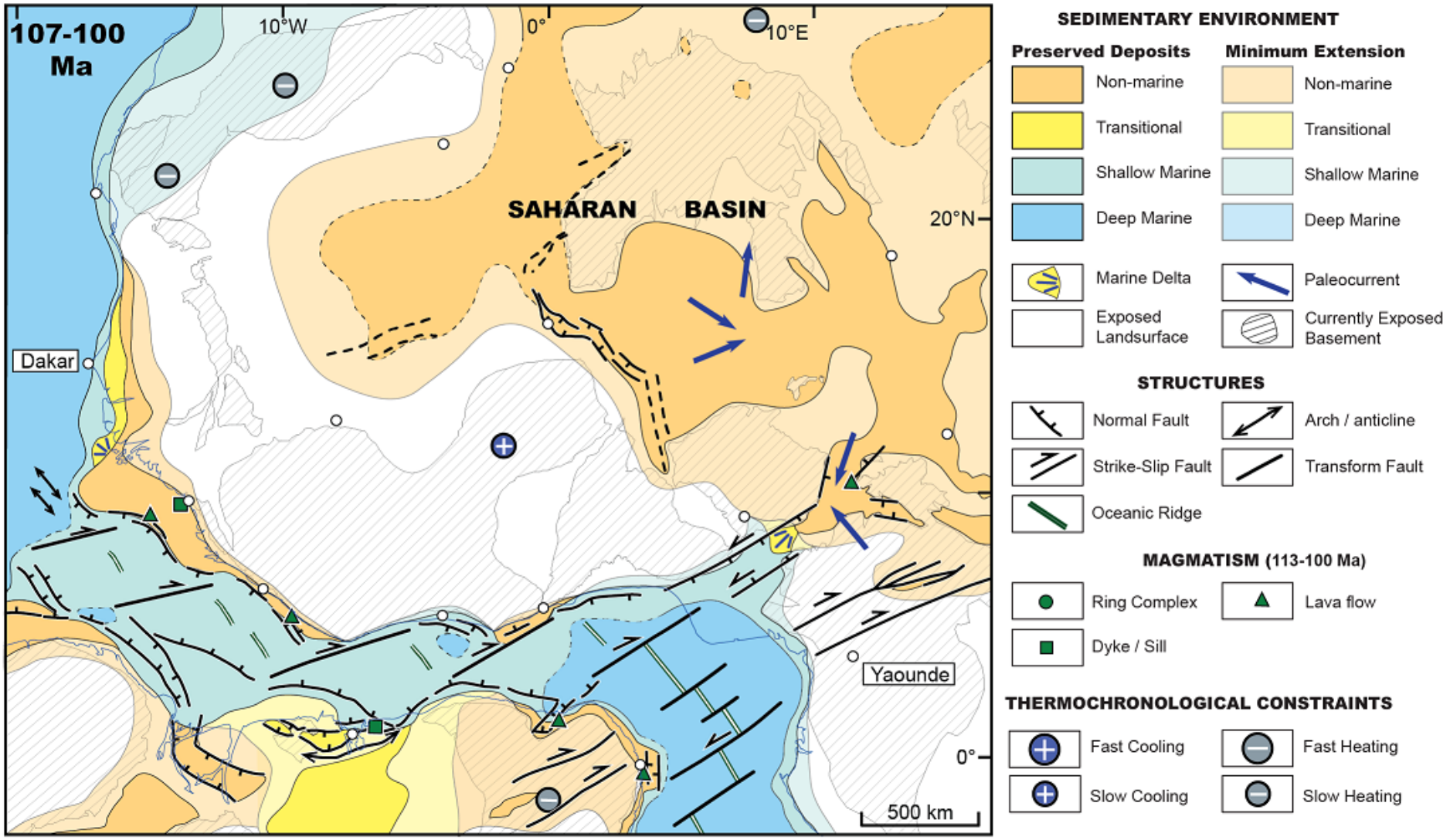

Figure 3-8 Geological configuration of Northwestern Africa, adjoining South America and the Eastern Central Atlantic Ocean during the Late Albian (107-100 Ma). Same conventions as in Figure 3-5.

3.4.2.5. Late Cenomanian (97-93Ma): Maximum Continental Flooding (Figure 3-9)

The global maximum transgression during the Late Cenomanian-Early Turonian allows the flooding of the Hoggar Shield. This 'Trans-Saharan Seaway' connects the Tethys Ocean, in the north, to the Equatorial Atlantic Ocean, in the south (Reyment, 1980; Luger, 2003), and shallow marine brackish shales and limestones are deposited above the 'Continental Intercalaire' (Dufaure et al., 1984; Zanguina et al., 1998). Thermochronological data suggest burial of the Hoggar and Reguibat shields ((Rougier et al., 2013; Leprêtre et al., 2014; English et al., 2016), consistent with subsidence under the 'Trans-Saharan seaway" and the northwestern Sahara basin, respectively. A wide lagoonal and coastal domain forms between these two domains, undergoing alternating transgressions and regressions (Fabre et al., 1996). The Upper Benue trough still receives deltaic and coastal sediments mostly provided by the South Atlantic marginal upwarp. Upper Cenomanian-Turonian marine transgression is recorded along the Central and Equatorial Atlantic margin without significant inland shoreline migration (Brownfield and Charpentier, 2003; Baby et al., 2014). This suggests a relatively steep seaward topographic slope of the continent. That transgression is documented further inland in South America in at least two embayments, suggesting a lower seaward topographic slopes on that side of the Equatorial Atlantic. Transform faults are still active during the Late Cenomanian, as the mid-ocean ridges slide against the Ivory Coast-Ghana marginal ridge (i.e., the 'active transfrom margin' stage of Basile et al., 2005). During this stage, anticlines form at the African tip of the Romanche and Saint Paul transform faults as a result of transpressional reactivation. The Equatorial Atlantic Ocean deepens and develops restricted bottom water circulation as attested by paleontological evidence (black shales and Oligosteginid limestone) (Chierici, 1996; Dumestre and Carvalho, 1985; Brownfield and Charpentier, 2006).

In Africa, the area exposed to erosion does not change significantly. The marginal upwarp north of 20°N is flooded but a wider surface corresponding to the Man-Leo shield and the southern Taoudeni basin is now undergoing erosion. The South Atlantic marginal upwarp feeds the Trans-Saharan Seaway and a river system in the Chad basin connecting potential source areas in East Africa to the Trans-Saharan Seaway may not be precluded.

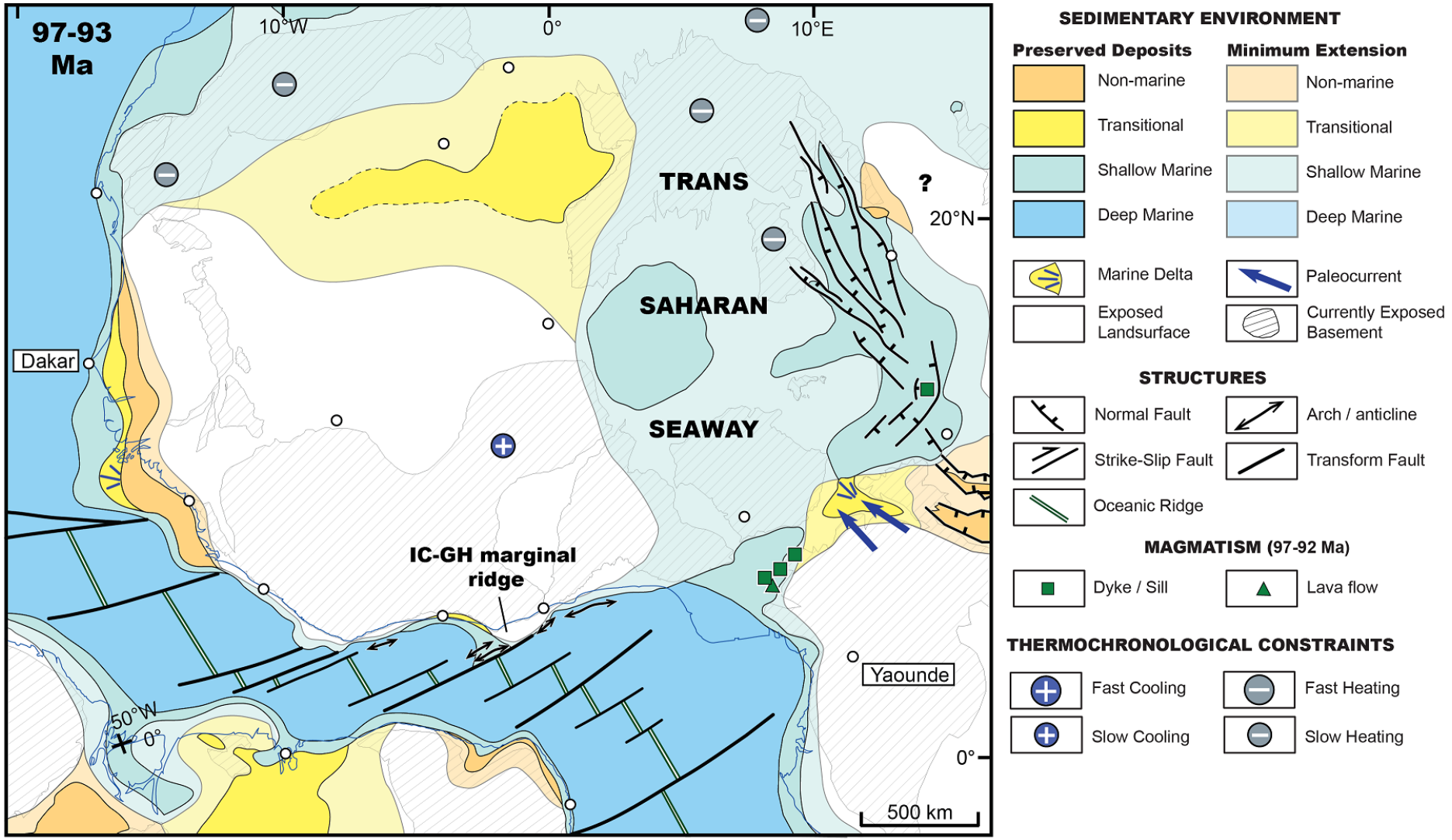

Figure 3-9 Geological configuration of Northwestern Africa, Northern South America and the Equatorial and Eastern Central Atlantic Ocean during the Late Cenomanian (97-93 Ma). Same conventions as in Figure 3-5

3.4.2.6. Santonian (86-84 Ma): Regional Tectonic Inversion (Figure 3-10)

During the Santonian, sinistral transpression leads to the inversion of the Benue Trough, producing regional folds, cleavages and schistosities and forming a mountain range that recorded ca.12 km of shortening (Benkhelil and Guiraud, 1980; Benkhelil, 1987, 1988; Benkhelil et al., 1988). The shortening direction varies from N to NW. Transpressional structures are also documented in the Western and Central Rift System (Guiraud and Bosworth, 1997), with shallow marine sediments deposited during inversion. A narrow seaway of the Tethys floods the Western and Central Rift System. This seaway is probably bounded by lagoonal environments to the West (Fabre et al., 1996). The Hoggar Shield remains buried, as suggested by thermochronological data.

Stratigraphic architectures of the Equatorial Atlantic margins' basins record more than 200 meters of relative sea level fall, suggesting uplift in those basins. The Santonian sedimentary hiatus along the Sierra Leone-Liberia margin also indicates uplift and erosion at that time. Furthermore, vitrinite reflectance data from certain boreholes along the Equatorial Atlantic margin suggest at least 400-500 m of erosion during the Late Cretaceous, which may result from this Santonian event. Transform-controlled anticlines continue to grow along the Ghana-Benin margin. Reactivation of the Romanche transform fault leads to more than 1 km of erosion on the IC-GH marginal ridge (Figure 3-1 and Figure *3-9*) during the Late Cretaceous according to vitrinite reflectance data. In Northwestern Africa, the area exposed to erosion has grown significantly, suggesting very-long wavelength uplift that could tentatively be linked to the inversion event. The eroding domain seems to form a very wide continuous marginal upwarp between the Benue Trough and the Reguibat shield.

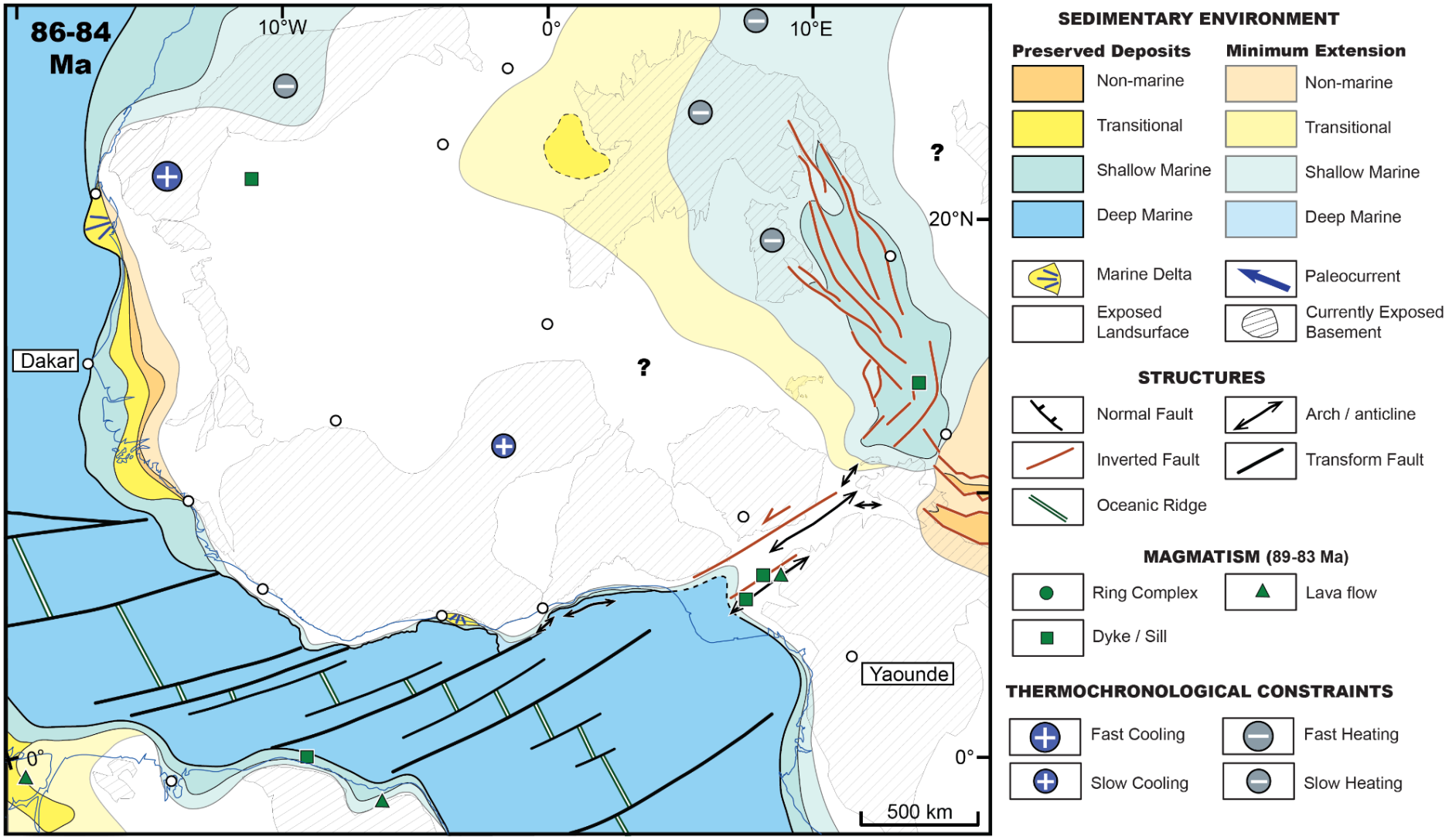

Figure 3-10 Geological configuration of Northwestern Africa, Northern South America and the Equatorial and Eastern Central Atlantic Ocean during the Santonian (86-84 Ma). Same conventions as in Figure 3-5.

3.4.2.7. Maastrichtian (72-66 Ma): Brief Continental Flooding and Re-establishment of the Trans-Saharan Seaway (Figure 3-11)

During the Maastrichtian, marine transgression also occurs briefly in West Africa but on a smaller scale than the Cenomanian transgression. Marine sediments interbedded within brackish water deposits are preserved East of the subsiding Hoggar Shield. The Trans-Saharan seaway is probably re-established, as suggested by the faunal similarities and exchanges between the Equatorial Atlantic Ocean and the Trans-Saharan Seaway (Reyment, 1980; Luger, 2003). It is likely that the connection is made through the Bida rift, which begins to form in the Campanian and continues to develop during the Maastrichtian under shallow marine environment (Kogbe et al., 1983; Akande et al., 2005; Ojo and Akande, 2009). Transgression is also recorded on the Ivory Coast-Ghana and Ghana-Benin margins by the flooding of the coastal basins.

The Western and Central Rift System is reactivated in extension and accommodates the deposition of alluvial sandstones (Zanguina et al., 1998). A rapid filling of the rifts may explain the change in depositional environment from marine to continental, even though more accommodation space is created. Folding is probably still active in the Upper Benue Trough, resulting in a Maastrichtian unconformity (Benkhelil, 1982). Reactivation of folding at the African tip of the Romanche transform fault is also active. Regional deformation seems to result from a W to WNW extension (and potentially shortening normal to that direction). Magmatism only affects the Lower Benue Trough and the adjoining Cameroun Line (Figure 3-1B). Transgression leads to a slight reduction of the erosional area, as a consequence of the flooding of the Nigerian shield and the Saharan portion of the marginal upwarp. The installation of large deltaic systems along the Central Atlantic coast could suggest a drainage reorganization and/or positive vertical movements along that margin. The Western and Central Rift System could still be fed by distant source areas to the East of the Chad Basin.

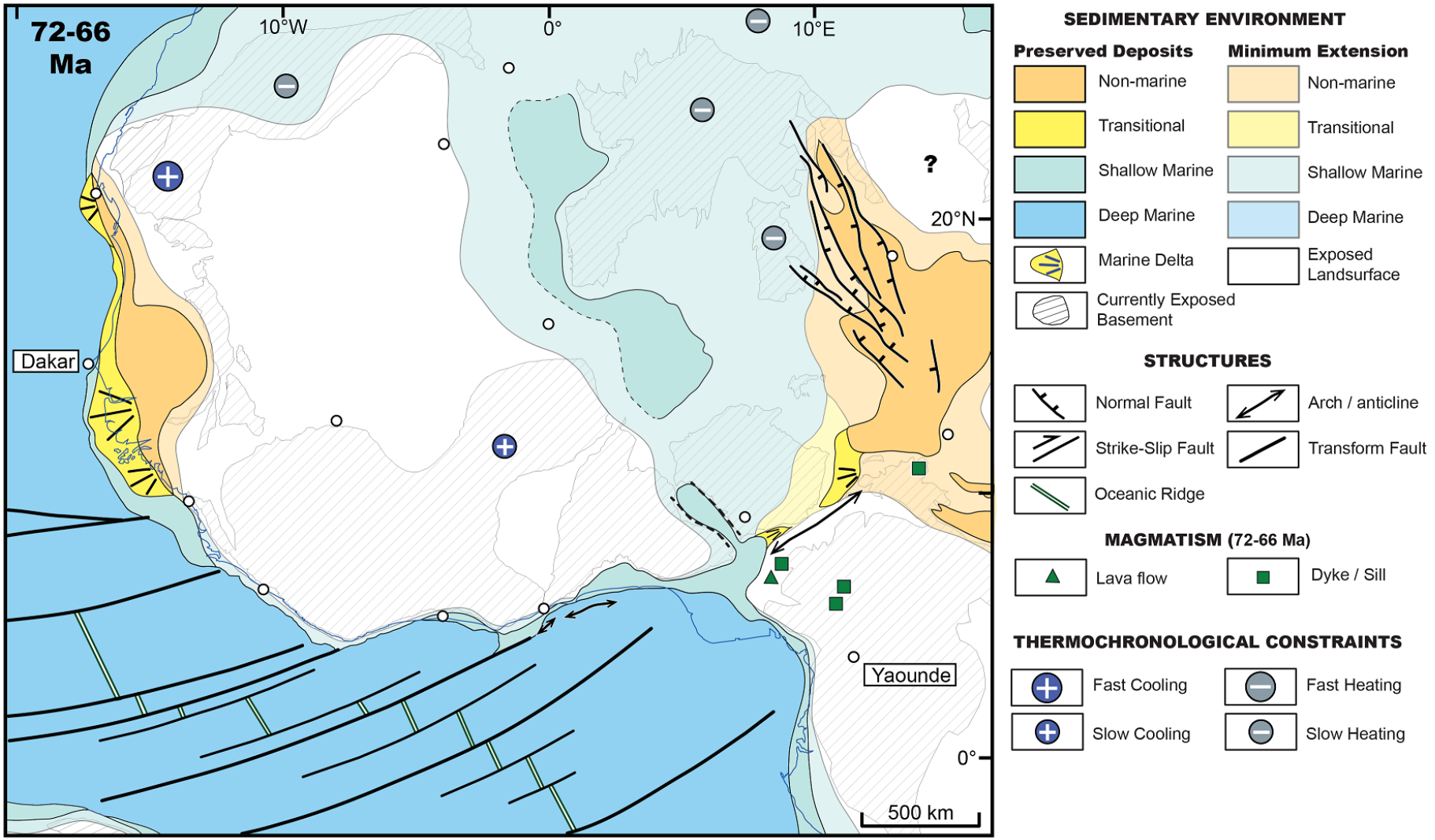

Figure 3-11 Geological configuration of Northwestern Africa and the Equatorial and Eastern Central Atlantic Ocean during the Maastrichtian (72-66 Ma). Same conventions as in Figure 3-5.

3.4.2.8. Late Paleocene (61-56 Ma): Last Flooding and Intense Continental Weathering (Figure 3-12)

Following the latest Maastrichtian regression, a last transgression affects Northwestern Africa during the Paleocene, and inland shoreline migration is documented along the Central and Equatorial Atlantic margins. Marine limestones and shales are preserved in the coastal basins (Davison, 2005; Brownfield and Charpentier, 2006), as well as in the Iullemmeden basin, recording southward transgression from the Tethys at the location of the former Trans-Saharan Seaway without reaching the Equatorial Atlantic Ocean. Extension in the Western and Central Rift System has stopped and the Chad basin undergoes long-wavelength thermal subsidence and fluvial sediments filling. No active tectonic fault is documented in the study area. Intense weathering is favored by the peak greenhouse climate, allowing bauxites to develop all over the emerged lands (Beauvais and Chardon, 2013; Chardon et al., 2016). The preservation of bauxites over the Nigerian Shield and the Bida rift (Valeton, 1991) precludes the connection between the Equatorial Atlantic Ocean and the Tethys (Chardon et al., 2016). As continental chemical weathering is favored, correlative carbonates and phosphates are found in all West African basins and clastic fluxes through the river systems are subdued (e.g., Lang et al., 1990; Valeton, 1991; Johnson et al., 2000). The size of the erosional domain did not evolve significantly and a continuous marginal upwarp re-installs.

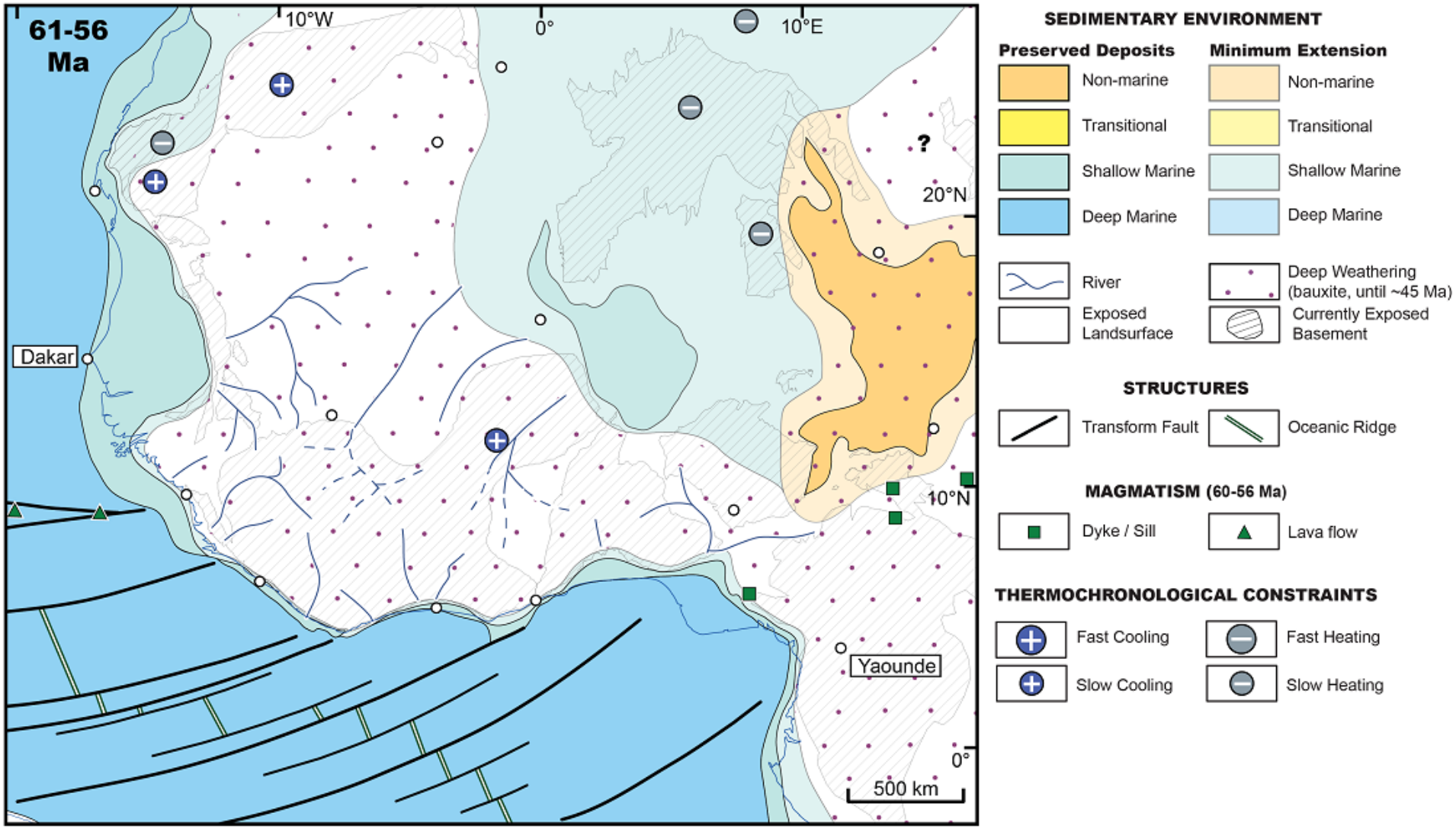

Figure 3-12 Geological configuration of Northwestern Africa and the Equatorial and Eastern Central Atlantic Ocean during the Late Paleocene (61-56 Ma). Same conventions as in Figure 3-5.

3.4.2.9. Oligocene (34- 23 Ma): Development of Basin-and-Swell Topography (Figure 3-13)

Volcanism develops on the African plate from the Late Eocene onward at various locations outside the frame of the West African craton (Burke, 1996). On the Hoggar shield and along the Cameroon line, this volcanism is interpreted as "hot-spot" related (e.g., Ait-Hamou and Dautria, 1994; Liégois et al., 2005; Ait-Hamou, 2006; Ngako et al., 2006; Appendix 1). The Hoggar Shield would undergo exhumation since the Late Eocene (40-30 Ma) as suggested by cooling temperature-time paths of apatites (Rougier et al., 2013; English et al., 2016). The products of its erosion are emplaced in mega fans of the 'Continental Terminal' around the massif that is undergoing uplift (Chardon et al., 2016). Doming of the Hoggar shield leads to the individualization of the present-day intracontinental basins of Northwestern Africa by fragmentation of a single Saharan basin into the Taoudeni, South Algerian, Murzuk, Chad and Iullemmeden basins. This fragmentation contributed to the development of the "basin-and-swell" topography of the continent (Burke, 1996). This triggered definitive retreat of the sea from the continent and a major drainage reorganization, which led to the establishment of the modern river network during the Early Oligocene, allowing for the building of the Niger delta (Chardon et al., 2016). As a consequence of possible uplift by the development of the basin-and-swell topography, numerous canyons incise the shelf and slopes of the Equatorial and South Atlantic margins of Africa, starting in the late Early Oligocene (Simon and Amakou, 1984; Burke, 1996; Seranne and Nze Abeigne, 1999; this work). Some authors suggest that the Western and Central Rift System is reactivated in the Eocene-Early Oligocene, allowing for the deposition of fluvial-lacustrine sediments (Genik, 1992, 1993; Zanguina et al., 1998). A phase of lateralization affects the entire sub region until the Latest Oligocene (Chardon et al., 2016). No sediment accumulates on the continent from that time on, except in the intracontinental Chad basin that still subsides during the Neogene (Burke, 1976).

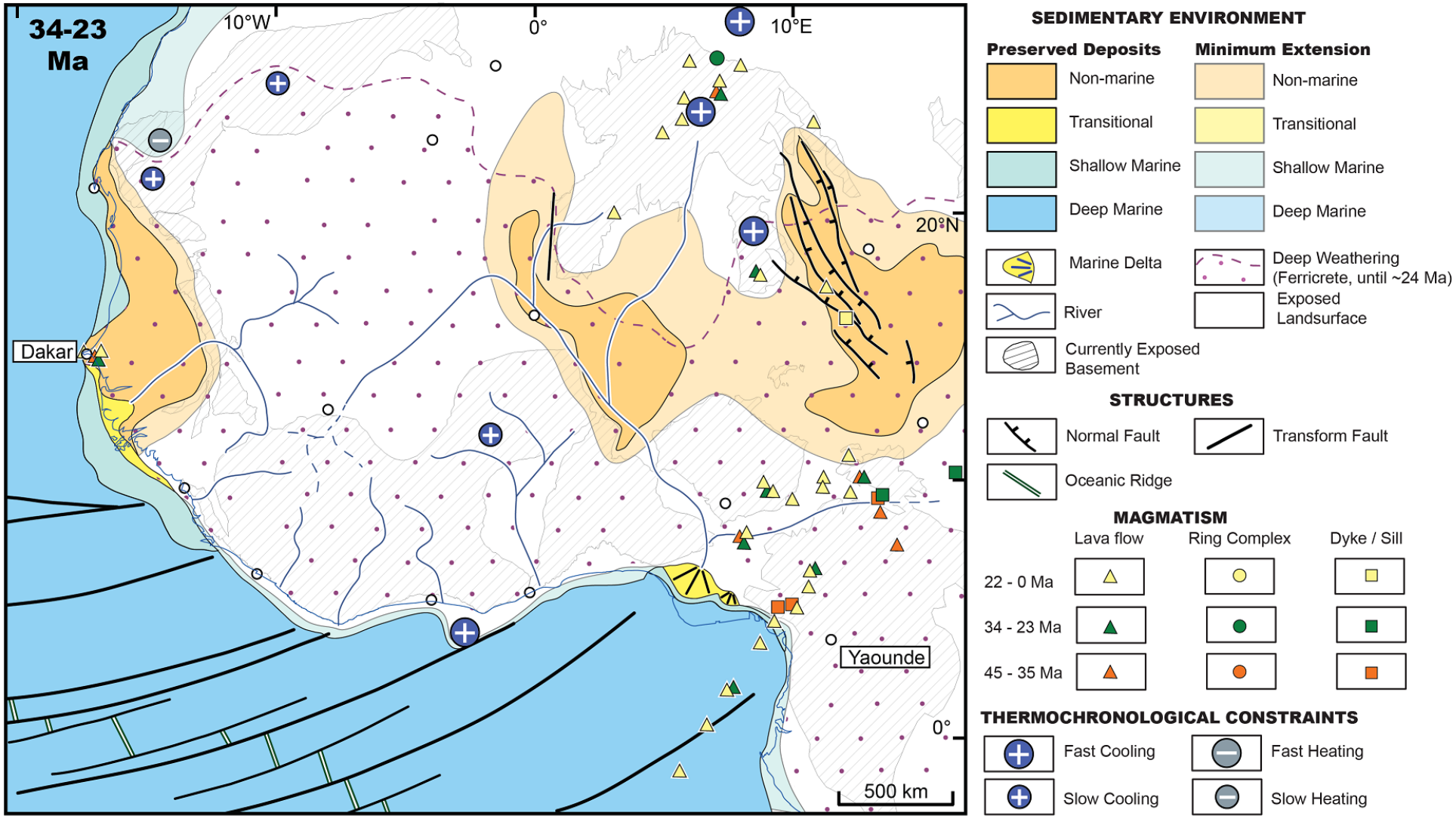

Figure 3-13 Geological configuration of Northwestern Africa and the Equatorial and Eastern Central Atlantic Ocean during the Oligocene (34-23 Ma). Same conventions as in Figure 3-5.

3.5. Discussion

3.5.1. Rifting and Large-scale Kinematics

Our reconstruction of the Albo-Aptian rifting stage (Figure 3-7) shows that the network formed by the Equatorial rift system and the intracontinental African rifts subdivides the continent areas into 7 microplates (Figure 3-14). This configuration allows for refining the kinematic framework for Early Cretaceous rifting that is usually based on a 4 microplates model (South America, NW Africa, Nubia and Central/Southern Africa; e.g., Guiraud and Maurin, 1992; Maurin and Guiraud, 1993). A central Microplate 1 (Leo-Man and Nigerian shields, Figure 1B) is bounded to the SW by the en-échelon Equatorial rift system and to the E by the Gao-Bida rift system (Figure 3-14). The northwestern limit is a transfer fault system in the direction of the Guinea-Demerara plateaus bounding fault, the Nara rift and the Amded rift (Figure 3-14). To the North, Microplate 2 represents the continental lithosphere of Central Atlantic affinity remaining stable during Cretaceous rifting. Microplate 3 accommodates the NE- extension between Microplate 1 and the Nubian plate (4) drifting northeastward (Figure 3-14). Microplate 5 occupies an intermediate position between Microplate 1, 3, 4, 6 (Central and Southern Africa block) and 7, and has therefore a complex behavior given the various kinematic incompatibilities it has to absorb along its various boundaries. Nevertheless, microtectonic data along its northern and southern boundary faults could suggest escape tectonic of that block towards the ENE, in the direction of divergence of Nubia (4).

The shape and kinematic boundary conditions of microplate 1 requires internal deformation (shearing) and rotation during rifting, in particular to accommodate (i) the distributed, en-échelon transtensional kinematics of the Equatorial margin, (ii) extension along its boundaries with microplate 3, and (iii) transfer faulting at the boundaries with microplate 2 (Figure 3-14). Internal deformation in the vicinity of the Equatorial margin requires reactivation of the basement faults inside microplate 1, which acted as terminations of the transforms into the continent.

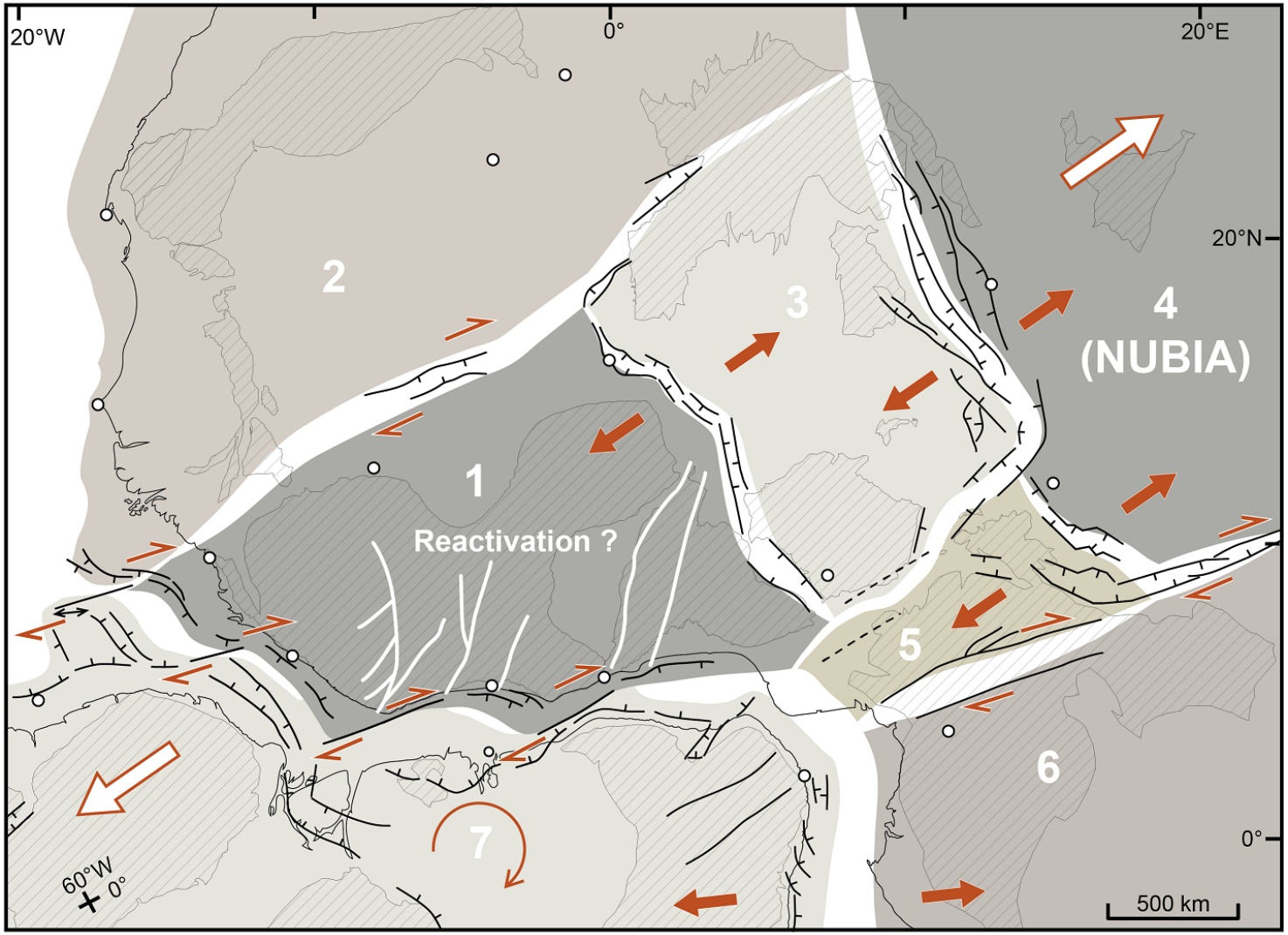

Figure 3-14 Microplate model for northwestern Africa and adjoining northern South America during Aptian rifting (based on the reconstruction shown in Figure 3-7). Six microplates are distinguished in intracontinental Africa. Open circles are the localities from Figure 3-1 and Figure 3-2B.

The deformation history in the Equatorial Atlantic Ocean appears to be more complex than a simple combination of coeval dextral transform and normal faulting at the scale of the entire margin. Crustal stretching began during the Valangian-Barremian along the Guinea-Liberia margin and its conjugate counterpart (Figure 3-15A). Seafloor spreading or mantle exhumation initiated locally during the Aptian within isolated basins in Ivory Coast and Guinea bounded by major transform faults (Figure 3-15B). The African Equatorial margin acquired its segmented shape only after final breakup in the Late Albian (Figure 3-15C).

The reason why the Guinea-Liberia margin was rifted first is that it may correspond to an aborted Jurassic rift (or aulacogene) of the Central Atlantic Ocean and therefore constitute a weakness zone (e.g., Figure 3-5). The Ivory Coast-Ghana and Ghana-Benin margins were rifted after, during the Barremian - Albian. The fact that the South American rifts of the Equatorial Atlantic have more complicated geometry and kinematics is probably related to the presence of a small craton (the Sao Luis craton, Figure 3-15) that originally belonged to the Leo-Man Shield (Klein and Moura, 2008a) and formed a lateral contrasts in the rheology of the lithosphere. Our reconstruction of the Equatorial Atlantic rift system allows to refining a pre-opening fit on the basis of the updated rift-bounding fault map, assuming it can be used to define the continents limits (Figure 3-15C). The specificities of the Equatorial Atlantic Ocean opening in a transform context may be summarized as follows. Mantle exhumation/sea floor spreading initiation processes created a Continental-Oceanic transition at an early time in isolated patches at the beginning of rifting (Figure 3-8 and Figure *3-15*B). The paleo-bathymetry of those newly formed 'ocean basins' increased slowly with restricted water circulation during the Albian-Cenomanian, due to potential barriers formed by transform-related marginal ridges (Figure 3-10 and Figure *3-15*C). Final "separation'' between continents occurred along the Ivory Coast-Ghana marginal ridge, which is the longest of the Equatorial domain (Figure 3-15C).

Many regional unconformities can be interpreted from seismic data. Some of these unconformities have formed during the so-called "rift phase" as consequences of repeated episodes of rifting / sagging. One of those unconformities should correspond to the "continental break-up unconformity", which should mark the end of faulting of the continental crust. At the end of the rift / mantle exhumation processes, a younger regional unconformity should form (i.e., the "lithospheric break-up unconformity") actually signing the onset of sea floor spreading. Therefore,

a number of diachronous “break-up unconformities” are expected at the scale of a single margin segment (from the necking zone to the hyperextended zone) and at the scale of the entire Equatorial Atlantic margins. A significant sedimentary hiatus (> 10 Ma) may be recorded by a “break-up unconformity” in proximal domains during extension /exhumation phases. Such a hiatus becomes shorter or sedimentation may even be quasi-continuous in distal parts of the margin.

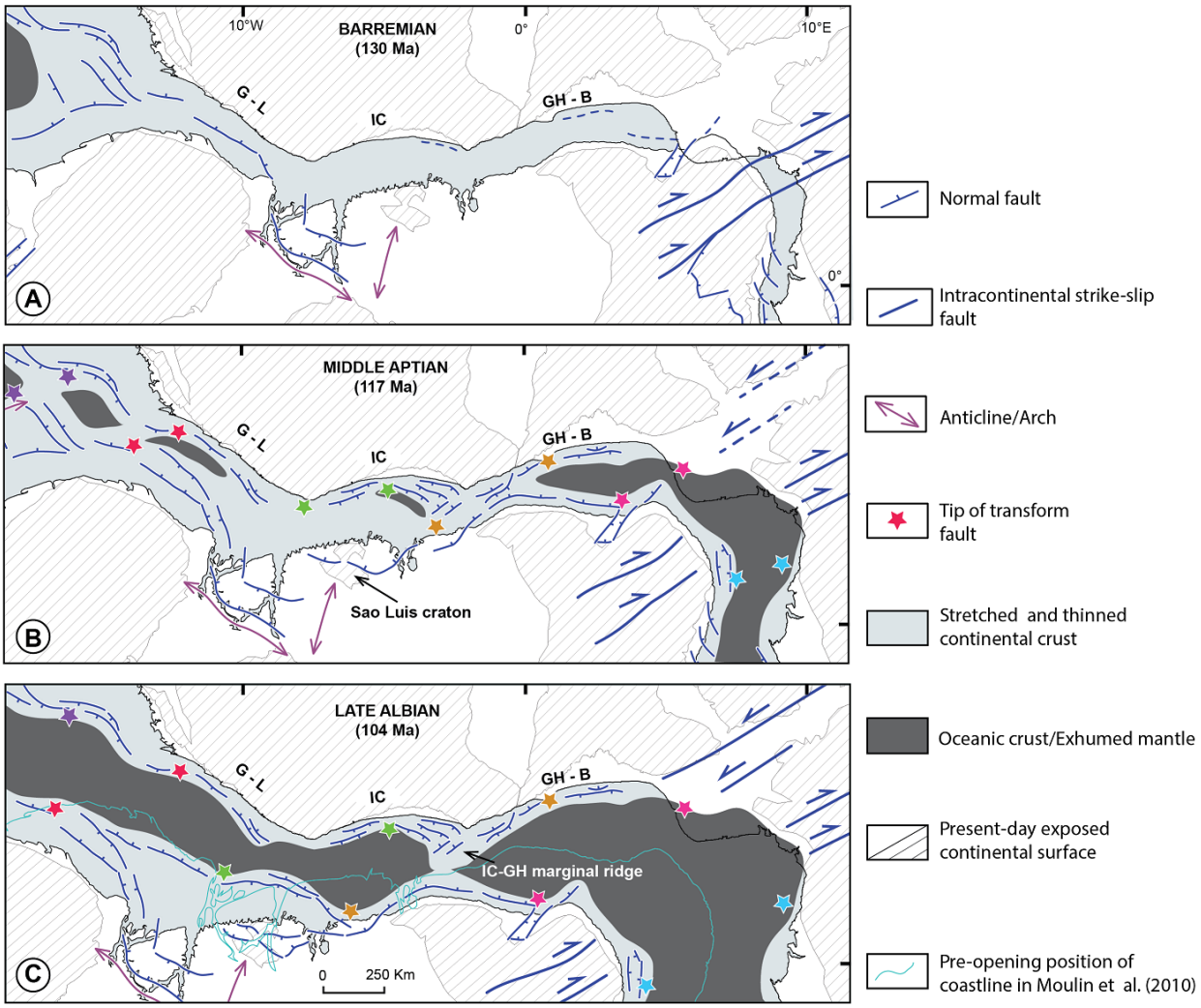

Figure 3-15 Successive configurations of the Equatorial Atlantic Ocean during the Early Cretaceous. G-L: Guinea-Liberia margin; IC: Ivory Coast margin; GH-B: Ghana-Benin margin. (A) Barremian: the Guinea-Liberia margin was undergoing rifting, whereas rifting only initiated along the Ivory Coast and Ghana-Benin margins. (B) Main Aptian rifting stage: all the Equatorial Atlantic margins underwent interference between dextral strike-slip (along incipient transforms) and normal faulting. Oceanic spreading was active between the South Atlantic Ocean and the eastern half of the Ghana-Benin margin. Spreading also initiated along the Ivory Coast-Ghana and Guinea-Liberia margins, forming two isolated domains of oceanic crust. (C) Late Albian break-up stage. A WNW trending rift branch formed

during the earlier stage on the South American side and was still active at the time. Rifting then ceased, and ultimate break-up took place along the Ivory Coast-Ghana marginal ridge.

3.5.2. Long-wavelength Deformation, Marginal Upwarps and Sedimentary Basins

Our work suggests the repeated or sustained occurrence of erosional marginal upwarp(s) between intracratonic and marginal basins around northwestern Africa. Figure 3-16 shows a stack of the limits (minimum extension) of the sedimentation areas from the Latest Triassic to the Oligocene over intracontinental Africa (compiled from Figure 3-5 to Figure *3-13*). This allows visualizing the evolving shape and size of the maximum erosional areas associated with marginal upwarp(s) through time. Four upwarp segments with contrasted exposition histories may be distinguished (Figure 3-16).

The largest and widest upwarp segment (I) roughly coincides with the current exposure of the Leo-Man shield. It is 1000- to 1400 km wide and may have undergone continuous erosion since the Triassic. All the kimberlites documented in West Africa are located within the Segment I (Figure 3-6), suggesting specific asthenosphere or lithospheric mantle process under this part of the West African craton that allowed sustaining uplift and/or topography over that region. The very-long wavelength of that upwarp (>1500 km) suggests an asthenospheric control, with limited impact of the continental margin's evolution. Indeed, rifting is expected to produce deformation at a shorter wavelength related to flexure. Upwarp segment (II) occurs along the southeastern edge of the Reguibat shield and has a NE trend. It has a shorter wavelength with significant variation in width (300-700 km; Figure 3-16), and it has been flooded at least once. Given its trend parallel to the Reguibat shield, segment II is likely an expression of the vertical movement history of this basement high. Leprêtre (2015) and Leprêtre et al. (2015) suggested that the Reguibat shield underwent upward vertical movements several times during the Mesozoic in response to plate-boundary forces. Upwarp segment III is N- trending (i.e., parallel to the coast) and narrow (400-450 km). It roughly coincides with the Mauritanides mobile belt and the westernmost fringe of the current Taoudeni basin (Figure 3-16 and Figure 3-2). It may have been episodically flooded during the Mesozoic. It most likely reflects the long-term evolution of the Senegalese segment of the

Central Atlantic margin. The last upwarp segment (IV) relates to the evolution of the South Atlantic margin. Its considerable width (up to more than 500 km) and the uplift it has undergone during the Neogene (Guillocheau et al., 2015) suggest at least a recent mantle support.

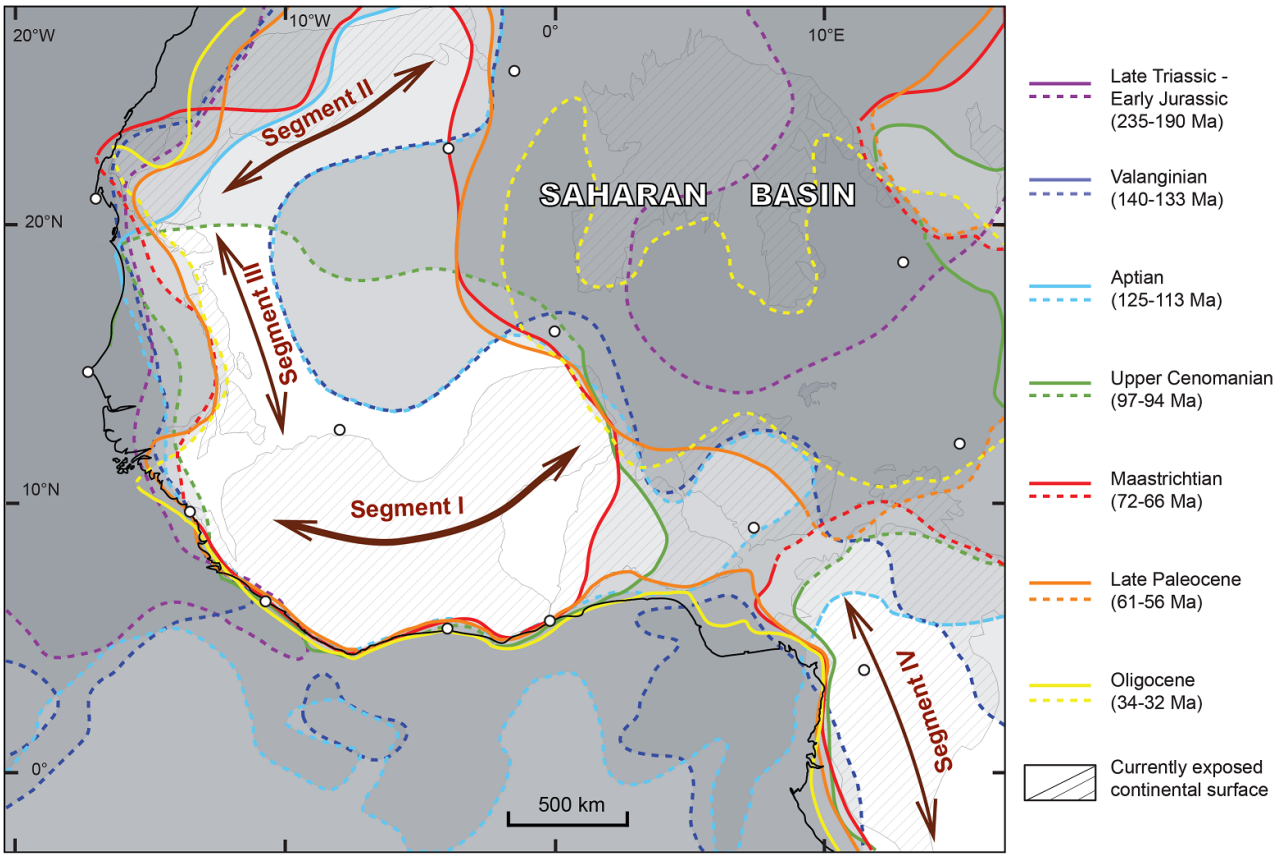

Figure 3-16 Synthetic paleogeographic map of northwestern Africa showing the evolving positions of shorelines (solid lines) or minimum extent of non-marine sedimentary deposits (dashed lines) through the Meso-Cenozoic (synthetized from Figure 3-5 to Figure 3-13). Depositional areas are filed with levels of grey color. Darker zones represent longer-lived depositional / sediment preservation area. Four segment types are distinguished along the marginal upwarp.

Rouby et al. (2013) have shown that the flexure-related rift-shoulders of a passive margin are often eroded away 10 to 20 Myr after the onset of rifting and therefore cannot explain the maintenance of those segments for more than 100 Myr. On another hand, Gilchrist and Summerfield (1990) have shown that denudational flexural isostasy could sustain marginal upwarps over long period. However, flexurally sustained upwarps very short wavelength (not more than a few hundreds of km) and cannot explain the large width (> 1000 km) of the northwestern African upwarps. To summarize, the documented marginal upwarps are somehow linked to the formation and/or the long-term evolution of the continental margins around northwestern Africa.

But their width and/or the evolution of their width through time suggests that asthenosphere dynamics or lithosphere-asthenosphere interactions were involved in their maintenance or rejuvenation.

3.5.3. Implications for Paleogeographic and Source-to-Sink studies

The space / time relationships between margins, marginal upwarps, intracratonic basins and hot-spot swells revealed by the present work have implications for understanding long-wavelength continental deformation and associated sedimentary processes of paired shield areas/continental margin systems.

Marginal upwarp segments constitute long-lived source areas for clastic sediments. However, beyond the two Paleogene time steps (Figure 3-12 and Figure *3-13*), the past river networks and continental divides may not be inferred. Yet, the present work helps addressing key issues for the understanding of passive margin – cratonic areas source-to-sink systems. Our reconstructions and paleocurrent data suggest that river systems draining the upwarp(s) fed both the intracratonic Saharan basin and the Central and Equatorial Atlantic margins since at least lithospheric break-up. The source-to-sink sediment budget of marginal upwarp should therefore consider both the margin and - potentially distant - intracratonic sinks, be they marine or continental. Given that the Saharan basin was a large embayment of the Tethys Ocean located north of the study area, remobilization and northward transport of its sediments have occurred. Furthermore, our reconstructions indicate that Meso-Cenozoic sediments have been tapped from the intracratonic basin and transported to the margin basins by rivers cutting across upwarp(s). This implies that intracratonic basins are transient sediment reservoirs (i.e., sinks) that have to be taken into account for source-to-sink investigations of marginal upwarps. This issue is further amplified by the Late Paleogene upheaval of the Saharan basin as a consequence of hot-spot swell growth (Figure 3-3D), which renders assessment of Mesozoic intracratonic sedimentary accumulation uncertain. In any case, our study provides ways to assess the past areal extent of erosional marginal upwarps, which may be used to estimate volumetric erosional export of such upwarps using long-term denudation laws such as those calibrated by Beauvais and Chardon (2013) or Grimaud et al. (2014, 2015).

As a result of long-wavelength lithospheric deformation and coeval erosion, the current West African intracratonic basins are only residual fragments of a large Saharan basin that once covered up to two thirds of the pre-Mesozoic continental substrate of Northwestern Africa. Therefore, those basins should not be studied as separate entities as it has been done since early geological exploration of Northwestern Africa. Likewise, the present compilation of paleogeography, paleocurrent, and thermochronological data shows that the Hoggar shield, which was considered as a large massif since the Early Mesozoic by most authors, only emerged since the Late Eocene. It is the result of the bursting, distortion and erosion of the Saharan basin by the Hoggar hot-spot swell.

3.6. Conclusion

The construction of Meso-Cenozoic paleo-geological / palinspastic maps allows reassessing the opening mode of the Equatorial Atlantic Ocean and constraining the structural, sedimentary and erosional history of its African continental margins. The maps further allow linking the evolution of the continental margins to that of their far African hinterland, with implications for the understanding of the coupling between long-wavelength deformation and sediment transfer processes over paired shield area-continental margin systems.

Oblique rifting of the Equatorial Atlantic domain started in the Valanginian (140-133 Ma), following plate reorganization and abandonment of a rift system that was propagating from the Central Atlantic Ocean across northern South America. Rifting of the Equatorial Atlantic propagated eastward from the Guinea margin until the Aptian (ca. 113 Ma). The rift system consisted in en-échelon dextral strike-slip faults (future tranforms) alternating with normal fault and was connected with an inland rift network under an overall regime of NE-SW extension in present coordinates. The whole rift-transform system almost split the Northwestern African continental domain into 6 microplates and a new syn-rift kinematic model is proposed that allows refining the pre-opening fit of Africa and North America. Final continental breakup occurred at the Ivory Coast-Ghana marginal ridge during the Late Albian.

The geological reconstructions reveal the persistent / renewed occurrence of eroding upwarps along the African continental margins that provided sediments both for the margin basins and for a very large, persistent intracratonic basin. But as an embayment of the Tethys Sea, such a basin acted as a transient sediment reservoir because the products of it erosion were transferred both to the Tethys (by north-flowing rivers) and the Equatorial Atlantic Ocean (by rivers crossing the marginal upwarp(s)). The source-to-sink investigation of the paired shield area-continental margin system is further complicated by Late Paleogene upheaval of the intracratonic basin as a result of hot-spot swell growth that led to the distortion and further massive erosion of its Meso-Cenozoic sediments. Upheaval resulted in the fragmentation of the intracratonic basin into the current, smaller residual basins, whose pre-hot-spot evolution should not be considered separately from one another. Hot-spot swell growth triggered a major reorganization of both the continental area and its margins in the Early Oligocene, so has the Northwest African source-to-sink system.

3.7. Acknowledgments

This study was funded by Total Exploration and Production through the Transform Source-to-Sink Project (TS2P). We acknowledge Total for providing data and for allowing publication of the study. Total R&D research group is thanked for discussions as well as scientific and technical support. We are grateful to Maryline Moulin and Daniel Aslanian for kindly providing us with their kinematic model of the Equatorial Atlantic Ocean.

CHAPTER 4 : STRUCTURE AND MESOZOIC STRATIGRAPHY OF THE EQUATORIAL ATLANTIC MARGIN

PAPER 2 - Structural variability of the African Equatorial Atlantic margin and post-rift stratigraphic implication

Manuscript in preparation

Abstract

We investigated the structural variability and the early post-rift stratigraphic architecture along the African Equatorial Atlantic margin. The segmentation of the margin results from the obliquity of each segment with respect to the orientation of transform faults bounding the main depot-centres (Sierra Leone-Liberia, Ivory-Coast, Ghana-Togo-Benin). This produced variable widths of the necking zone of the crust and the continent-ocean transition from one segment to the other. We show that this has a significant impact on the early post-rift stratigraphic architecture of the margin segments. In particular, the proximal parts of this sedimentary wedge are only preserved along divergent segments of the margin and not along transform segments. We interpret this differential preservation as the result of a greater flexural uplift, during the immediate post-rift, in the proximal parts of the transform segments, preventing the preservation. We also documented, in the proximal part of the divergent margins, a regional uplift event (x100m) during the Santonian (ca. 84 Ma) that could be related to either mantle driven dynamics or regional changes in lateral stress regime.

Résumé

Nous avons analysé la variabilité structurale et l'architecture stratigraphique de l'immédiat post-rift le long de la marge Atlantique Equatoriale africaine. La segmentation de la marge résulte de l'obliquité de chaque segment de la marge par rapport à l'orientation des failles transformantes délimitant des dépôt-centres principaux (Sierra Leone-Liberia, Côte d'Ivoire, Ghana-Togo-Benin). Ceci se traduit par des variations, d'un segment à l'autre, de la largeur de la zone d'amincissement de la croûte *(necking zone)* et de la transition océan-continent. Nous montrons que cette segmentation a un très fort impact sur l'architecture stratigraphique de l'immédiat post-rift des segments. En particulier, les parties proximales du prisme sédimentaire ne sont préservées que dans des segments divergents et pas sur des segments transformants. Nous interprétons cette

préservation différentielle comme le résultat d'une flexure plus importante des parties proximales des segments transformants au début du post-rift, qui empêche la préservation. Nous avons également pu documenter, dans la partie proximale des segments divergents, un soulèvement régional (x 100 m) durant le Santonien (ca. 84 Ma) qui pourrait être lié à la dynamique mantellique ou à une réorganisation intraplaque des contraintes.

4.1. Introduction

The African Equatorial Atlantic margin is known for its transform-controlled evolution, leading to the final opening of the Atlantic Ocean (Mascle et al., 1997; Basile et al., 2005). Most of previous investigations have focused on the evolution of the Ghana transform margin at the intersection of the Romanche transform fault with the West African craton (Mascle and Blarez, 1987; Attoh et al., 2004; Antobreh et al., 2009). As a spectacular feature of that part of the transform margin, the Ivory Coast-Ghana marginal ridge has been investigated by geophysical cruises, scientific drilling (Ocean Drilling Program, Leg 159) and deep-sea dives (Mascle and Blarez, 1987; Mascle et al., 1997; Benkhelil et al., 1997; Clift et al., 1998; Bouillin et al., 1998; Pletsch et al., 2001, Figure 4-1). These studies mainly showed the structure of the ridge, the geometry of the shallow Eastern Ivory Coast and highlighted vertical displacements of the marginal ridge during the intracontinental rift and syn-transform stages. Most of the other studies (e.g., Sierra Leone-Liberia, Eastern Ivory Coast segments) focused mainly on the structuration and sedimentation during the syn-rift or, locally, the post-rift stratigraphic architecture in terms of petroleum potential, as increasing interests have been given on deep-water turbidite reservoirs (Grillot et al., 1985; Kjemperud et al., 1992; Bennett and Rusk, 2002; MacGregor et al., 2003; Flinch, 2009).

The equatorial Atlantic margin does however show a very complex 3D pattern of lithosphere stretching, alternating segments where the stretching is fully controlled by the transform fault and segments where the stretching is more oblique or simply divergent (e.g. Basile, 2015; Basile and Braun, 2016; Mercier de Lépinay et al., 2016). Mercier de Lépinay et al. (2016) defined a typology of segment based on present-day geometries of the margin, however, the impact of this complex 3D stretching distribution on the post-rift evolution of the margin in general and the stratigraphic architecture in particular, has not been addressed. This spatial variability of lithosphere stretching is nonetheless expected to have very different impacts on vertical motions of the margin, especially in the necking domain, as it acts on the thermal and gravity driven isostasy,

as well as on the subsidence/uplift patterns related to the flexural isostasy response of the lithosphere to both stretching and (un)loading effects of surface processes.

The aim of this study is to establish the impact of the spatial variations of lithosphere stretching during the rifting on the post-rift stratigraphic architecture by analyzing the difference in behavior of different segments of the same margin during the post-rift. To do this, we used seismic and well data to study the tectonic and stratigraphic history of each segment at the scale of the whole African Equatorial Atlantic margin, and compared them. We analyzed the immediate post-rift stratigraphic architecture in the light of the geometry of crustal thinning pattern and obliquity with respect to the direction of the transforms, and discussed the post-rift vertical displacements associated with different margin segment types.

4.2. Regional Settings

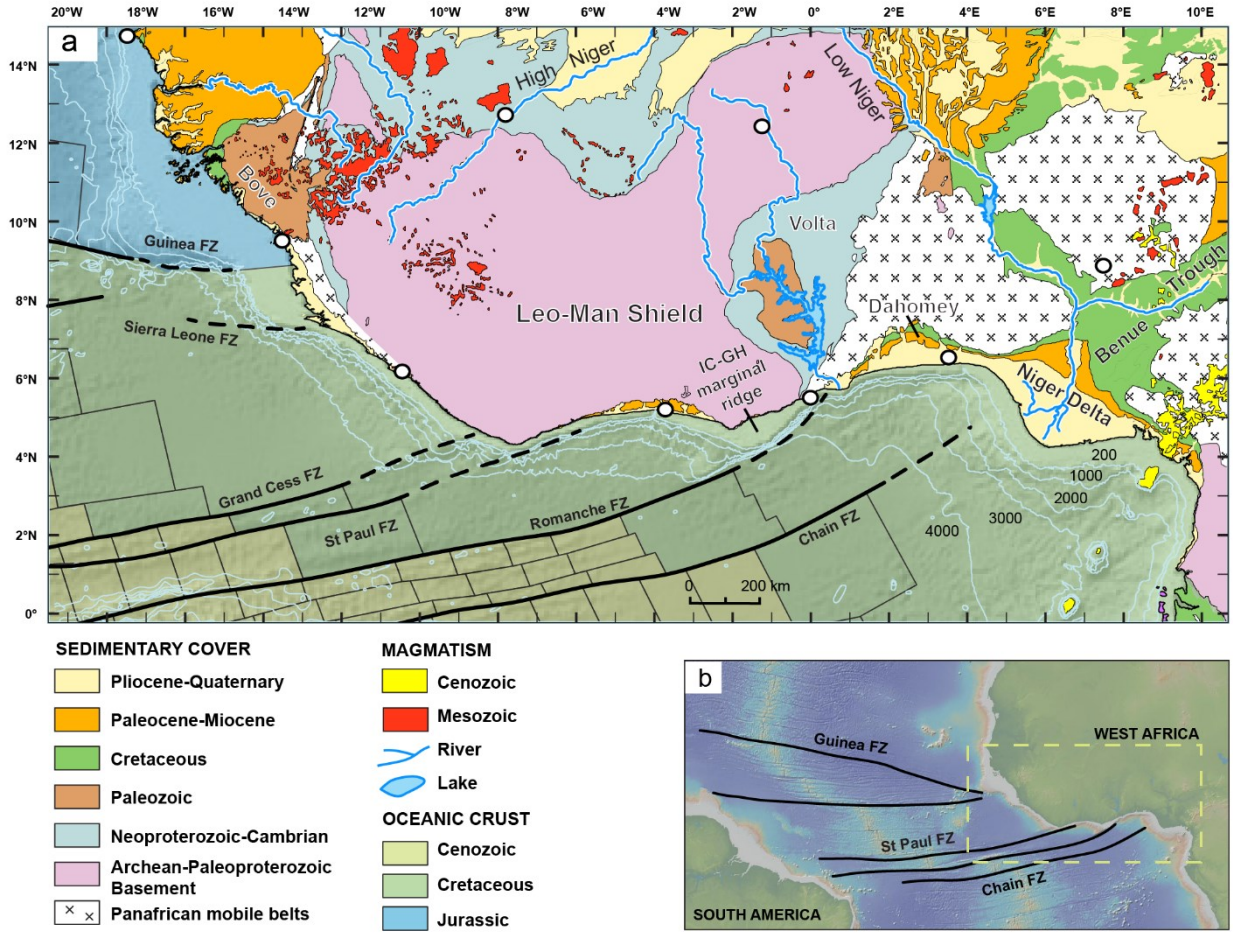

Figure 4-1 (a) Simplified geological map (modified from Choubert and Faure-Muret, 1988) and (b) the location of the study area. Topographic map is from www.noaa.gov.

The African Equatorial Atlantic margin (3-10°N latitude, 20°W-5°E longitude) is separated from the Central Atlantic Ocean by the Guinea Fracture Zone and from the South Atlantic Ocean by the Chain Fracture Zone (Figure 4-1). The present-day shelf is generally narrow (< 10 km), as a results of the these transform faults that divide the margin into four main margin segments: Sierra Leone-Liberia, Ivory Coast, Ghana and Togo-Benin margin segments (Figure 4-2).

Inland, the continent is composed of (i) the southern part of the West African craton corresponding to he Archean-Paleoproterozoic Leo-Man Shield bordered by Panafrican mobile belts; (ii) the Volta basin of Neoproterozoic-Paleozoic age, located East of the Leo-Man Shield, and; (iii) the coastal basin of the Dahomey embayment along the Togo-Benin margin that preserved Maastrichtian to Cenozoic deposits (Figure 4-1; Da Costa et al., 2009). The Dahomey embayment connects, to the East, with (iv) the Benue Trough that openned as a pull-apart basin by a senestral strike-slip deformation during the Aptian-Albian (125-100 Ma) (Benkhelil, 1988, 1989).

The rifting of the Equatorial Atlantic Ocean propagated eastward from the Central Atlantic between the Valanginian (ca. 140 Ma) and the Aptian (ca. 112 Ma) as an en-échelon transform-rift system (e.g. MacGregor et al., 2003; Brownfield and Charpentier, 2006) with a main rift phase in the Middle Aptian (120-115 Ma; Ye et al., Submitted). This rift was connected to a large inland rift network (Moulin et al., 2010; Heine and Brune, 2014, Ye et al., Submitted) and initially formed continental pull-apart basins. The breakup of the continent leading to the formation of the Equatorial Atlantic Ocean started later on, although the deformation history appears to be more complex than a simple combination of coeval transform and normal faulting (Ye et al., submitted). It is not well constrained because the age of the first oceanic crust was not precisely dated during the 'Cretaceous Quiet Magnetic Period' (Moulin et al., 2010; Heine et al., 2013; Ye et al., Submitted). Seafloor spreading or mantle exhumation initiated locally, during the Aptian-Early Albian (125-107 Ma), within isolated basins in Ivory Coast and Guinea bounded by major transform faults in Ivory Coast and Guinea. The paleobathymetry of these newly formed "oceanic basins" deepened slowly. They were flooded during the Late Albian although they remained under restricted water circulation during the Albo-Cenomanian (Chierici, 1996; Ye et al., Submitted). The final break-up between continents occurred during the Late Albian (104 Ma, Moulin et al.,

2010) achieving the segmentation of the African Equatorial margin. This break-up was associated with a major regional unconformity, the "Breakup Unconformity", also observed on the conjugate Brazilian margins (Zalan and Matsuda, 2007; Trosdtorf Junior et al., 2007; Soares Júnior et al., 2011). An 'active-transform' stage lasting until the Late Santonian (ca. 84 Ma) can be defined during the passage of oceanic spreading ridge along the transform segments in Western Ivory Coast and Ghana (Basile et al., 2005). A "Senonian Unconformity" was identified as a strong angular unconformity, corresponding to a hiatus of Turonien-Early Senonian (94-84 Ma) in Eastern Ivory Coast and Santonian-Campanian (86-72 Ma) in Benin (Elvsborg and Dalode, 1985; Chierici, 1996). Its origine is debated, but it could be related to the Santonian tectonics in the Benue Trough or the last transtensional movements affecting the Equatorial Atlantic margin (Chierici, 1996; Brownfield and Charpentier, 2006). Once the oceanic ridges passed beyond their outer corner tip, the transform margins entered a passive-margin stage (Basile, 2015).

4.3. Material and Method

4.3.1. Dataset

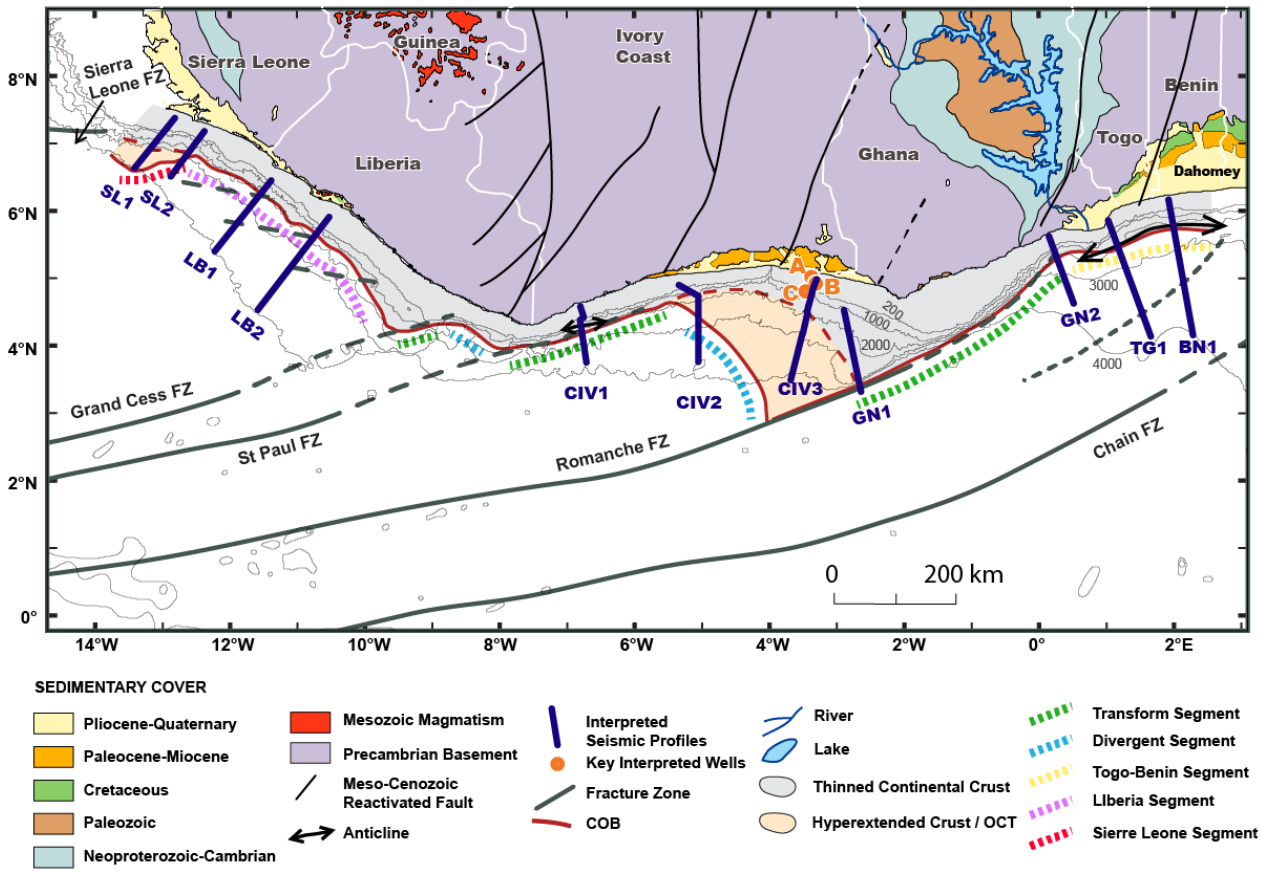

Figure 4-2 Location of interpreted seismic sections and the exploration wells used for proximal deposits analysis. Segmentation of the Equatorial Atlantic margin used in this study is shown by dashed color lines.

Our study of the African Equatorial Atlantic margin was based on a large set of subsurface data (about 1000 seismic reflection lines and 70 exploration wells) located along the margin from Sierra Leone to Benin (an area of c. $2.3x10^5$ km^2, Figure 4-2) among which we selected eleven composite regional sections perpendicular to the shoreline and extending from the present-day shelf to the abyssal plain (Figure 4-2). Thirty-eight of those wells have been recently evaluated in terms of biostratigraphy (palynology, nanofossil, foraminifera dating) by TOTAL, most of them located on the present-day shelf. We used them for calibration in ages of the stratigraphic surfaces. For three wells of the shelf of Western Ivory Coast (Figure 4-2), we also used well-logs, including Gamma Ray (GR, for radioactivity), Spontaneous Potential (SP, for permeability), Sonic (Dt), Netron (NPHI), Density (RHOB) and Resistivity as well as available cuttings reports, for lithologic calibration and paleo-environemental interpretations (Van Wagoner et al., 1988, 1990; Homewood et al., 1992).

4.3.2. Seismic Stratigraphy

We defined the stratigraphic architecture using the offlap migration method (Vail et al., 1977; Helland-Hansen and Martinsen, 1996; Homewood et al., 1992). It is based on the identification of offlap breaks that correspond to the slope rupture of clinoforms (Figure 4-3). They represent either past shorelines or past shelf-breaks. Their nature (shoreline or shelf-break) is identified by the upstream sedimentary environments that can be constrained by well-logs data. When an offlap break is identified as a shoreline, its migration trajectory allows to define trends of propagradation/regression (seaward migration), aggradation (vertical migration) and retrogradation/transgression (landward migration). Key stratigraphic surfaces are distinguished when combining the shoreline trajectory and truncations associated to the surface (onlap, toplap, downlap and erosional truncation, Figure 4-3b). An subaerial unconformity (UN) is defined when the shoreline migrates seaward and/or downward during an acceleration of propagation (Figure 4-3b). It can be correlated seaward to a marine conformity or the bottom of basin-floor mass-transport deposits. A maximum flooding surface (MFS) is defined when a retrogradation evolves

into a propagradation. Flooding surfaces (FS), also called as maximum regressive surfaces (MRS) or transgressive surfaces (TS), mark the inversion from a propagradation to a retrogradation.

Transgression/regression sequences are determined as bordered by these key surfaces including a propagradational system tract (highstand, lowstand and forced regression system tracts) and a retrogradational system tract (transgressive system tract, Figure 4-3c). A highstand system tract is separated from a lowstand or forced regression system tracts (downward shift of offlap break) by an unconformity, and from transgressive system track by a maximum flooding surface. A transgressive system track, usually less well preserved, is separated from lowstand system track by a flooding surface.

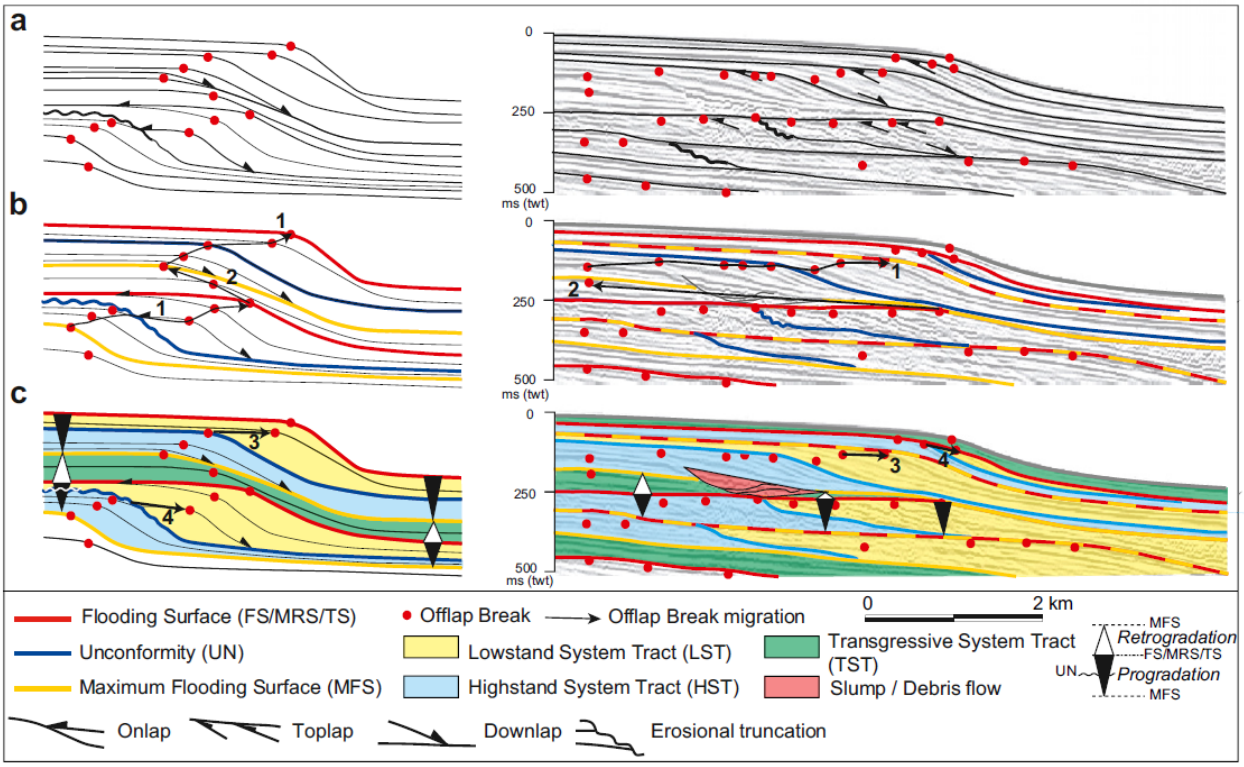

Figure 4-3 Seismic stratigraphy method used in this study (after Jermannaud et al., 2010). Definition of the (a) offlap break, (b) the offlap break migration and associated stratigraphic surfaces and (c) the systems tracts and depositional

sequences illustrated by a theoretical example (left column) and a natural example of the eastern Niger Delta (right column).

4.4. Structural and Stratigraphic Characteristics of the Segments

We mapped the continent-ocean boundary (COB) and the different crustal domains (thinned continental crust, hyperextended curst/continent-ocean transition, oceanic crust, Figure 4-2). We then focused on the early post-rift history of the margin, i.e., the Upper Cretaceous stratigraphic architecture. We mapped four regional horizons in every basin (Figure 5-2). Regional unconformities, such as the Late Albian Breakup and Senonian (probably Santonian, ca. 84 Ma) unconformities were correlated from one margin segment to the other, as well as the major Cenomano-Turonian maximum flooding surface (ca. 94 Ma). The Campanian sub-regional unconformity surface (ca. 72 Ma) was mapped only along the Sierra Leone-Liberia and Ivory Coast margins. We then classified each margin segments according its structural and stratigraphic characteristics (Figure 4-2).

4.4.1. Ivory Coast Margin

Crustal structures of Ivory Coast margin vary from the West to the East. The western transform segment is controlled by the Saint Paul transform fault, whereas the eastern one is a NW-SE trending divergent segment (Figure 4-2 and Figure *4-4*). During the Lower Cretaceous, the Western transform segment underwent mainly strike-slip syn-rift faulting and is associated with a relatively narrow necking width (ca. 40 km; Figure 4-4a). Continent-ocean transition (COT) is almost clear-cut with an oceanic crust clearly identified and marked by the strong reflector of the Moho. Anticlines formed locally by reactivation of syn-rift faults during the Upper Cretaceous. Along the Eastern divergent segment, the syn-rift normal faulting is better expressed. On the other hand, the continent-ocean boundary (COB) is less clear. Indeed, a hyperextended domain, considered also as COT, has been identified between a thinned continental crust and a typical oceanic crust (Figure 4-4b and c). Faulting and thinning of that domain seems to support its continental nature. This hyperextended crust domain is widening from the NW to the SE (Figure

4-2). Whatever the exact nature of that COT domain, the necking zone is wider than along the divergent transform segment (> 80 km).

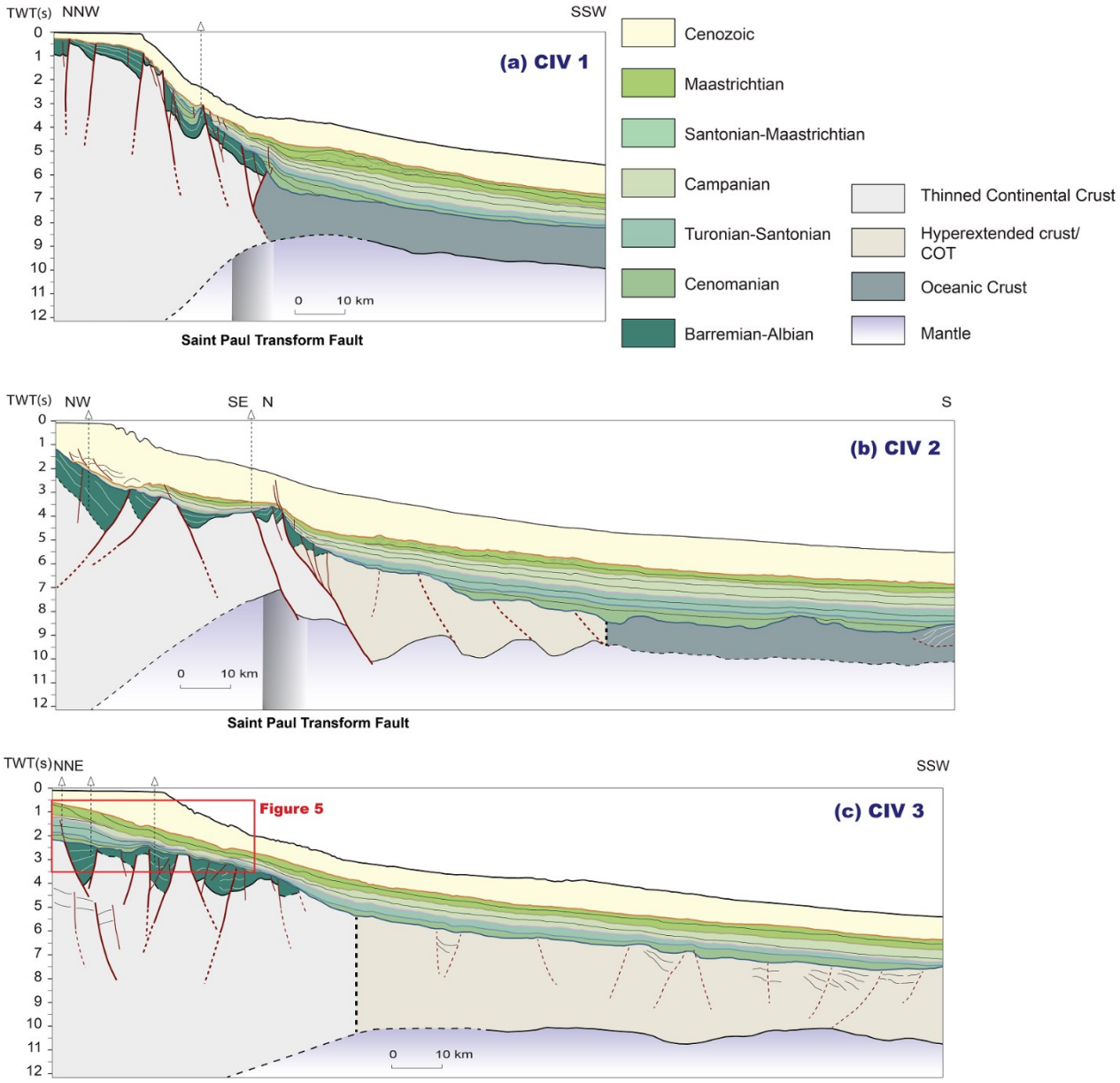

Figure 4-4 Structural and stratigraphic interpretation of cross-sections in the Ivory Coast Basin cross-sections. See location in Figure 4-2 and text for details.

The preservation of the proximal terms of the Upper Cretaceous (early post-rift) sedimentary wedge is, as well, very different between the eastern and western segments. Along the

eastern transform segment, only the distal terms (deep water deposits) of the early post-rift units are preserved at the foot of continental slope. Landward, they onlap upon the Late Albian breakup unconformity and, seaward, downlap upon the oceanic crust. This Upper Cretaceous wedge preserves remarkable Maastrichtian turbiditic channel-levee complexes, stacking on the abyssal plain (Figure 4-4a). In the proximal domain, the Upper Cretaceous is only represented by a hiatus and Cenozoic sediments lay directly upon the syn-rift deposits or the basement (Figure 4-4a and b). As a difference, along the divergent segment, the proximal terms of the immediate post-rift are preserved as clinoforms, marking the migration of the continent-ocean transition during the Upper Cretaceous (shorelines; Figure 4-4c and Figure *4-5*). We were able to identify there five major transgressive/regressive sequences with a mean durations of 6-7 Ma (Figure 4-5c). The Cenomanian (100-94 Ma), is marked by a propagradation / retrogradation cycle. The Turonian-Santonian (94-84Ma) is dominated by a regression recorded by a transition from deltaic to fluvial environment in Well A and from deep marine to deltaic environment in Well B (coarsening upward sequences, Figure 4-5c). A major relative sea level drop of over 200 m marked the end of Santonian (c. 84 Ma). This fall cannot be only related to eustasy that was less than 100 m at that time (e.g. Miller et al., 2005). Therefore, an uplift of the margin shelf must have at least amplified, or even driven, this accommodation reduction during the Santonian. As along the western segment, the distal terms of the immediate post-rift units are preserved at the foot of continental slope. This distal wedge appears to have preserved more turbiditic systems onto the basin-floor during the Campanian-Maastrichtian (84-66 Ma). They may have been triggered by the Santonian accommodation reduction documented on the shelf. The Maastrichtian ends by a regression phase (Figure 4-5c).

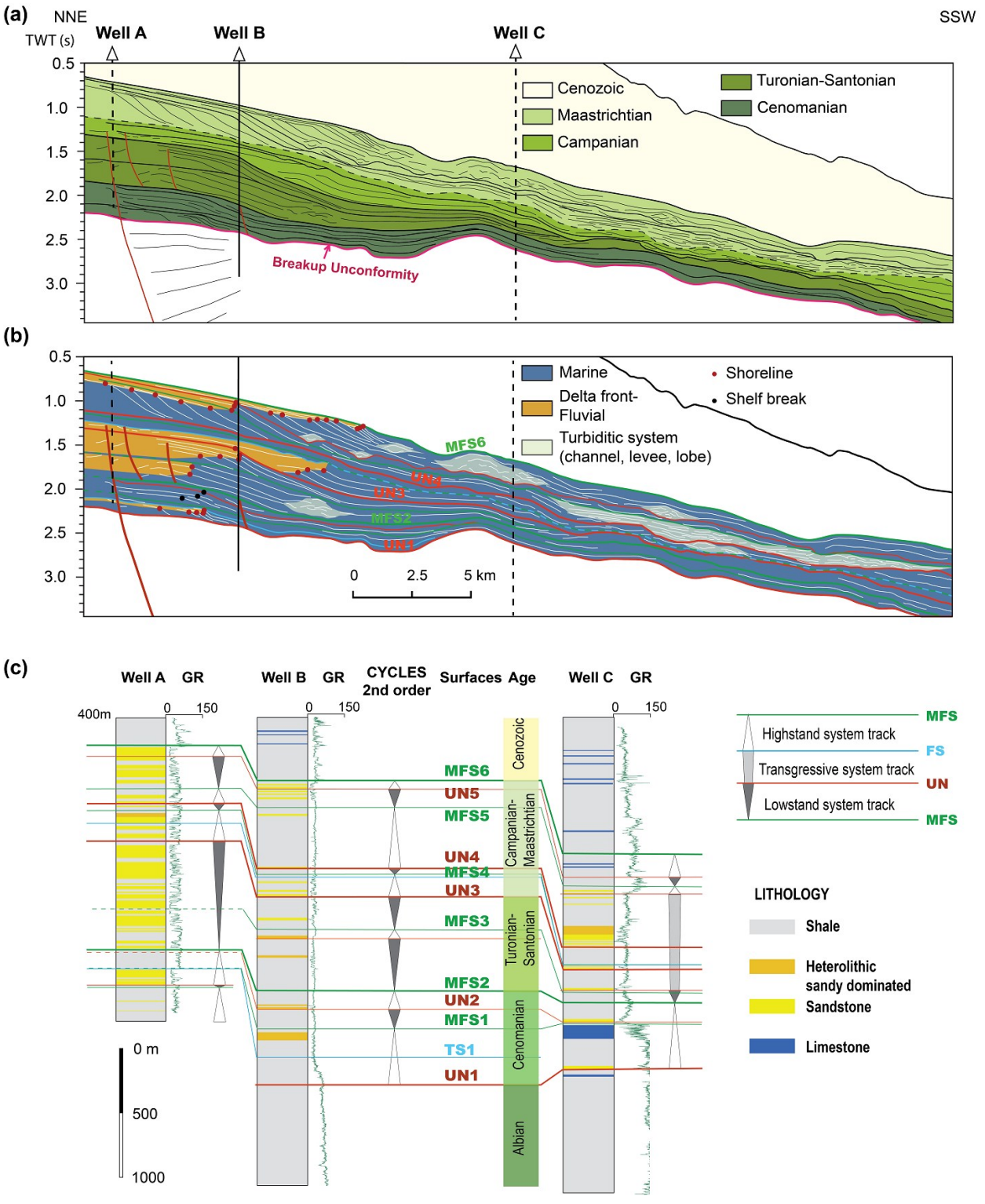

Figure 4-5 Sequence stratigraphic interpretation (a and b) of Upper Cretaceous sequences preserved on the shelf of the Eastern Ivory Coast divergent margin (see location in Figure 4-2 and Figure 4-4c), based on the offlap break migration method and well correlation (c). Projected wells are shown by dashed lines.

4.4.2. Ghana Margin

The Ghana segment has been previously investigated but mostly at its Western tip, at the location of the Ivory Coast-Ghana marginal ridge (Mascle and Blarez, 1987; Basile et al., 1998; Bouillin et al., 1998; Clift et al., 1998; Bigot-Cormier et al., 2005; Figure 4-2 and Figure *4-6*). Syn-rift faults are well imaged below the shallow Eastern Ivorian basin and have been locally reactivated during the early post-rift, deforming Upper Cretaceous units. The marginal ridge is a structural high forming a sharp transition between the relatively shallow Eastern Ivorian basin and the oceanic basin. The onlap of the Eastern Ivorian basin sedimentary units onto the ridge shows that this structure remained a relief on the sea floor since the end of the Albian (100 Ma; Figure 4-6a). The development of the marginal ridge has been extensively discussed and different mechanisms have been invoked including crustal thickening, oceanic ridge related thermal uplift or flexural response of the lithosphere to erosion (Mascle and Blarez, 1987; Sage et al., 2000; Basile and Allemand, 2002; Attoh et al., 2004). Thermochronological analysis of samples collected on the seaward slope of the ridge revealed a cooling during the Lower Cretaceous followed by a heating during the Upper Cretaceous. Although a striking and often investigated feature, the marginal ridge does not characterize Ghana transform segment, nor the Ivory Coast segment, as a whole (Figure 4-4c and Figure *4-6*b). It is indeed very restricted spatially to the intersection between the transform segment and the Eastern Ivorian divergent segment (Figure 4-2) and is probably a local interference of extensional processes between the transform and divergent segments.

The crustal structure and stratigraphic architecture of the main Ghana transform segment, (between the marginal ridge to the Volta River's mouth) is similar to the Western Ivory Coast segment (Figure 4-6c). It is indeed characterized by (i) syn-rift faults affecting pre-rift Paleozoic-Jurassic units, (ii) a very narrow continent-ocean transition without a structural high, (iii) no Upper Cretaceous sediments preserved in the proximal part of the margin. Those are only preserved at the foot of continental slope onlapping upon the Late Albian breakup unconformity and, seaward, downlapping upon the oceanic crust.

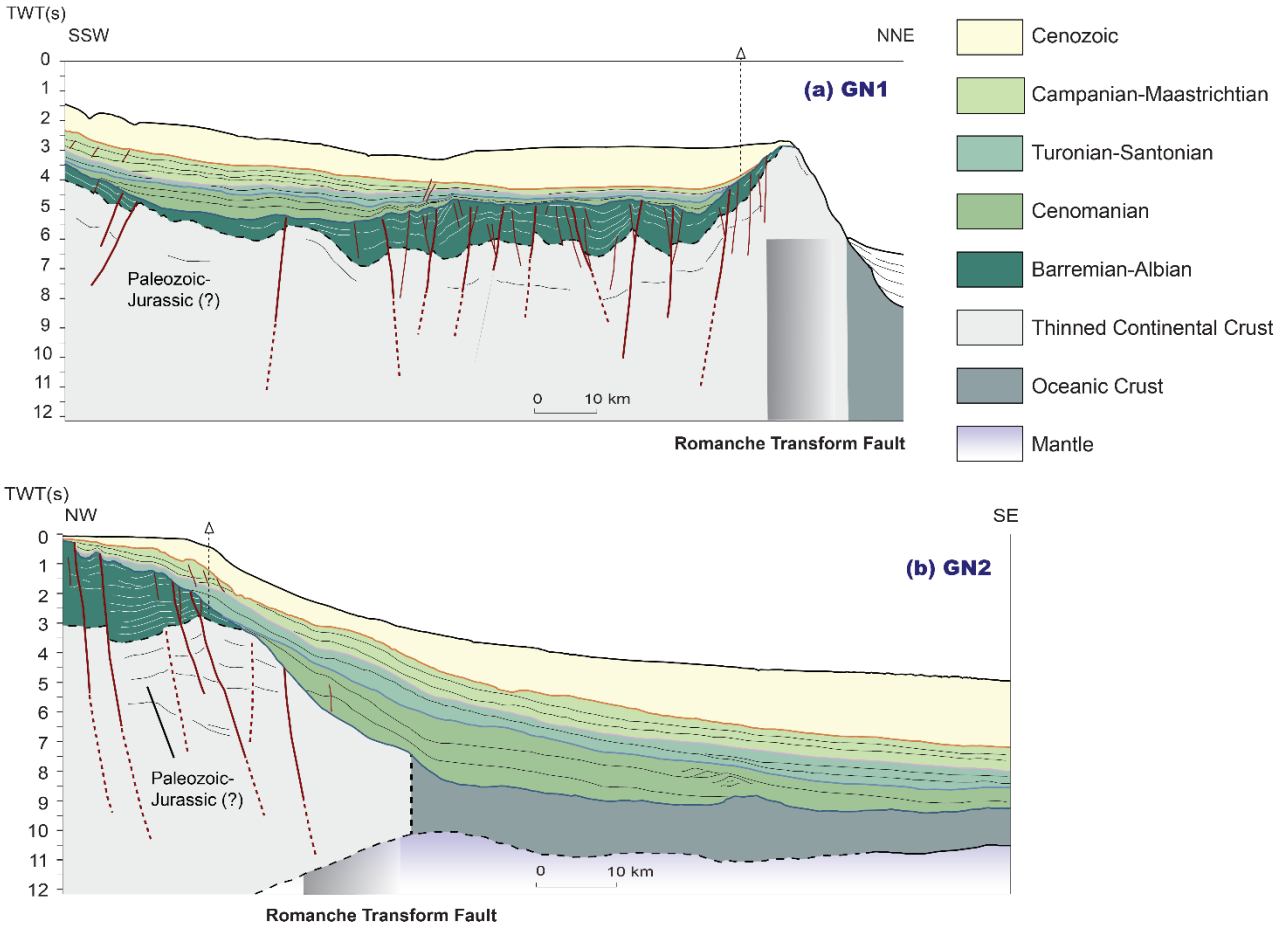

Figure 4-6 Structural and stratigraphic interpretation of regional cross-sections along the Ghana margin segment. See location in Figure 4-2.

4.4.3. Togo-Benin Margin

Along the Togo-Benin margin segment, about 30° oblique to the Romanche transform, the crustal structure of the margin appears to be strongly influenced by the Romanche transform fault, associated with a local upwarping of the Moho (Figure 4-7). Syn-rift faults were reactivated in the Upper Cretaceous (until at least Maastrichtian) forming a large anticline above the Romanche transform fault (Figure 4-2 and 4-7a). Recent seismicity observed along onshore faults at the prolongation of the transform fault is consistent with their recent reactivation (Bellion et al., 1984; Bellion and Robineau, 1986)-.

Along this segment, a few Late Cretaceous sediments (Campanian-Maastrichtian, 84-66 Ma) are preserved in the proximal part of the margin without preserved off-lap break. Most of the early post-rift stratigraphic units are preserved in the distal parts of the segment segment with abundant mass-transport deposits (MTD: slump, debris flows) indicating a significant reworking of Cretaceous to Cenozoic proximal deposits. The thick Cenozoic sedimentary units in the very distal parts of the margin, upon the oceanic crust, suggest a significant lateral contribution of Niger delta since its emplacement in the Early Oligocene (34-29 Ma, Chardon et al., 2016). The Senonian unconformity (c. 84 Ma) can be identified in wells and on seismic profiles.

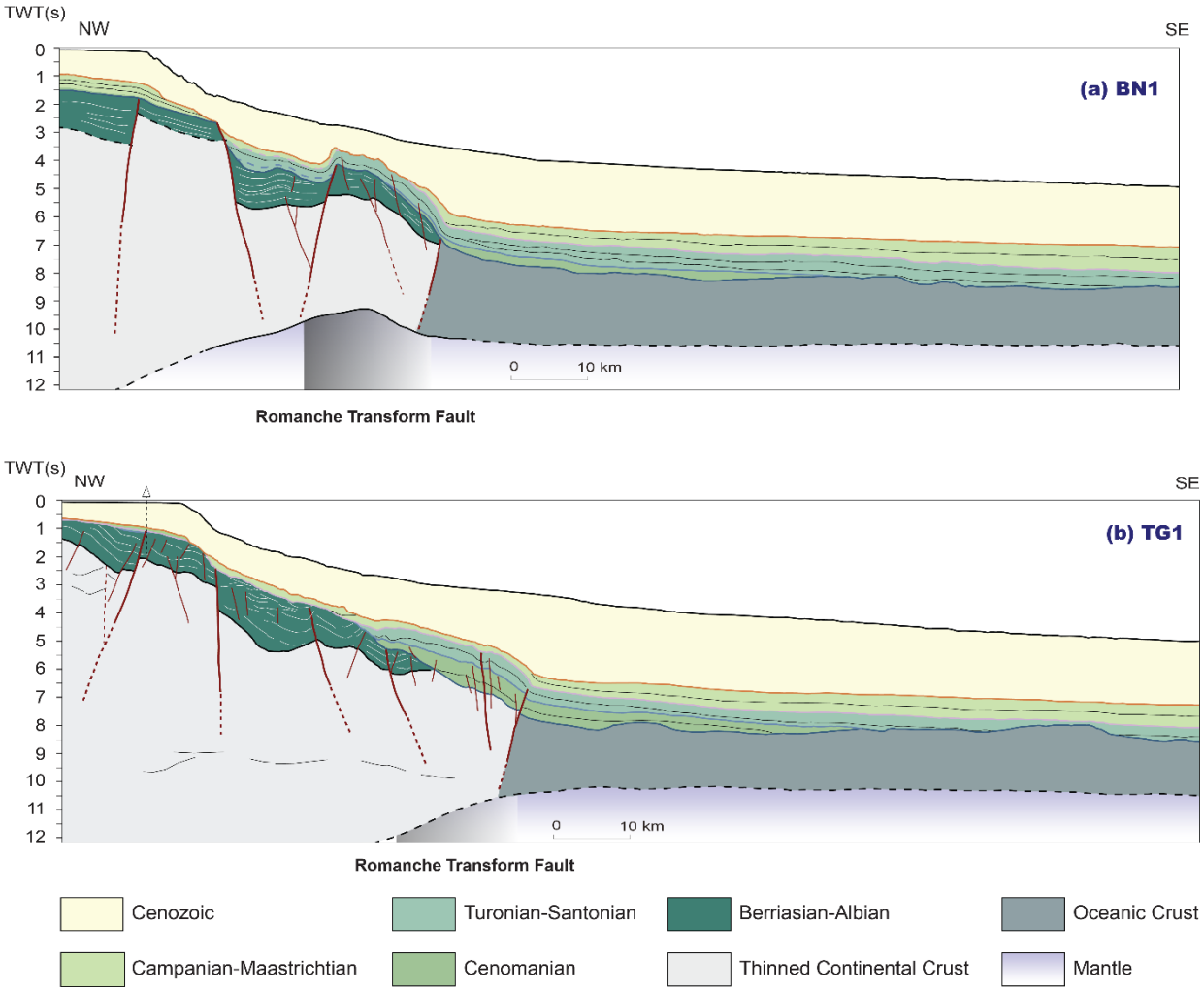

Figure 4-7 Structural and stratigraphic interpretation of regional cross-sections along the Togo- Benin margin segment. See location in Figure 4-2.

A specificity of this segment is the preservation of a large coastal basin, the Dahomey Embayment (Figure 4-1 and 4-2), that preserved shallow marine deposits in the latest Cretaceous (Maastrichtian) and Cenozoic (Bankole et al., 2007; Da Costa et al., 2009; Durugbo and Aroyewun, 2012, Figure 4-1). It demonstrates that this segment developed under marine conditions and underwent later on uplift of the proximal part of the margin, during the Cenozoic, to bring those marine deposits into their current continental position.

4.4.4. Sierra Leone-Liberia Margin

The Sierra Leone-Liberia margin is composed of both the Sierra Leone segment and the Liberia segments (Figure 4-1). Syn-rift structures vary along (from NW to SE) and across the margin (from proximal to distal domains; Figure 4-8). To the northwest of the Sierra Leone segment, syn-rift deformation is associated with strike-slip faulting (Figure 4-8a), whereas, to the southeast, it formed more classic tilted blocks (Figure 4-8b). To the northwest, a distal crustal domain, thinner than the oceanic crust has been identified and interpreted as a hyperextended continental crust. That domain is associated with a slight Moho upwarp and buried under a thick sedimentary unit showing normal faults and strike-slip flower structures (Figure 4-2 and Figure *4-8*a). The width of the necking zone along that segment is about 80 km (Figure 4-8a and b).

As a difference, the Liberia segment shows a narrower necking zone (ca. 30 km; Figure 4-8c and d). The syn-rift fault pattern is not well imaged, but could be associated with landward tilted blocks with fan-shape syn-rift deposits observed only very locally in one proximal half-graben. Most of syn-rift deposits form seaward reflectors, suggesting interbeded volcanic lava flows. Aptian-Albian and Jurassic interbedded basalts and tuffs have indeed been drilled (Bennett and Rusk, 2002). If these reflectors are indeed Jurassic in age, i.e. contemporaneous of the Central Atlantic Magmatic Province (CAMP), this suggests an earlier phase of stretching of the crust of this segment during the Central Atlantic rifting. Triassic to Early Jurassic desertic sands and basalts have indeed been identified in the Foz do Amazonas basin, along the South American conjugate margin of the Sierra Leone-Liberia segment (Figueiredo et al., 2007). Furthermore, the NW- trend of the Sierra-Leone margin segment matches the Central Atlantic opening direction, as well as a NW-trending transform system identified along the Liberia margin segment on the seafloor

bathymetry (Bennett and Rusk, 2002). These observations would be consistent with deformation of the Liberia margin segment during the Triassic-Early Jurassic prior to the Equatorial Atlantic rifting.

We therefore suggest that the Sierra Leone-Liberia margin experienced a first extensional deformation during the Triassic-Early Jurassic, related to the Central Atlantic rifting, forming the southernmost rifts of that system. The main rifting followed during the Lower Cretaceous rifting of the Equatorial Atlantic. The structural contrast between the Sierra Leone and the Liberia margin segments also suggests different syn-rift deformation regime (Figure 4-2 and Figure *4-8*). Along the Liberia segment, deep structures have been identified within the crust that may be attributed to older deformations events, such as the Neoproterozoic Panafrican and Hercynian orogens. These may have imprinted the continental lithosphere rheology, and in doing so, influenced the segmentation.

The Upper Cretaceous early post-rift stratigraphic architecture also varies between the Sierra Leone to Liberia segments. In Liberia, Upper Cretaceous deposits were mostly preserved in the distal part of the margin, forming a fan-shape wedge onlapping landward and downlapping seaward as along the Western Ivory Coast and Ghana transform segments. As a difference, along the Sierra Leone segment, the distal Upper Cretacous geometry seems to be affected by a complexe paleo-relief of the margin basement at the end of the rifting. Numerous turbiditic systems can be observed within those distal deposits, suggesting multiple point sources along the margin during the Upper Cretaceous (e.g. Reading and Richards, 1994).

These observations suggest that the difference in syn-rift deformation regimes along the Liberia - Sierra Leone segments has also had a strong influence on the immediate post rift history of this segment.

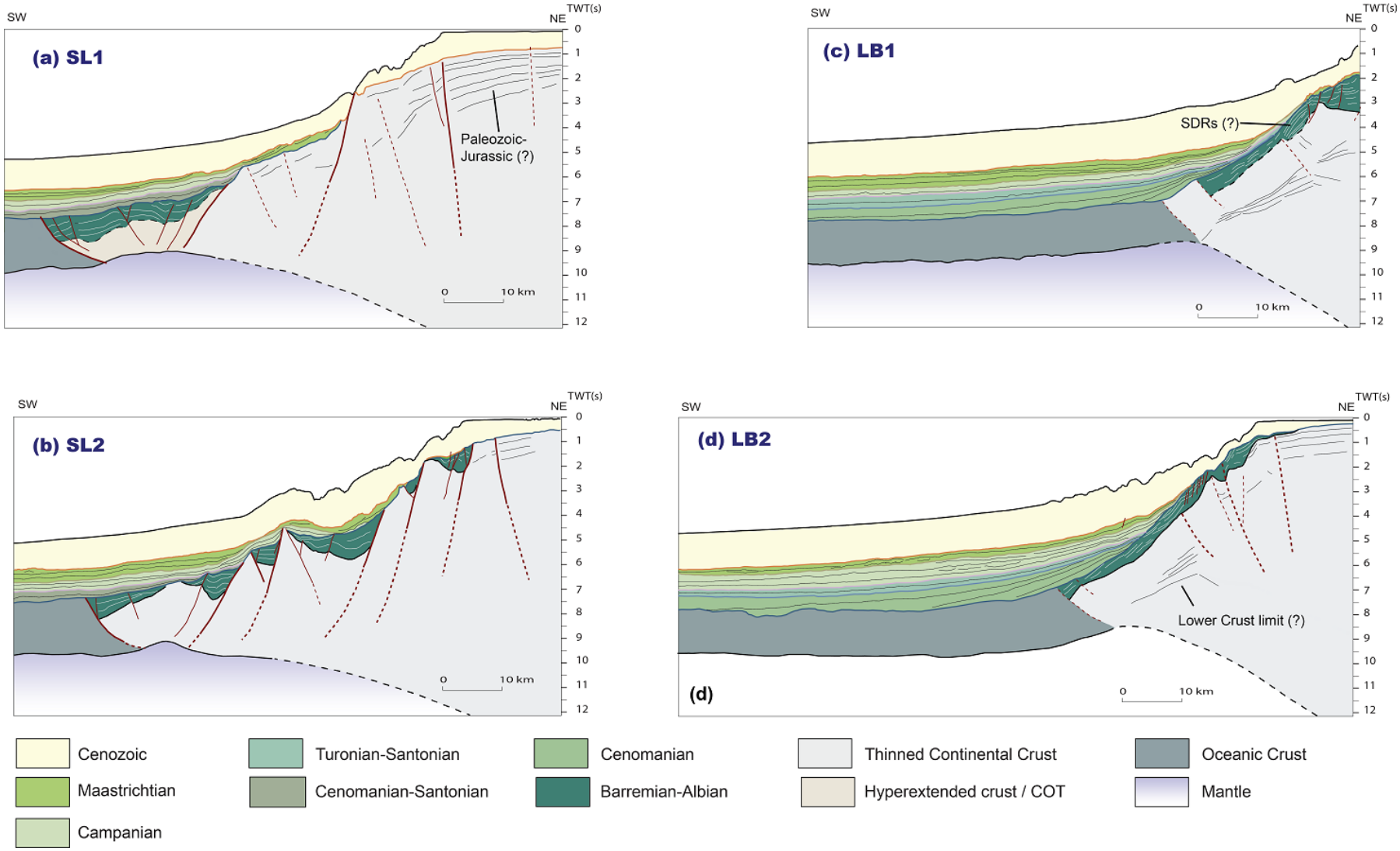

Figure 4-8 Structural and stratigraphic Interpretation of regional cross-sections along the Sierra Leone-Liberia margin segment. See location in Figure 4-2.

4.5. Margin Segmentation

The segmentation of the African Equatorial Atlantic margin from Sierra Leone to Benin is controlled by transform faults (Figure 4-2). The early post-rift stratigraphic architectures vary from one segment to another, with different deformation regimes (Figure 4-9). We discuss here the impact of this segmentation on present day crustal geometry and on post-rift stratigraphic architecture. To do this, we first measured the obliquity of each segment as the angle between the relative plate motion direction (given by the orientation of transform fault) and the regional trend of margin segment (given by the orientation of the COB). Transform margin segments have therefore a 0° obliquity, whereas divergent segments of the Equatorial Atlantic have a 75° obliquity (Figure 4-10). The Togo-Benin segment, with a 30° obliquity is an intermediate oblique segment. Also, the Sierra Leone-Liberia segment is transform with respect to the Central Atlantic system, but oblique with respect to the Equatorial Atlantic.

4.5.1. Regimes of Crustal Stretching and Obliquity

The width of the necking zone increases with the obliquity of the margin segments: from less than 40 km along transform segments to over 100 km along divergent ones (Figure 4-10). Different 3D deformation regimes along transform and divergent segments (strike-slip vs normal faulting) can explain this relationship between obliquity and the necking width of a segment. This relationship is however not preserved, when crustal stretching involved several stages. Indeed, from the Sierra Leone to the Liberia segments, the obliquity increases with regard to both Central and Equatorial Atlantic opening directions, whereas the necking width decreases. This could result from the fact that they may have experienced two extension phases in different directions during both the Central and Equatorial Atlantic rifting. Occurrence of older structures (e.g. Panafrican mobile belts) may also have impacted the localization of syn-rift deformation and, in doing so, impacted the necking zone width.

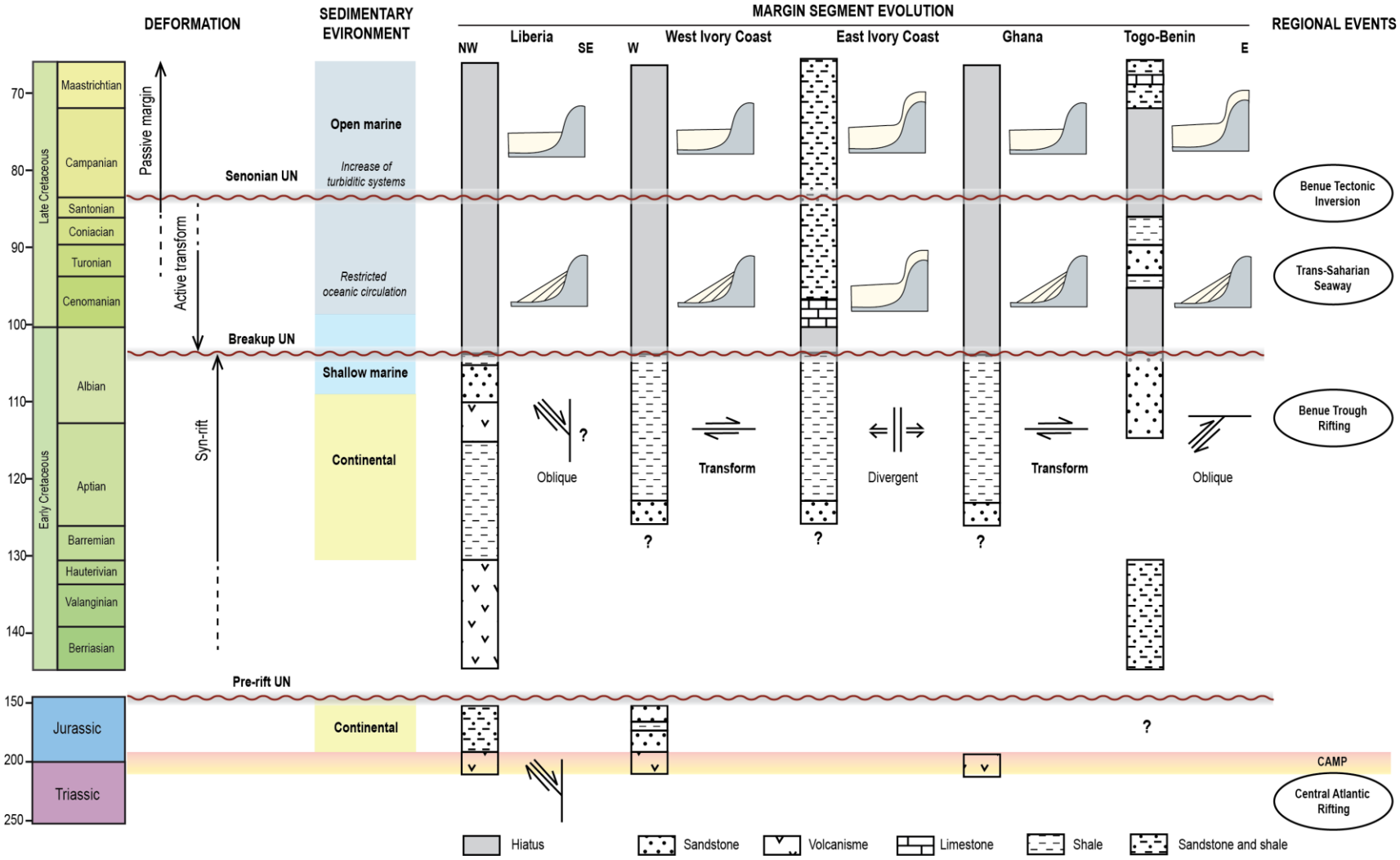

Figure 4-9 Synthetic chart summarizing the deformation regimes and the regional depositional environments along the Equatorial Atlantic margin, as well as major deformation or sedimentary events of the African plate. Tectonic and stratigraphic evolution of each margin segment is presented by a synthetic lithologic log of the shelf and carton-illustrated depositional patterns.

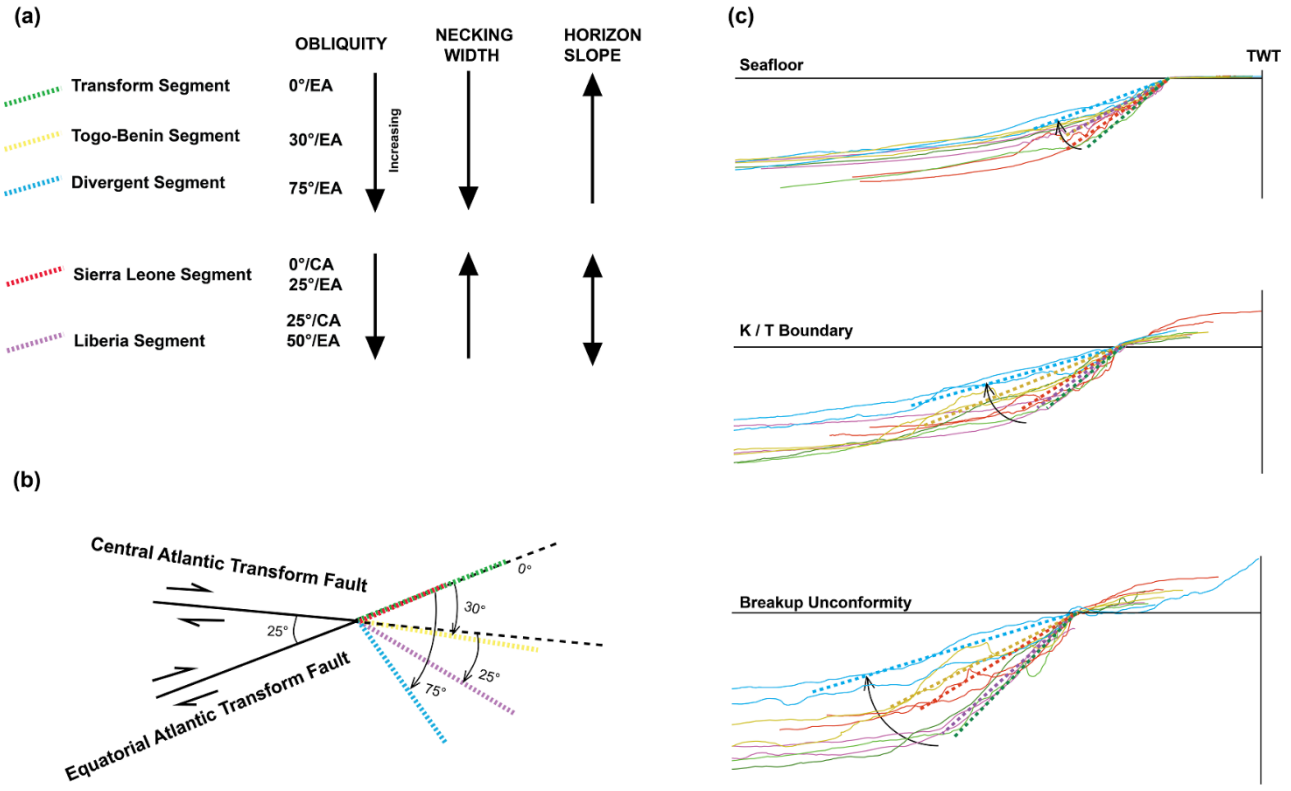

Figure 4-10 Segmentation of the Equatorial Atlantic margin based on obliquity, width of crustal stretching and thinning, and post-rift stratigraphic geometry of each segment. Seafloor horizon, Cretaceous-Cenozoic boundary and the Breakup unconformity were compiled from regional sections and superposed at the major slope rupture of horizon. Note that the horizons were with a two-way time axe, but not in depth, and only the relative angle between horizons of different margin segments should be considered.

The cause of variations of obliquity from one segment to the other is not clear. Pre-existing crustal weakness (e.g. Panafrican orogeny) or fault patterns may act as inheritance and influence the localization of deformation and syn-rift faulting orientations. Nevertheless, the Ivory Coast margin formed by cutting through the West African craton, separating the southernmost part on the South American side (Klein and Moura, 2008b) and this does not support an inheritance controlled obliquity. Deep mantle anomalies may impact lithospheric deformation localization by modifying the thermal field (Koptev et al., 2015, 2016). This may be expressed by magmatism on the surface during the rifting that has been documented only sparsely along the Equatorial Atlantic margins during the Valanginian-Late Albian (140-100 Ma, Ye et al., Submitted).

4.5.2. Early Post-rift Stratigraphic Architecture

The stratigraphic architecture of the early post-rift (Upper Cretaceous) in the proximal domain also shows major differences in the two end-members type of segments (transform and divergent; Figure 4-9). The proximal parts of the early post-rift sedimentary wedges are preserved only on the shelf of divergent segments. Along transform segments, they are represented by an erosion surface on the shelf and the distal parts of the wedge are preserved only on the slope and abyssal plain (Figure 4-9).

To further characterize the geometry of the early post-rift wedge, we measured, along every segment, the present-day averaged maximum slopes of the reflectors corresponding to the seafloor, the K-T boundary reflector and the Breakup Unconformity reflector (Figure 4-10). This analysis shows that the present-day slope of those surfaces increases as the obliquity of margin decreases (from transform to divergent segments) everywhere except along the Liberia segment. This suggests that a first-order control on the post-rift stratigraphic architecture is the structuration of margin segment during the syn-rift, and in particular, its obliquity.

4.6. Vertical Displacements

Our observations suggests that the different segments of the African Equatorial Atlantic margin experienced contrasting histories of post-rift vertical displacements depending on their maegin type and obliquity (transform or divergent segments; Figure 4-11).

During the early post-rift (Upper Cretaceous), the divergent segment (Eastern Ivory Coast) experienced mostly thermal subsidence (except for a transient potential uplift event recorded on the platform during the Santonian; Figure 4-5 and Figure *4-9*). For transform margin segments (Western Ivory Coast and Ghana segments), the Upper Cretaceous is recorded by a hiatus on the shelf suggesting sediment by-pass across the platform and/or erosion. There are two possible scenarios in terms of vertical displacements on the shelf of transform margin segments during the early post-rift in that case (Figure 4-11): (1) Either Upper Cretaceous sediments were deposited

and eroded later on (along with some of underlying syn-rift deposits) in response to an accommodation reduction driven by an uplift event, or, (2) sediments by-passed the shelf throughout the Upper Cretaceous (also eroding away some syn-rift deposits) in absence of accommodation creation related to a steady uplift compensating thermal subsidence. In the first case, the uplift event could correspond to the Santonian event documented on the divergent segment (Eastern Ivory Coast). In the second case, the more steady uplift on the shelf throughout the Upper Cretaceous could be related to a progressive tilting of the margin and/or to the flexure response of the stretched lithosphere. Unpublished vitrinite reflectance data from wells located on the shelf indicate maximum burial temperatures compatible with over 500 km of erosion during the Upper Cretaceous (M. Dall'Asta, personal communication). These data are compatible with Upper Cretaceous sediments first deposited on the shelf, then removed, in response to uplift driven accommodation reduction on the shelf.

In the case of transient event of shelf uplift, several mechanisms could cause it during the Upper Cretaceous along the Equatorial Atlantic margin: (1) a regional tectonic compression that has been documented in the Benue Trough during the Santonian inversion (Benkhelil, 1989; Guiraud and Bosworth, 1997), (2) an uplift in response to a change in lateral stress regime and a change in spreading direction (Fairhead and Binks, 1991), or (3) mantle upwelling or edge convection under the margin (Matton and Jébrak, 2009). In the case of a more steady uplift counteracting subsidence of the proximal domain of the margin during the Upper Cretaceous, two main causes may be invoked. First, the flexural response of the stretched lithosphere to the thermal subsidence load and erosion/sedimentation (un)loading may induce an uplift in the proximal part of the margin, in particular during the early post-rift (e.g. Rouby et al., 2013). It has been shown that the narrower the necking zone, the larger the associated flexural uplift (e.g. van der Beek et al., 2001; Rouby et al., 2013). However, this Upper Cretaceous post-rift margin rejuvenation was also observed along other Atlantic margins, such as the North America margin (uplift at 85-65 Ma; Amidon et al., 2016), the NE Brazil margin (84-72 Ma; Turner et al., 2008; Japsen et al., 2012). The synchronous Upper Cretaceous rejuvenation over such a broad region suggests an alternative explanation of a very large-scale process (x 100-1000 km), such as mantle upwelling. Those two processes (flexure and mantle driven deformation) are not mutually exclusive.

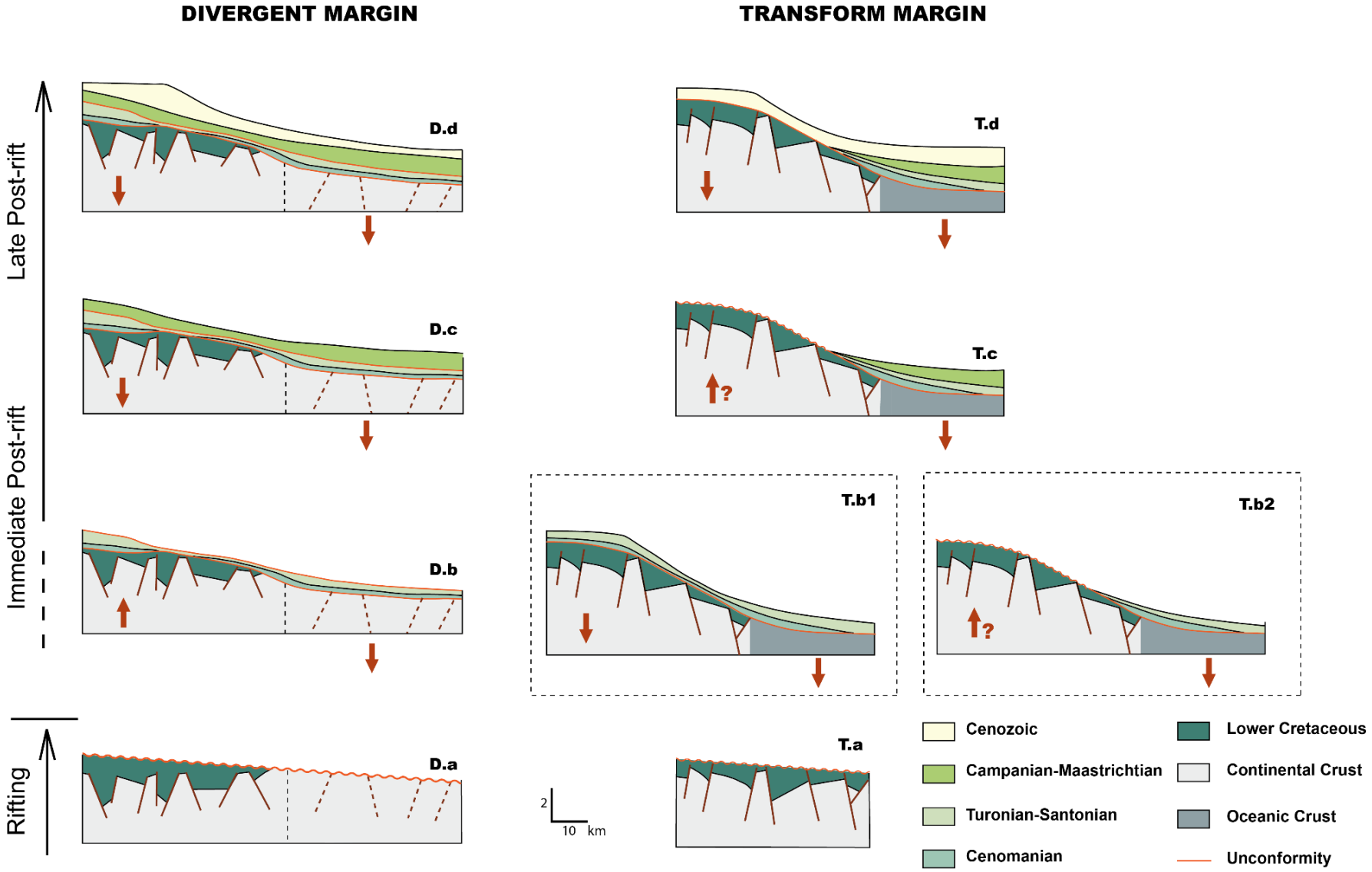

Figure 4-11 Schematic evolution of the different vertical displacement histories along divergent and transform margin segments. See text for details.

The distal parts of the transform margin basins experienced mainly thermal subsidence during the Upper Cretaceous, as evidenced by the tilting of initially horizontal turbidite deposits (Figure 4-4a and Figure *4-9*). Also, the seaward downlap of the immediate post-rift strata could result from the progressive tilts of initially flat lying strata by the cooling of newly-formed oceanic crust.

4.7. Conclusion

We analyzed the structural variability of the various segments of the African Equatorial Atlantic margin as well as the stratigraphic architecture of their early post-rift sedimentary wedge.

(i) Segmentation of the margin has been, at least partly, driven by transform faults, defining segments with different obliquities with respect to their orientation. Obliquity increases from transform to divergent segments, along with the width of the crustal necking zone.

(ii) Early post-rift stratigraphic architecture appears to be largely controlled by this obliquity: transform segments show steeper slopes of all the post-rift horizons than divergent segments. This correlation between obliquity and post-rift stratigraphy was however not observed, when the margin underwent a more complexe rifting history, such as the Sierra Leone-Liberia margin.

(iii) Also, the preservation of the early post-rift sedimentary wedge in the proximal domain differs in transform and divergent segments. Upper Cretaceous shallow deposits are preserved along divergent segments, whereas, on the shelf of transform segment, Cenozoic sediments lie directly on the Late Albian Breakup unconformity.

(iv) Transform and divergent segments accordingly underwent different histories of early post-rift vertical displacements. The divergent segment (Eastern Ivory Coast) experienced mostly thermal subsidence, allowing for the preservation of the proximal Upper Cretaceous wedge. It was nonetheless impacted by some transient uplift of the platform domain during the Santonian (84 Ma). Transform segments, with narrower necking zones than divergent segments, underwent larger flexural uplift in their proximal parts that would account for the lack of preservation of the early

post-rift wedge of most proximal terms. However, the Santonian post-rift rejuvenation event observed along several Atlantic margins, related to either mantle driven dynamics or regional changes in lateral stress regime, may superimpose along transform segments.

Further comparison with the conjugate margin in South America would provide insights in understanding the mechanisms driving margin segmentation and would allow for further deciphering of the relative contribution of syn-rift deformation inheritance and regional mantle or plate dynamics on the early post-rift evolution of those margins.

4.8. Ackowledgments

Total Exploration and Production funded this study through the Transform Source-to-Sink Project (TS2P). We acknowledge Total for providing data and for allowing publication of the study. Total R&D research group is thanked for discussions as well as scientific and technical support.

CHAPTER 5 : ESTIMATION OF ACCUMULATED SEDIMENTARY VOLUMES ON THE AFRICAN EQUATORIAL ATLANTIC MARGIN

5.1. Introduction

In order to investigate how the sedimentary accumulation history of the Equatorial Atlantic margin is related to changes in the continental erosion in the drainages areas of the craton, we evaluated the volumes of Meso-Cenozoic sediments of each basin (Master 2 project, A. Loparev). We used a cross section-based method (Guillocheau et al., 2012) where the terrigenous solid volume of accumulated sediments for each time interval is quantified by interpolation of regional cross-sections and then corrected from in situ carbonate production and remaining porosity after compaction. We also estimated uncertainties in the estimated solid volume. The temporal variation of accumulation gave insights into the filling history of each basin, as well as the variations in continental relief triggered by possible climate and deformation events.

5.2. Material and Method

5.2.1. Data

To estimate the volume of sediments accumulated in the Equatorial Atlantic basins (Ivory Coast, Ghana-Benin and Sierra Leone-Liberia basins), we used various types of data (Figure 5-1): exploration seismic profiles and well data provided by TOTAL, published vintage seismic profiles (Emery et al., 1975), bathymetric and basement maps (ETOPO5, Laske and Masters, 1997), and age of oceanic crusts (Milesi et al., 2010).

We used four Cretaceous horizons interpreted from Sierra Leone to Benin: Top Albian (~100.5 Ma), Top Cenomanian (~94 Ma), Top Santonian (~84 Ma) and Top Maastrichtian (~66 Ma) (Figure 5-2). In the Sierra Leone-Liberia Ivory Coast basins, we used a fifth Top Campanian (~72 Ma) horizon. In Ivory Coast and Ghana-Benin basins, we also used six Cenozoic horizons that were interpreted by D. Huyghe: Top Paleocene (~56Ma), Top Eocene (~34Ma), Oligocene unconformity (~ 31 Ma), and three Miocene horizons (Figure 5-2; Huyghe, 2016).

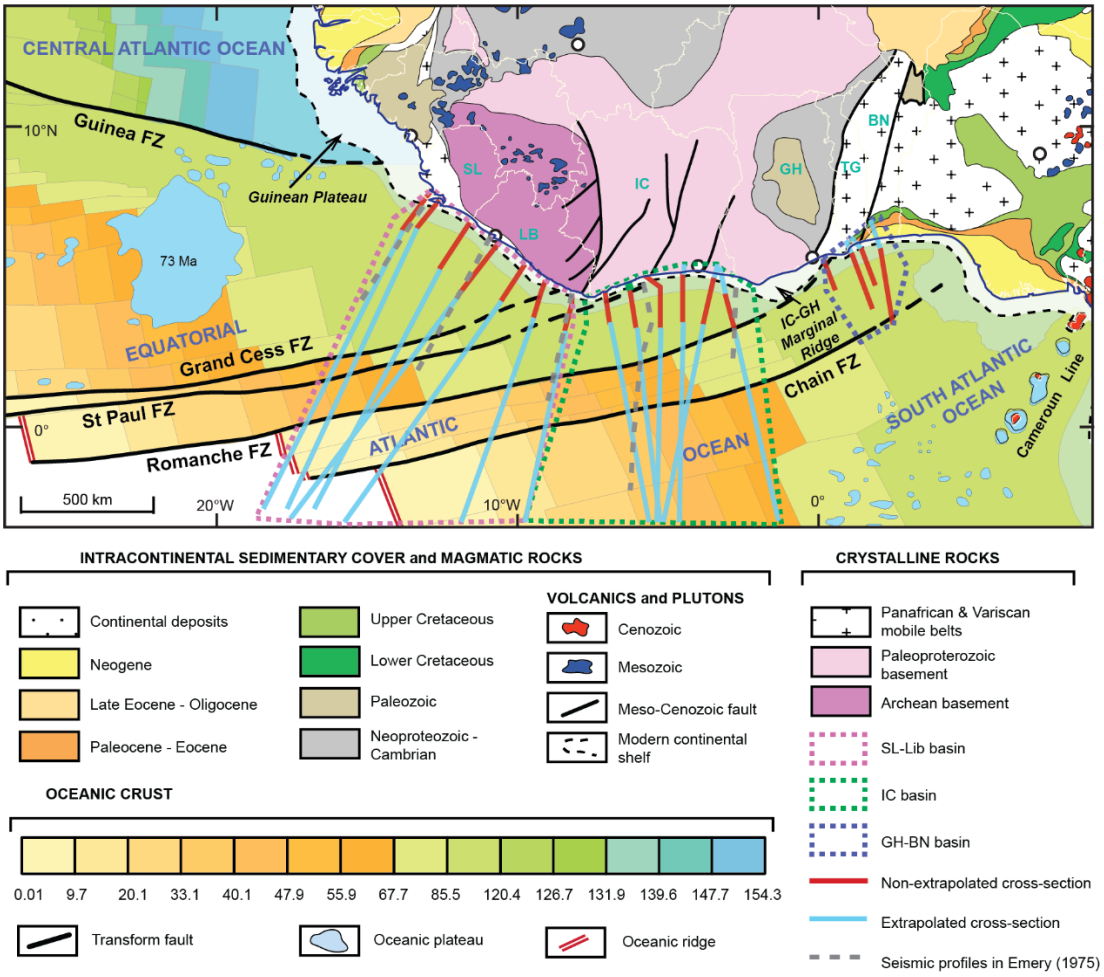

Figure 5-1 Simplified onshore geologic map and oceanic curst ages of study zone (modified from Choubert and Faure-Muret, (1988). Location of non-extrapolated and extrapolated cross-section are indicated, as well as used seismic profiles from Emery (1975). SL: Sierra Leone, LB: Liberia, IC: Ivory Coast, GH: Ghana, TG: Togo, BN: Benin.

The estimation of solid volume and accumulation rates include the following 6 steps:

- TWT to Depth Conversion,
- cross-sections extrapolation,
- volume and accumulation rate estimation,
- in situ production correction,
- porosity correction,
- uncertainties estimation.

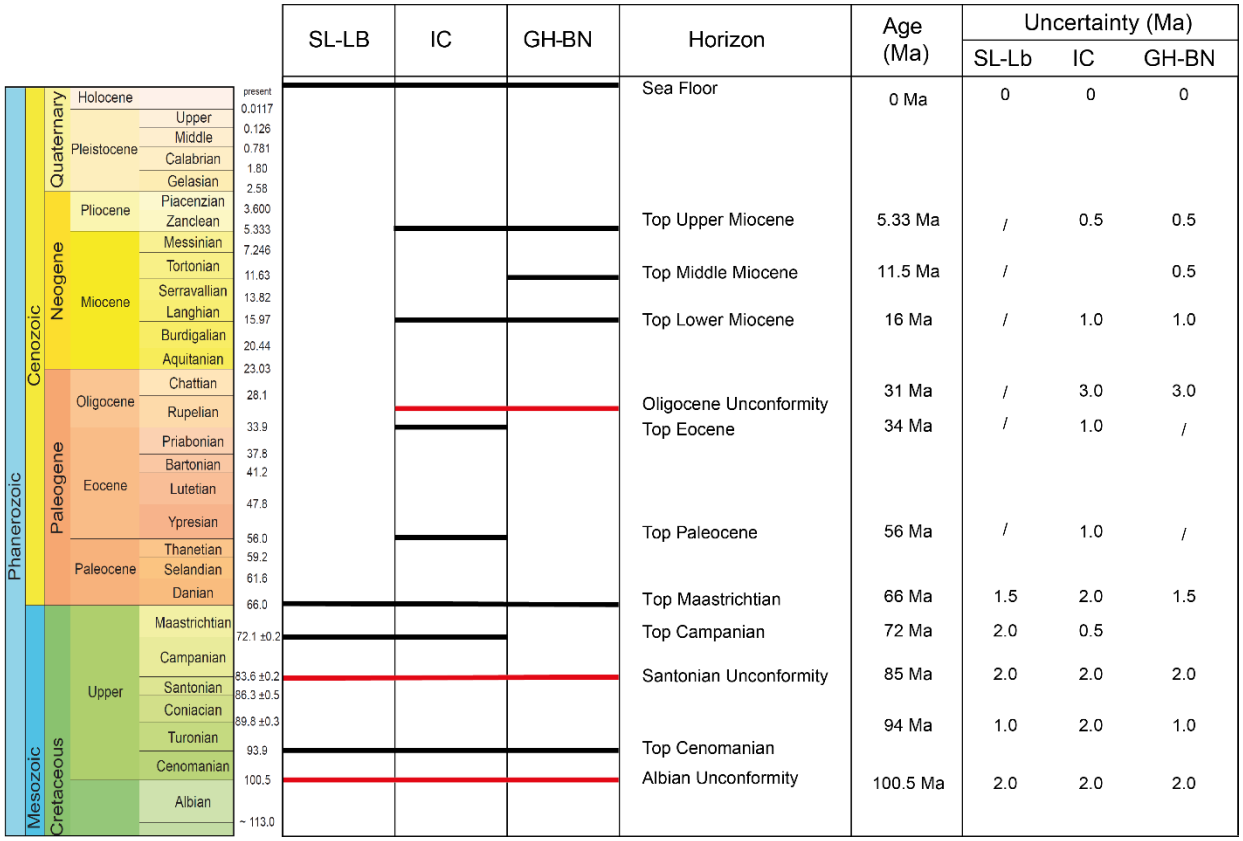

SL-LB	IC	GH-BN	Horizon	Age (Ma)	Uncertainty (Ma)		
					SL-Lb	IC	GH-BN
			Sea Floor	0 Ma	0	0	0
			Top Upper Miocene	5.33 Ma	/	0.5	0.5
			Top Middle Miocene	11.5 Ma	/		0.5
			Top Lower Miocene	16 Ma	/	1.0	1.0
			Oligocene Unconformity	31 Ma	/	3.0	3.0
			Top Eocene	34 Ma	/	1.0	/
			Top Paleocene	56 Ma	/	1.0	/
			Top Maastrichtian	66 Ma	1.5	2.0	1.5
			Top Campanian	72 Ma	2.0	0.5	
			Santonian Unconformity	85 Ma	2.0	2.0	2.0
			Top Cenomanian	94 Ma	1.0	2.0	1.0
			Albian Unconformity	100.5 Ma	2.0	2.0	2.0

Figure 5-2 Used regional horizons from seismic and well data interpretation in Sierra Leone-Liberia (SL-LB), Ivory Coast (IC) and Ghana-Benin (GH-BN) basins and their stratigraphic ages and associated uncertainties. Major erosional unconformities are in red lines, which present higher age uncertainties (modified from Loparev, 2016).

5.2.2. TWT to Depth Conversion

The first step is to convert selected horizons from two-way time (TWT) to depth (Km). For doing this, we defined a different velocity law for each basin.

In the Ghana-Benin basin, we used a two-layer velocity law: one layer for the Cenozoic, and another for the Upper Cretaceous. For each layer we used a linear function (1), taking into account the increase of velocity with depth due to compaction (see Japsen, 1993 for further explanation):

$$V(z) = Vo + kz \qquad (1)$$

where V(z) is the velocity at depth z, V_0 is the initial velocity, k is the velocity gradient (s^{-1}). V_0 and k were determined and calibrated to well log measurements. k is fixed here to be 0.5 s^{-1}. V_0 of 1500 m/s is used for the Cenozoic layer, 2350 m/s for the Upper Cretaceous layer.

In the Ivory Coast basin, we defined a polynomial law (2) from velocity measurements in 12 wells:

$$y = 0.7817x + 0.0002x^2 \qquad (2)$$

where x is the two-way time (s), and y is the depth (m).

In the Sierra Leone-Liberia basin, we defined another polynomial law (3) based on 8 wells:

$$y = 0.843x + 0.000146x^2 \qquad (3)$$

We checked depth conversion by measuring the deviation of depth converted horizons at wells and ensured that the uncertainty remains under 15%.

5.2.3. Cross-sections Extrapolation

We first constructed cross-sections from depth converted horizons. Since exploration seismic profiles are usually limited to the proximal part of the margin, onshore coastal basins (e.g., Togo-Benin embayment) and distal parts of the sedimentary system are not covered by those cross-sections. We first extrapolated cross-sections landward to bridge the gap between the seismic profiles and landward sediment onlaps in coastal basins using mostly the geological map. To incorporate sediments deposited in the distal part of the system into the abyssal plain, which constitute a non-negligible quantity of terrigenous sediments transported by gravity processes, we also extrapolated cross-sections towards the present-day oceanic ridge to the edge of the basin. We used published seismic profiles (Emery et al., 1975), bathymetric and basement maps (ETOPO5; Laske and Masters, 1997), and the age of oceanic crusts to avoid older sediments to be extended upon younger oceanic crust. We constructed 7 extrapolated cross-sections in the Sierra Leone-Liberia basin (Figure 5-3) and 6 cross-sections in Ivory Coast (Figure 5-4). We did not extrapolate the 4 cross-sections of the Ghana-Benin basin (Figure 5-5), because the distal parts of this margin segment received a large sedimentary input from the Niger Delta. This input has been studied separately at Geosciences Rennes (G. Beseme, Master 2 project, 2016).

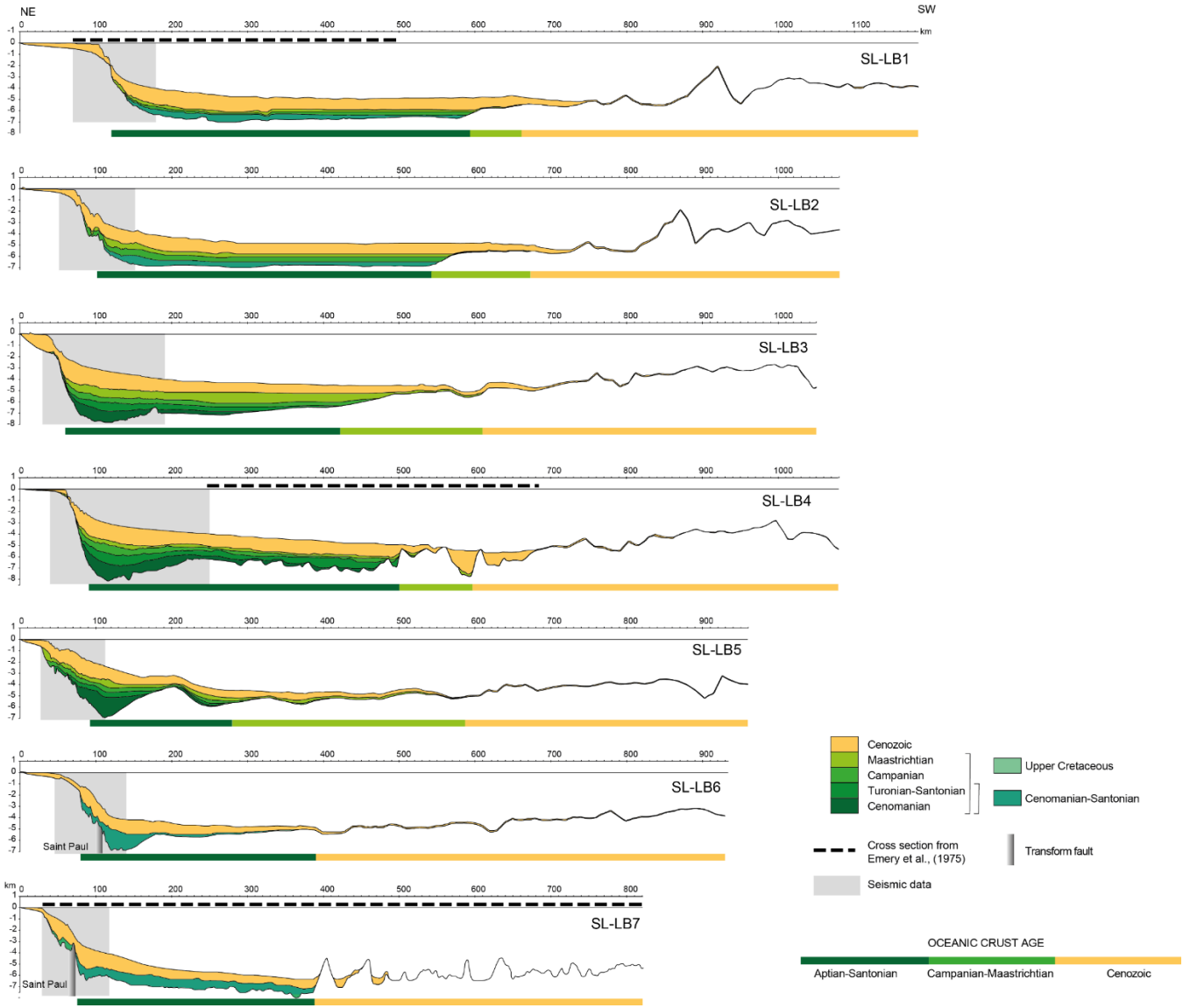

Figure 5-3: Seven extrapolated cross-sections along the Sierra Leone-Liberia margin from North to South (SL-LB1 to SL-LB7). Location is indicated in Figure 5-1.

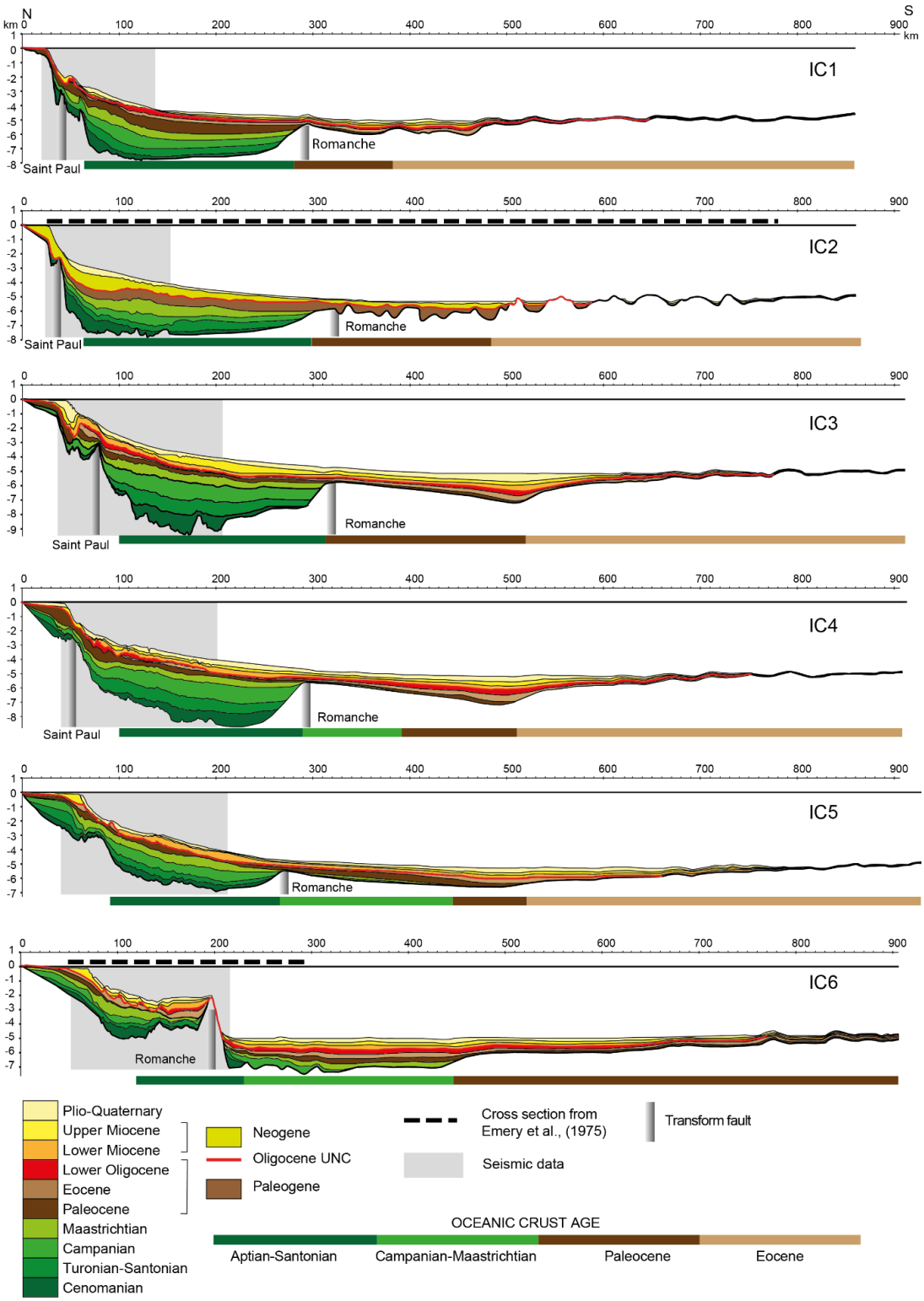

Figure 5-4 Extrapolated cross-sections along the Ivory Coast margin from West to East (IC1 to IC7). Location is indicated in Figure 5-1.

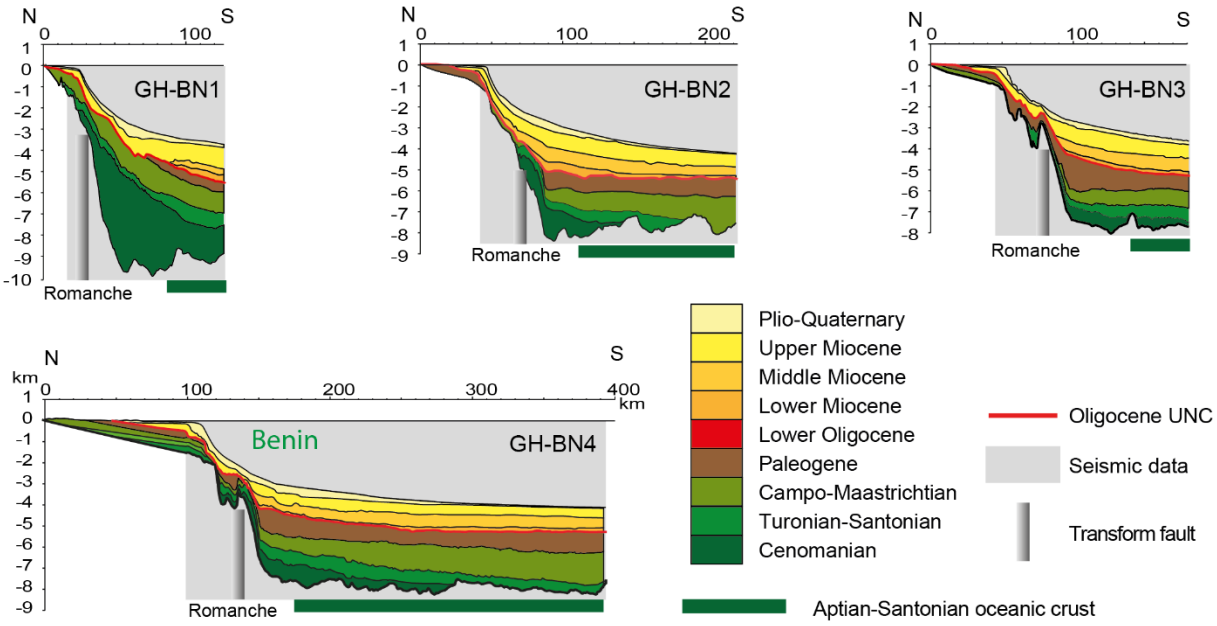

Figure 5-5 Non-extrapolated cross-sections along the Ghana-Benin margin from West to East (GH-BN1 to GH-BN7). Locations are indicated in Figure 5-1.

5.2.4. Volume and Accumulation Rate Estimation

The principle of the method (Guillocheau et al., 2012) is to interpolate cross-sections representing the variability of the stratigraphic architecture of the basin along the margin (Figure 5-6). For each time interval, the mean thickness and accumulation rate are then interpolated between the cross-sections. The product of the mean thickness and the deposition area gives the accumulated volume for each time interval (Figure 5-1).

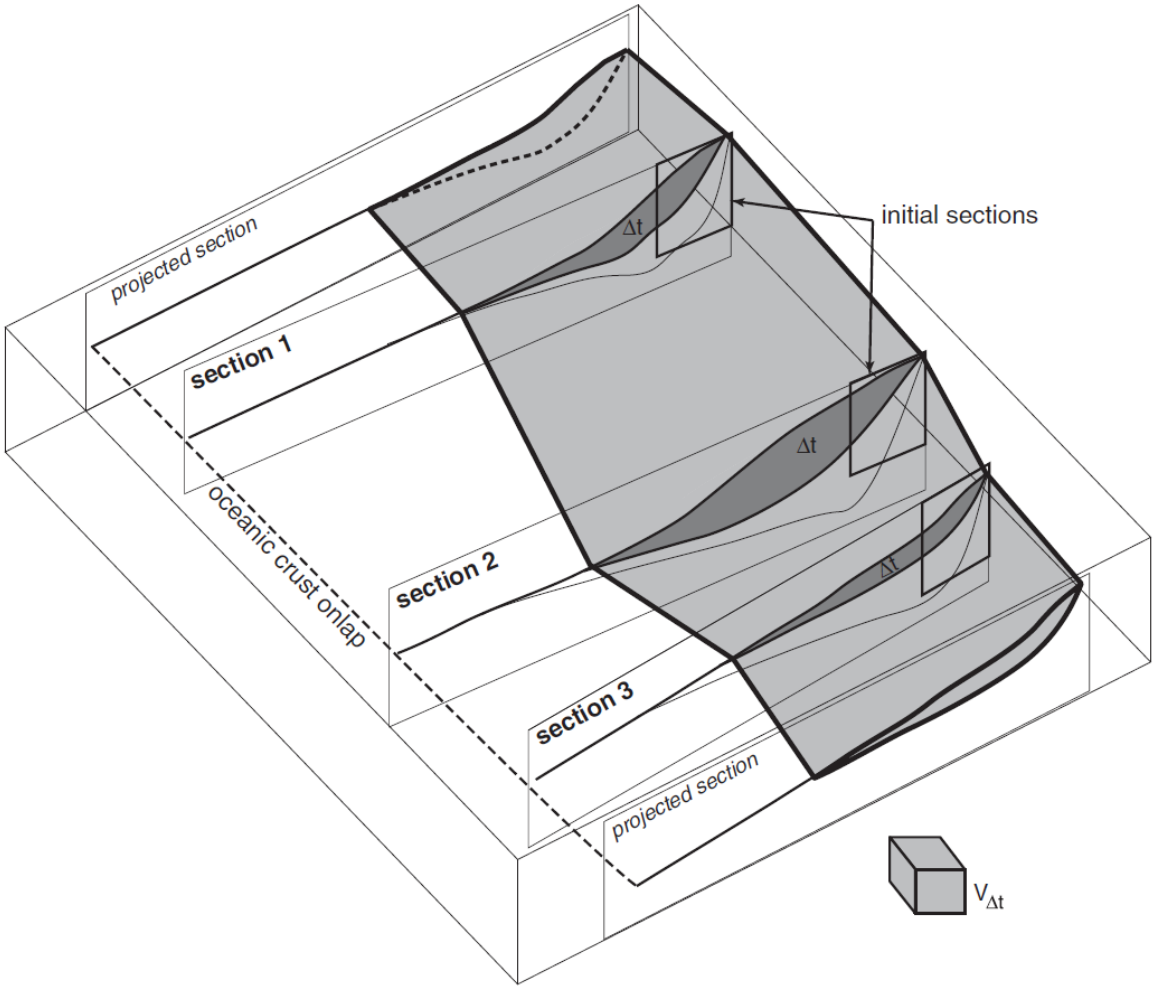

Figure 5-6 Method used for sedimentary volume and accumulation rate estimation. The volume of sediment VΔt in the basin during the time interval Δt is estimated by an interpolation between cross-sections. Cross-sections are selected to represent the variability of stratigraphic architecture of the basin and cover the whole sedimentary wedge from onshore to the distal oceanic basin. (After Guillocheau et al., 2012)

5.2.5. *In situ* Production Correction

In order to extract the terrigenous portion of the deposited volume, which is the only part of the sediments that can be compared with eroded crust, we estimated and removed the content of *in situ* sediment productions (i.e. carbonates). To do this we compiled the carbonate contents of 9 wells in Ghana-Benin proximal basin (mostly on the shelf), 9 wells in Ivory Coast proximal basin

and 5 wells in Sierra Leone-Liberia proximal basin (Figure 5-7a, b and c). We estimated the mean percentage of carbonates and its variability for each time interval in each basin (Figure 5-7d).

Other *in situ* productions, such as volcanics, cherts and organic matters were not estimated here assuming they were negligible since they had been observed only locally in a limited number of wells (Pletsch et al., 2001).

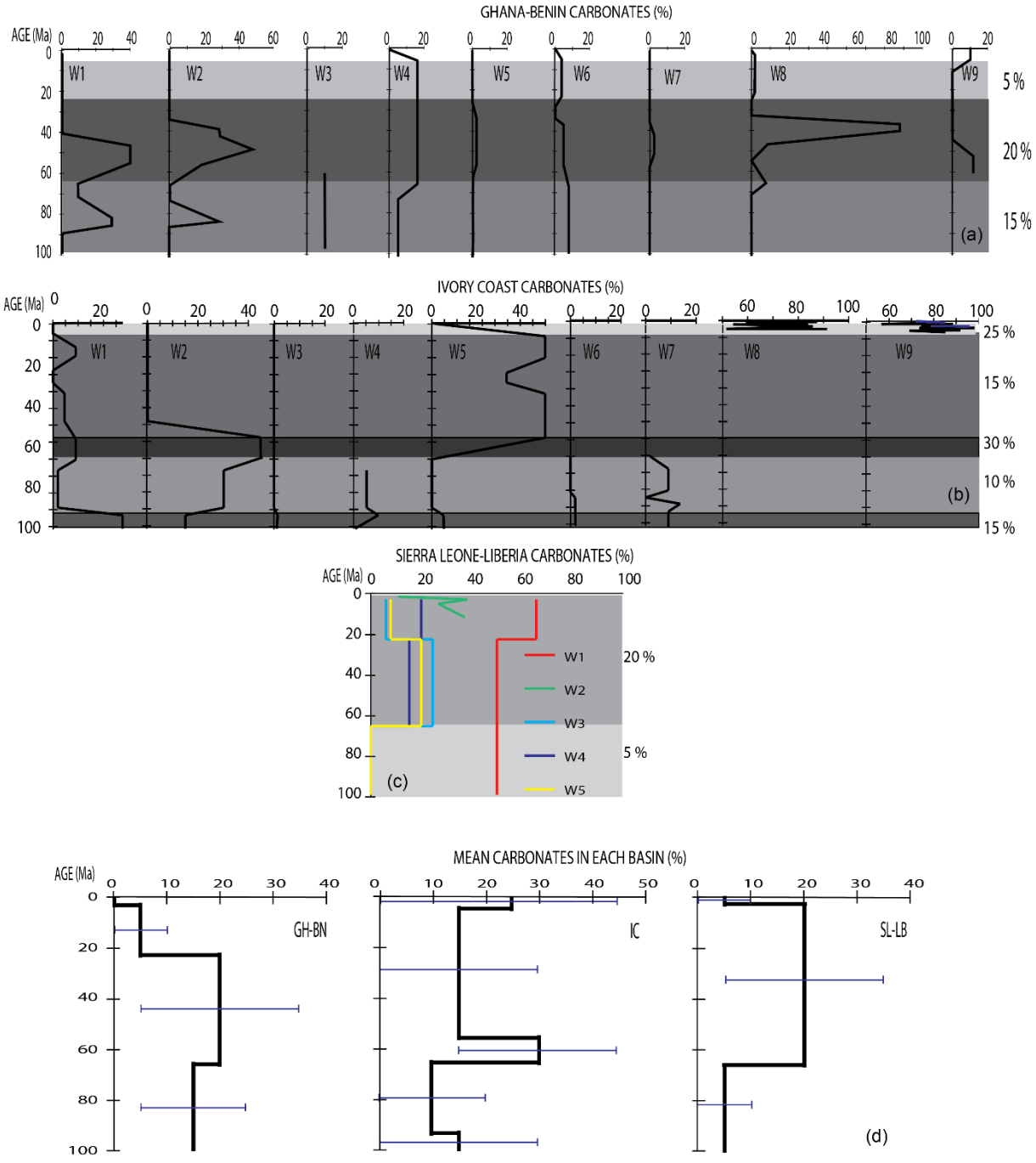

Figure 5-7 (a) 9 compiled wells with $CaCo_3$ percent in Ghana-Benin; (b) 9 compiled wells with $CaCo_3$ percent in Ivory Coast; (c) 5 compiled wells with $CaCo_3$ percent in Sierra Leone-Liberia; (d) Estimation of mean carbonate percent for the Ghana-Benin, Ivory Coast and Sierra Leone-Liberia basins with uncertainties.

5.2.6. Porosity Correction

Porosity remaining after compaction must be also corrected in order to obtain the solid volume of terrigenous sediments. Porosity decreases with depth and compaction and depends on the sediment lithology. We used an exponential law (4) (Figure 5-8):

$$\emptyset(z) = \emptyset_0 e^{-cz} \qquad (4)$$

Where $\emptyset(z)$ is the porosity at depth z, $\emptyset_0$ the porosity at the surface and c the compaction factor depending on the lithology. In this study, $\emptyset_0$ is equal to 49% for sand, and 63% for clay. c is 3700 km^{-1} for sand and 2000 km^{-1} for clay.

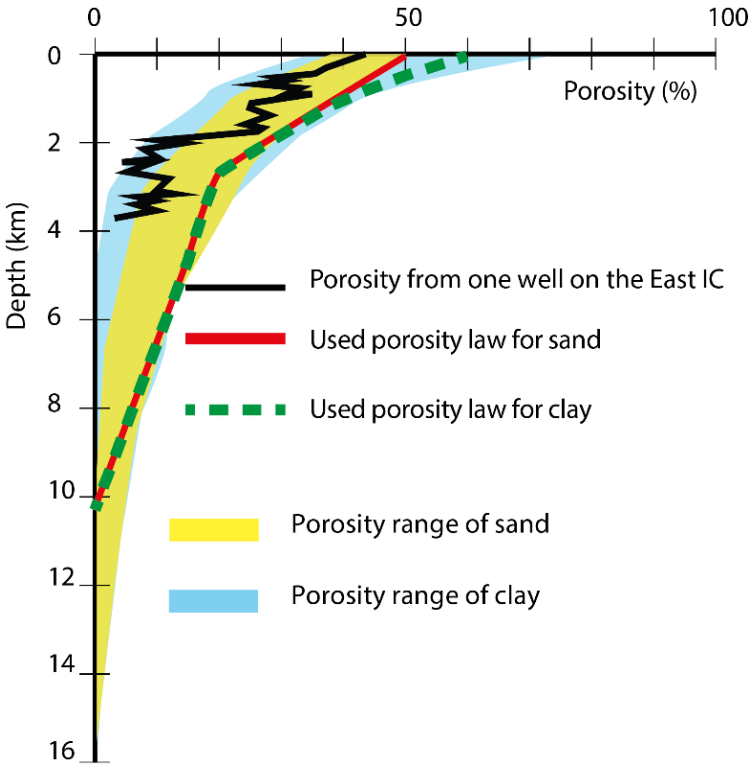

Figure 5-8 Used negative exponential law of porosity depending on the depth. Porosity range of sand and clay are from Dauteuil et al. (Submitted).

Averaged porosity ($\emptyset|$) between the depth z1 and z2 was then obtained by:

$$\emptyset| = (\frac{\emptyset_0}{c}) \frac{e^{-cz_1} - e^{-cz_2}}{z_1 - z_2} \quad (5)$$

The solid volume was estimated by the equation (6):

$$Vs = (1 - \emptyset|)Vt \quad (6)$$

where Vs is the solid volume, Vt the total volume.

5.2.7. Uncertainties on Absolute Ages

We used bio-stratigraphic data at well locations to attribute stratigraphic ages to depth converted horizons. We then ascribed absolute ages according to the UNESCO 2015 stratigraphic chart. Age attribution, whether stratigraphic or absolute, is associated with some uncertainty that we estimated for each horizon assuming larger uncertainties for unconfomities (Figure 5-2).

5.2.8. Uncertainties of Solid Accumulated Volume and Accumulation Rate

We estimated global uncertainties on estimated solid volumes and rates resulting from four sources of uncertainties:

- absolute ages of sediments,
- TWT-depth conversion law,
- carbonate content estimates,
- porosity correction.

To do this, volumes for each interval are calculated over 10000 times applying a random sampling of a value of each parameter within its variability. The standard deviation of the resulting values gave the uncertainty of the estimated volume or rate for each time interval.

5.3. Sedimentary Budget and Interpretation

Accumulated volumes and accumulation rates of the three basins, based on non-extrapolated cross-sections are shown in Figure 5-9A and on extrapolated cross-sections in Figure 9B. For Cenozoic, the number of time increments varies from one in Sierra Leone-Liberia to six in Ivory Coast and five in Ghana-Benin. For the Upper Cretaceous the number of time increments is more homogeneous: four increments in Sierra Leone-Liberia and Ivory Coast basins, and three in Ghana-Benin basin as the Campanian and Maastrichtian intervals were grouped.

5.3.1. Upper Cretaceous Sedimentary Budget

Non-extrapolated volumes show a peak of deposited volume during the Cenomanian in Sierra Leone-Liberia, which is followed by a decrease in volume (from about 9.1 to 6.7 $x10^{13}m^3$) until the Campanian (Figure 5-9A). A new peak of volume appears during the Maastrichtian (about $1.1x10^{14}$ m^3). The trend of accumulation rates is similar: they decrease from about $1.4x10^{13}$ m^3/Ma to $9.4x10^{12}$ m^3/Ma during the Cenomanian-Santonian, then increase to a maximum rate of about $1.9x10^{13}$ m^3/Ma. The accumulation volumes and rates follow the same trend in Ghana-Benin basin although with lower of magnitude. Maastrichtian peak was not observable because of the lower time resolution in this basin. Ivory Coast recorded a different accumulation history with a peak during the Campanian (about $8.2x10^{13}$ m^3). Accumulation rates show a Maastrichtian peak and Cenomanian increase in accumulation cannot be excluded given uncertainties. Extrapolation of cross-sections increases the accumulated volume values in Sierra Leone-Liberia and Ivory Coast basin, but they remain within the same order of magnitude (Figure 5-9B). In terms of accumulation rates, the trend is similar in Sierra Leone-Liberia and Ivory Coast, with one peak in the Cenomanian (about $1.1x10^{13}$ m^3/Ma) and the other in the Maastrichtian (about $2.0x10^{13}$ m^3/Ma).

These results show that sediment accumulation along the whole African Equatorial Atlantic margin during the Late Cretaceous is associated with two peaks: one during the Cenomanian and the other one in the Maastrichtian. The Cenomanian peak could be associated with the erosion of rift shoulders, which formed by lithospheric flexural isostasy (Rouby et al., 2013). The erosion of

rift shoulders takes usually less than 10 Ma (Rouby et al., 2013), which could explain the decrease of sedimentary flux during the Turonian-Santonian. The Maastrichtian peak maybe related to a relief reorganization triggered by a tectonic event along the margin. Indeed, a Santonian tectonic inversion affected the Benue Trough, which seems to have been reactivated during the Maastrichtian (Benkhelil, 1989; Benkhelil et al., 1988). The Santonian event seems to be a continental-scale tectonic event, which affected the margin by producing uplift. This would be attested by a forced regression wedge of Santonian age followed by Maastrichtian progradation in Eastern Ivory Coast (Chapter 4). The reason why no increase in sedimentary flux is observed during the Campanian following the Santonian event is unclear.

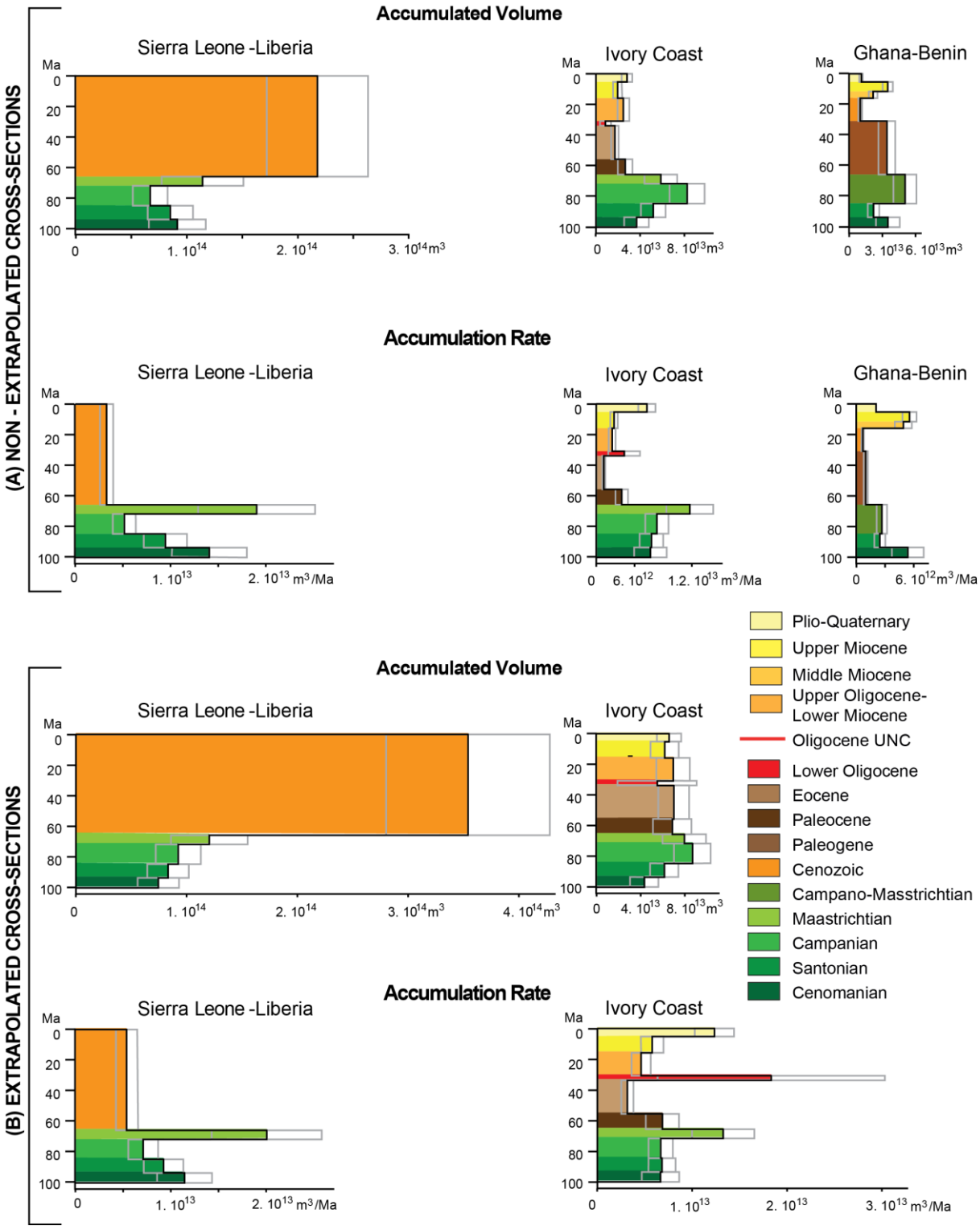

Figure 5-9 (A) Accumulated volumes and rates and their uncertainties, based on non-extrapolated cross-sections in Sierra Leone, Ivory Coast and Ghana-Benin; (B) Accumulated volumes and rates and their uncertainties estimated based on extrapolated cross-sections in Sierra Leone and Ivory Coast.

5.3.2. Cenozoic Sedimentary Budget

During the Cenozoic, higher variations in accumulated volumes and accumulation rates with higher frequency are recorded in Ivory Coast and Ghana-Benin thanks to the higher time resolution than during the Late Cretaceous. In Ivory Coast, the trends in volumes and rates are similar for the extrapolated and non-extrapolated cross-sections (Figure 5-9). Accumulation decreases during the Paleocene-Eocene (from about 6.8 to 3.1 $x10^{12}m^3$/Ma), increased in the Lower Oligocene (about $1.8x10^{13}m^3$/Ma), decreased again from the Early Oligocene to the Late Miocene before a second peak (about $1.2x10^{13}m^3$/Ma) in the Plio-Quaternary. The trends of volumes and rates are different in Ghana-Benin with a single peak in accumulated volumes (about $3.5x10^{13}m^3$/Ma) and rates (about $5.5x10^{12}m^3$/Ma) during the Late Miocene assuming extrapolation would not modify these trends.

The accumulation peak during the Early Oligocene could be more significant, as Oligocene erosion might have reworked a large quantity of older sediments (Huyghe, 2016). It may be related to the major drainage reorganization observed onshore during the Late Eocene-Early Oligocene, when the Niger River and the Volta significantly increased their catchment areas (Chardon et al., 2016). Meanwhile, the Hoggar Shield was uplifted and submitted to erosion (Ye et al., submitted). The absence of Early Oligocene accumulation peak in Ghana-Benin could be attributed to the reworking of Lower Oligocene sediments by later erosions (from Oligocene until Late Miocene) producing a large number of voluminous mass-transport deposits (MDTs: slumps, debris flows, etc., Huyghe, 2016). The Late Miocene peak could therefore be artificial because it could result from such reworkings. Contourites were also recognized (Huyghe, 2016) that could have brought sediments from the Southern African margins. The role of MDTs and contourites should be further investigated, in order to reduce the uncertainties on sedimentary volume estimation.

5.4. Conclusion

We quantified the accumulated solid volumes and the accumulation rates of terrigenous sediments preserved in the Sierra Leone-Liberia, Ivory Coast and Ghana-Benin basins of the African Equatorial margin. The methodology is based on interpolation of regional cross-sections and multiple corrections (carbonates, remaining porosity). Accumulation histories show two peaks during the Late Cretaceous: a Cenomanian peak, which could be explained by erosion of rift shoulders during the immediate post-rift, and a Maastrichtian peak that could be related to a plate-scale inversion event. During the Cenozoic, an Early Oligocene accumulation peak could be associated with the onshore drainage reorganization due to the Hoggar uplift. However, multiple Oligocene-Late Miocene erosional events may have disturbed the pre-Late Oligocene sedimentary record by reworking by mass-transport deposits.

Despite the uncertainties, these accumulation histories (Sink) form the basis for our 'source-to-sink' analysis along the African Equatorial Atlantic margin. Their comparison with onshore continental denudation histories and relief changes (Source) will be carried out bellow (Chapter 6).

CHAPTER 6 : CONTINENTAL DENUDATION HISTORY: LOW-TEMPERATURE THERMOCHRONOLOGY

6.1. Introduction

In this chapter, we quantify de denudation history of the onshore domain of the African Equatorial margin (Source study), in order to compare denudated volumes with that of the sediments accumulated on the margin (Chapter 5) by taking into account the evolving paleogeographic evolution of the onshore domain (Ye et al., submitted).

Two commonly used ways exist for quantifying erosion providing clastic sediments that fill sedimentary basins: mapping relict paleolandsurfaces of known age and thermochronological analyses. Study of paleolandsurfaces characteristic of West Africa has been carried out by Grimaud, (2014), which revealed the landscape evolution and denudation history during the Cenozoic. This method allows reconstructing ancient drainage systems and quantifying denudated volume at fairly high-resolution spatial and geological temporal scales (1-10 Ma / 10-1000 km). In this study, we focus on the pre-Cenozoic denudation history in West Africa, by using low-temperature thermochronology (AFTA, Apatite (U-Th-Sm)/He), which reveals the exhumation and burial histories of the first 3-4 km of the continental crust. The temporal resolution of this approach is relatively low, but it allows for a first-order quantification of denudation.

Sampling was carried out along three transects from Guinea to Benin, two of which were sampled by D. Chardon, D. Huyghe and D. Webster in 2014. A third transect in Ivory Coast was established by samples donated by A. Kouamelan used in his PhD work (Kouamelan, 1996). Analyses and dating of these samples were done by D. Webster (AHe dating) and M. Wildman (AFTA) at the School of Geographical and Earth Sciences, University of Glasgow.

In this chapter, I will present the main outcomes of the thermochronological study in terms of ages and thermal history models. Denudation histories along each transect were computed on the basis of temperature-time paths obtained by inversion of the data assuming a constant thermal gradient of 25°C. Denudated volumes and denudation rates were quantified by an interpolation between three transects.

6.2. Apatite Fission-Track and Apatite (U-Th-Sm)/He Dating Method

Apatite is a common phosphorous-bearing accessory mineral [$Ca_5(PO_4)_3(F,Cl,OH)$], found in the Earth's crust. Uranium and thorium are important trace elements in apatite. Three isotopes exist in natural uranium-bearing minerals: ^{238}U, ^{235}U and ^{234}U. The dominant ^{238}U with an abundance of 99.3 % experiences nuclear decay by two processes: spontaneous fission which allows apatite fission-track analysis, and α-decay (emission of a ^{4}He nucleus) on which apatite (U-Th-Sm)/He dating is based.

6.2.1. Apatite Fission-Track Analysis (AFTA)

6.2.1.1 Fission Track Age

a) Formation of fission tracks

Fission tracks occur as a result of spontaneous fission of uranium atoms (principally ^{238}U) which splits uranium nucleus into two fragments. They are considered as radiation-damage trails when positively charged fragments repel each other through the lattice with large amount of liberated energy (Figure 6-1). Fission tracks found in natural samples are called 'spontaneous tracks' or 'latent tracks'. They can be selectively enlarged by an acid etchant, such as HNO_3 solution for apatite.

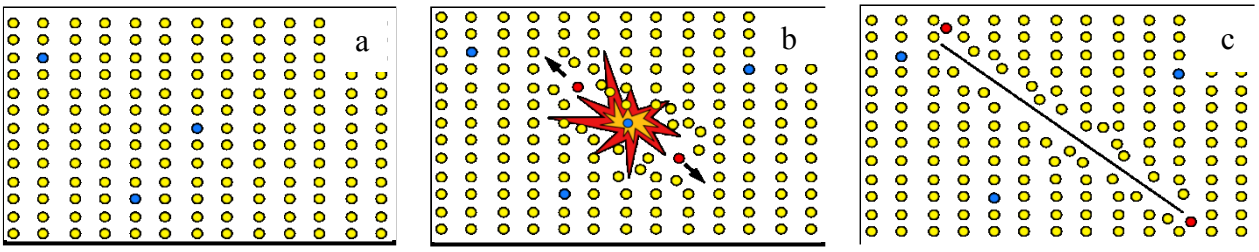

Figure 6-1 Formation of fission tracks in three steps. (a) Trace amounts of unstable radioactive 238U are present in the crustal lattice (dark circles). (b) Spontaneous fission of ^{238}U produces two highly charged heavy particles with mass numbers in the ranges of 85-105 and 130-150. They repel each other and interact with other atoms in the lattice by

electron stripping or ionization. (c) The fission particles slow down until they come to rest as the particles' energy is reduced and leaves a damage trail or fission track (modified from Fleischer et al., 1975).

b) Fission Track Age Determination

As a decay phenomenon, fission track density is a function of uranium concentration and time. So a fission track age can be calculated by measuring fission track density and the uranium content. The former is obtained by counting the number of spontaneous tracks per unit area (ρ_s). The uranium concentration is measured by counting tracks that are induced in specimen by irradiation with thermal neutrons in a nuclear reactor. The induced tracks are principally related to the fission of ^{235}U which has a large thermal-neutron capture cross-section (Donelick et al., 2005). As the ratio of ^{238}U to ^{235}U is constant in natural minerals, ^{238}U content can be deduced.

The age equation is expressed as following (Naeser and Faul, 1969; Fleischer et al., 1975):

$$t = \frac{1}{\lambda_D} \ln\left(1 + g \frac{\lambda_D \phi \sigma I}{\lambda_f} \frac{\rho_s}{\rho_i}\right) \qquad (1)$$

Where:

λ_D = total decay constant for ^{238}U, 1.55125×10^{-10} yr^{-1}

λ_f = spontaneous fission decay constant for ^{238}U

I = isotopic ration $^{235}U/^{238}U$, 7.2527×10^{-3}

σ = thermal neutron cross-section for ^{235}U, $580.2 \times 10^{-24} cm^{-2}$

φ = thermal neutron fluence

ρ_s = spontaneous track density

ρ_i = induced track density

g = geometry factor for spontaneous fission track registration

The zeta calibration (ζ) is used for eliminating unknown parameters in Equation (1), such as the value of the decay constant for spontaneous fission of ^{238}U (λ_f) and the thermal neutron fluence (φ) used to induce fission of ^{235}U. The thermal neutron fluence (φ) is related to the track

density in the mica (the external detector, see below) (ρ_d) by : $\phi = B\rho_d$, where the B is a constant calibration factor.

As zeta (ζ) is equivalent to $\frac{\sigma IB}{\lambda f}$, equation (1) is simplified as:

$$t = \frac{1}{\lambda_D}\ln(1 + g\zeta\rho_d\frac{\rho_s}{\rho_i}) \qquad (2)$$

Each fission track worker should have his own zeta (ζ) parameter by averaging over many separate measurements on age standards.

c) Procedure and Technique

Two procedures are commonly used for determining a fission track age: the population and external detector methods. The population method measures the spontaneous and induced track densities separately on two aliquots from the same sample based on an assumption of uniform uranium distribution within grains from the same sample. However, the external detector method, which is adopted in this study, avoids this assumption and dates grains individually from one aliquot (Figure 6-2). The surface of a given apatite mineral is firstly grinded and polished, and then etched by 5N HNO3 for around 20s under 20°C. After the etching treatment, surface fission tracks which intersect the etched surface are revealed. The confined tracks can also be reached by the etchant through surface tracks, cleavage or fracture. An external detector, such as a sheet of mica is put on this surface and then set to a nuclear reactor. The irradiation induces fission events in ^{235}U. They are registered in the mica by the formation of induced fission tracks. The mica is etched afterward to reveal the induced tracks. In the end, one grain mount is obtained for measuring spontaneous track density (ρ_s) and another one for estimating induced track density (ρ_i). The fission track age for each single grain is then obtained by using the Equation (2) above.

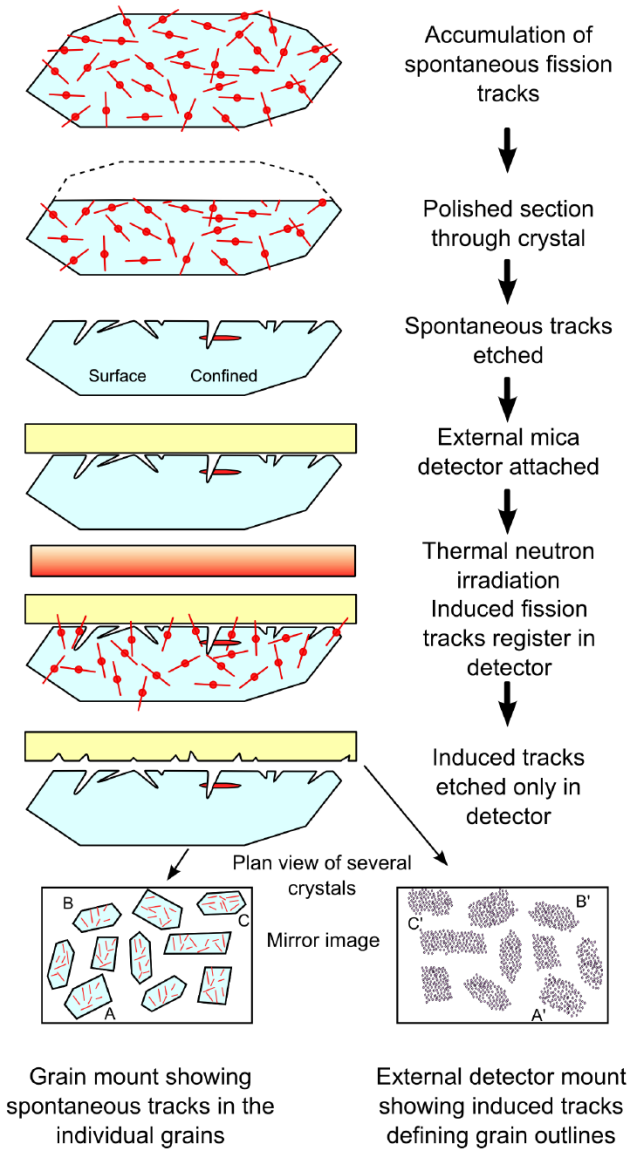

Figure 6-2 The external detector method (Hurford and Carter, 1991). The apatite crystal is polished and etched to reveal spontaneous tracks and certain confined tracks reached by the etchant. A uranium free external detector is placed over the crystal and irradiation induces fission of ^{235}U. Induced fission tracks cross into the external detector which is etched to reveal the tracks.

The problem encountered with this method is that the spontaneous tracks are produced by ^{238}U atoms located on both sides of the etched surface, whereas the induced tracks in the external detector result from only ^{235}U atoms located within the specimen. So a correction is suggested by some authors by increasing the measured U concentration by two or reduced the spontaneous track density (Faure, 1986).

6.2.1.2 Annealing and Fission Track Length

Apatite fission track ages have been found decreasing at depth with a temperature more than 100°C in deep drill holes. In fact, spontaneous fission tracks remain stable only at low temperature. Partial annealing happens when temperature increases, which shortens the length of fission track or removes totally the tracks. A temperature range over which annealing occurs is defined as 'partial annealing zone (PAZ)'. For apatite, PAZ ranges from 60° to 110±10°C with an uncertainty of 10°C according to the annealing model (Gallagher et al., 1998).

Track lengths are measured directly using a digitalized tablet and a microscope stage graticule calibrated by a micrometer. Only confined tracks entirely below and parallel to the etched surface are measured, which give a reliable real length distribution. The identification of confined track is possible by combining reflected and transmission light of the TEM. The track length data are then reported in a histogram with mean value, standard deviation and other parameters, such the angle between tracks and crystallographic c-axis. Because the etching and annealing processes are both anisotropic and controlled by crystal's crystallographic structure. Annealing is slower and the etching faster in the direction of the crystal's crystallographic c-axis. A correction of track length is proposed by some authors by using the angle to the c-axes of each track to deduce a supposed track length parallel to the c-axes, which is debatable for some other authors (Donelick et al., 1999; Ketcham, 2003).

Reduction on track length is controlled by temperature as well as time. A kinetic model of fission track annealing is firstly proposed by Laslett et al., (1987) on which subsequently published models are based. It describes a fanning Arrhenius plot with straight lines of equal track length reduction formed in a plot of log of time against inverse absolute temperature. All the lines converge to a point at infinite temperature because the slope increases with higher degree of annealing.

The composition of apatite also controls the annealing process, especially the Cl, F and OH contents. For example, apatite richer in Cl is more resistant to annealing than F-apatite. So they give longer fission track lengths.

6.2.1.3 Interpretation of Fission Track Data in Terms of Thermal History

Fission track ages can not be used without a combination with track-length data to interpret the thermal history of samples. If an apatite crystal experiences a continuous heating, all fission tracks formed at different times will be shortened to the almost same degree (Figure 6-3a). The resulted track-lengths have a short mean value. The fission track age does not represent any discrete event. In contrast, a continuous cooling will shorten fission tracks produced through time to different degrees. The final track-lengths are characterized by a negatively skewed length distribution (Figure 6-3b). The resulted fission track age tends to be younger than the onset of cooling. The lower probability of shorter tracks intersecting the etched surface results in lower measured fission track age. Only when minerals cooled rapidly and fission tracks did not have enough time to be annealed and stay relatively long, fission track ages can be considered approximately as those of the onset of cooling (Figure 6-3c). In an ideal case, a finite spread of length is expected. If the tracks formed after a heating experienced a cooling afterwards, the track-length distribution is typically bimodal (Figure 6-3d). We can not directly relate the fission track age to the timing to cooling.

6.2.1.4 Limitation and Uncertainty of the Method

The limitation of the AFT method is that only a recent thermal history after the last passage through PAZ is recorded. No information for the history prior to the onset of cooling can be obtained with precision by this method. Uncertainty persists due to the counting of the track numbers and the length measurement. The uranium concentration should not be too low or too high for a countable number of spontaneous fission tracks to accumulate. The possible uneven distribution of uranium in the specimen is also a source of error.

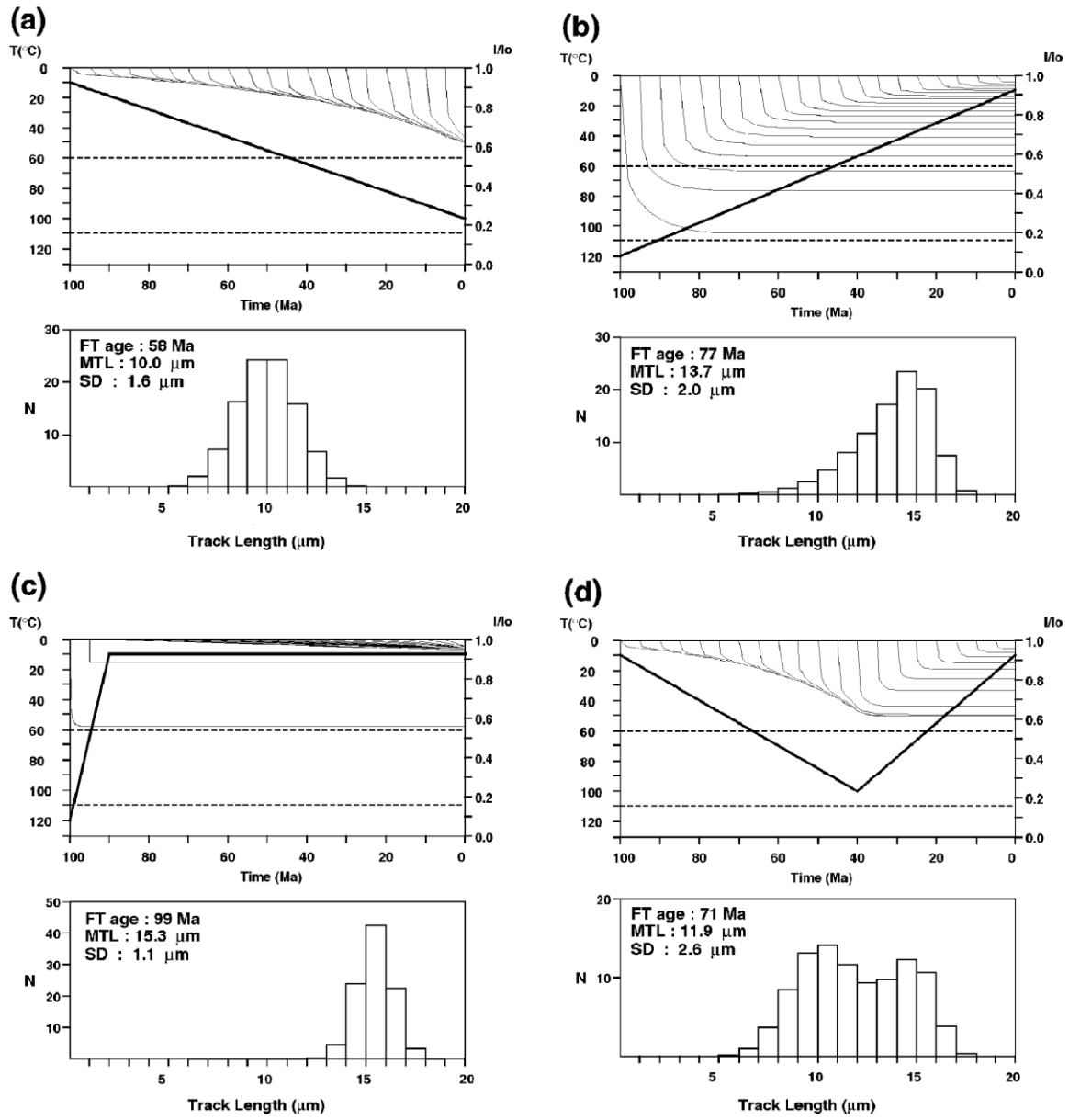

Figure 6-3 Predicted track-length reduction with time for different thermal histories with a continuous heating (a), a continuous cooling (b), a rapid cooling (c) and a heating/a cooling (d). The length reduction trajectories and track-length distribution are calculated with the annealing model of Laslett et al. (1987) (after Gallagher et al., 1998).

6.2.2. Apatite (U-Th-Sm)/He dating method (AHe)

6.2.2.1 AHe Age

a) Principles

Apatite (U-Th-Sm)/He dating method is based on the alpha decay of uranium, thorium isotopes and to some extent, samarium isotopes. The number of helium nuclei (or α particle) accumulated in apatite grain is a function of uranium, thorium and samarium content and time as below:

$$^{4}He = 8*^{238}U\ (e^{\lambda_1 t}-1) + 7*^{235}U\ (e^{\lambda 2^{t}}-1) + 6*^{232}Th\ (e^{\lambda 3^{t}}-1) + ^{147}Sm\ (e^{\lambda 4^{t}}-1)$$

Where ^{4}He, ^{238}U, ^{235}U, ^{232}Th, ^{47}Sm are isotope contents, $\lambda_{1,2,3,4}$ are decay constants.

Assuming that all produced helium nucleus are retained in the crystal and no other extraneous source of helium (e.g. inclusions of other minerals), an AHe age can be obtained by measuring the U, Th and Sm amounts.

b) Techniques and procedures

The adopted procedure for measuring He, U, Th and Sm concentrations involves firstly a careful selection of apatite grains (size, shape and inclusion free). Afterwards, helium extraction is processed using a Quadrupole mass spectrometer. Apatite crystals are degassed inside a platinum capsule by heating with a laser. The helium gas is purified by passing through liquid nitrogen before going into the mass spectrometer where helium concentration is measured. A calibration is made by repeat measurement of a ^{4}He standard throughout the analysis.

After helium extraction, the apatite crystals are dissolved and spiked with a solution with a known concentration of ^{235}U, ^{230}Th and ^{149}Sm. Samples are then analyzed using Inductively Coupled Plasma Mass Spectrometry (ICP-MS). The concentrations of ^{238}U, ^{232}Th and ^{147}Sm can be obtained and calibrated by a known ^{238}U.

6.2.2.2 Helium Diffusion and Radiation Damage

What makes (U-Th-Sm)/He dating a thermochronometer is the fact that He nuclei experiences thermal diffusion within apatite through time. In fact, helium nuclei can only be retained within the crystal below a certain temperature and the diffusive loss of He decreases

through a cooling trajectory. A theoretical partial retention zone (PRZ) is defined as a temperature range where the retention of helium begins and increases with temperature, which has a similar fashion of the partial annealing zone (PAZ) for AFT dating. The PRZ was estimated to be a temperature range of ~ 40 to 75± 5 °C by early studies of He diffusion (Farley, 2000). This makes the understanding of the thermal history of the very upper part of the crust (1-3 km) possible.

However, recent investigation revealed that radiation damages caused by alpha recoil had influence on diffusion by increasing the retention of helium within apatite. Alpha recoil is in return controlled by the effective uranium concentration ([eU]=[U]+0.24*[Th]). The higher effective uranium concentration creates more radiation damages, then increases the temperature range of PRZ and the measured age will be older. However if effective uranium concentration is very significant, He diffusion can be promoted (Shuster et al., 2006; Flowers et al., 2009; Gautheron et al., 2009).

6.2.2.3 Alpha-ejection

In addition to diffusion of helium, a process of alpha-ejection was discovered to increase the loss of helium in the crystal. In reality, when α particles are emitted from their parent isotope, they possess enough energy to travel up to ~ 20 µm before coming to rest, called 'stopping distance' (R) (Farley et al., 1996). As a result, a proportion of alpha particles may be lost from the crystal when the ejection happens within 20 µm from the crystal edge (Figure 6-4). When U and Th rich minerals (e.g. zircon, titanite, monazite) are aside or inside of the apatite grain, long stopping distance of α-particles may result in implantation or inclusion of alpha particles into the apatite (Figure 6-4). A correction factor (F_t) is proposed to be used for calculation of AHe ages, which depends largely on the grain size. But this correction is debated when α-decay comes to interplay with diffusion and it's considered to over-correct ages in case of significant diffusion (Gautheron et al., 2012).

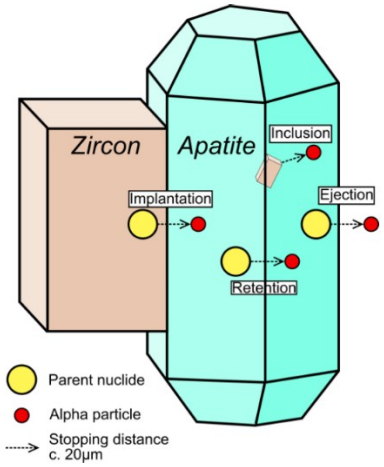

Figure 6-4 Cartoon representing of the effects of implantation, ejection and inclusions during alpha-ejection (Wildman, 2015).

6.2.2.4 Limitation and Uncertainties

Consequently, it is difficult to define sets of kinetic parameters for the AHe system by taking into account all factors, such as composition, crystal size, radiation damage and zonation of U, Th and Sm. Several kinetic models of helium diffusion have been proposed with differently defined relations between parameters (Shuster et al., 2006; Flowers et al., 2009; Gautheron et al., 2009). Uncertainty still exists within AHe analysis due to these aspects.

6.2.3. Power of Combination of Two Methods

Since two methods cover different ranges of temperature (60-110°C for AFTA and 40-80°C for AHe, Figure 6-5), AHe dating can only provide information about the very recent thermal history of crystal, while AFTA can constraint the older thermal history with cooling rate revealed by the track-length distribution. So the combination of both methods allows a better understanding of the thermal history of samples and then provide more precise information on denudation histories.

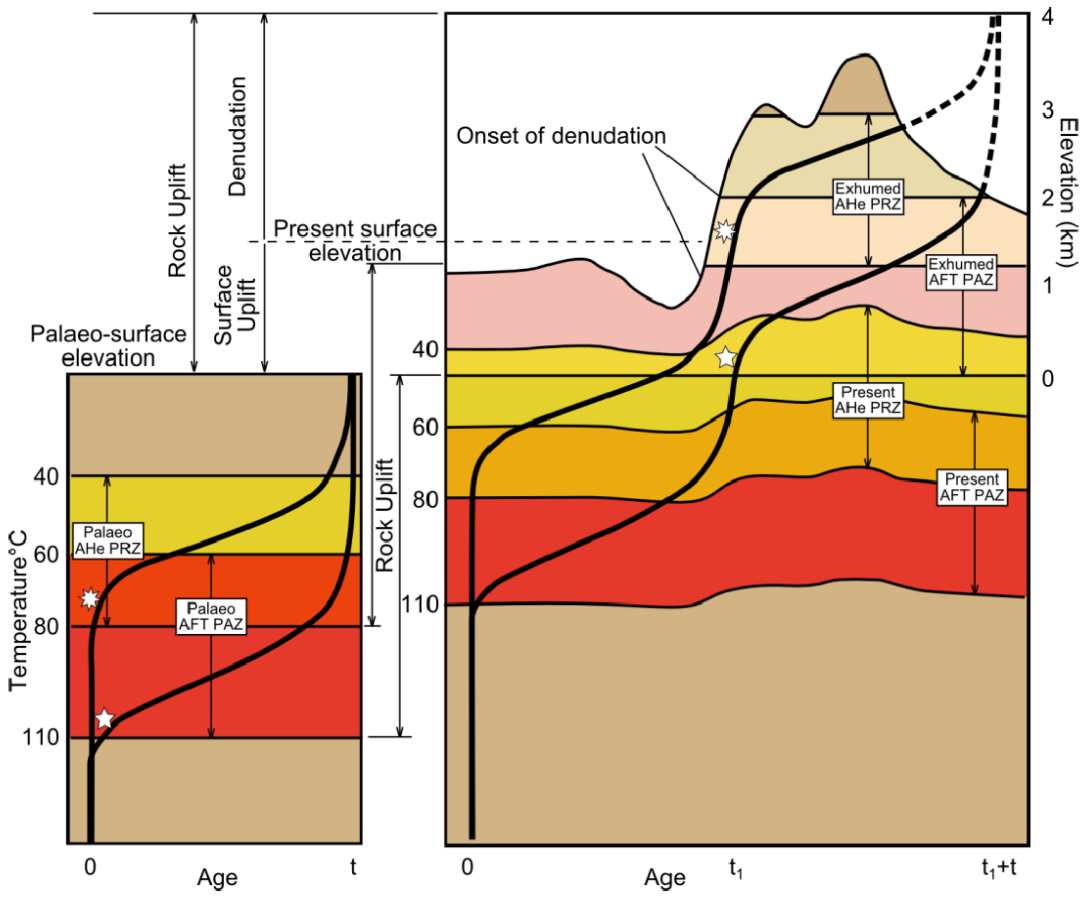

Figure 6-5 Left hand figure shows the structure of the theoretical PAZ and PRZ beneath a flat topography and the expected age profile with depth for both AFT and AHe thermochronomters. Asterix and star represent samples currently at depth. Right hand figure shows these samples now exhumed following a period of rapid uplift and denudation producing high relief topography. The high relief topography perturbs the present day PAZ and PRZ at depth. In high relief areas the age profile may have preserved the structure of the profile through the now exhumed palaeo-PAZ and palaeo-PRZ (Wildman, 2015).

In the case of complex episodic cooling, the combination of two methods appears to be absolutely necessary. Imaging a sample experienced two different cooling episodes (Figure 6-6), AFTA or AHe dating alone can only provide a single old or young age with a simple cooling path, although both results fulfill the separate thermochronological data. But the true thermal history can only be obtained by combining both AFTA and AHe methods.

The combination of both methods is used widely in tectonically stable cratonic areas. In fact, in tectonically active domains, such as mountain belts, crystals pass through the PAZ or PRZ with relatively higher velocity. We obtain often similar AFT and AHe ages. In cratonic areas, the

cooling is much slower. This has been revealed by the fission track length distribution with a low mean length value (from 11 to 13 μm) and a high standard deviation. We expect a bigger difference of AFT and AHe ages in cratonic domains and to have more precision on possible cooling rate by combing the two sets of ages. However AFT and AHe ages are sometimes difficult to be interpreted. For example, AHe ages are found in some cases older than AFT ages of the same samples, while we expect older AFT ages according to the higher AFTA temperature range. This incoherence is explained by some authors as a result of radiation damage related to a high eU concentration (Shuster et al., 2006; Flowers et al., 2009; Gautheron et al., 2009). This means radiation damage could act as a retaining trap and result in older AHe age. But when eU concentration goes beyond a certain level, radiation damage may in reverse make diffusion more efficient. A more explicit radiation damage related diffusion model for AHe dating is still demanded.

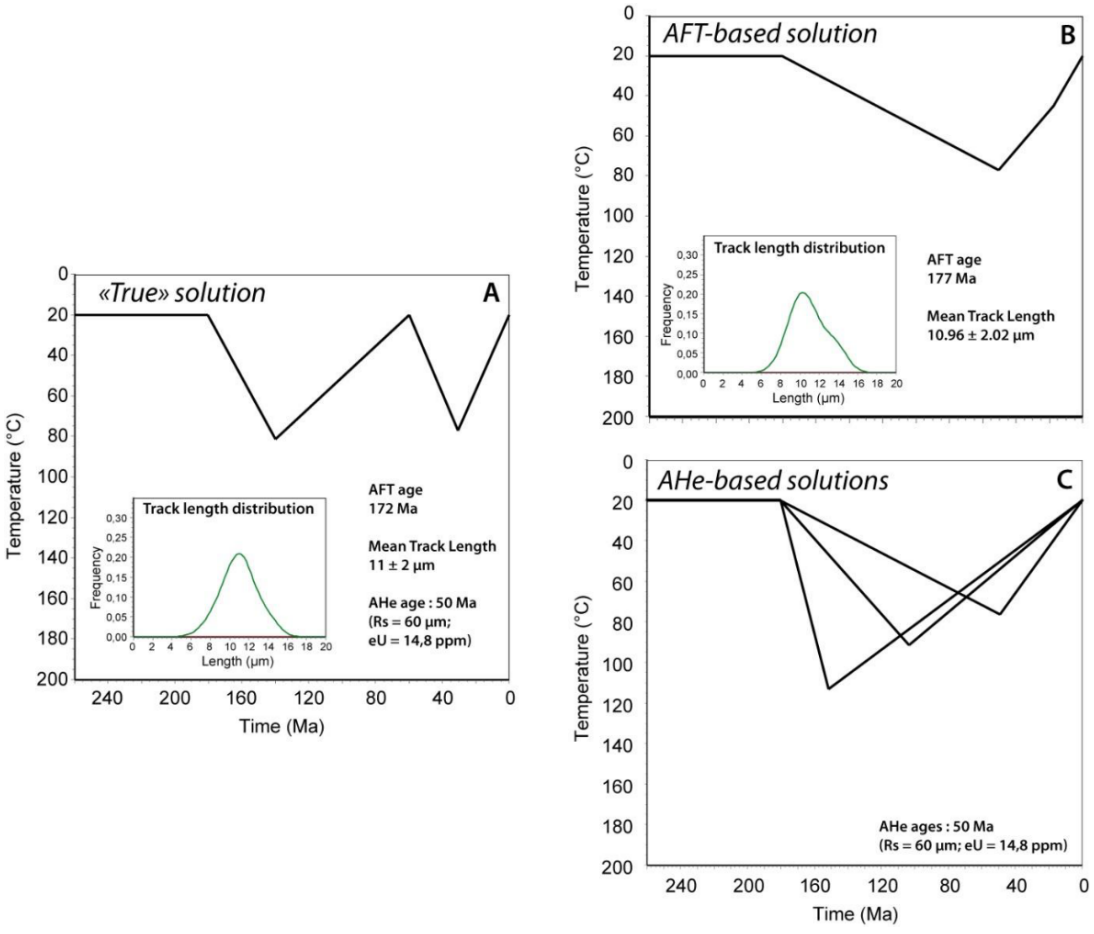

Figure 6-6 Comparison of determined thermal histories by both AFTA and AHe methods (A), only AFTA (B) and only AHe dating (C). All thermal histories are compatible with thermochronological data and have been modelled by HeFTy (Leprêtre, 2015).

6.3. TS2P Sampling

Earlier low-temperature thermochonological analysis in West Africa were carried out on samples from the Reguibat and Hoggar Shield (Cavellec, 2006; Rougier et al., 2013; Leprêtre, 2015; English et al., 2016, Figure 6-7). Only one study was undertaken on the Leo-Man Shied in Burkina Faso (Gunnell, 2003, Figure 6-7), far from the Equatorial Atlantic margin. Other studies were made on samples from ODP Leg 159 (Clift et al., 1998; Bouillin et al., 1998; Bigot-Cormier et al., 2005, Figure 6-7), in order to investigate vertical movements of the Ivory Coast-Ghana marginal ridge. No study on the Mesozoic denudation history of the basement along the Equatorial Atlantic margin exist yet.

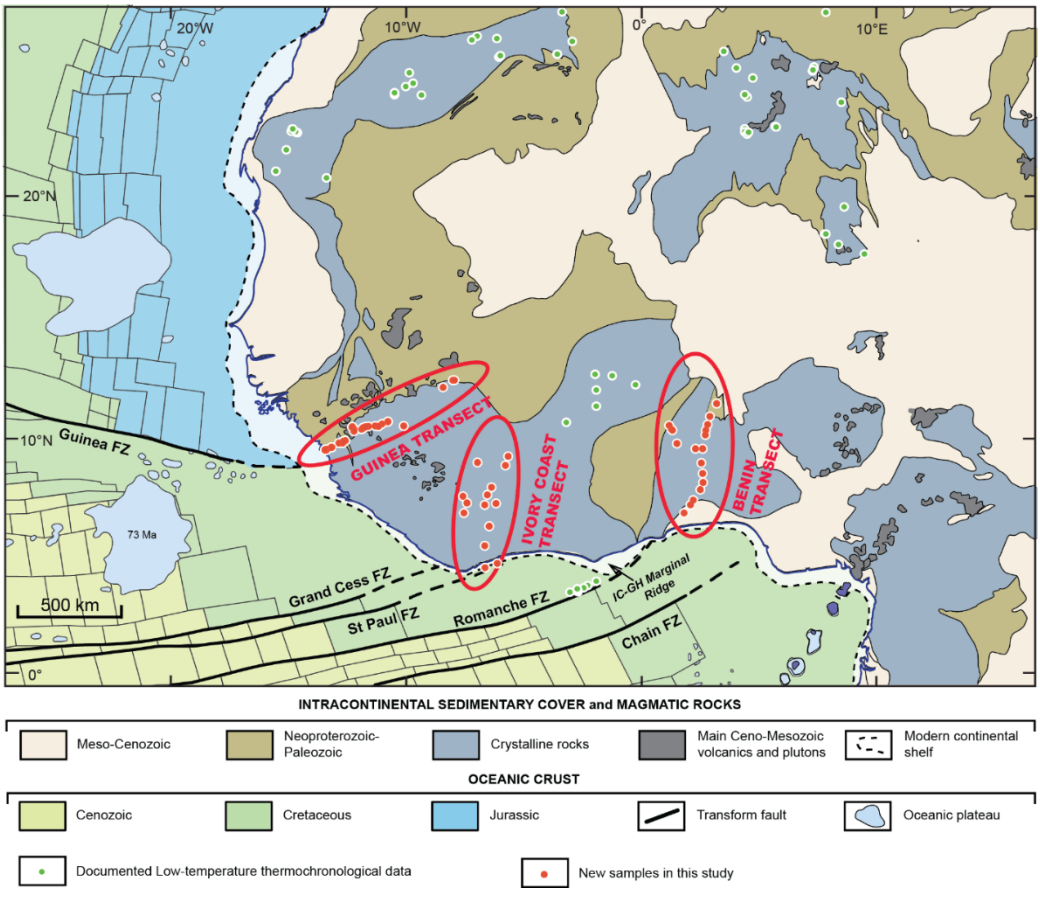

Figure 6-7 Location of earlier published low-temperature thermochronological data (AFTA and AHe) from Bouillin et al. (1998), Clift et al. (1998), Gunnell (2003), Bigot-Cormier et al. (2005), Cavellec (2006), Rougier et al. (2013), Leprêtre (2015), English et al. (2016), and new samples along three transects in Guinea-Benin. Quaternary sand was removed from the simplified geological map.

The TS2P project allowed sampling the margin from Guinea to Benin for the purpose of low-temperature thermochronological analysis (AFTA and AHe dating, Figure 6-7). Three transects were established from West to East, in Guinea, Ivory Coast and Benin (Figure 6-7). They aimed to reveal the thermal and denudation history of three major segments of the margin, which also correspond to long-lived drainage basins whose Cenozoic evolution was investigated in details (Chardon et al., 2016).

6.3.1. Guinea Transect

20 samples were collected along a transect from Conacry to Bamako by D. Chardon, D. Huyghe and D. Webster in 2014 (Figure 6-8). The transect is 700 km long and covers a range of altitude from 0 to 1200 m. The space between samples is of 40-50 km, except an empty zone from the Eastern Guinea to the Southern Mali, due to poor outcorp conditions.

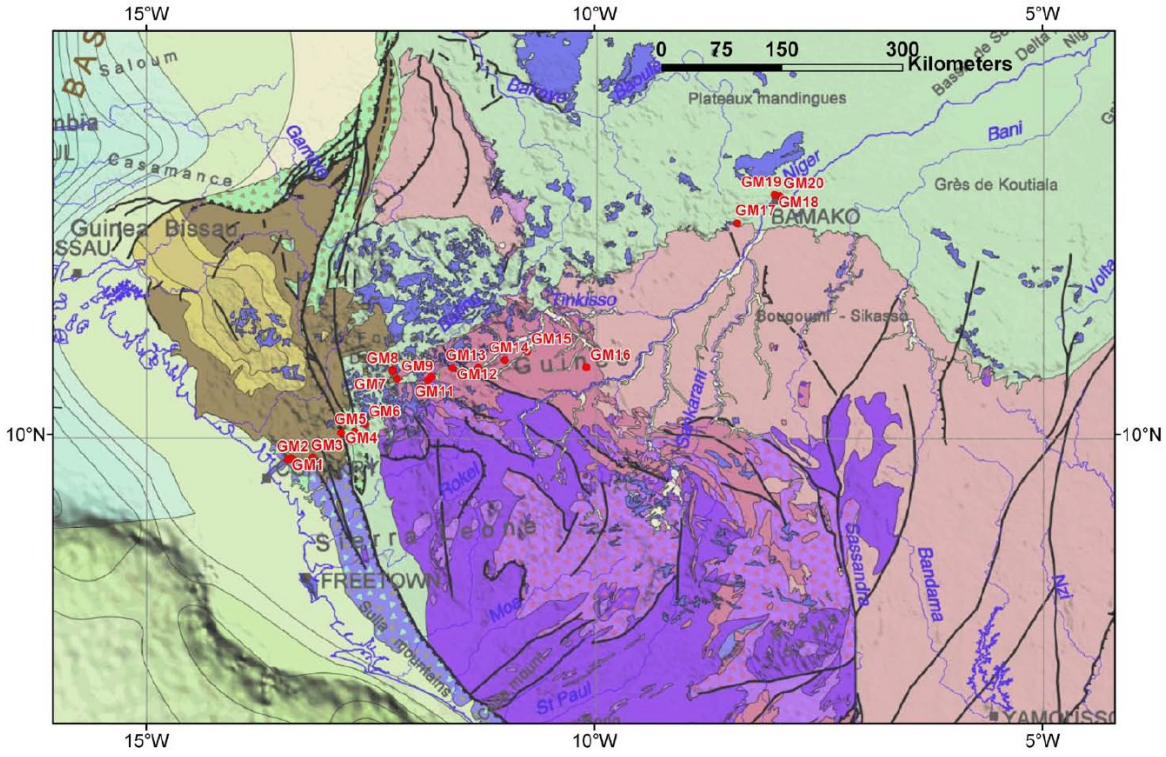

Figure 6-8 Guinea sample locations on the tectonic map of Milesi et al., (2010) (Provided by D. Chardon).

The lithology of samples varies from granitoids and gneiss of the Rockelide Panafrican mobile belt and Archean craton, to sandstones of the Bove basin and the Taoudeni basin. Doleritic sills of the Central Atlantic Magmatic Province were also sampled. More details of Guinea samples can be found in Appendix 3.

6.3.2. Ivory Coast Transect

The Ivory Coast transect consists of 13 samples given by A. Kouamelan (Université Félix Houphouêt-Boigny, Cocody, Ivory Coast) that have been collected during his PhD work for the purpose of a U-Pb geochronological study (Figure 6-9, Kouamelan, (1996)). They were mostly heavy mineral separates comrising apatites, which are suitable for thermochronological analysis (AFTA and AHe dating). The spatial distribution of the samples forms a wide latitudinal corridor covering a range of 0-471 m in elevation. Most samples are granodiorites and gneisses which yielded a large amount of apatites. More details on Ivory Coast samples are summarized in Appendix 4.

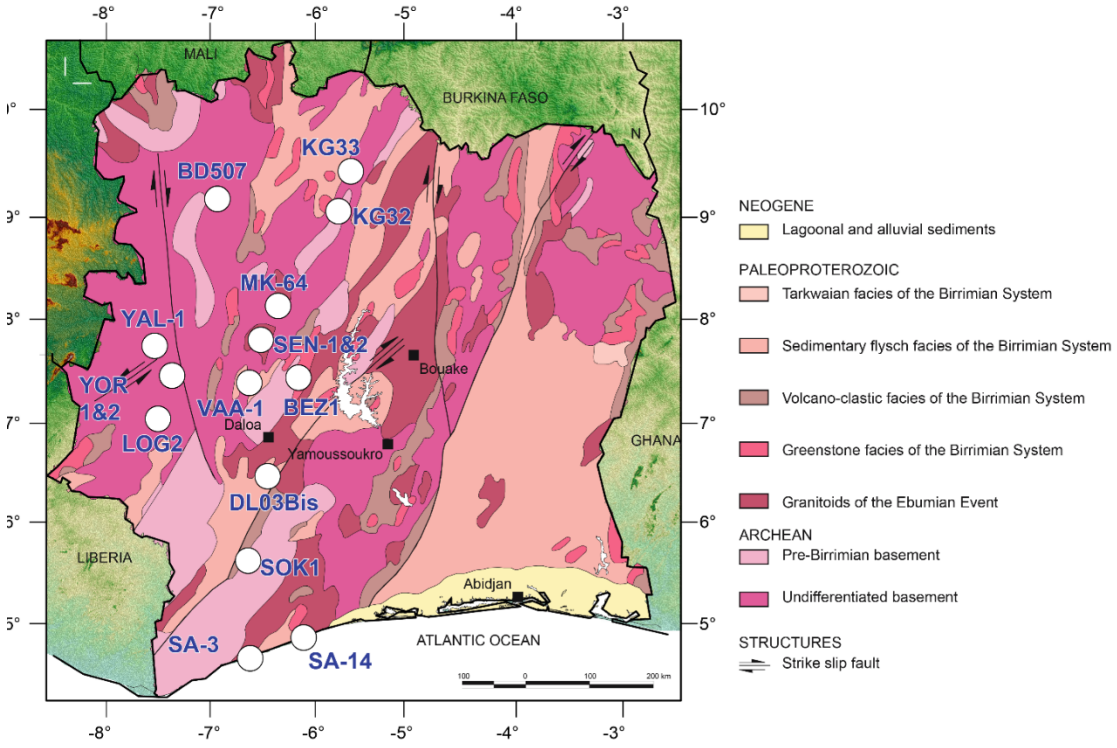

Figure 6-9 Ivory Coast sample locations on the geological map of Ivory Coast.

6.3.3. Benin Transect

18 Benin samples were collected by D. Chardon in 2014 along a long NNE-trending transect of 600 km across the country and a shorter NNW-trending one of 100 km in the northeasternmost part of the country (Figure 6-10). The space between samples is of 30-50 km. They cover a zone of weak topographic relief from 140-500m, extending from the coastal basin (i.e. the Dahomey embayment) to the Iullemmeden basin, in the north. The main transect passes through the granitoids and gneisses of the Panafrican mobile belt and the Cambrian-Silurian sandstones of the Kandi basin. The short transect covers mostly sandstones involved in the foreland fold-and-thrust belt of the Panafrican orogen. See Appendix 5 for more details on the Benin samples.

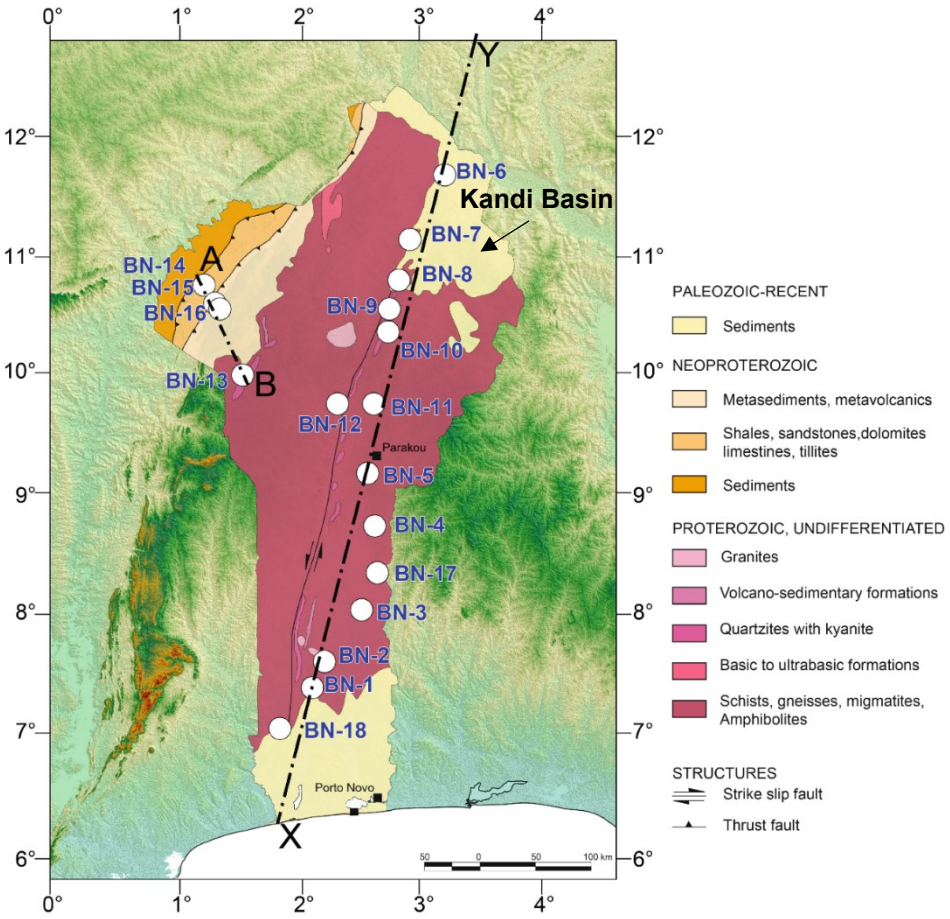

Figure 6-10 Benin sample locations on the geological map of Benin.

6.4. AFT and AHe Ages

6.4.1. AFT Ages

Guinea Transect

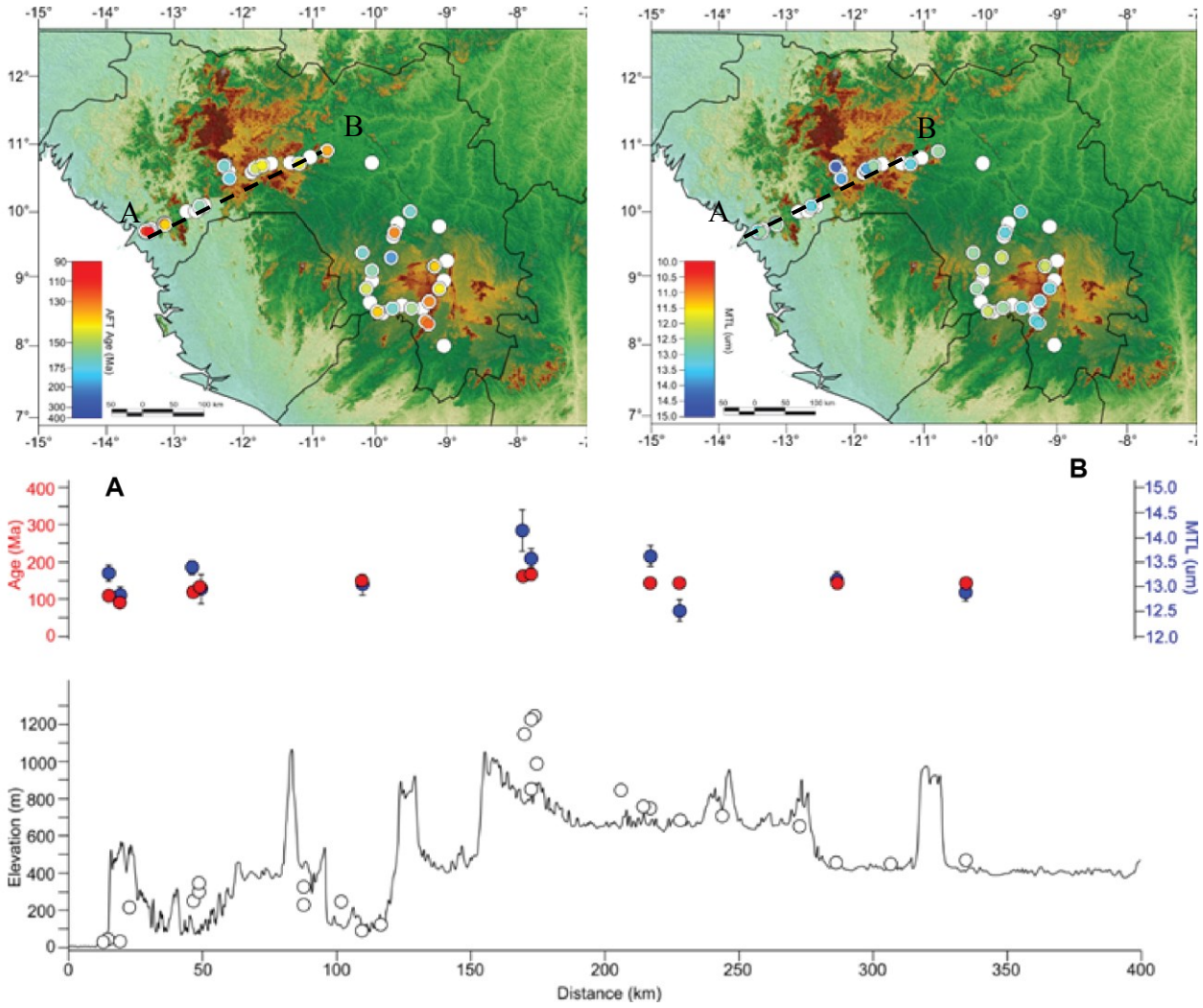

Figure 6-11 Measured central AFT ages (top left) and MTLs (top right) in Guinea plotted on a topographic map, and cross-section of samples of the Guinea transect on the topography with a plot of their central AFT ages and MTLs with uncertainty bars (bottom) (Provided by M. Wildman).

AFT ages obtained for 11 samples of the Guinea transect range from Jurassic to Early Cretaceous (from 170.7± 9.0 to 109.3±5.1 Ma) with mean track length varying from12.5±0.2 to 14.1±0.4µm (Figure 6-11, Appendix 6). Oldest measured ages were found mostly in highest elevation with longest MTLs (Figure 6-11). A positive correlation of AFT ages with elevation is

observed (Figure 6-11and Figure 6-12) with elevation increasing with AFT ages. Long MTLs (> 13.5µm) obtained on samples with old ages (140-170 Ma) could suggest a rapid cooling event during the Late Jurassic-Early Cretaceous. Youngest ages of 120-110 Ma are found close to the coastline. Additional samples in Southern Guinea were provided by Rod Brown as supplementary data which generated ages from 202.1±19.1 to 122.4±6.4 Ma with MTLs ranging from 12.2 to 13.4µm and showed no correlation between age and elevation. The standard deviation of track length measurements range from 1.64 to 2.59 with the majority of < 2. This means that most samples have a moderately broad track length distribution.

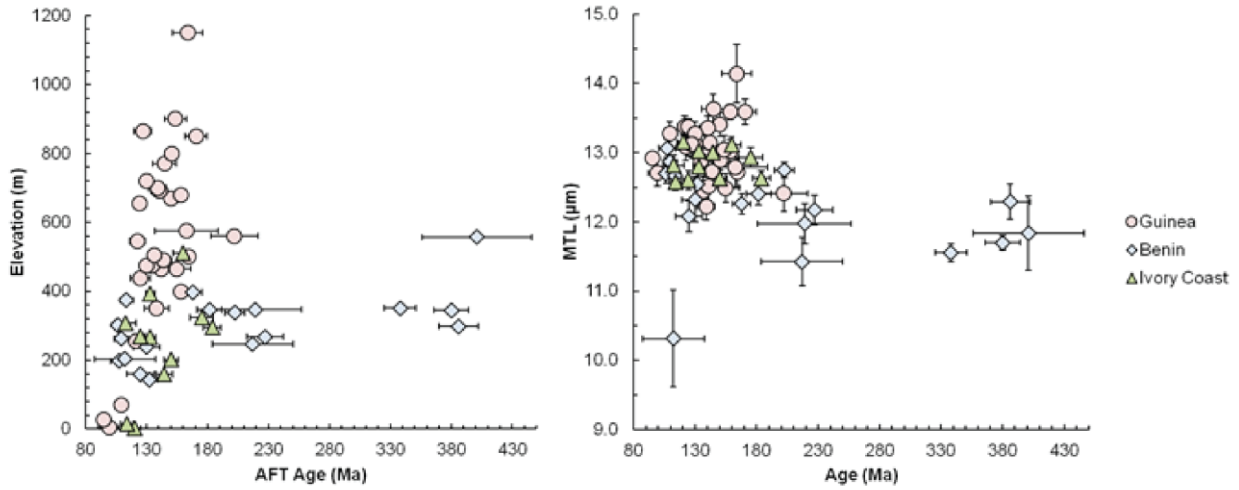

Figure 6-12 Plot of AFT ages against elevation (left) and mean track lengths (MTLs) against AFT ages (right) of three transects. AFT ages are Central AFT ages with 1σ standard error, as well as MTLs (Provided by M. Wildman).

Ivory Coast Transect

AFT ages of 11 samples in Ivory Coast ranging from 183.8±7.2 to 112.5±8.7 Ma and show a less obvious positive correlation of AFT ages with elevation than the Guinea transect (Figure 6-12 and Figure 6-13, Appendix 6). The AFT ages show a complex spatial distribution from the coastline to the inland with younger ages alternating with older ages. As for the Guinea transect, coastal samples yielded younger Aptian-Early Albian ages (120-110 Ma). Mean track lengths have a narrow distribution varying from 12.6±0.1 to 13.1±0.1µm. Compared to the Guinea samples,

Ivory Coast samples record a partially annealed cooling events of different ages from Jurassic to Early Cretaceous.

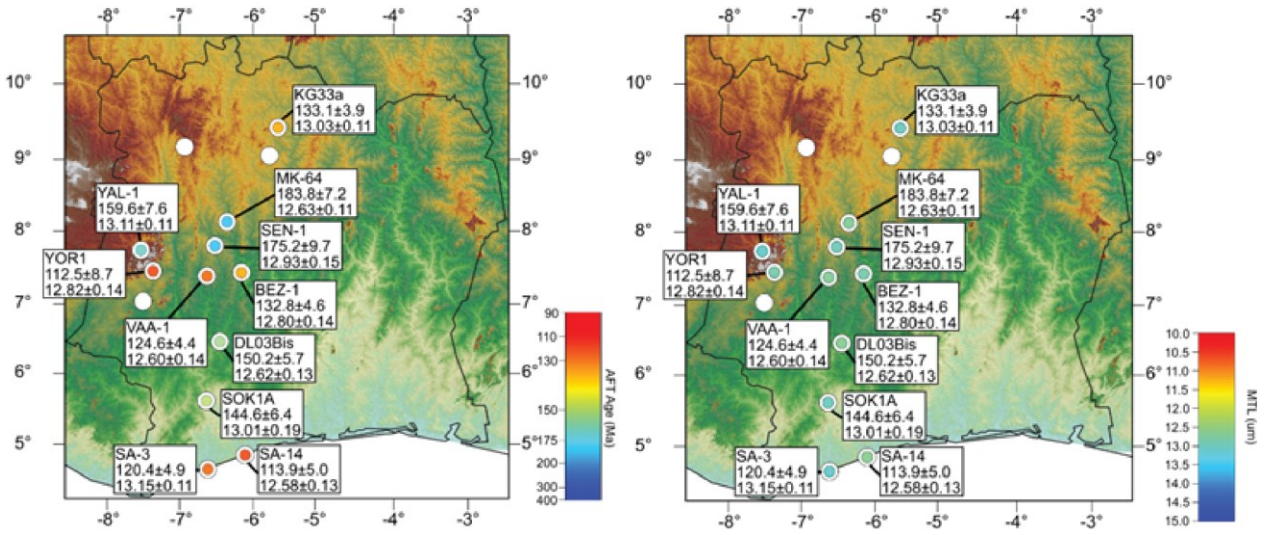

Figure 6-13 Measured Central AFT ages (top left) and mean track lengths (top right) with uncertainties in Ivory Coast plotted on a topographic map (Provided by M. Wildman).

Benin Transect

AFT ages of 18 samples in Benin show a clear altitudinal distribution with young ages (106.3±4.5 to 132.0±7.1 Ma) obtained close to the coastline and older ages (167.9±7.3 to 401.1±45.0 Ma) on the Northern inland (Figure 6-14, Appendix 6). A young AFT age (130.0±11.0 Ma) was yielded again by the northernmost sample (BN-6), which could be associated with the independent thermal history of the Gao rift that is nearby (see the paleogeographic study). However, no clear correlation of AFT ages with elevation is observed (Figure 6-12). Mean track lengths range from 10.3±0.7 to 13.1±0.1 µm with a majority under 12.5 µm. Cooling events were a priori slow in Ivory Coast, as annealing of fission tracks was more intense.

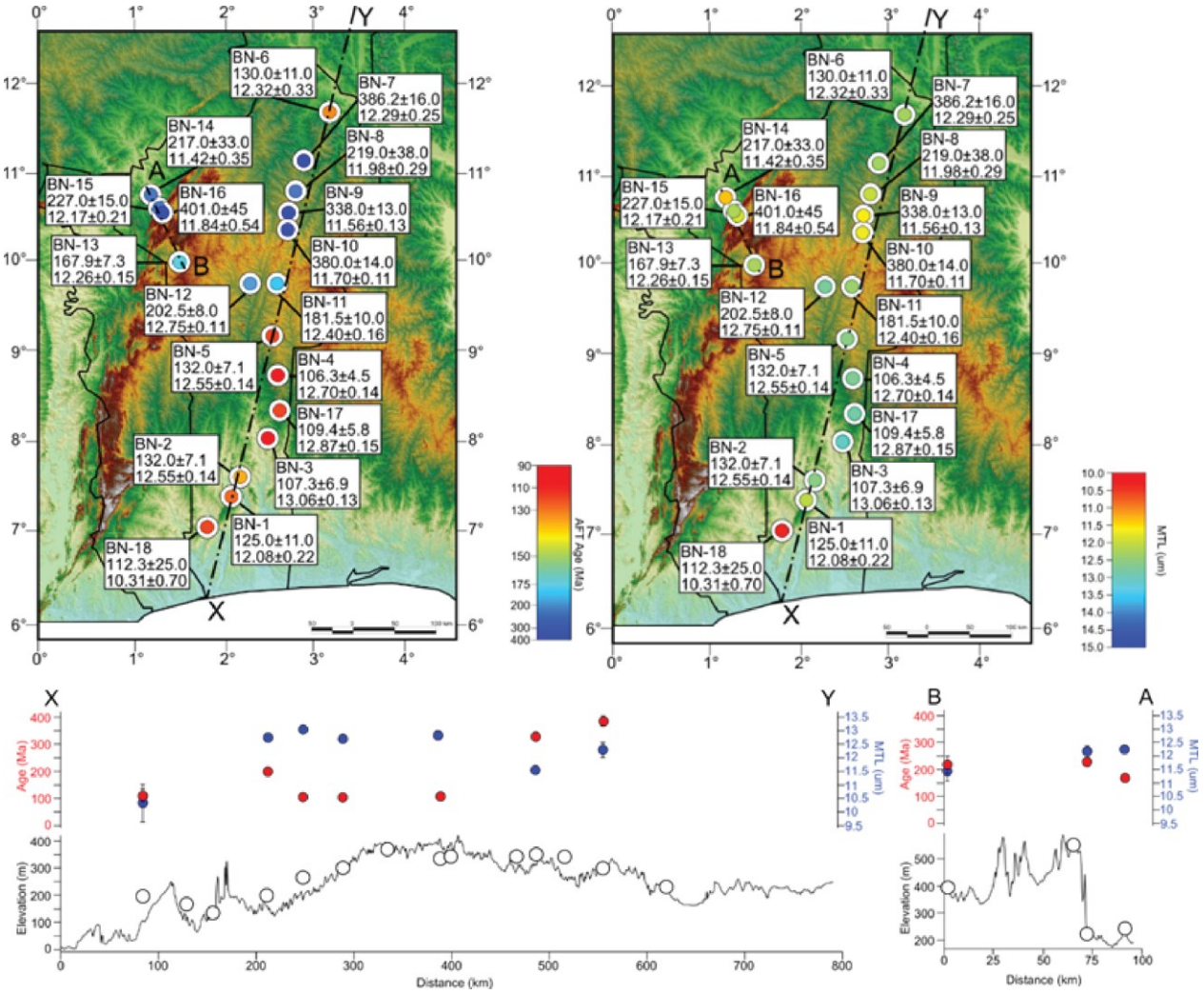

Figure 6-14 Measured AFT ages (top left) and MTLs (top right) in Benin localized on a topographic map and a plot of topography, AFT ages and MTLs of two Benin transects (bottom) (Provided by M. Wildman).

AFT and track length data were interpolated on a map (Figure 6-15). Additional AFT data published in Burkina Faso (Gunnell, 2003) were also incorporated. The resulting distribution of ages shows a spatial variability from North to South, and from West to East. Young AFT Early Cretaceous ages (100-150 Ma) are concentrated mostly along a coastal corridor of c. 400 km wide. Older AFT ages (> 150 Ma) are found far on the Northeast, and are also presented at local spots in Guinea and Ivory Coast. The distribution of MTLs is rather homogenous with a value of c. 13 µm. Short MTLs (< 12µm) were found only in Benin on the East, but the longest MTLs were yielded in Guinea. The fact that the southernmost Benin sample yielded shortest MTLs could be related to

its independent uplift and burial history due to its location within the Dahomey Embayment. Overall, the whole dataset supports a dominant phase of crustal cooling for the coastal corridor during the Early Cretaceous, which is the syn-rift stage of the Equatorial Atlantic margin (140 – 107 Ma, Figure 3-6 and Figure *3-7*). It also highlights pontentially complex spatial and temporal cooling patterns across the study area with samples recording differentiate thermal events.

6.4.2. AHe Ages

Not all samples have successfully yielded an AHe age, due to sample quality (Appendix 7). Single grains of one sample can yield ages with a great dispersion, which implies the influence of different chemical and structural characteristics of each grain, such as eU and grain size (R*). Obtained mean sample AHe ages are in agreement with AFT ages in general, ranging from 282.2 to 51.7 Ma (Appendix 7). Oldest AHe ages were also obtained in Benin, where they are comparable to the AFT ages. Several samples yielded AHe ages exceeding their corresponding AFT ages (BN12, BN18, SA-14, MK-64 and GN02). It is common in cratonic areas where effective uranium content is high and radiation damage effect is important. The relationships between the accumulation of radiation defects and alpha trapping are still unclear, considering the influence of grain radius and fragmented grains in addition. In general, samples do not show any positive age-R* and age-eU relationships. Overcorrection of AHe age using a single alpha-correction may also contribute to the overlap of AHe ages on AFT ages (Wildman et al., 2016). Therefore, the AHe data cannot be interpreted based only on the observed ages.

AFT and AHe ages do not essentially indicate a specific event. They need to be interpreted, taking into account other parameters (e.g., track length, eU content). We can only assess the thermal histories by using inverse modeling

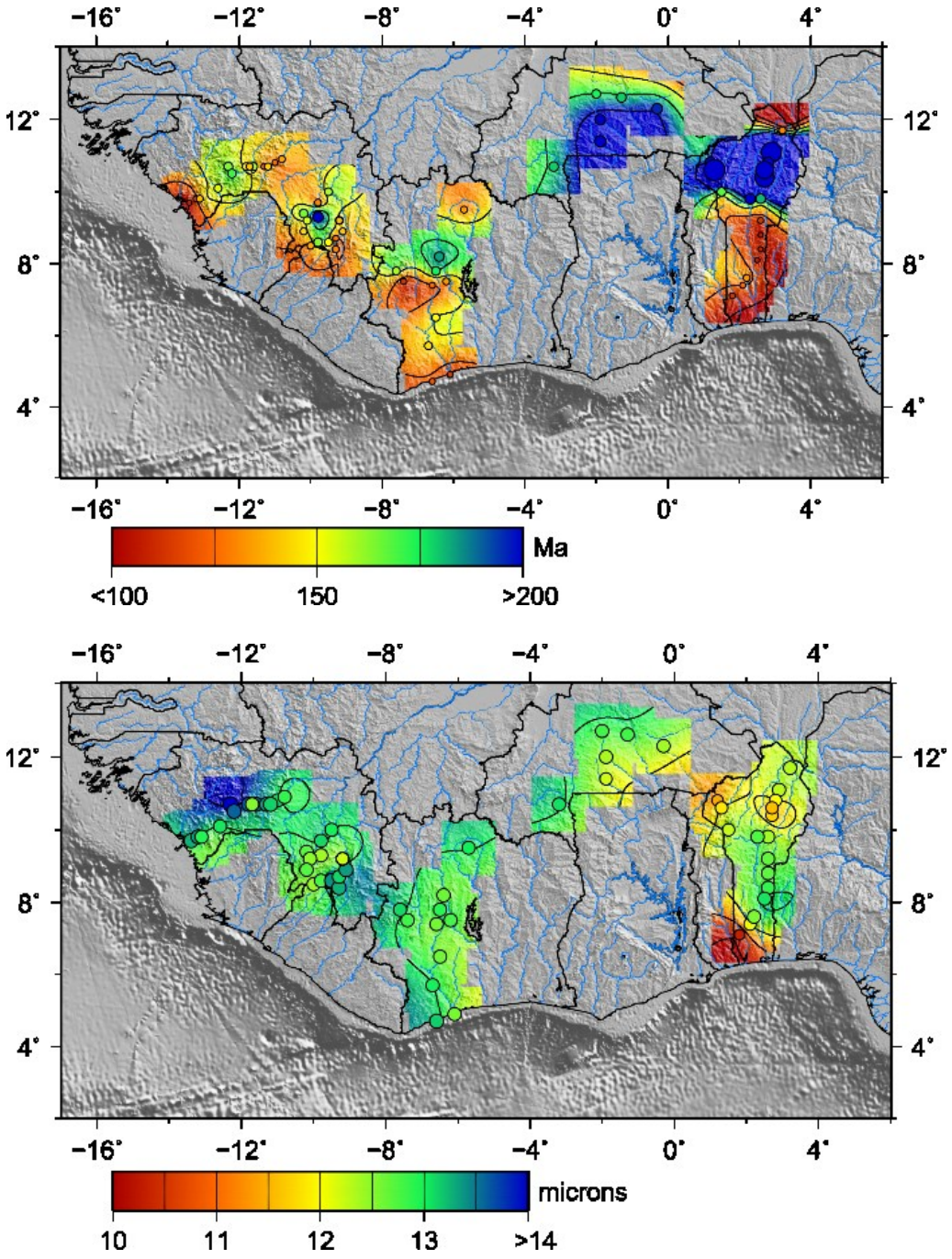

Figure 6-15 Distribution of AFT ages (top) and mean track lengths (bottom) of the study area, after narrow interpolation of three TS2P transects and additional Guinea and Burkina Faso data (Provided by M. Wildman).

6.5. Thermal History Modeling

6.5.1. Approach: QTQt

In order to generate thermal history and quantify surface processes (e.g. erosion and burial) that fit the observed data, inverse modelling is usually performed on specific software (e.g. QTQt, HeFTy). In this study, QTQt, a Bayesian transdimensional approach to data inversion is used (Gallagher, 2012).

A fundamental input for the modelling is a theoretical annealing or diffusion model defining how AFT or AHe thermochronometer evolves as a function of temperature and time. For the AFT, the multi-kinetic fission track annealing model of Ketcham et al. (2007) is applied in QTQt, which accounts for the differences in annealing rate in apatite grains with different chemistry (e.g. F and Cl content) and different angles of tracks to the c-axis. The Durango diffusion model of Farley (2000) is adopted for AHe data inversion. It defines the activation energy of alpha production for the U, Th and Sm decay, alpha stopping distances and thermal diffusivity for grains with a spherical approximation. Additional different radiation damage annealing models can be assessed separately (Shuster et al., 2006; Flowers et al., 2009; Gautheron et al., 2009).

The modelling approach of QTQt uses Bayesian transdimensional Markov Chain Monte Carlo (MCMC) method. It defines a wide range of possible thermal history models to be considered as prior information (a limited range of temperature and timescale). Sampling is based the MCMC approach through which the current model is perturbed to generate a proposed model which is then accepted or rejected according to its likelihood fitting the observed model (Gallagher, 2012). A posterior probability distribution of the model parameter values given the data can be constructed by calculating:

$$\mathrm{P}(M|D)=\mathrm{P}((M))\mathrm{P}(D|M)$$

Where P (M|D) is the posterior probability density function of the model parameters given the data; P(D|M) is the likelihood probability function of obtaining the data given the model and P(M) is the prior probability density function given to the model.

The main advantage of the Bayesian approach is that the number of T-t points is treated as unknown parameter and models with fewer T-t points are preferred during sampling. This avoids over complex thermal history model and propose simple models which fit adequately to the observed data.

The MCMC sampling should be run for a minimum of c. 200.000 iterations and all tested thermal history models, each with a related posterior probability of fitting the observed data are collected to produce a summary probability distribution map of temperature-time. Then the expected model can be determined by the mean thermal history model weighted for its posterior probability. The maximum likelihood model is considered as the model which fits the observed data best, but it is often too complicated to be justified by geological constraints. Therefore, the expected model tends to provide the most suitable insight to thermal history.

6.5.2. Modeling Results of TS2P Samples

The measured data (AFT and AHe data) of each sample were preferentially modelled jointly to provide better constraints for possible T°C/t models to be tested. The AHe data help constraining the thermal history through lower temperatures (40 – 80 °C), whereas the AFT data constrain that through higher temperatures (60 – 110 °C). Integrating both AFT and AHe data is crucial to define distinct transition in cooling style over time.

Other geological constraints (e.g. deposition age for sedimentary rocks, overlying volcanic or sedimentary rock, age of erosional surfaces) were used as constraints in modelling to predict a more robust thermal history (Appendix 8 to 10).

6.5.2.1 Guinea Transect

Data from samples in Ivory Coast were inverted using the procedure above. Only the AFT data and geological constraints were used, because the AHe data are limited in Guinea. The onset of cooling for resulting thermal histories occurs within three time periods (Figure 6-16): Early

Jurassic (200 – 180 Ma), Mid-Late Jurassic (175 – 145 Ma), Early Cretaceous (145-100 Ma). Spatial distribution of thermal histories and cooling rates were evaluated.

Early Jurassic (200 – 180 Ma): Slow cooling

Interior samples (GN6 – GN10) at 100 - 225 km distance from the coastline record cooling beginning in the Early Jurassic and continuing until the Cenozoic in an almost linear manner (Figure 6-16). The cooling rate is slow (0.5 to 0.8 °C/Myr) which is common in cratonic domains. The temperature at the beginning of cooling should be more than 120 °C. Because this region was heated by the CAMP event, thermal history older than 200 Ma should not be preserved and so is not considered here.

Mid-Late Jurassic (175 – 145 Ma): Slow to Rapid Cooling

Mid-Late Jurassic cooling event was recorded by samples landward of the above mentioned samples (GM12 and GM14, Figure 6-16). GM12 was cooled rapidly at a rate of 3.0 °C/Myr from 110 ± 20°C at c. 175 Ma to near surface conditions at c. 120 Ma. However, GM14 recorded a slow cooling at 0.6 °C/Myr which lasted for c. 160 Myr.

Early Cretaceous (145-100 Ma): Moderate to Rapid Cooling

Coastal samples (GN1, GM2 and GN3) at less than 50 km of distance from the coastline experienced cooling beginning in the Early Cretaceous (Figure 6-16). GM2 recorded a rapid cooling at c. 3.00 °C/Myr, which rapidely brought the sample under near surface conditions. However, GN1 and GN3 recorded a continuous cooling until the Cenozoic with a cooling rate of c. 1.8 °C/Myr. The timing of this cooling would fit with the rifting of the Guinea-Liberia margin which initiated during the Valanginian – Barremian (140-125 Ma). This means rifting affected the onshore domain only on a narrow coastal strip (less than 50 km from the coastline). An interior sample (GM13) also recorded Early Cretaceous cooling at a rate of c. 1.8 °C/Myr, which probably suggests another local tectonic event and needs further investigations.

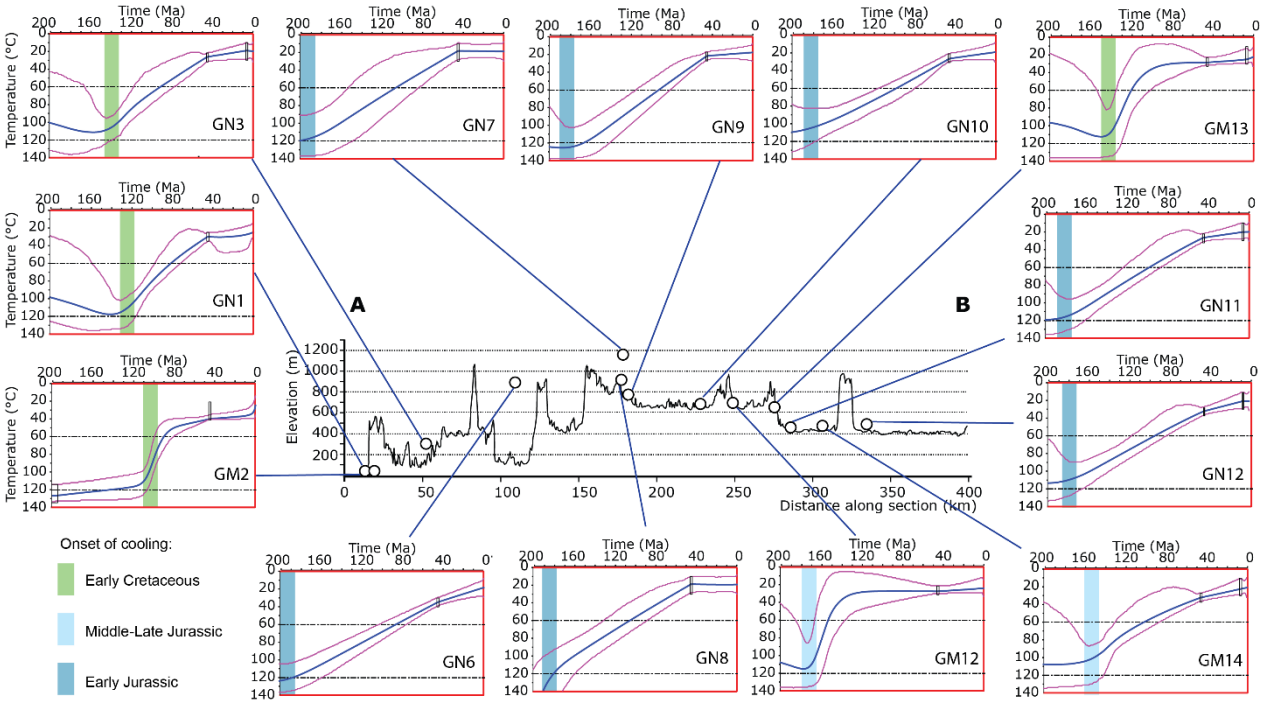

Figure 6-16 T°C/ time modelling results of samples projected on the Guinea transect in Ivory Coast. Only AFT data and geological constraints were used for modelling. The onset of cooling of each model during three time periods is indicated. Thermal models were produced and provided by M. Wildman.

6.5.2.2 Ivory Coast Transect

Modelling results of 9 samples projected on an N- trending transect of Ivory Coast were presented below. They were modelled with AFT and available AHe data, as well as geological constraints where available (Appendix 9). Samples close to each other (<50 km distance) were modelled together. In general, the onset of cooling occurs within one of three time periods: Early Jurassic (190 – 170 Ma), Mid-Late Jurassic (170 – 150 Ma), Early Cretaceous (140-130 Ma). Different cooling rates were recorded within these time intervals models, which also indicate spatial variabilities in the regional cooling pattern.

Early Jurassic (190 - 170 Ma): Extremely Slow Cooling

Samples which recorded cooling beginning in the Early Jurassic occupy large areas between 100 to 400 km inland of the coastline (Figure 6-17). The cooling is extremely slow in a linear manner until the present day with a cooling rate ranging from c. 0.2 to 0.5 °C/Myr. The temperature is estimated at the beginning of the cooling to be 110 ± 10°C for SOK1A and DLO3 Bis. However, northerner samples (SEN-1 & MK-64) record a cooling at 50 °C/Myr at the same time following an earlier more rapid cooling whose initial conditions are unconstrained.

Mid-Late Jurassic (170 – 150 Ma): Slow cooling

Samples (KG33a, VAA-1 and BEZ-1) on the northern part of the transect recorded slightly faster cooling than those described above during the Mid-Late Jurassic. They have cooling rate of c. 0.6-1.6 °C/Myr (Figure 6-17). This cooling initiates at a temperature of 110 ± 10°C at c. 160 Ma. KG33a recorded a change in cooling rate from 0.3 to 1.6 °C/Myr at c. 110 Ma, which differs from the continuous cooling recorded by VAA-1 and BEZ-1 until the present day.

Early Cretaceous (140-130 Ma): Rapid Cooling

Rapid cooling was only recorded by near coast samples (SA-3 and SA-14) during the Early Cretaceous with a cooling rate of c. 3.0 °C/Myr (Figure 6-17). Near surface temperature was reached shortly after this rapid cooling event and have been maintained for 100 Ma. The timing of this cooling coincides with the rifting of the margin during at the latest the Barremian (c.130 Ma). The rifting affects the onshore continent at a distance of less than 100 km from the coastline.

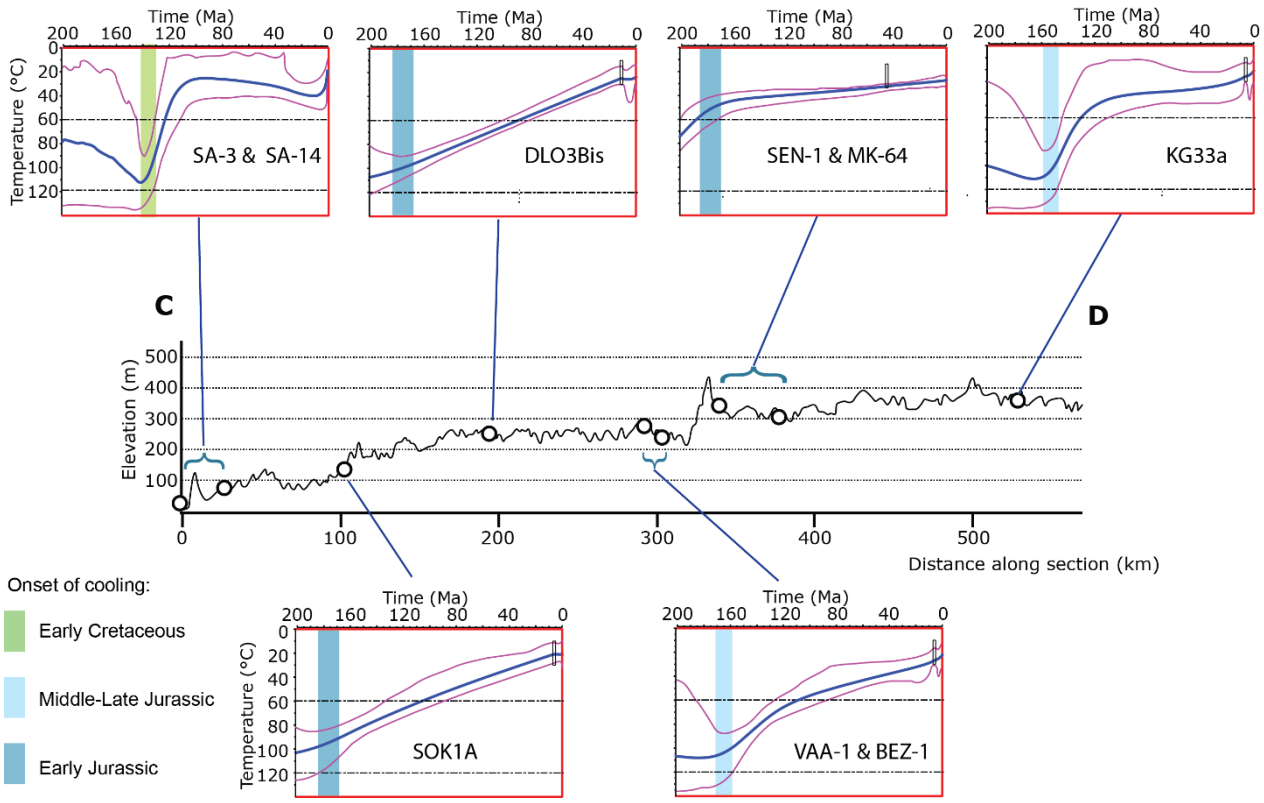

Figure 6-17 T°C/ time modelling results of samples projected on an N-trending transect in Ivory Coast. The onset of cooling of each model during three time periods is indicated. Thermal models were produced and provided by M. Wildman.

6.5.2.3 Benin Transect

Samples of the Benin transect were also modelled with both AFT and AHe data, and geological constraints. Considering the regional geology along the Benin transect (see above) samples were modelled with or without reheating permission according to the sample location. Samples near the coastal basin (BN-18 and BN-1) were modelled with reheating permitted due to their potential burial in the embayment, as well as samples close to the Kandi/Iullemmeden basin (BN-6, -7, -8, -9, Figure 6-18). Only interior samples far from both basins were modelled with no reheating permitted. Adjacent samples sharing the same geological constraints and have similar thermochronological data were modelled together.

Resulting thermal histories show great variabilities in terms of cooling onset time and cooling rate. Despite the variabilities, three major time periods of the onset of cooling were still observed: Mid-Late Jurassic (170 – 150 Ma), Early Cretaceous (140 - 120 Ma), Paleogene (40 - 20 Ma).

Mid-Late Jurassic (170 – 150 Ma): Slow Cooling

A cooling event during the Mid-Late Jurassic was only observed on the northernmost sample (BN-6, Figure 6-18). It is characterized by a slow cooling rate of 1.4 °C/Myr at c. 160 Ma. Near surface temperature was reached at c. 100 Ma and was maintained until the present day.

Early Cretaceous (140-120 Ma): Slow to Rapid Cooling

The Early Cretaceous cooling event was recorded by samples near the coastal basin (BN-1 to -5, and -17). Between them, a first group (BN-1, -2, -3 and -17) encompassing a great distance along the transect (100-250 km) is characterized by a slow cooling rate of 0.5 °C/Myr with unconstrained initial conditions (Figure 6-18). A second group (BN-4 and -5) recorded a cooling event of 2.0 °C/Myr from c. 140 to 110 Ma (initiated at 110 ± 10°C). This cooling is comparable to the Early Cretaceous cooling event observed in Ivory Coast along a c. 50 km wide coastal strip. The difference between these two Early Cretaceous cooling events is the position of the samples which are located farther inland in Benin (> 300 km from the coastline), probably due to the denudation of the embayment that had a greater extent at the time.

Paleogene (40-20 Ma)

A recent cooling event was recorded by samples (BN-7, -8, -9 and -10) near the Kandi basin (Figure 6-10), which started near the surface at c. 50 °C during the Paleogene and brought the samples to the surface until the Miocene (Figure 6-18). The samples probably experienced burial during the Late Cretaceous when the Kandi basin was actively subsiding, before being exhumed in the Cenozoic.

Other samples (BN-11, -12 and -18) were revealed to be at a shallow depth (80- 50 °C) at c. 200 Ma and experienced extremely slow cooling (c. 0.2 °C/Myr) until the present-day (Figure 6-18). The beginning of the cooling could be much older for BN-11 and -12. The thermal history of BN-18 (Upper Cretaceous sandstone) is much more problematic, as it was submitted to possible complex burial and exhumation history within the coastal basin since the Upper Cretaceous.

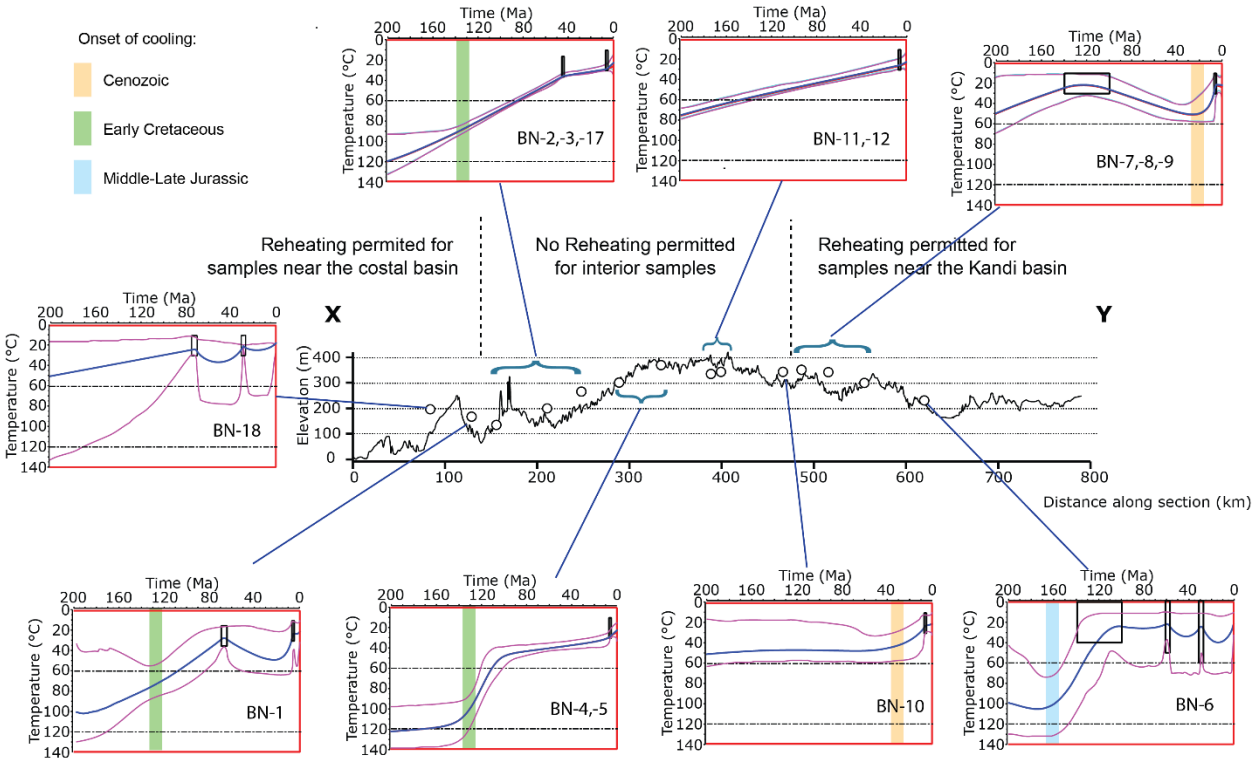

Figure 6-18 T°C/ time modelling results of samples along the Benin transect. The onset of cooling of each model during three time periods is indicated. Thermal models were produced and provided by M. Wildman.

Despite the variabilities between the three transects, general trends are still observed. Early Cretaceous cooling was all recorded by coastal samples at a moderate to rapid cooling rate. This event is probably related to rifting of the Equatorial Atlantic margin during the Valanginian - Late Albian (140-100 Ma). Interior samples recorded Early to Mid-Late Jurassic cooling (190 – 150 Ma) at a slow rate, which characterizes cratonic domains submitted to limited denudation. Cenozoic cooling event was only recorded by interior Benin samples close to the Kandi basin and may

therefore be related to the denudation of the edge of that basin. Deposition of the Mid-Eocene to Early Oligocene fluvial sediments of the « Continental Terminal » in the Iullemmeden basin was indeed shortly followed by long wavelength deformation and erosion of the basin as a consequence of the growth of the Hoggar hot spot swell (Figure 3-13, Chardon et al., 2016) .

6.6. Denudation Estimation

Magnitude of denudation was calculated for each transect based on T-t history predicted by expected thermal models, and assuming a thermal gradient of 25°C/km which is characteristic for cratonic domain. Eight time intervals were chosen with a duration of 20 or 25 Myr (except the Jurassic interval) for displaying denudation variation through time: 200 - 140 Ma, 140 - 120 Ma, 120 - 100 Ma, 100 - 85 Ma, 85 - 65 Ma, 65 - 45 Ma, 45 - 25 Ma, 25 - 0 Ma.

6.6.1 Guinea Transect (Figure 6-19A):

Total denudation since 200 Ma appears to be homogenous along the Guinea Transect, exceeding 4.0 km. Denudation between 200 and 140 Ma is uncertain due to poorly constrained thermal history models. Denudation increments vary in time and space. The southwesternmost area (0-75 km from the coastline) experienced denudation from the Valanginian (140 Ma) until the present-day. Maximum denudation occurred between 120 and 100 Ma, exceeding 1.0 km, which would correspond to the main syn-rift stage of the margin. Denudation decreases from Upper Cretaceous to Cenozoic, but remained significant during the Upper Cretaceous. Denudation in almost all the interior area (75 – 350 km from the coastline) has begun since the Early Jurassic, and decreased through time. The region at distance of 250 – 300 km from the coast is an exception, because it was submitted to negligible denudation since 140 Ma, after considerable denudation during the Jurassic (200 – 140 Ma). No burial is observed along the Guinea Transect during the Meso-Cenozoic.

6.6.2 Ivory Coast Transect (Figure 6-19B):

The Ivory Coast case reveals spatial and temporal variabilities of along-transect denudation history. Four regions can be distinguished from the coastline to the far inland (I – IV). The coastal region I (0 – 75 km) experienced the maximum total denudation (200 – 0 Ma) of the whole transect, up to almost 5.0 km. The pic of denudation (c. 2.5 km) in this region occurred during the Early Cretaceous (140 -120 Ma), followed by a rapid decrease in denudation during the Upper Cretaceous. Region I was shallowly buried during the Paleogene before being exhumed during the Neogene. Interior region II is characterized by a continuous and homogenous denudation since 200 Ma until the recent time at a denudation rate of 0.2 km/Myr. Interior region III was submitted to slight denudation since 140 Ma (less than 1 km). It could have been a long-lived divide between region I and IV. Innermost interior region IV recorded an increase in total denudation with maximum denudation occurring during the Early Cretaceous and could extend further on the north.

6.6.3 Benin Transect (Figure 6-19C):

As bounded by Meso-Cenozoic sedimentary basin, the Benin transect shows a more complex denudation history in terms of spatial variability and intensity. Three different regions are identified. The coastal region (I) was buried from the Campano-Maastrichtian to the Early Cenozoic (85-25 Ma) as part of the Dahomey Embayment. Interior region II experienced continuous denudation on the South since 200 Ma. However, denudation increases during the Lower Cretaceous to the North of the region before decreasing to a negligible value at the northern boundary of the region II. This increase could correspond to the erosion of the Gao rift shoulder formed during the Early Cretaceous rifting of the margin. Interior region III, close to the Kandi Basin, experienced rather burial than denudation during the Early Cretaceous-Cenozoic (120-25 Ma).

A. DENUDATION ALONG GUINEA TRANSECT

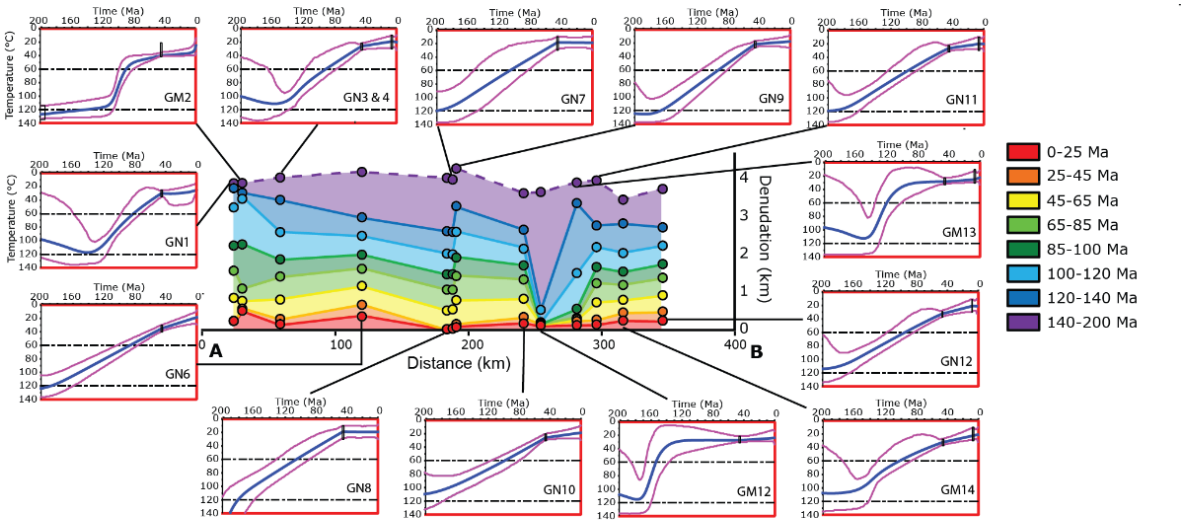

B. DENUDATION ALONG IVORY COAST TRANSECT

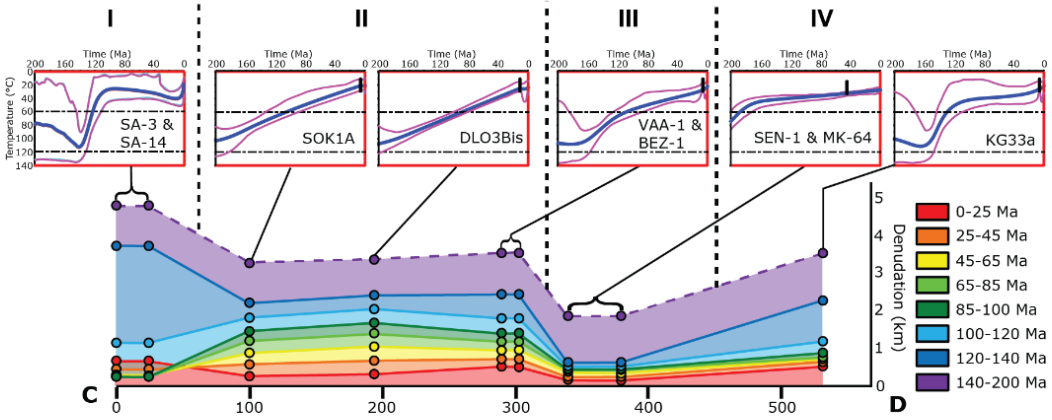

C. DENUDATION ALONG BENIN TRANSECT

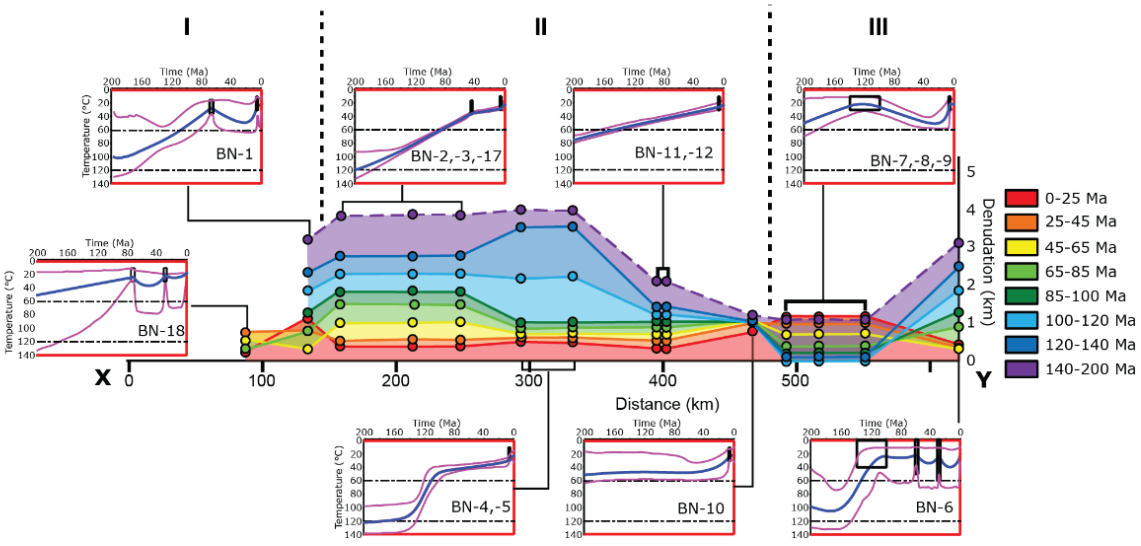

Figure 6-19 Three coast-perpendicular sections in Guinea (A), Ivory Coast (B) and Benin (C) with predictions on magnitudes of denudation over time intervals since 200 Ma and T-t models used for estimates. The geothermal gradient is assumed to be of 25°C/km.

6.7. Exported Volumes

6.7.1 Interpolation Procedure and Uncertainty Assessment

In order to calculate exported volumes of eroded materials, we interpolated the incremental denudation values of each TS2P samples, as well as the AFTA data of Gunnell (2003) in Burkina Faso. An area was defined for interpolation containing all the data points, and its Southern and Western boundaries coincide with the coastline. A triangulated surface was constructed for each time interval using the Gocad software. The resolution of the surface was adjusted by controlling the size of the triangles. Values of denudated volumes were then automatically obtained from each surface.

In order to assess the uncertainties associated with the interpolation procedure, a first set of surfaces was created with a free boundary, which allows any values at the boundary (Figure 6-20A, Figure 6-20B, Figure 6-21). This potentially increased the volumes by giving high values along the coastline and the inland boundary. The resulting volumes were so to be the maximum. A second set of surfaces was established as an end-member by fixing the denudation values to zero at the boundary (Figure 6-20C, 6-20D and Figure 6-22). The resulting volumes were decreased significantly and considered as the minimum values. Uncertainties in the volumes presented below are constrained by the difference between maximum and minimum volumes issued from each configuration (free or zero-value boundary condition).

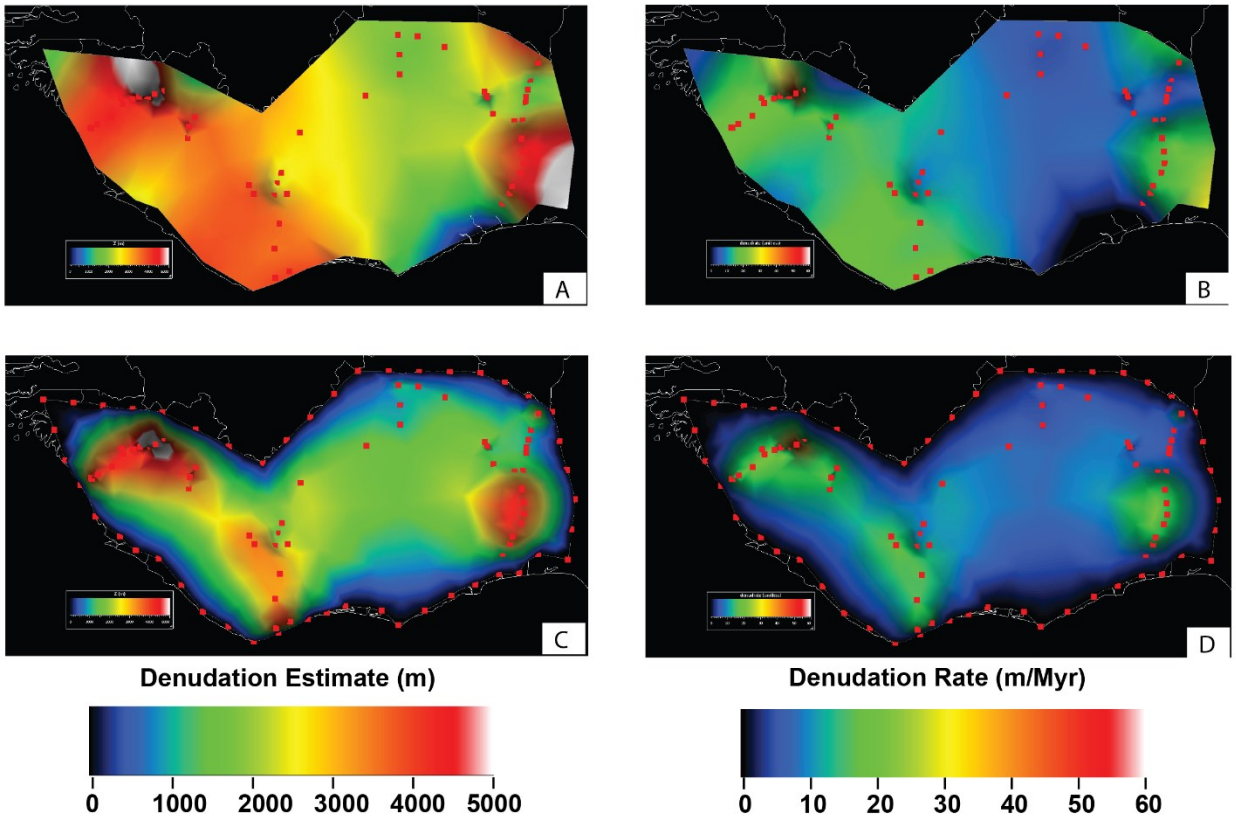

Figure 6-20 Maximum (A) and minimum (C) total denudation maps during 140 - 0 Ma obtained by triangulated surface, and maximum (B) and minimum (D) denudation rate maps.

6.7.2 Denudation Maps and Volumes

The denudation maps show the distribution of erosion in time and space. Despite the differences in values between the maximum and minimum denudation maps (Figure 6-20, Figure 6-21 and Figure 6-23), common general trends were observed:

- Denudation was systematically low (mostly < 1000 m) during the interval going from the Early Cretaceous (140 – 120 Ma) to the Neogene-Quaternary (25 – 0 Ma);
- Areas with relative high and low denudation values did not significantly evolve since the Jurassic (200 – 0 Ma). High values were concentrated at three regions

close to the boundaries, in the West (Guinea), the South (Western Ivory Coast) and East (Benin);

- A narrow corridor of intense denudation exists along the Western coastline of Ivory Coast between 140 and 100 Ma and disappears afterwards. We interpret this corridor to reflect Early Cretaceous rift shoulder topography that was eroded after the continental breakup.

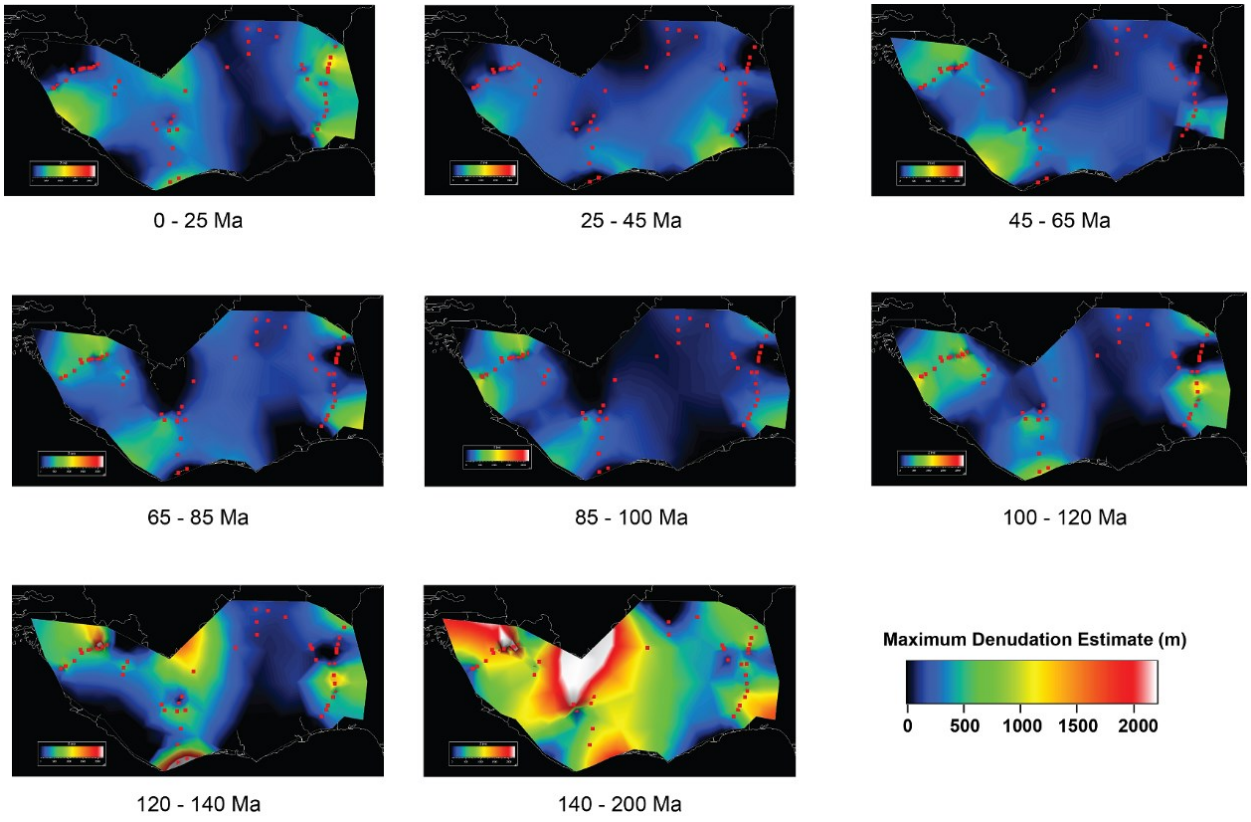

Figure 6-21 Maximum denudation maps from 140 to 0 Ma obtained by triangulated surface construction under a free boundary condition. Note that duration varies between time intervals.

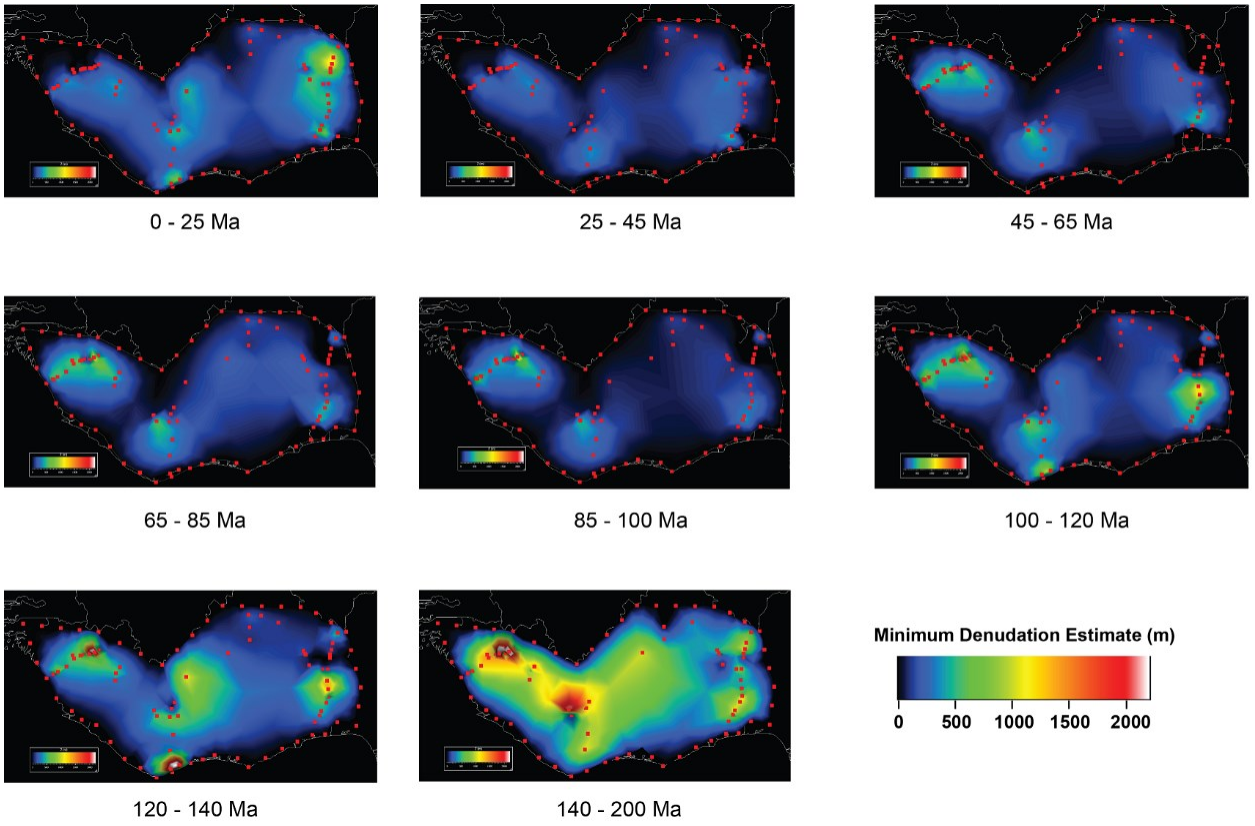

Figure 6-22 Minimum denudation maps from 140 to 0 Ma obtained by triangulated surface construction under zero denudation at the boundary. Note that duration varies between time intervals.

In order to analyze the geological meaning of the results, incremental volumetric denudation rates (m^3/Ma) were converted into averaged denudation rates at the scale of the study area (m/Ma) (Figure 6-23). No major change in volumetric denudation rates is observed since 200 Ma (2.1 to 1.1x10^{13} m^3/Ma). A small peak in volumetric denudation rate (2.1x10^{13} m^3/Ma) occurred during the Valanginian-Aptian (140 – 120 Ma), followed by a slow decrease in rate until the Miocene (20 Ma). Regionally averaged denudation rates show a range of 7 to 16 m/Ma through time, which is typical for cratonic domains (e.g., Beauvais and Chardon, 2013).

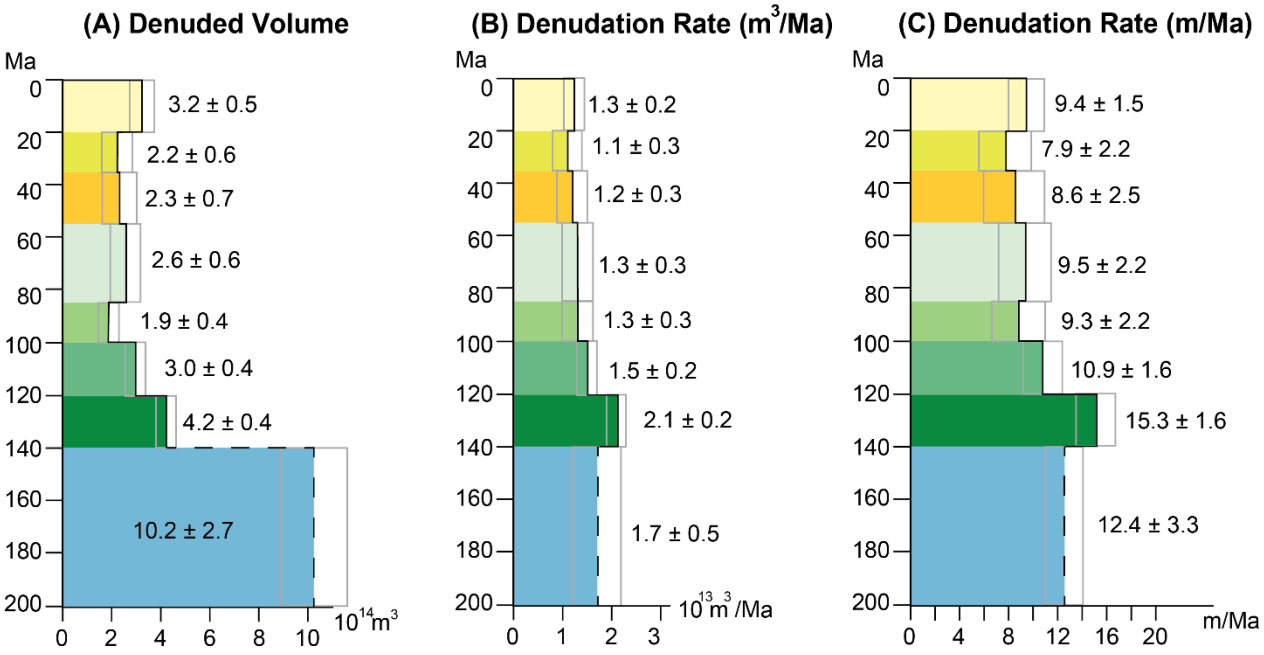

Figure 6-23 Diagrams showing the results of denuded volume (A), denudation rate in m^3/Ma (B) and in m/Ma (C) from 200 to 0 Ma.

6.8. Summary and Conclusions

Thermochronological data (AFTA and AHe dating) along three transects were obtained for the first time inland the African Atlantic Equatorial margin. AFT ages vary from 401 to 95 Ma with mean track lengths of 11.4 to 14.1 µm. AHe ages present a great dispersion; some of them are older than corresponding AFT ages due to the radiation damage effect. The data (AFTA and AHe) were preferentially modelled jointly, incorporating additional geological constraints, to produce the best-constrained thermal history of each sample. The obtained thermal histories show a diversity and spatial variability. Most of samples experienced a slow cooling (< 1.0°C/Myr) beginning in one of the three following time intervals: Early Jurassic (200-170 Ma), Middle-Late Jurassic (175-145 Ma) and Early Cretaceous (145-100 Ma). The CAMP (~200 Ma) may have impacted the study area by reseting thermochronological systems, so that no earlier event was preserved. The Early Cretaceous cooling is likely associated with the rifting of the Equatorial Atlantic Ocean, which influenced only a coastal corridor. Denudation was then estimated for each sample based on its expected thermal

history by assuming a constant thermal gradient of 25 °C/Ma. Denudation maps for a number of time intervals between 200 and 0 Ma were then computed by triangulated interpolation. These maps show the regional pattern of denudation, which remains nearly constant through time. Total denudated volumes were computed for each time interval and are of the order of magnitude of $10^{14}m^3$ since the Early Jurassic. The regionally averaged denudation rates range from from 7 to 16 m/Ma and show no major change since 200 Ma with only a small peak during 140 – 120 Ma. Instead of showing major denudation pulses (several kms) due to rifting and/or later tectonic events like that recorded by Southern Africa in the Late Cretaceous (e.g., Tinker et al., 2008), the Equatorial margin of Africa has recorded slow denudation typical of cratonic domains even though rifting may be detected in its Early Cretaceous denudation pattern.

CHAPTER 7 : OUTLINES OF A SOURCE-TO-SINK ANALYSIS, IMPLICATIONS FOR VERTICAL DISPLACEMENTS OF THE MARGIN

7.1. Introduction

This chapter presents the preliminary results of a source-to-sink analysis based on denudated (Chapter 6) and accumulated (Chapter 5) volumes and rates. The first-order Meso-Cenozoic changes in sedimentary fluxes and paleo-drainage system in West Africa are first discussed, as well as their implications for the understanding the Equatorial African sediment routing system. In a second section, vertical displacements of the margin induced by these sedimentary transfers are calculated for the Ivory Coast case, where the behavior of both the divergent and transform margin segments were simulated.

7.2. Source-to-Sink Sediment Budget

We compared the denudated and accumulated sediment budgets from the Late Cretaceous to the Cenozoic (100-0 Ma). The Middle Eocene-Quaternary (45-0 Ma) source-to-sink analysis is based on the accumulated volumes estimated in the course of this work (Chapter 5) and the eroded volumes of Grimaud (2014), which are based on the subtraction of dated relict lateritic landsurfaces. We used the denuded volumes retrieved from low-temperature thermochronological analysis (Chapter 6) and the accumulated volumes (Chapter 5) for the Late Cretaceous – Early Eocene (100-45 Ma) source-to-sink analysis. The Early Cretaceous syn-rift source-to-sink sediment budget was not interpreted because of the difficulty / impossibility to estimate syn-rift sediment volumes from the 2D seismic data. Moreover, some of the syn-rift depocenters are now located offshore the conjugate margin of South America, and the contribution of the South American continental surface to those depocenters must be significant.

7.2.1. Middle Eocene – Quaternary (45 - 0 Ma)

Clastic fluxes are first-order data to understand the transfer of eroded materials from their source to their basin sink. Post-Middle Eocene denudation history (45 - 0 Ma) of West Africa was well constrained by relictual lateritic landscapes at a much higher resolution than the thermochronological data (Grimaud, 2014; Chardon et al., 2016). Three regional-scale paleosurfaces were reconstructed by interpolation: the S1 (45 Ma), S2 (24 Ma) and S3 (11 Ma)

surfaces (Grimaud, 2014). Denudation maps for three intervals were obtained by subtracting successive paleosurfaces and the modern topography. Drainage divides were defined on the paleolandsurface geometries that had been corrected for the isostatic flexural deformation they have undergone since their abandonment as a consequence of erosional discharges and sedimentation charges (Chardon et al., 2016). A major shift in the drainage divide was documented between 34 and 29 Ma (after the abandonment of the S1 surface at 45 Ma and that of the S2 surface at 24 Ma) as a far-field effect of the growth of the Hoogar hot spot swell (Chardon et al., 2016) (Figure 7-1). At 29-24 Ma, the main divides of the sub region were established (Chardon et al., 2016). The quantification of eroded volumes was carried out for three major drainage areas contributing to the Equatorial margin (i.e., Short Atlantic drains, Long Atlantic drains, and Niger catchment), taking into account the uncertainties on drainage divides locations (Grimaud et al., in prep., Figure 7-1). Exported volumes were corrected by subtracting the Cenozoic volumes preserved in intracontinental basins to the eroded volumes. In the end, clastic exported volumes were extracted from exported volumes assuming a mean regolith porosity of 25%, as mostly regolith, as opposed to fresh bedrock, is the clastic material being provided to the river systems (Beauvais and Chardon, 2013; Grimaud et al., 2015; Grimaud et al., in prep.)

Overall, the sub region exported 928 $10^3 km^3$ of clastic sediments to the Equatorial Atlantic Ocean during the 45 - 0 Ma interval. More volumes were exported from the Niger catchment than the Long Atlantic drains (Table 7-1). The least of volumes were exported from the Short Atlantic drains, which represent the smallest contributing area. At first-order, exported rates increased in all basins between 45 – 24 Ma and 24 - 11 Ma, as contributing areas increased in size as a consequence of drainage reorganization. A decrease in exportation occurred for the 11-0 Ma period.

We compared the export rates with non-extrapolated accumulation rates measured in the nearby Equatorial basins (Chapter 5) and the Niger delta (Figure 7-1, Grimaud et al., in prep.). The reason why non-extrapolated accumulation rates were used is that the extrapolated accumulation rates could not be obtaiend in the Ghana-Benin basin (Figure 5-9), where the contribution of the Niger Delta is significant and should be distinguished. Overall, they fall within the same order of magnitude for each independent source-to-sink system roughly corresponding to a margin segment (Figure 7-1 and Table 7-1). The sediment budget is fairly well balanced during the 45 – 24 Ma and 24 – 11 Ma export periods taking into account the uncertainties, between the Long Atlantic drains

and their sink basins, and between the Niger catchment and its delta (Figure 7-1 and Table 7-1). However, the accumulation rate largely exceeds the export rate during the 11 – 0 Ma interval for these two systems. Different trends are observed for the Short Atlantic drains and the Sierra Leone-Liberia basin, as only the bulk (i.e., 45-0 Ma) accumulation rate was obtained (Figure 7-1 and Table 7-1). The total exported volume by Short Atlantic drains was estimated to be 111 ± 15 $10^3 km^3$, which is comparable to the accumulated volume of 148 ± 31 $10^3 km^3$.

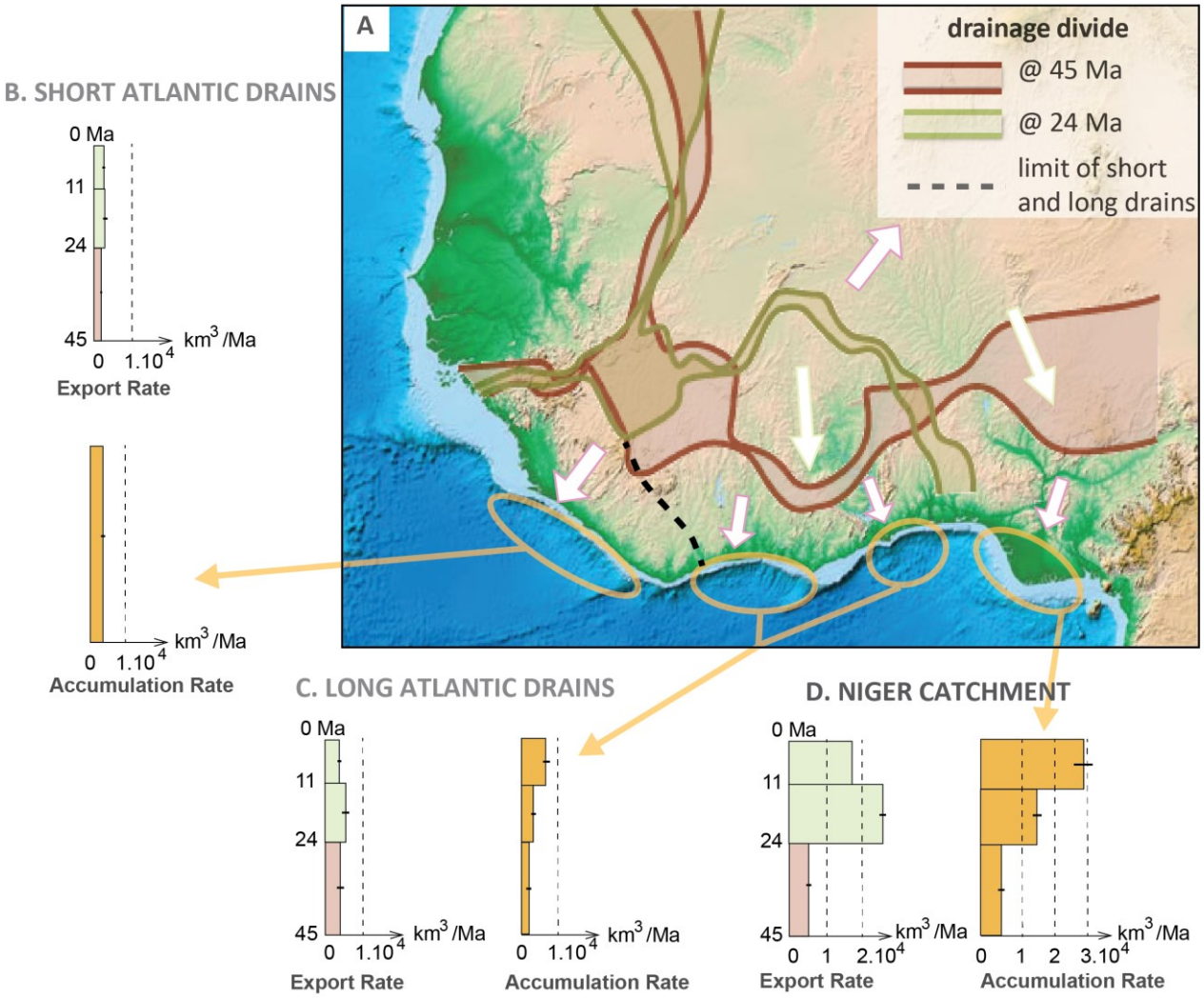

Figure 7-1 Middle Eocene – recent (45 - 0 Ma) volumetric source-to-sink budget. (A) Map of paleo-drainage divides at 45 and 24 Ma over a topographic map of West Africa. Arrows with the same color indicate general draining direction of three major drainage areas at 45 and 24 Ma. Clastic export rates and accumulation rates are shown for three source-to-sink systems: (B) the Short Atlantic drains and the Sierra Leone-Liberia basin, (C) the Long Atlantic drains and the Ivory Coast and the Ghana-Benin basins, and (D) the Niger catchment and the Niger Delta.

MIDDLE EOCENE – QUATERNARY CLASTIC SEDIMENT EXPORTATION Vs ACCUMULATION

Location	Interval (Ma)	Exported Volume (10^3km^3)	Clastic Export Rate (10^3km^3/Ma)	Accumulated Solid Volume (10^3km^3)	Accumulation Rate (10^3km^3/Ma)
Long Atlantic drains	11 - 0	44 ± 7	3.0 ± 0.5	85 ± 13	7.7 ± 1.2
	24 - 11	86 ± 22	5.0 ± 1.3	46 ± 10	3.8 ± 0.7
	45 - 24	97 ± 40	3.5 ± 1.4	47 ± 13	2.3 ± 0.6
Short Atlantic drains	11 - 0	29 ± 4	2.0 ± 0.3		
	24 - 11	37 ± 7	2.1 ± 0.4	148 ± 31	3.3 ± 0.7
	45 - 24	45 ± 4	1.6 ± 0.1		
Niger catchment	11 - 0	177 ± 11	12.1 ± 0.7	322 ± 43	29.3 ± 3.9
	24 - 11	260 ± 83	15.0 ± 4.8	173 ± 23	13.3 ± 1.8
	45 - 24	153 ± 136	5.5 ± 4.8	110 ± 15	5.2 ± 0.7

Table 7-1 45-0 Ma clastic export and accumulation budgets of the three West African source-to-sink systems (e.g., the Long Atlantic drains, the Short Atlantic drains and the Niger catchment with their corresponding sink basins, Figure 7-1).

7.2.2. Late Cretaceous – Early Eocene (100 – 45 Ma)

The denudation rates deduced from the thermochronology (Chapter 6) and accumulation rates determined offshore (Chapter 5) allow the Late Cretaceous-Early Eocene (100 – 45 Ma) overall sediment budget between the African Equatorial margin and its hinterland (Figure 7-2). The paleodrainage(s) for that time interval remains unknow due to the limitation of the thermochronological method and to the lack of paleolandscape remnants of that age. The contributing area may be different from that covered by the thermochronological data. However, the paleo-maps (Figure 3-9 to Figure 3-11) suggest that the area covered by thermochronological sampling roughly coincides with the area that was being eroded during the Cretaceous i.e., at the emplacement of the currently outcropping Léo-Man shield. Only non-extrapolated accumulation rates were used, due to the same raison as above. But volumes under-estimination is less important for the Late Cretaceous because the main depocenters were close to the shoreline and therfore included in the non-extrapolated volumes (e.g., Chapter 5).

The order of magnitude is the same for the total denudation and the cumulated accumulation on the whole Equatorial Atlantic margin (Table 7-2). A total volume of 6.8 ± 1.7 $10^5 km^3$ was denuded in West Africa during 100 - 45 Ma, of which 4.5 ± 1.0 $10^5 km^3$ were eroded during the Late Cretaceous (100 - 65 Ma). The total clastic volume accumulated in the Equatorial Atlantic basins was up to 8.1 ± 1.9 $10^5 km^3$, 6.9 ± 1.7 $10^5 km^3$ of which were deposited during the Late Cretaceous. The sedimentary volumes between the West African continental sources and the Equatorial Atlantic basins' sinks are therefore balanced within uncertainties. However, at a higher resolution, an excess of accumulated volume and rate occurred during the Cenomanian-Santonian (100 – 85 Ma) and the Campanian-Maastrichtian (85 – 65 Ma). Paleocene-Early Eocene (60-45 Ma) denudation rate in West Africa exceeds the accumulation rate in the Equatorial Atlantic basins (Figure 7-2 and Table 7-2).

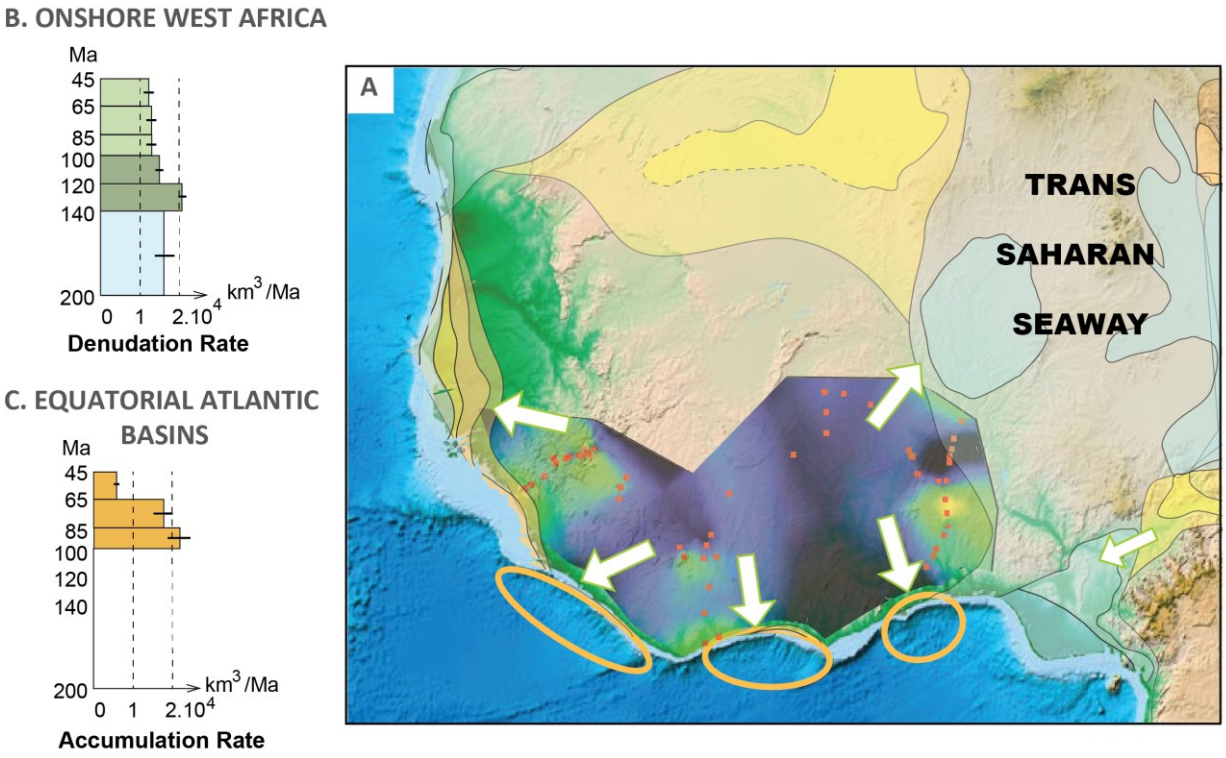

Figure 7-2 Late Cretaceous – Early Eocene (100 – 45 Ma) denudation and accumulation. (A) Cenomanian-Santonian denudation map (100 – 85 Ma, Figure 6-21) and Upper Cenomanian paleogeographic map (97 – 93 Ma, Figure 3-9) overlapping on the topographic map of West Africa. Arrows indicate potential draining directions of eroded materials. Denudation rate in West Africa (B) and accumulation rates in the Equatorial Atlantic basins (C) are shown.

UPPER CRETACEOUS – LOWER EOCENE DENUDATION Vs ACCUMULATION

Interval (Ma)	Denuded Volume ($10^5 km^3$)	Denudation Rate ($10^4 km^3/Ma$)	Accumulated Solid Volume ($10^5 km^3$)	Accumulation Rate ($10^4 km^3/Ma$)
45 - 65	2.3 ± 0.7	1.2 ± 0.3	1.2 ± 0.2	0.6 ± 0.1
65 - 85	2.6 ± 0.6	1.3 ± 0.3	3.7 ± 0.9	1.8 ± 0.5
85 - 100	1.9 ± 0.4	1.3 ± 0.3	3.2 ± 0.8	2.1 ± 0.6
100 - 120	3.0 ± 0.4	1.5 ± 0.2		
120 - 140	4.2 ± 0.4	2.1 ± 0.2		
140 - 200	10.2 ± 2.7	1.7 ± 0.5		

Table 7-2 Late Cretaceous - Early Eocene denuded volumes and denudation rates in West Africa based on thermochronology and total non-extrapolated accumulated volumes and accumulation rates in the Equatorial Atlantic basins from Chapter 5.

7.2.3. Interpretation

Overall, the clastic sedimentary volumes are well-balanced for the 45 – 11 Ma time interval between West African drainage systems and their sink basins. The higher values in exported and accumulated volumes during the 24 -11 Ma interval would support drainage reorganization before 24 Ma that led to dramatic increase in the size of the Niger and long Atlantic drains' catchments (Chardon et al., 2016). Since that reorganization, the Niger catchment incorporated the uplifting Hoggar Shield. Large quantities of sediments were then exported to the Niger delta. However, the higher accumulation rate during the 11-0 Ma interval in the Niger Delta and the Equatorial Atlantic is not supported by our export rate data. One explanation is the temporary storage of the previously eroded sediments in the intracontinental basins (e.g., Iullemmeden basin), that were exported only after 11 Ma (Grimaud et al., in prep.). In fact, less sediments were accumulated on the margin than exported during the 24 - 11 Ma interval for the Niger catchment and the Long Atlantic drains. The budget could therefore be better balanced for the 11 - 0 Ma interval as a consequence of the tapping of Paleogene (pre-24 Ma) sediments that were stored in the Iullemmeden basin (probably more than $10^5 km^3$). Lateral currents can also have brought sediments (i.e., contourites) from nearby margins, which would further explain the excess. Large quantities of contourites are indeed

observed on seismic data from offshore Ivory Coast to Nigeria since the Late Miocene (Huyghe, 2016).

The Late Cretaceous-Early Eocene (45-24 Ma) sediment budgets are balanced considering total eroded and deposited volumes. The excess of denudation during the Paleocene-Early Eocene (65-45 Ma) compared to offshore accumulations is more problematic. But the thermochronology-derived denuded volumes should be converted into clastic exported volumes by taking into account of the regolith porosity (as done for the 45-0 Ma period) and the potentially different geometry of the drainage system, as it has been done for the 45-0 Ma period. A second source for the source-to-sink discrepancy could be due to the fact that the accumulated volumes are non-extrapolated to distal basin (Chapter 5). Because the Equatorial Atlantic Ocean was fully opened during the Cenozoic and more sediments were deposited in distal plain, the accumulation is therefore underestimated.

The "excess" of accumulated volumes during the Late Cretaceous could have several causes. Lower Cretaceous syn-rift sediments exposed on the shelf of the margin could have been eroded and re-deposited on the slope of the margin and the distal basin. On seismic data, Cenozoic sediments rest directly upon the Late Albian breakup unconformity (Figure 4-4a and 4-8). Vitrinite reflectance data available in wells on the shelf of the margin show 500 – 1000 km of erosion during the Late Cretaceous hiatus (M. Dall'asta, personal communication). This supports erosional remobilization of Lower Cretaceous sediments or earlier Upper Cretaceous deposits. Moreover, mass-transport deposits and turbiditic systems were observed on seismic data in the Upper Cretaceous series (Chapter 4), which further support the remobilization hypothesis. Another cause for this discrepancy would be the existence of an extra source of eroded sediment. According to our paleogeographic maps (Ye et al., submitted), since the opening of the Equatorial Atlantic Ocean during the Late Albian, the area located South of the Benue Through was exposed to erosion and contributed sediments in the Atlantic Ocean. The paleogeography study further showed that Cretaceous sediments issued from the erosion of the marginal upwarp were temporarily stored in the Saharan intracratonic basin. Part of these sediments has been re-eroded and transported to the Equatorial Atlantic margins by river(s) crossing the upwarp. As the Saharan basin always lies outside the area covered by the thermochronology study (Figres 6-9), such sediment transfers may have contributed to the "extra" volume now found in the margin basins.

7.3. Induced Vertical Displacements of the Margin

Denudation and sediment deposition loading can cause uplift and subsidence, in response to the isostatic flexure of lithosphere. In order to simulate such vertical displacements induced by sediment mass transfers documented by the present study, we used a numerical modelling approach (Flex3D) applied to the Ivory Coast case where two margin types, transform and divergent, are present (Chapter 4). The two configurations were tested separately and combined with the onshore 2D denudation transect (Chapter 5).

7.3.1. Approach

We used the numerical Flex3D model of Braun et al., 2013, which calculates the flexural response of the lithosphere subjected to an instantaneous stretching that represents rifting. It incorporates the thermal relaxation following stretching and diffusion-type surfaces processes. The surface deflection can be calculated, assuming a thin elastic plate, whose effective elastic thickness (EET) is controlled by a given isotherm. The lithospheric stretching parameters (REF) are defined as follows. For the lithosphere, $\delta = h^0_m/h_m$, and for the crust, $\beta = h^0_c/h_c$, where h^0_m and h^0_c are initial thicknesses of the lithosphere and crust, and h_m and h_c are thickness of the lithosphere and crust at the end of the stretching.

In this work, we first defined a 2D stretched geometry (h_m and h_c) of the lithosphere inspired from offshore seismic profiles and African crustal and lithospheric thickness model (Bajolet et al., in prep.). Densities of the continental and oceanic crusts are referred to published geophysical data along the Atlantic Equatorial margin (Edwards et al., 1997; Sage et al., 2000). By defining a reference crustal thickness (h_0r, with this thickness, the surface of the crust is at the altitude of 0 m) of 29 km, a topo-bathymetric profile for the stretched lithosphere is reproduced in Flex3D, in response to the isostatic flexure of the lithosphere. In order to calculate the vertical displacements resulting from onshore denudation (d) and/or offshore sedimentary loading (s), we defined the above stretched geometry of the lithosphere as a reference, and a new geometry of the lithosphere is obtained by subtracting the denudation from the continental crust thickness of the reference and/or adding sedimentary loading on the reference oceanic crust thickness. A new topographic

and bathymetric profile of this geometry is then obtained and compared with that of the reference case. The difference between these two topographic and the bathymetric profiles (Δh) gives the value of vertical movements (U), using the relations: $U = d - \Delta h$ and/or $U = s + \Delta h$.

In doing so, no surface processes were incorporated, neither the variation of the EET in time and in space. The limitation of this model is that the difference between continental and oceanic crusts is only expressed by different densities. The thermal evolution of the oceanic crust and its impact on the vertical movements were not taken into account.

7.3.2. Model Setting

The thermochronological transect of Ivory Coast was used for inland denudation history. Two seismic profiles crossing the transform and the divergent parts of the margin, were used for sedimentary loading estimation (Figure 7-3). The transform and divergent margins with distinguishable necking widths (140 km VS 40 km) were modelled separately. For each margin, 6 cases were tested (Table 7-3):

(1) Denudation only during 140 – 0 Ma;

(2) Denudation and sedimentary loading during 140 – 0 Ma inverval;

(3) Averaged Denudation and sedimentary loading during 140 – 0 Ma inverval;

(4) Denudation and sedimentary loading during 140 – 100 Ma inverval;

(5) Denudation and sedimentary loading during 100 – 65 Ma inverval;

(6) Denudation and sedimentary loading during 65 – 0 Ma inverval;

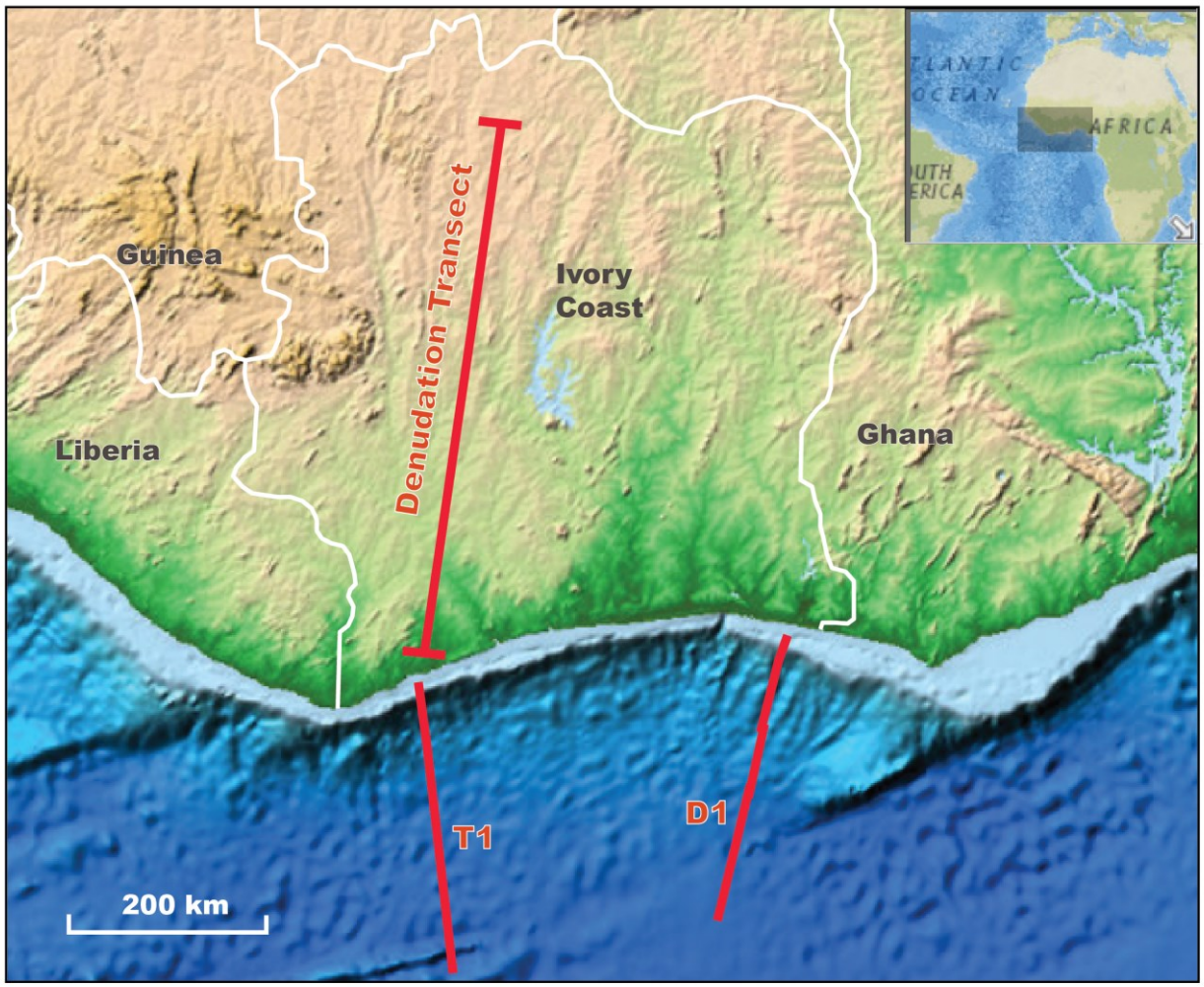

Figure 7-3 Location of the thermochronological denudation transect and seismic profiles in Ivory Coast used for modelling of vertical movements of Coast Ivory transform and divergent margins. T1: Seismic profile used for transform margin; D1: Seismic profile used for divergent margin.

TESTED CASES IN FLEX3D

	Case tested	Time interval	w_m (km)
ExpD0	Reference model	/	140
ExpD1	Denudation	140-0 Ma	140
ExpD2	Denudation + offshore sedimentary loading	140-0 Ma	140
ExpD3	Averaged denudation + offshore sedimentary loading	140-0 Ma	140
ExpD4	Denudation + offshore sedimentary loading	140-100 Ma	140
ExpD5	Denudation + offshore sedimentary loading	100-65 Ma	140
ExpD6	Denudation + offshore sedimentary loading	65-0 Ma	140
ExpT0	Reference model	/	40
ExpT1	Denudation	140-0 Ma	40
ExpT2	Denudation + offshore sedimentary loading	140-0 Ma	40
ExpT3	Averaged denudation + offshore sedimentary loading	140-0 Ma	40
ExpT4	Denudation + offshore sedimentary loading	140-100 Ma	40
ExpT5	Denudation + offshore sedimentary loading	100-65 Ma	40
ExpT6	Denudation + offshore sedimentary loading	65-0 Ma	40
Constant parameter		value	
Thermal gradient		35°C/km	
EET (km)	effective elastic thickness	15	
zn (km)	necking depth	10	
h°m (km)	initial lithosphere thickness	140	
h°c (km)	initial curst thickness	34	
TL (°C)	LAB temperature	1330	
ρs (kg m-3)	sediment density	2500	
ρm (kg m-3)	mantle density	3300	
ρcc (kg m-3)	continental crust density	2800	
ρnc (kg m-3)	crust density in necking zone	2900	
ρoc (kg m-3)	oceanic crust density	3000	
h0r (km)	reference crustal thickness	29	
E (Pa)	young's module	7x1010	
ν	poisson's ration	0,25	

Table 7-3 Parameters of tested cases in Flex 3D. ExpD0-D6 are experiences done for the divergent Ivorian margin, and ExpT0-T6 are for transform margin. Wm: Necking width.

7.3.3. Results

The results show the denudation-induced uplift of the continent and the sediment loading-induced subsidence (Figure 7-4). The geometry of the vertical movement profile (purple line) roughly mimics the denudation and sedimentary thickness profiles (dotted red line). An uplift average of 1207 m is obtained, which is slightly less than the denudation average of 1510 m. The maximum thickness (4300 m) of the sedimentary accumulation induced a maximum subsidence of 5200 m of the margin.

Incremental vertical displacements evolve through time and space since 140 Ma (Figure 7-4b). An area of intense uplift (close to 2 km) is revealed within a narrow coastal zone (100 -0 km of distance) between 140 and 100 Ma. It disappeared afterwards during the Late Cretaceous and the Cenozoic (100 – 0 Ma). Uplift pattern inland of this zone shows low values, with a minimum (close to 0) around 400 – 350 km. Subsidence induced by sediment loading in the transform margin evolves during the post-rift. The main depot-center seems to migrate southward (i.e., oceanward) during the Cenozoic (65 – 0 Ma).

The vertical displacement patterns obtained for the divergent Ivorian margin show an onshore uplift history comparable to that of the transform margin (Figure 7-4c and d). The uplift profile roughly parallel the denudation profile but is always less. Offshore subsidence is less than that of the transform margin after 100 Ma (Figure 7-4d). The maximum subsidence is located farther from the coastline (at c. 150 km), and seems to be fixed during the entire post-rift history (100 – 0 Ma) (Figure 7-4c).

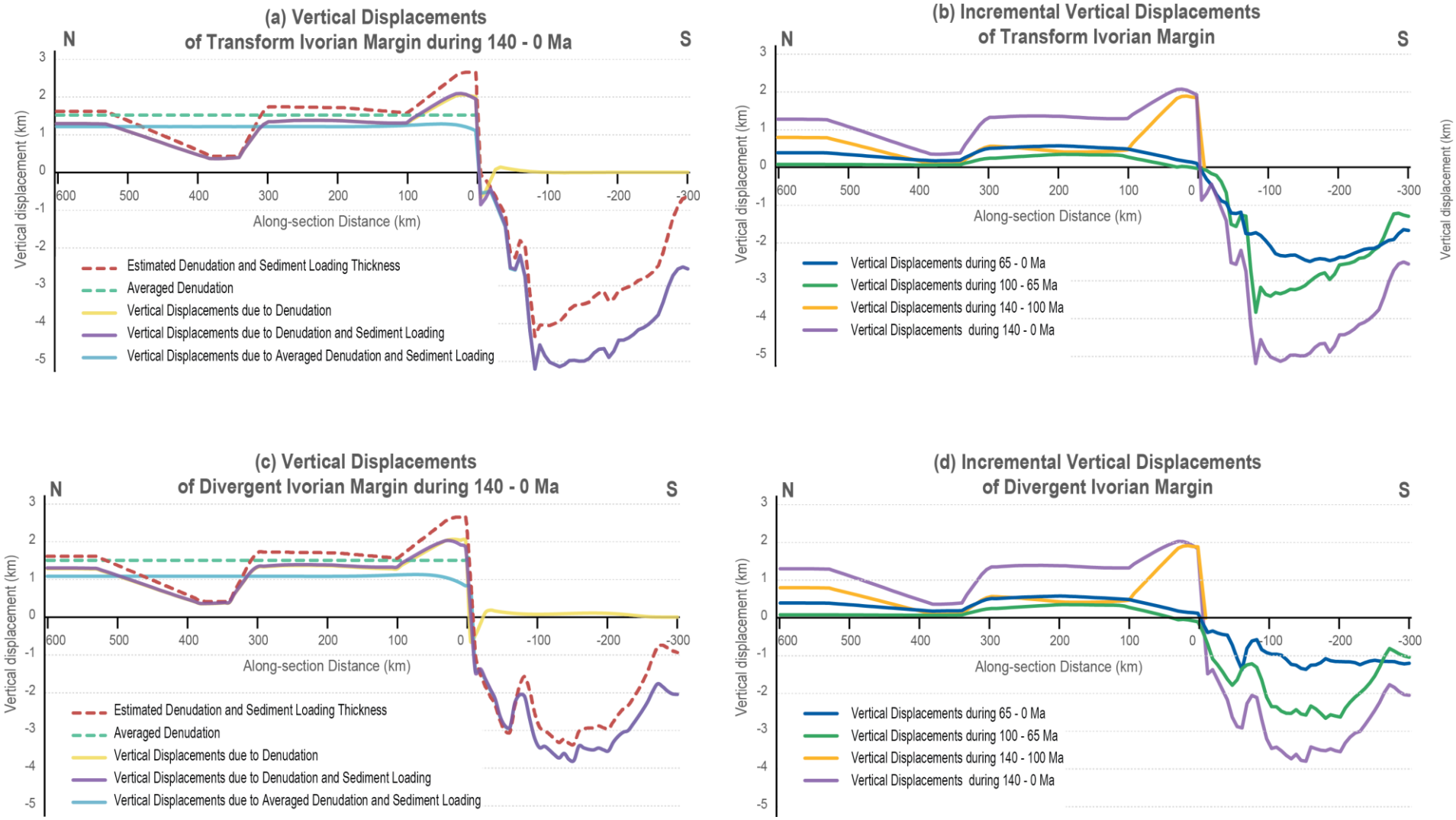

Figure 7-4 Results of the vertical displacements and the incremental values obtained on the transform (a and b) and divergent (c and d) margins in Ivory Coast. The coastline is at along-section distance of 0 km.

7.3.4. Interpretation

Sedimentary loading does not influence the onshore denudation-induced uplift pattern. Indeed, the denudation only-induced inland uplift profile (yellow line, Figure 7-4a and c) superimposes over the uplift profile resulting from the combination of denudation and offshore loading (purple line, Figure 7-4a and c).

Importantly, the onshore uplift pattern is comparable for the transform and the divergent margins although they have different necking widths and sedimentary histories. The same uplift profiles were obtained that are mostly controlled by the denudation pattern. The corridor of highest uplift closed to the shoreline between 140 and 100 Ma may correspond to the flexure-controlled rift shoulder formed and eroded during the syn-rift stage despite the very narrow zone of necking expected in a transform regime. The eroding coastal topography was not maintained later during the Late Cretaceous and Cenozoic as long-wavelength “cratonic” deformation may have exerted a growing influence on the cooling margin. Longer wavelength continental flexure may explains the attenuated inland uplift pattern.

7.4. Conclusion

New denudation and accumulation data acquired in this work allowed for a first-order source-to-sink study of the paired shield-margin system of Northwestern Africa along its Equatorial margin since the Early Mesozoic. Earlier works on Cenozoic denudation history and drainage systems (Grimaud, 2014; Grimaud et al., 2015; Chardon et al., 2016) were used to be compared to newly acquired Cenozoic accumulation history in the Equatorial Atlantic basins. Three source-to-sink systems related to three major catchments show similar trends of denudation and accumulation rates. The Late Oligocene reorganization of drainage systems was well recorded in the offshore basins by an increase in sedimentary input, which in turn confirms the paleo-drainage configuration and reorganization (Chardon et al., 2016). Mesozoic sediment budgets were evaluated at the scale of NW Africa and its Equatorial margin on the basis of an onshore thermochronological study and newly acquired offshore sediment accumulation history. The total sedimentary volumes were well-

balanced overall for the Late Cretaceous, post-rift history of the margin, within uncertainties. A slight excess of accumulation compared to erosion during the Late Cretaceous and since the Late Miocene reflects the complexities of source-to-sink sedimentary routing systems. Among those complexities, transient intracratonic storage of sediments issued from marginal upwarp erosion, and remobilization of older sediments on the margin is the most significant.

Source-to-sink sediment transfers in West Africa induced significant vertical movements due to flexural isostasy of the lithosphere. Onshore uplifts of ca. 1 km and maximum subsidence of 4 to 5 km may be produced, with a comparable impact on divergent or transform segments of the margin. Onshore uplift pattern is solely controlled by denudation, and the long-term thermal and sedimentary history of the adjacent margin did not influence inland vertical movement except for a narrow (2 km wide) coastal strip of higher uplift and denudation produced only during rifting.

CONCLUSION

Cette thèse présente une nouvelle approche de l'évolution paléo-géographique, structurale et sédimentaire de l'Afrique de l'Ouest et de sa marge atlantique équatoriale dans une perspective *source-to-sink*. Une nouvelle série de reconstructions paléogéographiques et structurales méso-cénozoïques a été produite sur la base d'une méthode innovante. Elle permet de proposer, outre un nouveau modèle structural et cinématique d'ouverture précoce de l'Atlantique Equatorial, une histoire intégrée terre-mer de la déformation lithosphérique à grande longueur et des transferts sédimentaires associés. Une synthèse de la structure et de l'architecture stratigraphique post-rift crétacée supérieure de la marge Atlantique Equatoriale a été réalisée à partir de l'interprétation de données inédites de subsurface. Elle a permis de quantifier ensuite les volumes sédimentaires clastiques accumulés dans les bassins de la marge. Ce travail a également incorporé de nouvelles données thermochronologiques basse-température acquises sur le domaine continental qui ont permis de caractériser l'histoire de l'érosion et de quantifier les volumes sédimentaires exportés depuis le Mésozoïque. Un bilan volumétrique *source-to-sink* a ensuite été réalisé.

Les domaines en érosion et en sédimentation en Afrique de l'Ouest évoluent depuis le début du rifting du futur Océan Atlantique Equatoriale. Un grand bassin continental saharien recevait les produits d'érosion du bourrelet marginal équatorial et communiquait vers l'aval (au Nord) avec la Téthys. Il a été ensuite envahi par la mer durant les transgressions crétacées supérieures et a pu, à plusieurs reprises, perdre des sédiments qui ont été re-exportés vers les bassins de la marge équatoriale. Les bassins intracratoniques actuels n'ont acquis leurs géométries qu'à partir de la fragmentation oligocène du bassin saharien par le percement du bombement du Hoggar, et ne constituent ainsi que des petits dépôt-centres résiduels. La portion de bourrelet marginal équatorial correspondant à l'affleurement actuel du craton ouest africain est la seule à être soumise à l'érosion depuis le pré-rift (ce qui est confirmé par les résultats thermochronologiques). Cet affleurement coïncide avec une grande province de magmatisme kimberlitique pré-rift qui pourrait être à l'origine d'une modification du manteau (métasomatisme) et acquérir ainsi une plus grande flottabilité que les domaines environnants.

La segmentation longitudinale de la marge atlantique équatoriale a été systématiquement étudiée du point de vue de son orientation, de la largeur de sa *zone de necking* et de son architecture

stratigraphique crétacée supérieure (immédiat post-rift). La géométrie de ce prisme stratigraphique varie selon la largeur de la *zone de necking* et les mouvements verticaux post-rift subis par les segments de la marge. Les sédiments proximaux crétacés supérieurs ont été seulement préservés sur la plateforme des segments de marge divergents, mais sont absents des segments transformants. Cette différence s'explique par des histoires différentes de mouvements verticaux post-rift des segments transformants et divergents. La plateforme des segments transformants a été probablement plus soulevée et plus longtemps durant le Crétacé Supérieur alors que seul un faible évènement d'érosion Santonien est enregistré par les segments divergents.

L'histoire de la dénudation déduite de la thermochronologie montre des taux d'érosion à l'échelle de la zone d'étude relativement constants dans le temps de l'ordre de 9 m/Ma, typiques des cratons. La seule exception à cette homogénéité est une phase initiale un peu plus rapide en lien avec l'érosion de reliefs issus du rift localisé sur une bande côtière. L'analyse *source-to-sink* des volumes de dénudation et d'accumulation montre que l'ordre de grandeur des volumes érodés correspond à celui des volumes déposés durant le Crétacé Supérieur et le Cénozoïque. La réorganisation des systèmes de drainage à l'Oligocène Supérieur s'est exprimée par une augmentation de flux sédimentaire dans les bassins de la marge équatoriale. Des excès d'accumulation ont été détectés au Crétacé Supérieur et depuis le Miocène Supérieur qui peuvent s'expliquer par le stockage temporaire de sédiments dans le bassin intracratonique ou sur la plateforme de la marge. La réponse en isostatie flexurale de la marge aux transferts terre-mer de sédiments a été estimée dan le cas du segment ivoirien. Les mouvements ainsi générés correspondent à un soulèvement moyen cumulé à terre de l'ordre de 1200 m sur 600 km de distance dans les terres et une subsidence offshore maximum de plus que 4000 m à 100-200 km de la côte. Le type de marge (transformante ou divergente) n'influence pas la quantité du soulèvement à terre.

La nouvelle méthode de reconstruction paléogéographique et structurale développée dans le cadre de cette thèse pourra être appliquée dans d'autres contextes comparables. Les caractères structuraux et stratigraphiques de la marge transformante ouest africaine qui contrastent largement de ceux des marges divergente pourraient être comparés avec d'autres marges transformantes dans le monde. La comparaison avec sa marge conjuguée sud-américaine devrait s'avérer de ce fait être très prometteuse.

REFERENCES

Abdelsalam, M.G., Liegeois, J.P., and Stern, R.J., 2002, The Saharan Metacraton: Journal of African Earth Sciences, v. 34, p. 119–136.

Aifa, T., Feinberg, H., and Pozzi, J.P., 1990, Devonian-Carboniferous paleopoles for Africa: consequences for Hercynian geodynamics: Tectonophysics, v. 179, p. 287–304.

Ait-Hamou, F., 2006, Le volcanisme cénozoïque à l'échelle du bombement de l'Ahaggar (Sahara Central Algerien): synthèse géochronologique et répartition spatio-temporelle quelques implications en relation avec l'histoire eo-Alpine de la plaque Afrique: Mémoires du Service Géologique de l'Algérie, v. 13, p. 155–167.

Ait-Hamou, F., and Dautria, J.M., 1994, Le magmatisme cénozoïque du Hoggar : Une synthèse des données disponibles. Mise au point sur l'hypothèse d'un point chaud: Bulletin du Service géologique de l'Algérie, v. 5, p. 49–68.

Akande, S.O., Ojo, O.J., Erdtmann, B.D., and Hetenyi, M., 2005, Paleoenvironments, organic petrology and Rock-Eval studies on source rock facies of the lower Maastrichtian Patti Formation, southern Bida Basin, Nigeria: Journal of African Earth Sciences, v. 41, p. 394–406.

Amidon, W.H., Roden-Tice, M., Anderson, A.J., McKeon, R.E., and Shuster, D.L., 2016, Late Cretaceous unroofing of the White Mountains, New Hampshire, USA; an episode of passive margin rejuvenation? Geology, v. Pre-Issue Publication.

Antobreh, A.A., Faleide, J.I., Tsikalas, F., and Planke, S., 2009, Rift–shear architecture and tectonic development of the Ghana margin deduced from multichannel seismic reflection and potential field data: Marine and Petroleum Geology, v. 26, p. 345–368.

Attoh, K., Brown, L., Guo, J., and Heanlein, J., 2004, Seismic stratigraphic record of transpression and uplift on the Romanche transform margin, offshore Ghana: Tectonophysics, v. 378, p. 1–16.

Baby, G., Caillaud, A., Calves, G., Guillocheau, F., Robin, C., and Leparmentier, F., 2014, Vertical movements in NW Africa margin: controls on accomodation and sedimentary partionning, *in* Geophysical Research Abstracts, Vienne, Austria, v. 16, p. 5318.

Bajolet, F., Rouby, D., and Chardon, D., in prep., Distorsion of the African plate, unraveling African plate structure from elevation, geoid and geology data.

Bankole, S.I., Schrank, E., and Erdtmann, B.D., 2007, Palynology of the Paleogene Oshosun Formation in the Dahomey Basin, southwestern Nigeria: Revista Espanola de Micropaleontologia, v. 39, p. 29–44.

Basile, C., 2015, Transform continental margins; Part 1, Concepts and models: Tectonophysics, v. 661, p. 1–10.

Basile, C., and Allemand, P., 2002, Erosion and flexural uplift along transform faults: Geophysical Journal International, v. 151, p. 646–653.

Basile, C., and Braun, J., 2016, The initiation of pull-apart basins and transform continental margins: results from numerical experiments of kinematic partitioning in divergent settings: Terra Nova, v. 28, p. 120–127.

Basile, C., Mascle, J., Benkhelil, J., and Bouillin, J.-P., 1998, Geodynamic evolution of the Cote d'Ivoire-Ghana transform margin; an overview of Leg 159 results: Proceedings of the Ocean Drilling Program, Scientific Results, v. 159, p. 101–110.

Basile, C., Mascle, J., and Guiraud, R., 2005, Phanerozoic geological evolution of the Equatorial Atlantic domain: Journal of African Earth Sciences, v. 43, p. 275–282.

Basile, C., Mascle, J., Sage, F., Lamarche, G., and Pontoise, B., 1996, Pre-cruise and site surveys; a synthesis of marine geological and geophysical data on the Cote d'Ivoire-Ghana transform margin: Proceedings of the Ocean Drilling Program, Part A: Initial Reports, v. 159, p. 47–60.

Beauvais, A., and Chardon, D., 2013, Modes, tempo, and spatial variability of Cenozoic cratonic denudation; the West African example: Geochemistry, Geophysics, Geosystems, v. 14, p. 1590–1608.

Begg, G.C., Griffin, W.L., Natapov, L.M., O'Reilly, S.Y., Grand, S.P., O'Neill, C.J., Hronsky, J.M.A., Poudjom Djomani, Y., Swain, C.J., Deen, T., and Bowden, P., 2009, The lithospheric architecture of Africa: Seismic tomography, mantle petrology, and tectonic evolution: Geosphere, v. 5, p. 23–50.

Bellion, J.C., 1987, Histoire géodynamique post-paléozoïque de l'Afrique de l'Ouest d'après l'étude de quelques bassins sédimentaires: Thèse Etat, Université d'Avignon et des Pays de Vaucluse, 306 p.

Bellion, Y., Hebrard, L., and Robineau, B., 1984, Sismicité historique de l'Afrique de l'Ouest. Essai d'inventaire. Remarques et commentaires: Bulletin de liaison - Association sénégalaise pour l'étude du quaternaire de l'ouest africain, p. 57–71.

Bellion, Y., and Robineau, B., 1986, Sismicité de l'Afrique de l'Ouest.

Benkhelil, J., 1982, Benue Trough and Benue Chain: Geological Magazine, v. 119, p. 155–168.

Benkhelil, J., 1988, Structure et évolution géodynamique du bassin intracontinental de la Bénoué (Nigeria): Sociéte Nationale Elf-Aquitaine, Pau, France, v. 12, p. 29–128.

Benkhelil, J., 1989, The origin and evolution of the Cretaceous Benue Trough (Nigeria): Journal of African Earth Sciences, v. 8, p. 251–282.

Benkhelil, J., Dainelli, P., Ponsard, J.F., Popoff, M., and Saugy, L., 1988, The Benue Trough; wrench-fault related basin on the border of the Equatorial Atlantic, *in* Manspeizer, W. ed.,

Triassic-Jurassic rifting, Elsevier, Amsterdam, Developments in Geotectonics, v. 22, p. 251–282.

Benkhelil, J., Mascle, J., and Guiraud, M., 1998, Sedimentary and structural characteristics of the Cretaceous along the Cote d'Ivoire-Ghana transform margin and in the Benue Trough; a comparison, *in* Mascle, J., Lohmann, G.P., and Moullade, M. eds., Proceedings of the Ocean Drilling Program, Scientific Results, v. 159: College Station, TX (Ocean Drilling Program), p. 93–99.

Benkhelil, J., Mascle, J., Guiraud, M., Basile, C., and Team, E.S., 1997, Submersible observations of Cretaceous deformations along the Côte d'Ivoire–Ghana transform margin: Geo-Marine Letters, v. 17, p. 49–54.

Benkhelil, J., Mascle, J., and Tricart, P., 1995, The Guinea continental margin; an example of a structurally complex transform margin: Tectonophysics, v. 248, p. 117–137.

Bennett, K.C., and Rusk, D., 2002, Regional 2D seismic interpretation and exploration potential of offshore deepwater Sierra Leone and Liberia, West Africa: The Leading Edge, v. 21, p. 1118–1124.

Bertrand, J.M., and Jardim de Sa, E.F., 1990, Where are the Eburnian-Transamazonian collisional belts? Revue canadienne des sciences de la Terre, v. 27, p. 1382–1393.

Bigot-Cormier, F., Basile, C., Poupeau, G., Bouillin, J.-P., and Labrin, E., 2005, Denudation of the Côte d'Ivoire-Ghana transform continental margin from apatite fission tracks: Terra Nova, v. 17, p. 189–195.

Binks, R.M., and Fairhead, J.D., 1992, A plate tectonic setting for Mesozoic rifts of West and Central Africa: Tectonophysics, v. 213, p. 141–151.

Bond, G., 1978, Evidence for Late Tertiary Uplift of Africa Relative to North America, South America, Australia and Europe: The Journal of Geology, v. 86, p. 47–65.

Bott, M.H.P., and Kusznir, N.J., 1979, Stress distributions associated with compensated plateau uplift structures with application to the continental splitting mechanism: Geophysical Journal International, v. 56, p. 451–459.

Bouillin, J.P., Poupeau, G., Basile, C., Labrin, E., and Mascle, J., 1998, Thermal constraints on the Cote d'Ivoire-Ghana transform margin; evidence from apatite fission tracks: Proceedings of the Ocean Drilling Program, Scientific Results, v. 159, p. 43–48.

Bouysse, P., and coll., 2014, Geological Map of the Word: CCGM-CGMW.

Braun, J., Deschamps, F., Rouby, D., and Dauteuil, O., 2013, Flexure of the lithosphere and the geodynamical evolution of non-cylindrical rifted passive margins; results from a numerical model incorporating variable elastic thickness, surface processes and 3D thermal subsidence: Tectonophysics, v. 604, p. 72–82.

REFERENCES

Braun, J., Guillocheau, F., Robin, C., Baby, G., and Jelsma, H., 2014, Rapid erosion of the Southern African Plateau as it climbs over a mantle superswell: Journal of Geophysical Research: Solid Earth, v. 119, p. 6093–6112.

Brownfield, M.E., and Charpentier, R.R., 2003, Assessment of the undiscovered oil and gas of the Senegal Province, Mauritania, Senegal, the Gambia, and Guinea-Bissau, Northwest Africa: U. S. Geological Survey 8755531X.

Brownfield, M.E., and Charpentier, R.R., 2006, Geology and total petroleum systems of the Gulf of Guinea Province of West Africa: U. S. Geological Survey, 32 p.

Burke, K., 1976, The Chad Basin: an active intra-continental basin: Tectonophysics, v. 36, p. 197–206.

Burke, K., 1996, The African Plate: South African Journal of Geology, v. 99, p. 339–409.

Burke, K., Macgregor, D.S., and Cameron, N.R., 2003, Africa's petroleum systems: four tectonic "Aces" in the past 600 million years, *in* Arthur, T.J., Gacgregor, D.S., and Cameron, N.R. eds., Petroleum Geology of Africa: New Themes and Developing Technologies, Geological Society, London, Special Publication, v. 207, p. 21–60.

Burke, K., and Whiteman, A.J., 1973, Uplift, Rifting and the Break-up of Africa, *in* Tarling, D.H. and Runcorn, S.K. eds., Implications of Continental Drift to the Earth Sciences, Academic Press, London&New York, p. 735–755.

Busson, G., and Cornée, A., 1991, The Sahara from the Middle Jurassic to the Middle Cretaceous: Data on environments and climates based on outcrops in the Algerian Sahara: Journal of African Earth Sciences, v. 12, p. 85–105.

Cavellec, S., 2006, Evolution diagénétique du bassin de Tim Mersoï et conséquences pour la genèse des minéralisations uranifères dans les formations carbonifères du Guezouman et du Tarat (district Arlit-Akokan, Niger) [Ph.D. thesis]: Université de Paris XI, Orsay, France, 449 p.

Chaboureau, A.C., Guillocheau, F., Robin, C., Rohais, S., Moulin, M., and Aslanian, D., 2013, Paleogeographic evolution of the central segment of the South Atlantic during Early Cretaceous times: Paleotopographic and geodynamic implications: Tectonophysics, v. 604, p. 191–223.

Chardon, D., Grimaud, J.L., Rouby, D., Beauvais, A., and Christophoul, F., 2016, Stabilization of large drainage basins over geological time scales: Cenozoic West Africa, hot spot swell growth, and the Niger River: Geochemistry, Geophysics, Geosystems, v. 17, p. 1164.

Chierici, M.A., 1996, Stratigraphy, palaeoenvironments and geological evolution of the Ivory Coast-Ghana basin, *in* Géologie de l'Afrique et de l'Atlantique Sud: Actes Colloques Angers 1994, p. 293–303.

Choubert, G., and Faure-Muret, A., 1988, International Geological Map of Africa: CCGM/UNESCO.

Choubert, G., Faure-Muret, A., Fabre, J., Perrodon, A., and Tunner, D.C., 1971, Couvertures de plate-forme: Tectonique de l'Afrique (Sciences de la terre), v. 6, p. 379–406.

Clift, P.D., Carter, A., and Hurford, A.J., 1998, Apatite fission track analysis of sites 959 and 960 on the transform continental margin of Ghana, West Africa: Proceedings of the Ocean Drilling Program, Scientific Results, v. 159, p. 35–41.

Conde, V.C., Lana, C.C., Pessoa Neto, O.C., Roesner, E.H., de Morais Neto, J., and Dutra, D.C., 2007, Bacia do Ceara: Boletim de Geociencias da PETROBRAS, v. 15, p. 347–355.

Cooper, M., and Warren, M.J., 2014, The geometric characteristics, genesis and petroleum significance of inversion structures: Geological Society, London, Special Publication, v. 335, 827–846 p.

Da Costa, P.Y.D., Johnson, A.K.C., and Affaton, P., 2009, Biostratigraphy and geodynamic impact in the uppermost part of the northeastern coastal basin of Togo: Comptes Rendus Palevol, v. 8, p. 511–526.

Dars, R., 1960, Les formations sédimentaires et les dolérites du Soudan occidental (Afrique de l'Ouest) [Ph.D. thesis]: Univiversité de Paris, 386 p.

Dauteuil, O., Bouffette, J., and Toteu, F., 2008, Visages du continent africain - Eléments de géologie africaine: CCGM, 48 p.

Dauteuil, O., Robin, C., Guillocheau, F., Linol, B., Calves, G., and Moreau, F., Submitted, Intracontinental basin subsidence: Terra Nova.

Davidson, L., Beswetherick, S., Craig, J., Eales, M., Fisher, A., Himmali, A., Jho, J., Mejrab, B., and Smart, J., 1998, The structure, stratigraphy and petroleum geology of the Murzuq Basin, Southwest Libya, *in* Sola, M.A. ed., Geological exploration in Murzuq Basin, Netherlands, Elsevier : Amsterdam, Netherlands, p. 295–320.

Davison, I., 2005, Central Atlantic margin basins of North West Africa: Geology and hydrocarbon potential (Morocco to Guinea): Journal of African Earth Sciences, v. 43, p. 254–274.

De Castro, D.L., Reinhardt, A.F., Jeffery, D.P., Roberta, M.V., Bezerra, F.H.R., and Dantas, E.L., 2014, Crustal structure beneath the Paleozoic Parnaíba Basin revealed by airborne gravity and magnetic data, Brazil: Tectonophysics, v. 614, p. 128–145.

De Matos, R.M.D., 1992, The northeast Brazilian rift system: Tectonics, v. 11, p. 766–791.

Delteil, J.-R., Valery, P., Montadert, L., Fondeur, C., Patriat, P., and Mascle, J., 1974, Continental margin in the northern part of the Gulf of Guinea, *in* Burk, C. and Drake, C.L. eds., The geology of continental margins, Springer-Verlag : New York, United States, p. 297–311.

Deynoux, M., Affaton, P., Trompette, R., and Villeneuve, M., 2006, Pan-African tectonic evolution and glacial events registered in Neoproterozoic to Cambrian cratonic and foreland basins of West Africa: Journal of African Earth Sciences, v. 46, p. 397–426.

Dillon, W.P., Schlee, J.S., and Klitgord, K.D., 1988, The development of the continental margin of eastern North America—conjugate continental margin to West Africa: Journal of African Earth Sciences, v. 7, p. 361–367.

Donelick, R.A., Ketcham, R.A., and Carlson, W.D., 1999, Variability of apatite fission-track annealing kinetics: II. Crystallographic orientation effects: American Mineralogist, v. 84, p. 1224–1234.

Donelick, R.A., O'Sullivan, P.B., and Ketcham, R.A., 2005, Apatite fission-track analysis: Reviews in Mineralogy and Geochemistry, v. 58, p. 49–94.

Doucouré, C.M., and de Wit, M.J., 2003, Old inherited origin for the present near-bimodal topography of Africa: Journal of African Earth Sciences, v. 36.

Dufaure, P., Fourcade, E., and Massa, D., 1984, Réalité des communications marines trans-sahariennes entre la Téthys et l'Atlantique durant le Crétacé supérieur: Comptes-Rendus de l'Académie des Sciences, Paris, v. 298 II, p. 665–670.

Dumestre, M.A., and Carvalho, F.F., 1985, The petroleum geology of the Republic of Guinea Bissau: Oil & Gas Journal, v. 83, p. 180–191.

Durugbo, E.U., and Aroyewun, R.F., 2012, Palynology and Paleoenvironments of the Upper Araromi Formation, Dahomey Basin, Nigeria: Asian Journal of Earth Sciences, v. 5, p. 50–62.

Edwards, R.A., Whitmarsh, R.B., and Scrutton, R.A., 1997, Synthesis of the crustal structure of the transform continental margin off Ghana, northern Gulf of Guinea: Geo-Marine Letters, v. 17, p. 12–20.

Ehlers, T.A., and Farley, K.A., 2003, Apatite (U-Th)/He thermochronometry; methods and applications to problems in tectonic and surface processes: Earth and Planetary Science Letters, v. 206, p. 1–14.

Elvsborg, A., and Dalode, J., 1985, Benin hydrocarbon potential looks promising: Oil and Gas Journal, v. 83, p. 126–131.

Emery, K.O., Uchupi, E., Phillips, J., Bowin, C.O., and Mascle, J., 1975, Continental margin off western Africa; Angola to Sierra Leone: AAPG Bulletin, v. 59, p. 2209–2265.

English, K.L., Redfern, J., Bertotti, G., English, J.M., and Yahia Cherif, R., 2016, Intraplate uplift: New constraints on the Hoggar dome from the Illizi basin (Algeria): Basin Research, doi: 10.1111/bre.12182.

Fabre, J., Arnaud-Vanneau, A., Belhadj, Z., and Monod, T., 1996, Evolution des terrains méso-cénozoïques d'une marge à l'autre du craton ouest africain, entre le Tanezrouft (Algérie) et l'Adrar de Mauritanie: Mémoires du Service Géologique de l'Algérie, p. 187–229.

Fairhead, J.D., 1988, Mesozoic plate tectonic reconstructions of the central South Atlantic Ocean: The role of the West and Central African rift system: Tectonophysics, v. 155, p. 181–191.

Fairhead, J.D., and Binks, R.M., 1991, Differential opening of the Central and South Atlantic Oceans and the opening of the West African rift system: Tectonophysics, v. 187, p. 191–203.

Farley, K.A., 2000, Helium diffusion from apatite: General behavior as illustrated by Durango fluorapatite: Journal of Geophysical Research: Solid Earth, v. 105, p. 2903–2914.

Farley, K.A., Wolf, R.A., and Silver, L.T., 1996, The effects of long alpha-stopping distances on (U-Th)/He ages: Geochimica et Cosmochimica Acta, v. 60, p. 4223–4229.

Faure, G., 1986, Principles of isotope geology: New York, John Wiley & Sons, 589 p.

Figueiredo, J.J.P., Zalan, P.V., and Soares, E.F., 2007, Bacia da Foz do Amazonas: Boletim de Geociencias da PETROBRAS, v. 15, p. 299–309.

Fleischer, R.L., Price, P.B., and Walker, R.M., 1975, Nuclear tracks in solids. Principles and Applications: Berkeley, California: University of California Press, 626 p.

Flinch, J.F., 2009, The Sierra Leone-Liberia Emerging Deepwater Province: AAPG Search and Discovery.

Flowers, R.M., Ketcham, R.A., Shuster, D.L., and Farley, K.A., 2009, Apatite (U-Th)/He thermochronometry using a radiation damage accumulation and annealing model: Geochimica et Cosmochimica Acta, v. 73, p. 2347–2365.

Frizon de Lamotte, D., Fourdan, B., Leleu, S., Leparmentier, F., and de Clarens, P., 2015, Style of rifting and the stages of Pangea breakup: Tectonics, v. 34, p. 1109–1120.

Gaina, C., Torsvik, T.H., Hinsbergen, D.J.J.V., Medvedev, S., Werner, S.C., and Labails, C., 2013, The African Plate: A history of oceanic crust accretion and subduction since the Jurassic: Tectonophysics, v. 604, p. 4–25.

Gallagher, K., 2012, Transdimensional inverse thermal history modeling for quantitative thermochronology: Journal of Geophysical Research, v. 117, p. 1–16.

Gallagher, K., Brown, R., and Johnson, C., 1998, Fission track analysis and its applications to geological problems: Annual Review of Earth and Planetary Sciences, v. 26, p. 519–572.

Gallagher, K., Hawkesworth, C.J., and Mantovani, M.S.M., 1995, Denudation, fission track analysis and the long-term evolution of passive margin topography: application to the southeast Brazilian margin: Journal of South American Earth Sciences, v. 8, p. 65–77.

Galloway, W.E., Whiteaker, T.L., and Ganey-Curry, P., 2011, History of Cenozoic North American drainage basin evolution, sediment yield, and accumulation in the Gulf of Mexico Basin: Geosphere, v. 7, p. 938–973.

Gautheron, C., Tassan-Got, L., Barbarand, J., and Pagel, M., 2009, Effect of alpha damage annealing on apatite (U-Th)/He thermochronology: Chemical Geology, v. 266, p. 166–179.

Gautheron, C., Tassan-Got, L., Ketcham, R.A., and Dobson, K.J., 2012, Accounting for long alpha particle stopping distances in (U-Th-Sm)/He geochronology; 3D modeling of diffusion, zoning, implantation, and abrasion: Geochimica et Cosmochimica Acta, v. 96, p. 44–56.

Genik, G.J., 1993, Petroleum geology of Cretaceous-Tertiairy rift basins in Niger, Chad, and Central African Republic: American Association of Petroleum Geologists Bulletin, v. 77, p. 1405–1434.

Genik, G.J., 1992, Regional framework, structural and petroleum aspects of rift basins in Niger, Chad and the Central African Republic (C.A.R.): Tectonophysic, v. 213, p. 169–185.

Gilchrist, A.R., and Summerfield, M.A., 1990, Differential denudation and flexural isostasy in formation of rifted-margin upwarps: Nature, v. 346, p. 739–742.

Gorini, M.A., and Asmus, H.E., 1981, The tectonic fabric of the Equatorial Atlantic and adjoining continental margins : Gulf of Guinea to northeastern Brazil. Projecto Remac-Reconhecimento global da margem continental brasileira, *in* Estruturas e tectonismo da margem continental brasileira, e suas implicacoes nos processos sedimentares e na avaliacao do potencial de recursos minerais, Petrobras, Rio de Janeiro, p. 11–16.

Gouyet, S., 1988, Evolution tectono-sédimentaire des marges guyanaise et nord-brésilienne au cours de l'ouverture de l'Atlantique Sud [Ph.D. thesis]: Université de Pau et des Pays de l'Adour.

Greigert, J., 1966, Description des formations crétacées et tertiaires du bassin des Iullemeden (Afrique occidentale): Editions BRGM, Paris, France, 236 p.

Grillot, L.R., Anderton, P.W., Haselton, T.M., and Dermargne, J.F., 1985, Three-dimensional seismic interpretation; Espoir Field area, offshore Ivory Coast: Memoir American Association of Petroleum Geologists, v. 42, p. 326–329.

Grimaud, J.L., 2014, Dynamique long-terme de l'érosion en contexte cratonique: l'Afrique de l'Ouest depuis l'Eocène [Ph.D. thesis]: Université Toulouse III Paul Sabatier.

Grimaud, J.L., Chardon, D., Metelka, V., Beauvais, A., and Bamba, O., 2015, Neogene cratonic erosion fluxes and landform evolution processes from regional regolith mapping (Burkina Faso, West Africa): Geomorphology, v. 241, p. 315–330.

Grimaud, J.L., Rouby, D., Chardon, D., and Beauvais, A., in prep., Balancing the sediment budgets of West Africa and the Niger delta over the Cenozoic: Basin Research,.

Guillocheau, F., Chelalou, R., Linol, B., Dauteuil, O., Robin, C., Mvondo, F., Callec, Y., and Colin, J.-P., 2015, Cenozoic Landscape Evolution in and Around the Congo Basin: Constraints from Sediments and Planation Surfaces, *in* de Wit, M.J., Guillocheau, F., de Wit, M.C.J.,

Maarten, J.W., Guillocheau, F., and Michiel, C.J.W. eds., Geology and Resource Potential of the Congo Basin, Berlin, Heidelberg, Springer Berlin Heidelberg, p. 271–313.

Guillocheau, F., Rouby, D., Robin, C., Helm, C., Rolland, N., Le Carlier de Veslud, C., and Braun, J., 2012, Quantification and causes of the terrigeneous sediment budget at the scale of a continental margin; a new method applied to the Namibia-South Africa margin: Basin Research, v. 24, p. 3–30.

Guiraud, R., 1986, Tectonique, Seismicité et volcanisme de la plaque africaine depuis le Méso-Cénozoïque, *in* INQUA, Dakar symposium 'Changments glocaux en Afrique', p. 179–182.

Guiraud, R., and Alidou, S., 1981, La faille de Kandi (Bénin), témoin du rejeu fini-crétacé d'un accident majeur à l'échelle de la plaque africaine: C. R. Acad. Sc. Paris, v. 293 II, p. 779–782.

Guiraud, M., Benkhelil, J., Mascle, J., Basile, C., Mascle, G., Bouillin, J.P., and Cousin, M., 1997, Synrift to syntransform deformation along the Côte d'Ivoire–Ghana transform margin: evidence from deep-sea dives: Geo-Marine Letters, v. 17, p. 70–78.

Guiraud, R., and Bosworth, W., 1997, Senonian basin inversion and rejuvenation of rifting in Africa and Arabia; synthesis and implications to plate-scale tectonics: Tectonophysics, v. 282, p. 39–82.

Guiraud, R., Bosworth, W., Thierry, J., and Delplanque, A., 2005, Phanerozoic geological evolution of Northern and Central Africa: An overview: Journal of African Earth Sciences, v. 43, p. 83–143.

Guiraud, M., Buta Neto, A., and Quesne, D., 2010, Segmentation and differential post-rift uplift at the Angola margin as recorded by the transform-rifted Benguela and oblique-to-orthogonal-rifted Kwanza basins: Marine and Petroleum Geology, v. 27, p. 1040–1068.

Guiraud, R., Issawi, B., and Bellion, Y., 1985, Les linéaments guinéo-nubiens : un trait structural majeur à l'échelle de la plaque africaine: C. R. Acad. Sc. Paris, v. 300 II.

Guiraud, R., and Maurin, J.C., 1992, Early Cretaceous rifts of Western and Central Africa: an overview: Tectonophysic, v. 213, p. 153–168.

Gunnell, Y., 2003, Radiometric ages of laterites and constraints on long-term denudation rates in West Africa: Geology, v. 31, p. 131–134.

Heine, C., and Brune, S., 2014, Oblique rifting of the Equatorial Atlantic; why there is no Saharan Atlantic Ocean: Geology, v. 42, p. 211–214.

Heine, C., Zoethout, J., and Müller, R.D., 2013, Kinematics of the South Atlantic rift: Solid Earth, v. 4, p. 215–253.

Helland-Hansen, W., and Martinsen, O.J., 1996, Shoreline trajectories and sequences; description of variable depositional-dip scenarios: Journal of Sedimentary Research, v. 66, p. 670–688.

Helm, C., 2009, Quantification des flux sédimentaires anciens à l'échelle d'un continent : le cas de l'Afrique au Méso-Cénozoïque [Ph.D. thesis]: Université Rennes 1.

Homewood, P., Guillocheau, F., Eschard, R., and Cross, T.A., 1992, Corrélations Haute Résolution et Stratigraphie Génétique: Une Démarche Intégrée: Bulletin Centre Recherche Exploration-Production Elf-Aquitaine, v. 16, p. 357–381.

Huismans, R.S., and Beaumont, C., 2008, Complex rifted continental margins explained by dynamical models of depth-dependent lithospheric extension: Geology, v. 36, p. 163–166.

Huismans, R.S., and Beaumont, C., 2014, Rifted continental margins; the case for depth-dependent extension: Earth and Planetary Science Letters, v. 407, p. 148–162.

Hurford, A.J., and Carter, A., 1991, The role of fission track dating in discrimination of provenance: Geological Society Special Publications, v. 57, p. 67–78.

Huyghe, D., 2016, Forçage des liens source-marge au Cénozoïque (marge Bénin-Sénégal): Internal Raport, 67 p.

Japsen, P., 1993, Influence of lithology and neogene uplift on seismic velocities in Denmark: Implications for depth conversion of maps: The American Association of Petroleum Geologists Bulletin, v. 77, p. 194–211.

Japsen, P., Bonow, J.M., Green, P.F., Cobbold, P.R., Chiossi, D., Lilletveit, R., Magnavita, L.P., and Pedreira, A., 2012, Episodic burial and exhumation in NE Brazil after opening of the South Atlantic: Geological Society of America Bulletin, v. 124, p. 800–816.

Jermannaud, P., Rouby, D., Robin, C., Nalpas, T., Guillocheau, F., and Raillard, S., 2010, Plio-Pleistocene sequence stratigraphic architecture of the eastern Niger Delta: A record of eustasy and aridification of Africa: Marine and Petroleum Geology, v. 27, p. 810–821.

Johnson, A.K., Rat, P., and Lang, J., 2000, Le bassin sedimentaire a phosphates du Togo (Maastrichtien-Eocene); stratigraphie, environnements et evolution: Journal of African Earth Sciences, v. 30, p. 183–200.

Jourdan, F., Marzoli, A., Bertrand, H., S.Cirilli, Lht., Kontak, D.J., McHone, G., Renne, P.R., and Bellieni, G., 2009, 40Ar/39Ar ages of CAMP in North America: Implications for the Triassic–Jurassic boundary and the 40K decay constant bias: Lithos, v. 110, p. 167–180.

Keen, C.E., Kay, W.A., and Roest, W.R., 1990, Crustal anatomy of a transform continental margin: Tectonophysics, v. 173, p. 527–544.

Ketcham, R.A., 2003, Observations on the relationship between crystallographic orientation and biasing in apatite fission-track measurements: American Mineralogist, v. 88, p. 817–829.

Ketcham, R.A., Carter, A., Donelick, R.A., Barbarand, J., and Hurford, A.J., 2007, Improved modeling of fission-track annealing in apatite: American Mineralogist, v. 92, p. 799–810.

Kjemperud, A., Agbesinyale, W., Agdestein, T., Gustafsson, C., and Yukler, A., 1992, Tectono-stratigraphic history of the Keta Basin, Ghana with emphasis on late erosional episodes, *in* Géologie Africaine: Colloque de Géologie de Libreville, recueil des Communications 6–8 May 1991, p. 55–69.

Klein, E.L., and Moura, C.A.V., 2008a, São Luís Craton and Gurupi Belt (Brazil): possible links with the West African Craton and surrounding Pan-African belts: Geological Society, London, Special Publications, v. 294, p. 137–151.

Klein, E.L., and Moura, C. a. V., 2008b, Sao Luis Craton and Gurupi Belt (Brazil); possible links with the West African Craton and surrounding Pan-African belts: Geological Society Special Publications, v. 294, p. 137–151.

Kogbe, C.A., 1981, Cretaceous and Tertiary of the Iullemmeden Basin in Nigeria (West Africa): Cretaceous Research, v. 2, p. 129–186.

Kogbe, C.A., 1980, The Trans-Saharan Seaway during the Cretaceous, *in* Salem, M.J. and Busrewil, M.T. eds., The Geology of Libya, Academic Press, p. 91–96.

Kogbe, C.A., Ajakaiye, D.E., and Matheis, G., 1983, Confirmation of a rift structure along the Mid-Niger Valley, Nigeria: Journal of African Earth Sciences, v. 1, p. 127–131.

Koptev, A., Burov, E., Calais, E., Leroy, S., Gerya, T., Guillou-Frottier, L., and Cloetingh, S., 2016, Contrasted continental rifting via plume-craton interaction: Applications to Central East African Rift: Geoscience Frontiers, v. 7, p. 221–236.

Koptev, A., Calais, E., Burov, E., Leroy, S., and Gerya, T.V., 2015, Dual continental rift systems generated by plume-lithosphere interaction: Nature Geoscience, v. 8, p. 388–392.

Kouamelan, A.N., 1996, Géochronologie et géochimie des formations archéennes et protérozoïques de la dorsale de Man de Côte d'Ivoire; implications pour la transition archéen-protérozoïque [Ph.D. thesis]: Geosciences Rennes, Rennes, France, 296 p.

Kuhlemann, J., Frisch, W., Szekely, B., Dunkl, I., and Kazmer, M., 2002, Post-collisional sediment budget history of the Alps; tectonic versus climatic control: International Journal of Earth Sciences, v. 91, p. 818–837.

Labails, C., Olivet, J.L., Aslanian, D., and Roest, W.P., 2010, An alternative early opening scenario for the Central Atlantic Ocean: Earth and Planetary Science Letters, v. 297, p. 355–368.

Lamarche, G., Basile, C., Mascle, J., and Sage, F., 1997, The Côte d'Ivoire–Ghana transform margin: sedimentary and tectonic structure from multichannel seismic data: Geo-Marine Letters, v. 17, p. 62–69.

Lang, J., Kogbe, C., Alidou, S., Alzouma, K.A., Bellion, G., Dubois, D., Durand, A., Guiraud, R., Houessou, A., de Klasz, I., Romann, E., Salard-Cheboldaeff, M., and Trichet, J., 1990, The continental terminal in West Africa: Journal of African Earth Sciences, v. 10, p. 79–99.

Lang, J., Kogbe, C., Alidou, S., Alzouma, K., Dubois, D., Houessou, A., and Trichet, J., 1986, Le Sidérolithique du Tertiaire ouest-africain et le concept de Continental Terminal: Bulletin de la Société géologique de France, v. 2, p. 605–622.

Laske, G., and Masters, G., 1997, A Global Digital Map of Sediment Thickness: EOS Trans. AGU, 78, F483.

Laslett, G.M., Green, P.F., Duddy, I.R., and Gleadow, A.J.W., 1987, Thermal annealing of fission tracks in apatite 2. A quantitative analysis: Chemical Geology: Isotope Geoscience section, v. 65, p. 1–13.

Le Heron, D.P., Craig, J., and Etienne, J.L., 2009, Ancient glaciations and hydrocarbon accumulations in North Africa and the Middle East: Earth-Science Reviews, v. 93, p. 47–76.

Le Pichon, X., and Hayes, D.E., 1971, Marginal offsets, fracture zones, and the early opening of the South Atlantic: Journal of Geophysical Research, v. 76, p. 6283–6293.

Lefranc, J.P., 1983, Corrélation vers le Nord et description stratigraphique detaillée du continental intercalaire (Mésozoïque continental) de la sebkha de Timimouns, Gourara, Sahara algerien: Comptes Rendus des Seances de l'Academie des Sciences, Serie 2, v. 296, p. 193–196.

Lefranc, J.P., and Guiraud, R., 1990, The continental intercalaire of northwestern Sahara and its equivalents in the neighbouring regions: Journal of African Earth Sciences, v. 10, p. 27–77.

Leprêtre, R., 2015, Evolution phanérozoïque du Craton Ouest Africain et de ses bordures Nord et Ouest [Ph.D. thesis]: Université Paris Sud - Paris XI, France, 423 p.

Leprêtre, R., Barbarand, J., Missenard, Y., Leparmentier, F., and Frizon de Lamotte, D., 2014, Vertical movements along the northern border of the West African Craton: the Reguibat Shield and adjacent basins: Geological Magazine, v. 151, p. 885–898.

Liégois, J.P., Benhallou, A., Azzouni-Sekkal, A., Yahiaoui, R., and Bonin, B., 2005, The Hoggar swell and volcanism: Reactivation of the Precambrian Tuareg shield during Alpine convergence and West African Cenozoic volcanism: Geological Society of America, Special Paper, v. 388, p. 379–400.

Liu Zhifei, Zhao Yulong, Colin, C., Stattegger, K., Wiesner, M.G., Huh, C.-A., Zhang Yanwei, Li Xiajing, Sompongchaiyakul, P., You, C.-F., Huang, C.-Y., Liu, J.T., Siringan, F.P., Le, K.P., et al., 2016, Source-to-sink transport processes of fluvial sediments in the South China Sea: Earth-Science Reviews, v. 153, p. 238–273.

Loparev, A., 2016, Architecture stratigraphique des bassins et Quantification des flux sédimentaires en Afrique Ouest-Équatoriale: Master thesis, Université Paul Sabatier, 34 p.

Lorenzo, J.M., Mutter, J.C., Larson, R.L., Buhl, P., Diebold, J.B., Alsop, J., Hopper, J., Falvey, D., Williamson, P., and Brassil, F., 1991, Development of the continent-ocean transform boundary of the southern Exmouth Plateau: Geology, v. 19, p. 843–846.

Luger, P., 2003, Paleobiogeography of late Early Cretaceous to early Paleocene marine Ostracoda in Arabia and north to Equatorial Africa: Palaeogeography, Palaeoclimatology, Palaeoecology, v. 196, p. 319–342.

MacGregor, D.S., Robinson, J., and Spear, G., 2003, Play fairways of the Gulf of Guinea transform margin: Geological Society, London, Special Publications, v. 207, p. 131–150.

Magnavita, L.P., Davison, I., and Kusznir, N.J., 1994, Rifting, erosion, and uplift history of the Reconcavo-Tucano-Jatoba Rift, northeast Brazil: Tectonics, v. 13, p. 367–388.

Mascle, J., 1976, Atlantic-type continental margins; distinction of two basic structural types: Anais da Academia Brasileira de Ciencias, v. 48, p. 191–197.

Mascle, J., and Blarez, E., 1987, Evidence for transform margin evolution from the Ivory Coast-Ghana continental margin: Nature, v. 326, p. 378–381.

Mascle, J., Lohmann, P., Clift, P., and Party, O. 159 S., 1997, Development of a passive transform margin: Côte d'Ivoire–Ghana transform margin – ODP Leg 159 preliminary results: Geo-Marine Letters, v. 17, p. 4–11.

Mateer, N.J., Wycisk, P., Jacobs, L.L., Brunet, M., Luger, P., Arush, M.A., Hendriks, F., Weissbrod, T., Gvirtzman, G., Mbede, E., Dina, A., Moody, R.T.J., Weigelt, G., El-Nakhal, H.A., et al., 1992, Correlation of nonmarine Cretaceous strata of Africa and the Middle East: Cretaceous Research, v. 13, p. 273–318.

Matenco, L., and Andriessen, P.A.M., 2013, Quantifying the mass transfer from mountain ranges to deposition in sedimentary basins; source to sink studies in the Danube Basin-Black Sea system: Global and Planetary Change, v. 103, p. 1–18.

Matton, G., and Jébrak, M., 2009, The Cretaceous Peri-Atlantic Alkaline Pulse (PAAP): Deep mantle plume origin or shallow lithospheric break-up? Tectonophysics, v. 469, p. 1–12.

Maurin, J.C., and Guiraud, R., 1993, Basement control in the development of the Early Cretaceous West and Central African Rift System: Tectonophysics, v. 228, p. 81–95.

McKenzie, D., 1978, Some remarks on the development of sedimentary basins: Earth and Planetary Science Letters, v. 40, p. 25–32.

Mercier de Lépinay, M., 2016, Iinventaire mondial des marges transformantes et évolution tecto-sédimentaire des plateaux de Demerara et de Guinée [Ph.D. thesis]: Université de Perpignan, 335 p.

Mercier de Lépinay, M., Loncke, L., Basile, C., Roest, W.R., Patriat, M., Maillard, A., and De Clarens, P., 2016, Transform continental margins – Part 2: A worldwide review: Tectonophysics, doi: 10.1016/j.tecto.2016.05.038.

Milesi, J.P., Frizon de Lamotte, D., De Kock, G., and Toteu, F., 2010, Tectonic Map of Africa: CCGM/CCGM.

Miller, K.G., Kominz, M.A., Browning, J.V., Wright, J.D., Mountain, G.S., Katz, M.E., Sugarman, P.J., Cramer, B.S., Christie-Blick, N., and Pekar, S.F., 2005, The Phanerozoic Record of Global Sea-Level Change: Science, v. 310, p. 1293–1298.

Mizusaki, A.M.P., Thomaz-Filho, A., Milani, E.J., and De Césero, P., 2002, Mesozoic and Cenozoic igneous activity and its tectonic control in northeastern Brazil: Journal of South American Earth Sciences, v. 15, p. 183–198.

Moody, R.T.J., and Sutcliffe, P.J.C., 1991, The Cretaceous deposits of the Iullemmeden Basin of Niger, central West Africa: Cretaceous Research, v. 12, p. 137–157.

Moulin, M., Aslanian, D., and Unternehr, P., 2010, A new starting point for the South and Equatorial Atlantic Ocean: Earth Science Reviews, v. 98, p. 1–37.

Naeser, C.W., and Faul, H., 1969, Fission track annealing in apatite and sphene: Journal of Geophysical Research, v. 74, p. 705–710.

Ngako, V., Njonfang, E., Aka, F.T., Affaton, P., and Nnange, J.M., 2006, The north-south Paleozoic to Quaternary trend of alkaline magmatism from Niger-Nigeria to Cameroon; complex interaction between hotspots and Precambrian faults: Journal of African Earth Sciences, v. 45, p. 241–256.

Ojo, O.J., and Akande, S.O., 2009, Sedimentology and depositional environments of the Maastrichtian Patti Formation, southeastern Bida Basin, Nigeria: Cretaceous Research, v. 30, p. 1415–1425.

Olsen, P.E., 1997, Stratigraphic record of the early Mesozoic breakup of Pangea in the Laurasia-Gondwana rift system: Annual Review of Earth and Planetary Sciences, v. 25, p. 337–401.

Pessoa Neto, O.C., Soares, U.M., Fernandes da Silva, J.G., Roesner, E.H., Pires Florencio, C., and Valentin de Souza, C.A., 2007, Bacia Potiguar: Boletim de Geociencias da PETROBRAS, v. 15, p. 357–369.

Pique, A., and Michard, A., 1989, Moroccan hercynides: a synopsis. The Paleozoic sedimentary and tectonic evolution at the northern margin of West Africa: American Journal of Science, v. 289, p. 286–330.

Pletsch, T., Erbacher, J., Holbourn, A.E.L., Kuhnt, W., Moullade, M., Oboh-Ikuenobe, F.E., Soeding, E., and Wagner, T., 2001, Cretaceous separation of Africa and South America; the view from the West African margin (ODP Leg 159): Journal of South American Earth Sciences, v. 14, p. 147–174.

Popoff, M., 1988, Du Gondwana à l'atlantique sud: les connexions du fossé de la bénoué avec les bassins du Nord-Est brésilien jusqu'à l'ouverture du golfe de Guinée au crétacé inférieur: Journal of African Earth Sciences, v. 7, p. 409–431.

Radier, H., 1959, Contribution à l'étude géologique du Soudan oriental (AOF). 2 Le bassin crétacé et tertiaire de Gao le détroit soudanais: Bulletin du Service de Géologie et de Prospection Minière, 556 p.

Reading, H.G., and Richards, M., 1994, Turbidite systems in deep-water basin margins classified by grain size and feeder system: AAPG Bulletin, p. 792.

Reyment, R.A., 1980, Biogeography of the Saharan Cretaceous and Paleocene epicontinental transgressions: Cretaceous Research, v. 1, p. 299–327.

Rogers, J.W., Unrug, R., and Sultan, M., 1995, Tectonic Assembly of Gondwana: Journal of Geodynamics, v. 19, p. 1–34.

Rouby, D., Braun, J., Robin, C., Dauteuil, O., and Deschamps, F., 2013, Long term stratigraphic evolution of Atlantic-type passive margins; a numerical approach of interactions between surface processes, flexural isostasy and 3D thermal subsidence: Tectonophysics, v. 604, p. 83–103.

Rougier, S., 2012, Interactions lithosphère-ssthénosphère et mouvements verticaux : le cas du Massif du Hoggar [Ph.D. thesis]: Université Paris-Sud, 276 p.

Rougier, S., Missenard, Y., Gautheron, C., Barbarand, J., Zeyen, H., Pinna, R., Liegeois, J., Bonin, B., Ouabadi, A., Derder, M.., and Frizon de Lamotte, D., 2013, Eocene exhumation of the Tuareg Shield (Sahara Desert, Africa): Geology, v. 41, p. 615–618.

Roussel, J., and Lesquer, A., 1991, Geophysics and the Crustal Structure of West Africa, *in* Dallmeyer, R.D. and Lécorché, J.P. eds., The West African Orogens and Circum-Atlantic Correlatives, Berlin, Heidelberg, Springer Berlin Heidelberg, p. 9–28.

Sage, F., Basile, C., Mascle, J., Pontoise, B., and Whitmarsh, R.B., 2000, Crustal structure of the continent-ocean transition off the Cote d'Ivoire-Ghana transform margin; implications for thermal exchanges across the palaeotransform boundary: Geophysical Journal International, v. 143, p. 662–678.

Sahabi, M., Aslanian, D., and Olivet, J.L., 2004, A new starting point for the history of the Central Atlantique: Comptes Rendus Geosiciences, v. 336, p. 1041–1052.

Sahagian, D., 1988, EPeirogenic motions of Africa as inferred from Cretaceous shoreline deposits: Tectonics, v. 7, p. 125–138.

Sapin, F., Davaux, M., Dall'Asta, M., Lahmi, M., Baudot, G., and Ringenbach, J.C., 2016, Post-rifting Subsidence of the French Guyana Hyper-Oblique Margin: Geological Society, London, Special Publications, v. 431, doi: 10.1144/SP431.11.

Schettino, A., and Turco, E., 2009, Breakup of Pangaea and plate kinematics of the central Atlantic and Atlas regions: Geophysical Journal International, v. 178, p. 1078–1097.

Scrutton, R.A., 1979, Crustal properties across passive margins On sheared passive continental margins: Tectonophysics, v. 59, p. 293–305.

Scrutton, R.A., and Dingle, R.V., 1976, Sedimentary basins of continental margins and cratons Observations on the processes of sedimentary basin formation at the margins of Southern Africa: Tectonophysics, v. 36, p. 143–156.

Sengör, A.M.C., and Burke, K., 1978, Relative timing of rifting and volcanism on Earth and its tectonic implications: Geophysical Research Letters, v. 5, p. 419–421.

Seranne, M., and Nze Abeigne, C.R., 1999, Oligocene to Holocene sediment drifts and bottom currents on the slope of Gabon continental margin (West Africa); consequences for sedimentation and Southeast Atlantic upwelling: Sedimentary Geology, v. 128, p. 179–199.

Shuster, D.L., Flowers, R.M., and Farley, K.A., 2006, The influence of natural radiation damage on helium diffusion kinetics in apatite: Earth and Planetary Science Letters, v. 249, p. 148–161.

Simon, B., 2015, Rift du Lac Albert, Ouganda, Rift Est Africain : Déformation, érosion, sédimentation et bilan de matière depuis 17 Ma [PhD thesis]: Université de Rennes 1, 418 p.

Simon, P., and Amakou, B., 1984, La discordance oligocène et les dépôts posterieurs a la discordance dans le bassin sédimentaire ivoirien: Bulletin de la Societé Géologique de France, v. 26, p. 1117–1125.

Sloss, L.L., 1963, Sequences in the Cratonic Interior of North America: Geological Society of America Bulletin, v. 74, p. 93–114.

Sloss, L.L., and Scherer, W., 1975, Geometry of sedimentary basins; applications to Devonian of North America and Europe: Memoir - Geological Society of America, p. 71–88.

Soares Júnior, A.V., Hasui, Y., Costa, J.B.S., and Machado, F.B., 2011, Evolução do rifteamento e paleogeografia da margem Atlântica Equatorial do Brasil: Triássico ao Holoceno: Geociências, v. 30, p. 669–692.

Somme, T.O., Martinsen, O.J., and Lunt, I., 2013, Linking offshore stratigraphy to onshore paleotopography; the Late Jurassic-Paleocene evolution of the south Norwegian margin: Geological Society of America Bulletin, v. 125, p. 1164–1186.

Spohn, T., and Schubert, G., 1982, Convective thinning of the lithosphere: A mechanism for the initiation of continental rifting: Journal of Geophysical Research: Solid Earth, v. 87, p. 4669–4681.

Summerfield, M.A., 1985, Plate tectonics and the evolution of the African landscape, *in* Morisawa, M. and Hack, J.T. eds., Tectonic Geomorphology, Allan and Unwin, p. 27–51.

Summerfield, M.A., 1996, Tectonics, geology and long-term landscape development, *in* Adams, W.M., Goudie, A.S., and R.Orme, A. eds., The Physical Geography of Africa, Oxford University Press, p. 1–17.

Tinker, J., de Wit, M., and Brown, R., 2008, Mesozoic exhumation of the southern Cape, South Africa, quantified using apatite fission-track thermochronology: Tectonophysics, v. 455, p. 77–93.

Toteu, S.F., Penaye, J., and Djomani, Y.P., 2004, Geodynamic evolution of the Pan-African belt in central Africa with special reference to Cameroon: Canadian Journal of Earth Sciences, v. 41, p. 73–85.

Trosdtorf Junior, I., Zalan, P.V., Figueiredo, J.J.P., and Soares, E.F., 2007, Bacia de Barreirinhas: Boletim de Geociencias da PETROBRAS, v. 15, p. 331–339.

Turner, J.P., Green, P.F., Holford, S.P., and Lawrence, S.R., 2008, Thermal history of the Rio Muni (West Africa)-NE Brazil margins during continental breakup: Earth and Planetary Science Letters, v. 270, p. 354–367.

Turner, J.P., Rosendahl, B.R., and Wilson, P.G., 2003, Structure and evolution of an obliquely sheared continental margin: Rio Muni, West Africa: Tectonophysics, v. 374, p. 41–55.

Vagnes, E., 1997, Uplift at thermo-mechanically coupled ocean-continent transforms; modeled at the Senja fracture zone, southwestern Barents Sea: Geo-Marine Letters, v. 17, p. 100–109.

Vail, P.R., Mitchum, R.M., and Thompson, S., 1977, Seismic Stratigraphy and Global Changes of Sea Level: Part 3. Relative Changes of Sea Level from Coastal Onlap, *in* Payton, C.W. ed., Seismic Stratigraphy-Applications to Hydrocarbon Exploration: American Association of Petroleum Geologists Memoir, v. 26, p. 83–97.

Valeton, I., 1991, Bauxites and associated terrestrial sediments in Nigeria and their position in the bauxite belts of Africa: Journal of African Earth Sciences and the Middle East, v. 12, p. 297–310.

Valsardieu, C., 1971, Etude géologique et paléogéographique du Bassin de Tim Mersoï, région d'Agadès (République du Niger) [Ph.D. thesis]: Université de Nice, 518 p.

Van der Beek, P., Pulford, A., and Braun, J., 2001, Cenozoic landscape development in the Blue Mountains (SE Australia); lithological and tectonic controls on rifted margin morphology: Journal of Geology, v. 109, p. 35–56.

Van Wagoner, J.C., Mitchum, R.M., Campion, K.M., and Rahmanian, V.D., 1990, Siliciclastic sequence stratigraphy in well logs, cores, and outcrops; concepts for high-resolution correlation of time and facies: Methods in Exploration Series, v. 7, 55 p.

Van Wagoner, J.C., Posamentier, H.W., Mitchum, R.M., Jr., Vail, P.R., Sarg, J.F., Loutit, T.S., and Hardenbol, J., 1988, An overview of the fundamentals of sequence stratigraphy and key

definitions: Special Publication - Society of Economic Paleontologists and Mineralogists, v. 42, p. 39–45.

Vaz, P.T., Wanderley Filho, J.R., and Bueno, G.V., 2007b, Bacia do Tacutu: Boletim de Geociencias da PETROBRAS, v. 15, p. 289–297.

Villeneuve, M., 1988, Corrélations et évolution des bassins sédimentaires de la marge NW du continent de Gondwana au cours du Paléozoïque inférieur (de la Mauritanie au Vénézuela): Journal of African Earth Sciences, v. 7, p. 451–461.

Villeneuve, M., 2005, Paleozoic basins in West Africa and the Mauritanide thrust belt: Journal of African Earth Sciences, v. 43, p. 166–195.

Villeneuve, M., Archi, A.E., and Nzamba, J., 2010, Les chaînes de la marge occidentale du Craton Ouest-Africain, modèles géodynamiques: Comptes Rendus Geosiciences, v. 342, p. 1–10.

Villeneuve, M., and Cornée, J.J., 1994, Structure, evolution and palaeogeography of the West African craton and bordering belts during the Neoproterozoic: Precambrian Research, v. 69, p. 307–326.

Wagner, T., and Pletsch, T., 2001, No major thermal event on the Mid-Cretaceous Cote d'Ivoire-Ghana transform margin: Terra Nova, v. 13, p. 165–171.

Walker, J.D., Geissman, J.W., Bowring, S.A., and Babcock, L.E., 2012, The Geological Society of America Geologic Time Scale: Geological Society of America Bulletin, v. 125, p. 259–272.

Watts, A.B., 2001, Isostasy and Flexure of the Lithosphere: Cambridge University Press, 508 p.

Wernicke, B., 1985, Uniform-sense normal simple shear of the continental lithosphere: Canadian Journal of Earth Sciences, v. 22, p. 108–125.

Wildman, M., 2015, Reassessing the structural and geomorphic evolution of a "classic" Atlantic type passive margin: an integrated study of the Namaqualand sector of the South African continental margin [Ph.D. thesis]: University of Glasgow, 375 p.

Wildman, M., Brown, R., Beucher, R., Persano, C., Stuart, F., Gallagher, K., Schwanethal, J., and Carter, A., 2016, The chronology and tectonic style of landscape evolution along the elevated Atlantic continental margin of South Africa resolved by joint apatite fission track and (U-Th-Sm)/He thermochronology: Tectonics, v. 35, p. 511–545.

Wilson, J.T., 1965, A New Class of Faults and their Bearing on Continental Drift: Nature, v. 207, p. 343–347.

Wilson, M., and Guiraud, R., 1998, Late Permian to Recent magmatic activity on the African-Arabian margin of Tethys, *in* Macgregor, D.S., Moody, R.T.J., and Clark-Lowes, D.D. eds., Petroleum Geology of North Africa, Geological Society, London, Special Publication, v. 132, p 231–263.

Withjack, M.O., Schlisch, P.W., and Olsen, P.E., 1998, Diachronous Rifting, Drifting, and Inversion on the Passive Margin of Central Eastern North America: An Analog for Other Passive Margins: AAPG Bulletin, v. 82, p. 817–825.

Wittmann, H., Malusà, M.G., Resentini, A., Garzanti, E., and Niedermann, S., 2016, The cosmogenic record of mountain erosion transmitted across a foreland basin: Source-to-sink analysis of in situ10Be, 26Al and 21Ne in sediment of the Po river catchment: Earth & Planetary Science Letters, v. 452, p. 258–271.

Ye, J., Chardon D., Rouby D., Guillocheau F., Dall'asta M., Ferry J.N., Broucke O., Submitted, Paleogeographic and structural evolution of northwestern Africa and its Atlantic margins since the Early Mesozoic: Geosphere.

Zalan, P.V., 2007, Bacias de Braganca-Viseu, Sao Luis e Ilha Nova: Boletim de Geociencias da PETROBRAS, v. 15, p. 341–345.

Zalan, P.V., and Matsuda, N.S., 2007, Bacia do Marajo: Boletim de Geociencias da PETROBRAS, v. 15, p. 311–319.

Zanguina, M., Bruneton, A., and Gonnard, R., 1998, An Introduction to the Petroleum Potential of Niger: Journal of Petroleum Geology, v. 21, p. 83–103.

Zattin, M., Pace, D., Andreucci, B., Rossetti, F., and Talarico, F.M., 2014, Cenozoic erosion of the Transantarctic Mountains; a source-to-sink thermochronological study: Tectonophysics, v. 630, p. 158–165.

APPENDIX

Appendix 1. Compilation of Meso-Cenozoic magmatic occurences in Northwestern Africa.

Paleogeographic maps: Fig 1- Late Triassic-Early Jurassic (235-190 Ma), Fig 2- Vanlanginian (140-133Ma), Fig 3- Middle Aptian (120-115 Ma), Fig 4- Late Albian (107-100 Ma), Fig 5- Late Cenomanian (97-93 Ma), Fig 6- Santonian (86-84 Ma), Fig 7- Maastrichtian (72-66 Ma), Fig 8- Late Paleocene (61-56 Ma), Fig 9- Oligocene (34-23 Ma).

Country	Ignous Province or Location	Emplacement mode	Age (Ma)	Method	Reference	Map
Nigeria	Benue Trough	Intrusion in Kerri-Kerri formation	41	Radiometrical dating	Adegoke et al. 1986	Fig 9
Algeria	Touareg Shield	Serouenout lava flows	18.1 ± 0.4, 6.3	K-Ar	Aït Hamou and Dautria, 1994; Aït Hamou, 2000	Fig 9
Algeria	Touareg Shield	Tahalgha lava flows	3.4 ± 0.1 - 2.43 ± 0.06	K-Ar	Aït Hamou and Dautria, 1994; Aït Hamou, 2000	Fig 9
Algeria	Touareg Shield	Taharaq lava flows	34.5 ± 3.5- 32.8 ± 2.6	Ar-Ar	Aït Hamou et al., 2000	Fig 9
Algeria	Touareg Shield	Taharaq lava flows, dykes	44 ± 0.8, 33.6 ± 0.7 - 24.4 ± 0.5	K-Ar	Aït Hamou et al., 2000	Fig 9
Sierra Leone	CAMP	Freetown Complex	232.1 ± 9 - 196.3 ± 3	Ar-Ar	Barrie et al., 2006; Barrie et al., 2010	Fig 1
Guinea	Offshore	Krausse Seamount	53.3 - 55.4	N.D.*	Bertrand et al., 1993	Fig 8
Guinea	Offshore	Nadir Seamount	58.6 ± 0.3	Ar-Ar	Bertrand et al., 1993	Fig 8
Algeria	CAMP	Reggane-Tindouf-Hank Sills & Fersiga Dykes & Bechar Lava flows	197.9 ± 2.0 -195.0 ± 1.6	Ar-Ar	Chabou et al., 2007	Fig 1
Liberia	CAMP	Paynesvill Sill	185.0 ± 4.4- 187.0 ± 3.4	Ar-Ar	Dalrymple et al., 1975	Fig 1
Liberia	CAMP	Liberia Dyke and Sills	192 ± 6 - 173 ± 4	K-Ar	Dalrymple et al., 1975	Fig 1
Guinea	CAMP	Kakoulima Laccolithic Complex & Fouta Djalon Dykes and Sills	200.4 ± 2.4 - 188.7 ± 1.9	Ar-Ar	Deckart et al., 1997	Fig 1

Nigeria	Younger Granites	Pankshin ring complexe	151	Rb-Sr	Van Breemen et al., 1975; Dickin et al., 1991	Fig 1
Nigeria	Younger Granites	Jos ring complexe	161	Rb-Sr	Van Breemen et al., 1975; Dickin et al., 1991	Fig 1
Nigeria	Younger Granites	Shere Hills ring complexe	161	Rb-Sr	Van Breemen et al., 1975; Dickin et al., 1991	Fig 1
Nigeria	Younger Granites	Amo ring complexe	162	Rb-Sr	Van Breemen et al., 1975; Dickin et al., 1991	Fig 1
Nigeria	Younger Granites	Zaranda ring complexe	186	Rb-Sr	Van Breemen et al., 1975; Dickin et al., 1991	Fig 1
Nigeria	CAMP	Oban-Obudu Dyke Swarm	219.9 ± 4.7-204.0 ± 9.9	K-Ar	Ekwueme et al., 1997	Fig 1
Nigeria	N.D.*	Oban-Obudu Dyke Swarm	140.5 ± 0.7	Ar-Ar	Ekwueme,1994	Fig 2
Nigeria	Cameroun Line	Mandara lava flows	36 - 30	K-Ar	Fitton and Dunlop, 1985	Fig 9
Nigeria	Cameroun Line	Biu Plateau lava flows	5 - 0.8	K-Ar	Fitton and Dunlop, 1985	Fig 9
Cameroun	Cameroun Line	Manengouba lava flows	3 – 0	K-Ar, Rb-Sr	Fitton and Dunlop, 1985; Halliday et al., 1990	Fig 9
Cameroun	Cameroun Line	Sao Tomé lava flows	13 – 0	K-Ar, Rb-Sr	Fitton and Dunlop, 1985; Halliday et al., 1990; Lee et al., 1994	Fig 9
Cameroun	Cameroun Line	Bambouto lava flows	23 - 14	K-Ar	Fitton and Dunlop, 1985; Marzoli et al., 2000	Fig 9
Cameroun	Cameroun Line	Oku lava flows	31 - 22	K-Ar	Fitton and Dunlop, 1985; Rankenburg et al., 2005	Fig 9
Chad	WCRS	Dilia (Langrin-1) granites, Termit	190 ± 7	N.D.*	Genik, 1992, 1993	Fig 1
Chad	WCRS	Doseo (Tega-1) sills	97 ± 1.2	N.D.*	Genik, 1992, 1993	Fig 5
Chad	WCRS	Bongor (Naramay-1) sills	52 - 56	N.D.*	Genik, 1992, 1993	Fig 8
Chad	WCRS	Doseo (Kikwey-1) sills	101.1 ± 1.1	N.D.*	Genik, 1992, 1993	Fig 4
Chad	WCRS	Termit (Kumia-1) sills	Cenomanian	Relative dating	Genik, 1992, 1993	Fig 5
Chad	WCRS	Sedigi dykes, Termit	Santonian	Relative dating	Genik, 1992, 1993	Fig 6
Chad	WCRS	Doseo (Keita-1) sills	Upper Aptian	Relative dating	Genik, 1992, 1993	Fig 3
Niger	WCRS	Gosso Lorom lava flows, Termit	10 - <1	N.D.*	Genik, 1992, 1993	Fig 9
Niger	WCRS	Termit (Iaguil-1) sills	8.6 ± 0.5	N.D.*	Genik, 1992, 1993	Fig 9
Nigeria	Nigeria Shield	Jos Plateau lava flows	2.1 ± 0.1 - 0.9 ± 0.2	K-Ar	Grant et al., 1972	Fig 9
Nigeria	Benue Trough	South Gombe plugs	22.8 - 11.2	K-Ar	Grant et al., 1972	Fig 9
Nigeria	Cameroun Line	Biu Plateau lava flows	5.0 ± 0.2 - 0.8	K-Ar	Grant et al., 1972	Fig 9
Nigeria	Benue Trough	South Gombe plugs	7.4 - 2.5	K-Ar	Grant et al., 1972	Fig 9
Cameroun	Cameroun Line	Mt Cameroon lava flows	3 – 0	Rb-Sr	Halliday et al., 1990	Fig 9

APPENDIX

Cameroun	Cameroun Line	Bioko lava flows	1 – 0	Rb-Sr	Halliday et al., 1990	Fig 9
Cameroun	Cameroun Line	Principe lava flows	31 – 0	Rb-Sr	Halliday et al., 1990; Lee et al., 1994	Fig 9
Cameroun	Cameroun Line	CL plutons	73 ± 6 - 39 ± 2	K-Ar, Ar-Ar, Rb-Sr	Kamdem et al., 2001	Fig 7
Cameroun	Cameroun Line	CL plutons	73 ± 6 - 39 ± 2	K-Ar, Ar-Ar, Rb-Sr	Kamdem et al., 2001	Fig 8
Cameroun	Cameroun Line	CL plutons	73 ± 6 - 39 ± 2	K-Ar, Ar-Ar, Rb-Sr	Kamdem et al., 2001	Fig 9
Liberia	CAMP	Liberia Dyke Swarm	196 ± 4 - 177 ± 4	K-Ar	Lanphere and Dalrymple, 1971; Lanphere and Dalrymple, 1976	Fig 1
Cameroun	Cameroun Line	Pagalu lava flows	5 – 0	Rb-Sr	Lee et al., 1994	Fig 9
Chad	Tibesti Shield	Tibesti lava flows	9.7-0.3	N.D.*	Liégeois et al., 2005	Fig 9
Mali	Touareg Shield	Tin Zaouatene lava flows	0	N.D.*	Liégeois et al., 2005	Fig 9
Niger	Touareg Shield	Tin Taralle and Todra lava	28-20; 15-8; 4-0.7	N.D.*	Liégeois et al., 2005	Fig 9
Mali	Touareg Shield	Tidjerazraze ring complexe	161 ± 5	Rb-Sr	Liégois et al., 1991	Fig 1
Mali	Touareg Shield	Anezrouf ring complex	184 ± 14	Rb-Sr	Liégois et al., 1991	Fig 1
Mali	Touareg Shield	Tirkine ring complexe	215 ± 11	Rb-Sr	Liégois et al., 1991	Fig 1
Nigeria	Benue Trough	Gowol lava flows	123.1 ± 1.6	Ar-Ar	Maluski et al., 1995	Fig 3
Nigeria	Benue Trough	Bima Hill lava flows	106.6 ± 19	Ar-Ar	Maluski et al., 1995	Fig 4
Nigeria	Benue Trough	Dumne lava flows	130.7 ± 2.7	Ar-Ar	Maluski et al., 1995	Fig 2
Nigeria	Benue Trough	Burashikai lava flows	146.7 ± 1.6 - 137.8 ± 1.9	Ar-Ar	Maluski et al., 1995	Fig 2
Nigeria	Benue Trough	Gboko dykes	93.5 ± 1.7, 92.3 ± 1.1	Ar-Ar	Maluski et al., 1995	Fig 5
Nigeria	Benue Trough	Wanakum Hills lava flows, sills, dykes and pyroclastic deposits	95.3 ± 1 - 71.4 ± 1.3	Ar-Ar	Maluski et al., 1995	Fig 5
Nigeria	Benue Trough	Katyo subvolcanic intrusions	97.1 ± 1.2, 68.4 ± 1.1	Ar-Ar	Maluski et al., 1995	Fig 5
Nigeria	Benue Trough	Okigwi subvolcanic intrusions	87.7 ± 1 - 81.1 ± 1.1	Ar-Ar	Maluski et al., 1995	Fig 6
Nigeria	Benue Trough	Wanakum Hills lava flows, sills, dykes and pyroclastic deposits	95.3 ± 1 - 71.4 ± 1.3	Ar-Ar	Maluski et al., 1995	Fig 6
Nigeria	Benue Trough	Wanakum Hills lava flows, sills, dykes and pyroclastic deposits	95.3 ± 1 - 71.4 ± 1.3	Ar-Ar	Maluski et al., 1995	Fig 7
Nigeria	Benue Trough	Katyo subvolcanic intrusions	97.1 ± 1.2, 68.4 ± 1.1	Ar-Ar	Maluski et al., 1995	Fig 7
Nigeria	Benue Trough	Makurdi intrusions	49.1 ± 1.1	Ar-Ar	Maluski et al., 1995	Fig 8
Nigeria	Benue Trough	Afikpo sills	55.2 ± 2	Ar-Ar	Maluski et al., 1995	Fig 8
Liberia	CAMP	Liberia Dyke Swarm	201± 2 - 186 ± 4	K-Ar	Mauche et al., 1989	Fig 1

Algeria	Touareg Shield	Achkal ring complexe, Amadhor	29 ± 0.6, 24 ± 0.4	K-Ar	Maza et al., 1995	Fig 9
Guinea	Offshore	Los Island instrusions	104.5 ± 1.6	Rb-Sr	Moreau et al., 1996	Fig 4
Mauritania	Taoudenni	Richat dome	85 ± 5	Fission track dating	Nettos et al., 1992	Fig 6
Cameroun	Cameroun Line	Garoua lava flows	39 - 34	K-Ar	Ngounouno et al., 1997	Fig 9
Nigeria	Benue Trough	Burashika-Shani lava flows	147 ± 7	K - Ar	Popoff et al., 1982	Fig 2
Nigeria	Benue Trough	Gowol and Bima-Wada lava flows	103 ± 5	K - Ar	Popoff et al., 1982	Fig 4
Nigeria	Younger Granites	Mada ring complexe	150 ± 2, 145 ± 4	Rb-Sr	Rahaman et al., 1984	Fig 1
Nigeria	Younger Granites	Tibchi ring complexe	171 ± 3	Rb-Sr	Rahaman et al., 1984	Fig 1
Nigeria	Younger Granites	Banke ring complexe	173 ± 3, 173 ± 2	Rb-Sr	Rahaman et al., 1984	Fig 1
Nigeria	Younger Granites	Kudaru ring complexe	175 ± 16, 173 ± 3	Rb-Sr	Rahaman et al., 1984	Fig 1
Nigeria	Younger Granites	Dutsen ring complexe	177 ± 3, 173 ± 3	Rb-Sr	Rahaman et al., 1984	Fig 1
Nigeria	Younger Granites	Ningi ring complexe	183 ± 7	Rb-Sr	Rahaman et al., 1984	Fig 1
Nigeria	Younger Granites	Shira ring complexe	186 ± 5	Rb-Sr	Rahaman et al., 1984	Fig 1
Nigeria	Younger Granites	Fagam ring complexe	191 ± 3	Rb-Sr	Rahaman et al., 1984	Fig 1
Nigeria	Younger Granites	Dutse ring complexe	213 ± 7	Rb-Sr	Rahaman et al., 1984	Fig 1
Nigeria	Younger Granites	Ririwai ring complexe	170-166	Rb-Sr	Rahaman et al., 1984; Dickin et al., 1991; Van Breemen et al., 1975	Fig 1
Cameroun	Cameroun Line	Ngaoundere lava flows	11 – 7	N.D.*	Rankenburg et al., 2005	Fig 9
Ghana	Offshore	Vocaniclastic deposits	125 - 120	N.D.*	Reyre, 1984	Fig 3
Algeria	Touareg Shield	Atakor basaltic lava flows	19.9 ± 1.9 - 12.4 ± 2; 6.7 ± 2 - 4.2 ± 0.2; 1.95 ± 0.2 - 1.5 ± 0.1	K-Ar	Rognon et al., 1981; Rognon et al., 1983	Fig 9
Algeria	CAMP	Ksi-Ksou Dyke	198.0 ± 1.8	Ar-Ar	Sebai et al., 1991	Fig 1
Mali	CAMP	Taoudenni Dyke Swarm	203.7 ± 2.7-200.9 ± 2.5	Ar-Ar	Sebai et al., 1991	Fig 1
Guinea	Kimberlite	Banakoro kimberlite pipe	139 ± 3	Ar-Ar	Skinner et al., 2004	Fig 2
Guinea	Kimberlite	Droujba kimberlite pipe	153 ± 3	Ar-Ar	Skinner et al., 2004	Fig 2
Sierra Leone	Kimberlite	Tongo kimberlite dyke	140	N.D.*	Skinner et al., 2004	Fig 2
Sierra Leone	Kimberlite	Koidu kimberlite pipe 1	143 ± 1	Ar-Ar	Skinner et al., 2004	Fig 2
Sierra Leone	Kimberlite	Koidu kimberlite pipe 2	146 ± 2	Ar-Ar	Skinner et al., 2004	Fig 2
Nigeria	Benue Trough	Gboko-Ikyuen rhyolites	113 ± 3	Rb-Sr	Umeji and Caen-Vachette, 1983	Fig 3
Nigeria	Younger Granites	Afu ring complexe	141 ± 2, 144 ± 2	Rb-Sr	Vail, 1989; Bowden et al., 1976	Fig 1

Mali	CAMP	Taoudenni Sills Drilling ONU	202.4 ± 1.6 - 198.9 ± 1.2	Ar-Ar	Verati et al., 2005	Fig 1
Mali	CAMP	Taoudenni Dyke Swarm	203.7 ± 2.7-196.6 ± 1.0	Ar-Ar	Verati et al., 2005	Fig 1
Nigeria	Kimberlite	Kuafur kimberlite	c.150	N.D.*	Wright, 1976	Fig 2
Nigeria	Nigeria Shield	Jos Plateau lava flows	34.7 ± 0.2, 27 ± 0.2, 8.4 ± 0.1	K-Ar	Zeese et al., 1994	Fig 9
Algeria	Touareg Shield	In Ezzane lava flows	0	N.D.*	Liégeois et al., 2005	Fig 9
Algeria	Touareg Shield	Manzaz lava flows	20-12; 7-4; 3-0.01	N.D.*	Liégeois et al., 2005	Fig 9
Algeria	Touareg Shield	Adrar n'Ajjer lava flows	3,5-2,5	N.D.*	Liégeois et al., 2005	Fig 9
Algeria	Touareg Shield	Eggere lava flows	3,5-2,5	N.D.*	Liégeois et al., 2005	Fig 9
Algeria	Touareg Shield	Serouenout lava flows	16.8 ± 0.6 - 4.7 ± 0.3	Ar-Ar	Maza et al., 1998	Fig 9
Guinea	Offshore	Drilled volcanic	Aptian-Albian	Relative dating	This study	Fig 3
Guinea	Offshore	Drilled volcanics	Aptian-Albian	Relative dating	This study	Fig 4
Liberia	Offshore	Drilled interbedded tuffs and basalts	Neocomian	Relative dating	This study	Fig 2
Liberia	Offshore	Drilled andesite	Neocomian	Relative dating	This study	Fig 2
Liberia	Offshore	Drilled interbedded tuffs and basalts	Neocomian	Relative dating	This study	Fig 2
Liberia	Offshore	Drilled tuffs	Albian	Relative dating	This study	Fig 4
Liberia	Offshore	St Paul lacoliths, volcanics	Tertiary	Relative dating	This study	Fig 8
Liberia	Offshore	St Paul lacoliths, volcanics	Tertiary	Relative dating	This study	Fig 9

*N.D. = not determined.

Appendix 2. Compilation of thermochronological data (AFTA and AHe) available over Northwestern Africa.

Sample's name, location, lithology, age and mean track length issue from AFTA, age of AHe dating and used reference are shown for each sample, when available.

Sample Name	Long	Lat	Location	Elevation (m)	Lithology	AFT_ Age (Ma)	Error	MTL (µm)	Error	MTL_ Std	AHE_Mean (Ma)	AHE_Correc (Ma)	Reference
TGH3163	-9,9	24,9	Reguibat Central	305	Granite	139	9	11,9	0,2	1,8	162-137	191-166	Leprêtre, 2015
TGH3111 B	-9,4	24,0	Reguibat Central	252	Granite	150	8	11,9	0,2	1,7			Leprêtre, 2015
TEN1185	-10,5	24,1	Reguibat Central	236	Gabbro	163	10	12,4	0,2	2,1	142-86	167-133	Leprêtre, 2015
YT7	-7,3	26,5	Reguibat Central	384	Monzogranite	166	8	11,4	0,3	1,8			Leprêtre, 2015

TEN4065	-10,0	24,3	Reguibat Central	258	Microgranite	172	13	11,7	0,3	2,0			Leprêtre, 2015
TGH4072 A	-9,7	24,5	Reguibat Central	273	Granite	199	13	12,4	0,2	1,6			Leprêtre, 2015
AL10	-7,1	26,6	Reguibat Central	394	Granodiorite	202	14	12,0	0,2	1,6	280-67	396-96	Leprêtre, 2015
TEN1153	-10,5	24,0	Reguibat Central	216	Grabbro	256	21	12,3	0,2	2,3	66-31	81-38	Leprêtre, 2015
TL3	-3,2	27,4	Reguibat East	381	Gabbro	237	21				99-31	133-40	Leprêtre, 2015
CH2	-3,6	25,6	Reguibat East	252	Gabbrodiorite	264	21	12,0	0,2	1,7			Leprêtre, 2015
CH1	-3,6	25,6	Reguibat East	252	Gabbrodiorite	307	26	11,5	0,2	2,1	178-26	234-32	Leprêtre, 2015
CH3	-3,6	25,6	Reguibat East	252	Gabbrodiorite	315	24	11,5	0,3	2,3	175-99	222-138	Leprêtre, 2015
DEG6	-3,0	26,1	Reguibat East	355	Gabbro	355	25	11,2	0,4	2,1			Leprêtre, 2015
GH3	-6,1	25,5	Reguibat East	360	Trondhjemite	359	27	11,5	0,2	1,9	256-88	326-104	Leprêtre, 2015
IG3	-6,2	26,2	Reguibat East	366	Rhyolite	393	36	0,0	0,0		277-120	384-166	Leprêtre, 2015
GH20	-6,0	25,6	Reguibat East	350	Gabbro						61-27	87-41	Leprêtre, 2015
AOS2	-14,3	22,5	Reguibat West	400	neph. syen.	107	8	11,8	0,2	1,8	65-21	81-27	Leprêtre, 2015
TAS29	-15,6	21,0	Reguibat West	110	Gneiss	115	6	12,2	0,3	1,8	138-62	185-94	Leprêtre, 2015
AG169	-13,4	20,7	Reguibat West	137	Charnockite	118	10						Leprêtre, 2015
TAS233	-15,6	21,0	Reguibat West	110	Volcanite	126	7	12,5	0,2	1,8	77-35	111-43	Leprêtre, 2015
TCH7	-15,1	21,9	Reguibat West	194	Granite	127	8	9,4	0,3	2,0	55-23	67-29	Leprêtre, 2015
AOS3	-14,3	22,5	Reguibat West	400	neph. syen.	128	6	11,9	0,2	1,6	74-38	95-47	Leprêtre, 2015
AOS5	-14,3	22,5	Reguibat West	400	neph. syen.	128	8	11,8	0,2	1,8	39-12	52-14	Leprêtre, 2015
AG167	-13,4	20,7	Reguibat West	125	Charnockite	137	12						Leprêtre, 2015
SC12	-14,5	22,6	Reguibat West	292	Granite	141	8	12,2	0,2	1,8	64-55	82-63	Leprêtre, 2015
SC9	-14,3	22,6	Reguibat West	318	Granite	143	13	11,2	0,4	1,9	71-42	93-52	Leprêtre, 2015
SC5	-14,5	22,7	Reguibat West	284	Granite	156	15	10,7	0,3	1,7	77-28	101-35	Leprêtre, 2015
SC11	-14,4	22,6	Reguibat West	293	Granite	160	11	12,1	0,3	1,8	71-35	92-24	Leprêtre, 2015
SC15	-14,5	22,7	Reguibat West	282	Granite	175	16				67-21	80-27	Leprêtre, 2015
SC-31	7,8	18,5	Air		granite pegmatitic granite	34	3	12,5	0,7				Cavellec, 2006
SC-56	7,8	18,5	Air		Leucocratic granite	36	2	12,8	1,2				Cavellec, 2006
SC-71	8,4	18,0	Air		prthoclase-phenocryst	44	3	12,6	0,2				Cavellec, 2006
BF 3	-2,0	12,7	Burkina Faso	400	Granite	175	10	12,8	0,2	1,6			Gunnell, 2013

BF 1	-1,3	12,6	Burkina Faso	340	Granite	179	10	12,8	0,2	1,5		Gunnell, 2013
BF 7	-3,2	10,7	Burkina Faso	320	Granite	179	9	13,1	0,2	1,5		Gunnell, 2013
BF 4	-0,3	12,3	Burkina Faso	380	quartz syenite	196	19	12,4	0,2	1,9		Gunnell, 2013
BF 5	-1,9	12,0	Burkina Faso	400	Granodiorite	211	8	12,4	0,2	1,6		Gunnell, 2013
BF 2	-1,9	11,4	Burkina Faso	380	Granite	218	7	12,2	0,2	1,8		Gunnell, 2013
IT05	5,7	22,8	Hoggar	1523	Granite	75	8				55	Rougier, 2012
BLN12-2	9,6	17,6	Hoggar	671	Rhyolite	91	10				64	Rougier, 2012
IT22	5,7	22,8	Hoggar	1537	Granite	96	11				71	Rougier, 2012
ALG3	4,5	22,5	Hoggar	707	Granodiorite	99	6				43	Rougier, 2012
TOD17	7,3	25,0	Hoggar	1341	Granite	111	10				41	Rougier, 2012
ARO113	8,5	23,7	Hoggar	1037	Granite	114	10				17	Rougier, 2012
ALG1	4,4	22,7	Hoggar	705	Granodiorite	166	10					Rougier, 2012)
ALG2	4,4	22,6	Hoggar	699	Granodiorite	166	9	10,4	0,2		41	Rougier, 2012
TOD27	7,3	25,1	Hoggar	1372	Granodiorite	179	20	0,0	0,0		22	Rougier, 2012
TOD30	7,3	25,0	Hoggar	1416	Granite	285	29				14	Rougier, 2012
ALG4	4,6	22,5	Hoggar	722	Granodiorite						42	Rougier, 2012
FRZ1	3,5	25,7	Hoggar	625	Cambro-Ordovician sandstone						78	Rougier, 2012
BLN400	8,6	19,6	Hoggar	802	Mylonitic metatonalite						37	Rougier, 2012
TZA14	4,5	23,9	Hoggar	827	Imelehatene granite						49	Rougier, 2012
TZA28	4,4	24,0	Hoggar	754	Tidjelamine granite						49	Rougier, 2012
TZA182	4,0	25,1	Hoggar	834	Mouydir granodiorite						71	Rougier, 2012
TZA204	4,7	24,7	Hoggar	912	Tesnou granite						43	Rougier, 2012
ARO108	8,5	23,7	Hoggar	1037	Tin Ghoras granite						41	Rougier, 2012
EN06-5	-2,5	3,6	IC-GN marginal ridge	-3465	Early Cretaceous sandstone	68						Bouilin et al., 1997
EN04-9	-2,3	3,7	IC-GN marginal ridge	-2405	Early Cretaceous sandstone	69						Bouilin et al., 1997
EN09-9	-2,7	3,5	IC-GN marginal ridge	-2675	Early Cretaceous sandstone	78						Bouilin et al., 1997

EN01-3	-1,9	3,9	IC-GN marginal ridge	-3479	Early Cretaceous sandstone	83	Bouilin et al., 1997
EN09-4	-2,7	3,5	IC-GN marginal ridge	-3524	Early Cretaceous sandstone	90	Bouilin et al., 1997
EN09-2	-2,7	3,5	IC-GN marginal ridge	-3905	Early Cretaceous sandstone	92	(Bouilin et al., 1997
961	-3,1	3,5	IC-GN marginal ridge	-365	Bajocian-Maastrichtian siltstone	92	Bouilin et al., 1997
960	-2,7	3,6	IC-GN marginal ridge		sandstone, claystone, limestone		Bouilin et al., 1997;Clift et al., 1998
959	-2,7	3,6	IC-GN marginal ridge		Sandstone		Clift et al., 1998

References cited in Appendix 1. and 2.

Adegoke, O.S., Agumanu, A.E., Benkhelil, M.J., and Ajayi, P.O., 1986, New stratigraphic, sedimentologic and structural data on the Kerri-Kerri Formation, Bauchi and Borno states, Nigeria: Journal of African Earth Sciences, v. 5, p. 249–277.

Akpati, B.N., 1978, Geologic structure and evolution of the Keta basin, Ghana, West Africa: Geological Society of America Bulletin, v. 89, p. 124–132.

Barrie, I.J., 2006, Tectono-thermal evolution of the Sierra Leone passive continental margin, West Africa; constraints from thermochronology, *in* Geochimica et Cosmochimica Acta, Melbourne, Victoria, Australia, v. 70, p. A36–A36.

Barrie, I.J., Wijbrans, J., Andriessen, P., Beunk, F., Strasser-King, V., and Fode, D., 2010, Combined (super 40) Ar/ (super 39) Ar and fission-track study of the Freetown layered igneous complex, Freetown, Sierra Leone, West Africa; implications for the inital break-up of Pangea to form the central Atlantic Ocean and insight into the Post-rift Evolution of the Sierra Leone Passive Margin, *in* Geophysical Research Abstracts, v. 12, p. 7322.

Bertrand, H., Mascle, J., Marinho, M., and Villeneuve, M., 1988, Volcanics from the Guinea continental margin: geodynamic implications: Journal of African Earth Sciences, v. 7, p. 181–188.

Bouillin, J.P., Poupeau, G., Basile, C., Labrin, E., and Mascle, J., 1998, Thermal constraints on the Cote d'Ivoire-Ghana transform margin; evidence from apatite fission tracks: Proceedings of the Ocean Drilling Program, Scientific Results, v. 159, p. 43–48.

Bouillin, J.-P., Poupeau, G., Labrin, E., Basile, C., Sabil, N., Mascle, J., Mascle, G., Gillot, F., and Riou, L., 1997, Fission track study: heating and denudation of marginal ridge of the Ivory Coast–Ghana transform margin: Geo-Marine Letters, v. 17, p. 55–61.

Bowden, P., Van Breemen, O., Hutchinson, J., and Turner, D.C., 1976, Palaeozoic and Mesozoic age trends for some ring complexes in Niger and Nigeria: Nature, v. 259, p. 297–299.

Cavellec, S., 2006, Evolution diagénétique du bassin de Tim Mersoï et conséquences pour la genèse des minéralisations uranifères dans les formations carbonifères du Guezouman et du Tarat (district Arlit-Akokan, Niger) [Ph.D. thesis] [Thèse doctorat]: Université de Paris XI, Orsay, France, 449 p.

Clift, P.D., Carter, A., and Hurford, A.J., 1998, Apatite fission track analysis of sites 959 and 960 on the transform continental margin of Ghana, West Africa: Proceedings of the Ocean Drilling Program, Scientific Results, v. 159, p. 35–41.

Dalrymple, G.B., Gromme, C.S., and White, R.W., 1975, Potassium-argon age and paleomagnetism of diabase dikes in Liberia; initiation of central Atlantic rifting: Geological Society of America Bulletin, v. 86, p. 399–411.

Deckart, K., Feraud, G., and Bertrand, H., 1997, Age of Jurassic continental tholeiites of French Guyana, Surinam and Guinea: implications for the initial opening of the central Atlantic Ocean: Earth and Planetary Science Letters, v. 150, p. 205–220.

Dickin, A.P., Halliday, A.N., and Bowden, P., 1991, A Pb, Sr and Nd isotope study of the basement and Mesozoic ring complexes of the Jos Plateau, Nigeria: Chemical Geology, v. 94, p. 23–32.

Ekwueme, B.N., 1994, Basaltic magmatism related to the early stages of rifting along the Benue Trough; the Obudu dolerites of South-east Nigeria: Geological Journal, v. 29, p. 269–276.

Ekwueme, B.N., Itaya, T., and Yabe, H., 1997, K-Ar ages of intrusive rocks in the Oban-Obudu Massif and their significance for the tectonic and plutonic history of southeastern Nigeria: The Island Arc, v. 6, p. 353–360.

Fitton, J.G., and Dunlo, H.M., 1985, The Cameroon line, West Africa, and its bearing on the origin of oceanic and continental alkali basalt: Earth and Planetary Science Letters, v. 72, p. 23–38.

Genik, G.J., 1993, Petroleum geology of Cretaceous-Tertiairy rift basins in Niger, Chad, and Central African Republic: American Association of Petroleum Geologists Bulletin, v. 77, p. 1405–1434.

Genik, G.J., 1992, Regional framework, structural and petroleum aspects of rift basins in Niger, Chad and the Central African Republic (C.A.R.): Tectonophysic, v. 213, p. 169–185.

Grant, N.K., Rex, D.C., and Freeth, S.J., 1972, Potassium-Argon Ages and Strontium Isotope Ratio Measurements from Volcanic Rocks in Northeastern Nigeria: Contributions to Mineralogy and Petrology, v. 35, p. 277–292.

Gunnell, Y., 2003, Radiometric ages of laterites and constraints on long-term denudation rates in West Africa: Geology, v. 31, p. 131–134.

Halliday, A.N., Davidson, J.P., Holden, P., DeWolf, C., Lee, D.C., and Fitton, J.G., 1990, Trace-element fractionation in plumes and the origin of HIMU mantle beneath the Cameroon Line: Nature, v. 347, p. 523–528.

Kamden, J.B., Kraml, M., Keller, J., and Henjes-Kunst, F., 2001, Cameroon Line magmatism: conventional K/Ar and single-crystal laser 40Ar/39Ar ages of rocks and minerals from the Hossere Nigo anorogenic complex Cameroon: Journal of African Earth Sciences, v. 35, p. 99–105.

Lanphere, M.A., and Dalrymple, G.B., 1971, A test of the (super 40) Ar/ (super 39) Ar age spectrum technique on some terrestrial materials: Earth and Planetary Science Letters, v. 12, p. 359–372.

Lanphere, M.A., and Dalrymple, G.B., 1976, Identification of excess (super 40) Ar by the (super 40) Ar/ (super 39) Ar age spectrum technique: Earth and Planetary Science Letters, v. 32, p. 141–148.

Lee, D.C., Halliday, A.N., Fitton, J.G., and Poli, G., 1994, Isotopic variations with distance and time in the volcanic islands of the Cameroon Line; evidence for a mantle plume origin: Earth and Planetary Science Letters, v. 123, p. 119–138.

Leprêtre, R., 2015, Evolution phanérozoïque du Craton Ouest Africain et de ses bordures Nord et Ouest [Ph.D. thesis]: Université Paris Sud - Paris XI, France, 423 p.

Leprêtre, R., Barbarand, J., Missenard, Y., Leparmentier, F., and Frizon de Lamotte, D., 2014, Vertical movements along the northern border of the West African Craton: the Reguibat Shield and adjacent basins: Geological Magazine, v. 151, p. 885–898.

Liégois, J.P., Benhallou, A., Azzouni-Sekkal, A., Yahiaoui, R., and Bonin, B., 2005, The Hoggar swell and volcanism: Reactivation of the Precambrian Tuareg shield during Alpine convergence and West African Cenozoic volcanism: Geological Society of America, Special Paper, v. 388, p. 379–400.

Liégois, J.P., Sauvage, J.F., and Black, R., 1991, The Permo-Jurassic alkaline province of Tadhak, Mali: Geology, geochronology and tectonic significance: Lithos, v. 27, p. 95–105.

Maluski, H., Coulon, C., Popoff, M., and Baudin, P., 1995, 40Ar/39Ar chronology, petrology and geodynamic setting of Mesozoic to early Cenozoic magmatism from the Benue Trough, Nigeria: Journal of Geological Society, London, v. 152, p. 311–326.

Mauche, R., Faure, G., Jones, L.M., and Hoefs, J., 1989, Anomalous isotopic compositions of Sr, Ar and O and the Mesozoic diabase dikes of Liberia, West Africa: Contributions to Mineralogy and Petrology, v. 101, p. 12–18.

Moreau, C., Ohnenstetter, D., Demaiffe, D., and Robineau, B., 1996, The Los Archipelago nepheline syenite ring-structure: a magmatic marker of the evolution of the Central and Equatorial Atlantic: The Canadian Mineralogist, v. 34, p. 281–299.

Netto, A.M., Fabre, J., Poupeau, G., and Champenois, M., 1992, Datation par traces de fission de la structure circulaire des Richat (Mauritanie): C.R. Acad. Sci. Paris, v. 314 II, p. 1179–1186.

Ngounouno, I., Deruelle, B., Demaiffe, D., and Montigny, R., 1997, Données nouvelles sur le volcanisme cénozoïque du fossé de Garoua (Nord du Cameroun): Comptes Rendus de l'Academie des Sciences, Serie II, v. 325, p. 87–94.

Popoff, M., Kampunzu, A.B., Coulou, C., and Esquevin, J., 1982, Découverte d'un volcanisme mésozoïque dans le NE du Nigeria: datations absolues, caractères magmatiques et signification dans l'évolution du rift de la Bénoué., *in* Popoff, M. and Tiercelin, J.J. eds., Rifts et Fossés anciens, Résumés de communication des travaux du laboratoire de Science de la Terre, Saint Jérome, Marseille, France, p. 47–49.

Rahaman, M.A., Van Breemen, O., Bowden, P., and Bennett, J.N., 1984, Age migrations of anorogenic ring complexes in northern Nigeria: Journal of Geology, v. 92, p. 173–184.

Reyre, D., 1984, Remarques sur l'origine et l'évolution des bassins sédimentaires africains de la côte altantique: Bulletin de la Societé Géologique de France, v. 26, p. 1041–1059.

Rougier, S., 2012, Interactions lithosphère-ssthénosphère et mouvements verticaux : le cas du Massif du Hoggar [Ph.D. thesis]: Université Paris-Sud, 276 p.

Rougier, S., Missenard, Y., Gautheron, C., Barbarand, J., Zeyen, H., Pinna, R., Liegeois, J., Bonin, B., Ouabadi, A., Derder, M.., and Frizon de Lamotte, D., 2013, Eocene exhumation of the Tuareg Shield (Sahara Desert, Africa): Geology, v. 41, p. 615–618.

Sebai, A., Feraud, G., Bertrand, H., and Hanes, J., 1991, 40Ar/39Ar dating and geochemistry of tholeiitic magmatism related to the early opening of the Central Atlantic rift: Earth and Planetary Science Letters, v. 104, p. 455–472.

Skinner, E.M.W., Morelli, C., Apter, D.B., and Smithson, N.K., 2004, Kimberlites of the Man craton, West Africa: Lithos, v. 76, p. 233–259.

Umeji, A.C., and Caen-Vachette, M., 1983, Rb-Sr isochron from Gboko and Ikyuen rhyolites and its implications for the age and evolution of the Benue Trough, Nigeria: Geological Magazine, v. 120, p. 529–533.

Van Breemen, O., Hutchinson, J., and Bowden, P., 1975, Age and origin of the Nigerian mesozoic granites: A Rb-Sr isotopic study: Contributions to Mineralogy & Petrology, v. 50, p. 157–172.

Vannucci, R., Calvino, F., Cortesogno, L., and Tolomeo, L., 1989, Jurassic volcanism findings in Sokoto State (NW-Nigeria): Journal of African Earth Sciences, v. 9, p. 245–258.

Verati, C., Bertrand, H., and Feraud, G., 2005, The farthest record of the Central Atlantic Magmatic Province into West Africa craton: Precise 40Ar/39Ar dating and geochemistry of Taoudenni basin intrusives (northern Mali): Earth and Planetary Science Letters, v. 235, p. 391–407.

Wright, J.B., 1976, Volcanic rocks in Nigeria, *in* Kogbe, C.A. ed., Geology of Nigeria, Elizabethan Publication Company, Surulere, Lagos, Nigeria, p. 93–142.

Zeese, R., Schwertmann, U., Tietz, G.F., and Jux, U., 1994, Mineralogy and stratigraphy of three deep lateritic profiles of the Jos plateau: Catena, v. 21, p. 195–214.

Appendix 3. Localization and features of samples collected in Guinea

(Provided by Dominique Chardon)

SAMPLE	Lat N	Long E	Alt. (m)	Lithology	Locality	Country	Comments
GM1	9,7164	-13,41813	4	Granitoid	Manéah (Conakry)	Guinea	Industrial granite pit on the edge of lagoon/mangrove reached by the road to the Mahéah center. Light color granite (more or less porphyritic). Fk+Q+Bi +/- Pl.
GM2	9,72433	-13,37092	27	Gneiss	between Coyah and Kouria	Guinea	Western sided of the road. Migmatitic gneiss rich in quartz. Outcrops contains muscovite-rich facies. The sample is without muscovite. Shallowly deeping schistosity to the NW.
GM3	9,73388	-13,14382	303	Sandstone	Tabili (?), climing up Friguiady	Guinea	Chenalised sandstone with coarsing up evolution. Strong grading of size from siltstone to corase sandstone with ripples rich in quartz +/- +/- Felspars and heavy minerals.
GM4	10,01673	-12,82185	324	Sandstone	Eastern exit of Kindia	Guinea	Sandstone with tidal structures, herring bones and channels
GM5	10,02741	-12,67767	255	Dolerite	several kms from Bokaria	Guinea	Well-crystallized and fresh dolerite at the foot of the « Cocherie » pit.
GM6	10,1125	-12,55918	125	Sandstone	4 km before Souguela	Guinea	Well-classified sandstone, without visible sedimentary structures, stongly weathered. Stratigraphic position: bottom of the Bove Basin.

GM7	10,71441	-12,24887	1247	Sandstone	Dalaba (3,5 km on the north of the city)	Guinea	First pass 3.5 km outside the city on the Labé road. Saprolite of sandstone. No visible sedimentary structures. Sample is from the slope of a 1370m high mountain.
GM8	10,7017	12,25725	1228	Dolerite	Dalaba (northern exit)	Guinea	Northern exit of the city. Well-crystallized and fresh dolerite collected in a holl surrounded by rocks with saprolitic facies
GM9	10,61369	-12,19874	980	Dolerite	12 km on the South of Dalaba	Guinea	Hurge doleritic sill (>100m). Centimetric-scale hornblende bearing diorite (coarse-grained facies in the middle of the sill)
GM10	10,6038	-11,85709	840	Dolerite	4 km before Timbo	Guinea	Hundreds meters before the panel on the left for Dar el Salam. Dolerite preserved in weathering profil of high glacis. Coarse-grain hypovolcanic texture.
GM11	10,6364	-11,81488	784	Granitoid	Slope of RN1 of the northern exit of Timbo	Guinea	Mylonitic orthogneiss (senestral shearing). Deformation in green shale with probably syn-crystallization hydrothermalism. Fk, Pl et Cl. Schistosity N84, 90.
GM12	10,73259	-11,57986	679	Granitoid	Several kms from Sarramousaya	Guinea	Granodiorite (2 pieces) connected laterally to a migmatitic shear zone (~15m far). Shchistosity: N130, 90.
GM13	10,73559	-11,29056	656	Granitoid	around 24 km on the South of Dabola	Guinea	Foothill of 950m high Inselberg (altitude difference between the sample and the inselberg top: 295 m). Absence of visible quartz. Prophyritic granodiorite with pink feldspars. Schistosity / banding : N129,30NE.

GM14	10,82268	-10,99629	438	Granitoid	17 km on the East of Dabola, 6,7 km before Bissikrima	Guinea	Foothill of a granitic mount with 890m height, 1 km on the North of the road. Altitude difference between the sample and the mount top: 398 m. Granitoide with Fk + Q + Pl + Hb +/- Bi. Hb, weathered.
GM15	10,91783	-10,74739	496	Granitoid	Kouroukoro	Guinea	Slope of the inselberg of Kouroukoro. Fresh porphyritic granite, absence of Hb. Height of the inselberg: 620 m (difference: 130 m).
GM16	10,73857	-10,08871	415	Granitoid	8 km on the East of Moussaya	Guinea	500 m on the north of the road, bank of the river (outcrops indicated on the map of BRGM). Granite similar with GM15 but non-porphyritic. Visible weathering.
GM17	12,347	-8,40856	430	Sandstone	South of Siby	Mali	Foot of the Monts Mandingues. Coarse sandstone with quartz. Sample collected from channel-facie sandstone without pebble. Sample was collected at ca. 8m on the foot of the cliff and 20-25 m above the plain level.
GM18	12,66357	-7,98985	438	Sandstone	Bamako, rebord sud de la colline du Pouvoir (Sud du CHU)	Mali	Sandstone pavement under a weathering profile of ~50m thick and topped by a cuirasse of glacis (height: 490 m). Coarse sandstone, rare sedimentary structures except several channels and ripples. Dark sandstone, quartz grains are angular, 2-3 mm. Cemented grains in a whith matrix.
GM19	12,66337	-7,98911	408	Sandstone	Bamako, Southern edge of the hill of Pouvoir (South of CHU)	Mali	Sample on the foot of the slope on the same location. Coarse sandstone, relatively weathered. Many channels underlined by more conglometric levels.

GM20	12,64776	-7,93109	324	Sandstone	Bamako, 3rd bridge on the Niger river	Mali	Sanstone-levels forming the knickpoint of the river near the old bridge. Sample collected on the Northern bank. Dark fin-grain sandstone. Erozion and the streaming of the river erase the possible sedimentary structures.

Appendix 4. Localization and features of samples in Ivory Coast

(Kouamelan, 1996)

SAMPLE	Lat N	Long W	Alt. (m)	Lithology	Locality	Comments	PhD page
BD507	9,19900	6,95217	471	leucocratic migmatitic gneiss	Siréba	W of the Bagoué basin. Foliation: 20°-70°E. Granoblastic texture, medium grained, locally cataclastic. Green biotite (sometimes brown), Allanite.	194
KG33a	9,46500	5,65417	393	leucocratic migmatitic gneiss	Korhogo	East of the Diaouala volcano-sedimentary series. Same as BD507.	194
KG32	9,07983	5,76900	407	leucocratic migmatitic gneiss	Dikodougou	Same as KG-33a.	194
MK64	8,15900	6,36383	295	granodiorite	5 km S of Kouroufia	Western edge of Séguéla massif. Quartz, plagioclase, microline, hornblende & biotite.	196
SEN-1	7,82833	6,53383	324	granodioritic gneiss	Between Kénégoué et Digila, 6 km S of Ména	South of Séguéla massif. Equigranulare, medium- to coarse grained . Pink K feldspar phenocrysts.Quartz, plagioclase, microcline & brown biotite. Foliation: N0° to N10°. Dextral shear N°40.	196
SEN-2	7,82833	6,53383	324	granodioritic gneiss	Between Kénégoué et Digila, 6 km S of Ména	Same as SEN-1	196
YAL-1	7,77250	7,56183	511	granulitic grey gneiss	1.4 km NW of Bénomba, 7 km NE of Biankouma	Dark grey, fine- to medium grained. Predominance of quartz & feldspar	42

YOR-1	7,47733	7,39067	308	granodriorite	Yorogoué village 4.6 km WNW of Zouta	Domple massif. Deformation up to weak augen gneiss texture. Foliation: N40	41
YOR-2	7,47733	7,39067	308	granodriorite	Yorogoué village 4.6 km WNW of Zouta	Same as YOR-1	41
BEZ-1	7,45900	6,16400	266	granodioritic gneiss	7.8 km E of Zanzra, 5.7 km W of Klazra	Quartz, microline, plagioclase, green hornblende, biotite & euhedral allanite	197
VAA-1	7,41133	6,63650	270	granodioritic gneiss	1.5 km SE of Vaafla	Same as BEZ-1	197
LOG-2	7,05867	7,52883	269	biotite migmatitic gneiss	Logoualé village, 6 km E of Douonfapleu	Core of the Logoualé "band". Millimetric layering (more rarely centimetric). Foliation: N70.	47
DLO3bis	6,49950	6,45933	201	leucogranite	2.7 km E of Bïtapia, 6.7 W of Broma	Intrusives in schists. Predominance of microcline. Muscovite & green biotite.	198
SOK-1a	5,67650	6,64933	159	tonalitic gneiss	3.2 km SSW of Nibi II, 7.4 km NNW of Salékoragui	Melanocratic	198
SOK-1b	5,67650	6,64933	159	tonalitic gneiss	3.2 km SSW of Nibi II, 7.4 km NNW of Salékoragui	Coarse grained, hololeucocratic. Occurrence of quartz and microcline megacrysts, rare FeMg minerals.	198 & 199
SA-14	4,93300	6,10583	15	granodiorite	Batelebre 2	Sassandra massif. Mesocratic. Foliation: N120 to 130°. Dextro-normal shears.	200
SA-3	4.72695	6.6293	2	tonalitic gneiss	San-Pedro	More or less migmatitic. Mesocratic. Foliation N30°. Dextral shears (N80) intruded by pink pegmatites.	199

Appendix 5. Localization and features of samples collected in Benin

(Provided by Dominique Chardon)

Sample	lat N	long E	Elev. (m)	Lithology	Locality	Comments
BN 1	7.40153	2.08989	160	Granitoid	Abandoned quarry north of Dan	Fine-grained granodiorite with no apparent fabric, synkinematically intruding flat migmatitic gneisses. The gneisses undergo pervasive, syn-melt, top-to-the East apparent shearing. Bi + Hb + Pl +/- F_K + Q (+ Gt ?). *Sample the closest to the Coastal Sedimentary Basin.*
BN 2	7.61572	2.19132	144	Granulitic gneiss	Small quarry, East side of the road 3 km S of Dassa)	Hyperstene (granulitic) gneiss resulting from charnockitization of a hornblende gneiss. Foliation: N150, 90. Sample collected at the entrance of an inselberg bearing country (culminating at 398 m in Savé).
BN 3	8.04684	2.49882	197	Granitoid	Road cut, northern entrance of Savé	Syn-kinematic porphyritic granite forming the Savé inselbergs. Rich in Biotite. Facies go from randomly oriented phenocrysts to highly sheared augen gneiss. Feldspars are ductilely deformed; shears and CS fabrics indicate dextral kinematics. Foliation: N135, 90. Gray aplites intruding shears while active. The outcrop marks the intersection of the Savé inselberg with the road at a pass. Relief amplitude is of at least 200 m.
BN 4	8.74617	2.60651	302	Granitoid	Hill on the E side of the road at Goutogo	Porphyritic granite rich in Biotite (+/- Hb ?). Sampled on the northern hillslope. Visible banding and phenocryst preferential orientation.

BN 5	9.19113	2.55006	374	Granitoid	Artisanal quarry E side of road S of Parakou	Porphyritic granite showing transitional (fuzzy) facies with diatexitic gneisses suggesting genetic relationships. Parakou granite. Locally incipient or pervasive dextral CS fabrics. S: N20, 90 ; C: N50, 90.
BN 6	11.67882	3.19195	238	Sandstone	Ferricrete-capped cuesta, 1km E of the Road , N of Boiffo	Medium grained, weathered sandstone (« Cambro-Silurian » of the « Kandi basin »). The outcrop is mainly made of coase-grained beds and gravels. The sampled layer shows slightly oblique stratifications. *The sample is crucial* although it may not be too favorable at first sight. It is the northernmost of the transect i.e., the closest to the southern margin of the Iullemmeden basin.
BN 7	11.13767	2.90475	298	Gneiss	Outcrops along the Kandi - Banikouara road, less than 1 km from the entrance circle of Kandi	Banded (« straight ») hornblende gneiss of TTG composition (U/Pb conventional age of ca. 540 Ma). Upper amphibolite facies deformation conditions. A few, highly sheared concordant leucocratic veins (the sample is devoid of melt). Some isoclinal folds. The main fabric reworks an earlier, shallowly dipping foliation.
BN 8	10.80048	2.80781	347	Sandstone	Inselberg E side of the road 1 km N of Wéré	Pink weathered medium size grained sandstones (« Cambro-Silurian »). The sampled layer is the finest grained in an outcrop of conglomerates and heterogeneous coarse-grained sandstones. Oblique stratifications in the sampled bed. Bedding: N25, 35W. NE piedmont of a small inselberg.
BN 9	10.56113	2.73231	351	Gneiss	Small outcrop in crops E side of the road	Migmatitic, banded hornblende (TTG) gneiss (comparable to BN 7, but with clearer evidence of melting and melt remobilization, maybe due to lesser strain). Late C' shear bands (dextral).
BN 10	10.37225	2.72320	345	Gneiss	Road cut ca. 13 km N of Bembéréké	Migmatitic granitic augen gneiss (melt collection in concordant veins and individualization of phenocrysts in those veins).

BN 11	9.77403	2.60340	346	Granitoid	Small quarry N side of road, 3.5 km W of Ouenou	Very fresh porphyritic granite without clear preferential crystal orientation. Some Schlieren, rare aplitic concordant veins.
BN 12	9.77020	2.30326	338	Metamorphic rock	Big quarry ca. 2 km E of Sonoumon	Migmatitic volcano-sedimentary (?) rock. « Biotite rich, phenocrysts bearing banded migmatite » (augen gneiss-like). Highly strained.
BN 13	10.00532	1.50905	397	Granitoid	Small outcrop in crops NE side of the road	Sheared two-mica granite. Pervasive C' shear bands, slightly weathered. Fol : N132, 35SW ; L : N187 ; pervasive top-to-the N shearing.
BN 14	10.75895	1.19141	247	Sandstone	NE slope of inselberg, SE side of the road, NW of Tiélé	Homogenous sandstone with planar & parallel stratifications. Steep bedding. Slightly weathered. Lower Paleozoic.
BN 15	10.61275	1.27637	268	Sandstone	Tanguieta gate, southern entrance of town	Strained pink sandstone, partially recrystallized. Entrance of the gorge crossing the Western front of the Atacora range (culminating at ca. 530 m nearby). Minimum relief amplitude : 330 m.
BN 16	10.56254	1.32132	557	Sandstone	NE edge of the Atakora « plateau »	Strained pink sandstone, partially recrystalized.
BN 17	8.36322	2.62905	262	Gneiss	Small outcrops E side of the road, ca. 3 km S of Kokoro	Migmatitic hornblende gneiss. Hb bearing, coarse grained, concordant leucozomes nucleating syn- to late melt shears. The sample is devoid of leucozome. Fol : N144, 80W ; pitch Lin : 60N; Shears : N169, 90 dextral.
BN 18	7.05832	1.81862	203	Sandstone	1-2 km NE of Adjahomé, SW roadcut	Turonian - Cognacian. Wide (decametric) and thin (decimetric) channels with oblique planar stratifications. Weathered sandstone *but crucial* (only sample in the Mesozoic series of the Coastal Sedimentary Basin).

Appendix 6. Table of the AFTA data (age, mean track length, number of measured track lengths, standard deviation, Dpar, and the person who operated). Provided by Mark Wildman.

Country	Elevation_m	Lithology	AFT_Age_Ma	AFT_Age_Err	A_MTL_µm	A_MTL_Err	A_MTL_Std	Num_Lengths	Dpar	Person
Guinea	70	granite	109,3	5,1	13,28	0,17	1,73	100		R. W. Brown
Guinea	255	sandstone	121,6	4,8	13,38	0,15	1,46	100		R. W. Brown
Guinea	350	sandstone	138,1	10,0	12,95	0,30	2,35	60		R. W. Brown
Guinea	900	granite	153,7	8,9	13,04	0,21	2,09	100		R. W. Brown
Guinea	1150	sandstone	163,7	12,2	14,14	0,42	1,50	13		R. W. Brown
Guinea	850	diorite	170,7	9,0	13,59	0,18	1,79	100		R. W. Brown
Guinea	770	gneiss	144,8	9,6	13,63	0,21	1,65	63		R. W. Brown
Guinea	692	gneiss	140,9	4,9	12,52	0,22	2,17	100		R. W. Brown
Guinea	465	granite	142,2	4,9	13,14	0,17	1,65	100		R. W. Brown
Guinea	475	granite	134,7	5,3	12,88	0,17	1,68	100		R. W. Brown
Guinea	500	amphibolite gneiss	164,3	4,5	12,72	0,21	2,09	100		R. W. Brown
Guinea	490	granodiorite	143,6	7,3	12,73	0,20	1,97	100		R. W. Brown
Guinea	465	granite	154,8	11,5	12,49	0,21	2,12	100		R. W. Brown
Guinea	505	granite	136,3	4,9	12,44	0,22	2,18	100		R. W. Brown
Guinea	560	biotite gneiss	202,1	19,1	12,41	0,26	2,59	100		R. W. Brown
Guinea	575	granite	162,7	26,1	12,79	0,28	1,46	27		R. W. Brown

Guinea	475	granite	129,9	5,8	13,12	0,18	1,83	100		R. W. Brown
Guinea	400	amphibolite gneiss	158,4	4,7	13,02	0,16	1,64	100		R. W. Brown
Guinea	669	granodiorite	150,2	5,0	13,41	0,17	1,66	100		R. W. Brown
Guinea	720	gneiss	129,9	4,3	13,28	0,17	1,66	100		R. W. Brown
Guinea	545	gneiss	122,4	6,4	13,08	0,19	1,93	100		R. W. Brown
Guinea	864	granite	127,0	7,2	13,12	0,19	1,88	100		R. W. Brown
Guinea	800	granite	150,5	5,3	12,89	0,19	1,89	100		R. W. Brown
Guinea	700	granite	139,1	7,2	12,22	0,19	1,91	100		R. W. Brown
Guinea	691	granite	140,3	6,9	13,36	0,17	1,74	100		R. W. Brown
Guinea	27	Gniess	95,0	3,5	12,92	0,08	1,21	262	1,89	M. Wildman
Benin	160	Granitiod	125,0	11,0	12,08	0,22	1,55	49	1,78	M.Wildman
Benin	144	Gniess	132,0	7,1	12,55	0,14	1,44	100	1,78	M.Wildman
Benin	197	Granitiod	107,3	6,9	13,06	0,13	1,38	106	1,75	M.Wildman
Benin	302	Granitoid	106,3	4,5	12,70	0,14	1,45	104	1,66	M.Wildman
Benin	374	Granitiod	113,4	5,4	12,67	0,12	1,26	105	1,72	M.Wildman
Benin	238	Sandstone	130,0	11,0	12,32	0,33	1,42	19	1,87	M.Wildman
Benin	298	Gniess	386,2	16,0	12,29	0,25	1,36	134	2,04	M. Wildman
Benin	347	Sandstone	219,0	38,0	11,98	0,29	1,36	22	2,00	M. Wildman
Benin	351	Gniess	338,0	13,0	11,56	0,13	1,60	151	1,86	M. Wildman
Benin	345	Gniess	380,0	14,0	11,70	0,11	1,50	249	2,02	M. Wildman
Benin	346	Granitoid	181,5	10,0	12,40	0,16	1,63	102	1,73	M. Wildman

Benin	338	Migmatite	202,5	8,0	12,75	0,11	1,38	151	1,90	M. Wildman
Benin	397	Granitiod	167,9	7,3	12,26	0,15	1,66	120	1,69	M. Wildman
Benin	247	Sandstone	217,0	33,0	11,42	0,35	2,01	33	1,81	M. Wildman
Benin	268	Sandstone	227,0	15,0	12,17	0,21	1,58	55	1,78	M. Wildman
Benin	557	Sandstone	401,0	45,0	11,84	0,54	1,53	8	1,88	M. Wildman
Benin	262	Gniess	109,4	5,8	12,87	0,15	1,46	98	1,69	M. Wildman
Benin	203	Sandstone	112,3	25,0	10,31	0,70	1,85	8	1,76	M. Wildman
Ivory Coast	270	Granite-gniess	124,6	4,4	12,60	0,139	1,39	102	1,68	M. Wildman
Ivory Coast	15	Granodiorite	113,9	5	12,58	0,13	1,31	100	1,87	M. Wildman
Ivory Coast	201	Leucogranite	150,2	5,7	12,62	0,128	1,56	149	1,88	M. Wildman
Ivory Coast	393	Granite-gniess	133,1	3,9	13,03	0,11	1,25	103	1,84	M. Wildman
Ivory Coast	295	Granodiorite	183,8	7,2	12,63	0,11	1,17	116	1,85	M. Wildman

Appendix 7. Table of AHe data. Provied by David Webster.

Location	Sample Name	4He ncc/g	238U ppm	235U ppm	238+235 ppm	232Th ppm	147Sm ppm	eU ppm	Radius µm	R* µm	Terminations	Age_Ma	error
Guinea	GM14-01 (1)	1,76E+05	12,98	0,0942	13,08	12,69		16,06	40,5	47,04	1	90,11	9,01
Guinea	GM14-01 (2)	1,08E+05	6,18	0,0448	6,22	4,58		7,30	49,5	47,52	1	120,58	12,06
Guinea	GM14-01(8)	6,47E+04	1,16	0,0084	1,17	2,70		1,80	48,5	50,06	2	289,04	28,90
Guinea	GM14-01(12)	1,45E+05	5,34	0,0387	5,38	2,76		6,03	42	48,05	2	194,83	19,48
											Mean	**173,64**	**17,36**
Guinea	GM14-02 (2)	8,86E+05	52,74	0,3825	53,12	1,64		53,51	69	80,97	1	135,48	13,55
Guinea	GM14-02(3)										2	421,71	42,17
Guinea	GM14-02 (4)	3,49E+05	33,54	0,2433	33,79	1,07		34,04	98	98,33	1	84,27	8,43
Guinea	GM14-02 (5)	5,92E+05	42,05	0,3050	42,35	10,68		44,86	75,5	90,48	1	108,30	10,83
Guinea	GM14-02(6)	6,05E+05	6,66	0,0483	6,70	2,61		7,32	60	72,47	2	645,78	64,58
Guinea	GM14-02(10)	2,21E+05	14,61	0,1059	14,71	0,85		14,91	81,5	92,46	2	121,18	12,12
											Mean	**252,79**	**25,28**
Guinea	GM14-12 (1)	2,07E+05	12,96	0,0940	13,06	11,45		15,74	65,5	69,71	1	107,55	10,75
Guinea	GM14-12 (2)	2,15E+05	12,68	0,0920	12,77	14,93		16,28	73	69,53	1	108,36	10,84
Guinea	GM14-12 (3)	2,19E+05	14,45	0,1048	14,56	10,93		17,12	64	74,96	1	104,87	10,49
Guinea	GM14-12(4)	9,71E+04	12,70	0,0921	12,79	9,94		15,13	44	54,10	2	52,83	5,28
Guinea	GM14-12(13)	7,85E+04	10,54	0,0765	10,62	4,72		11,73	53,5	65,26	2	55,14	5,51
											Mean	**85,75**	**8,57**
Guinea	GM14-13(1)	1,02E+05	1,55	0,0112	1,56	15,50	13,80	5,20	57	71,81	2	157,38	15,74
Guinea	GM14-13(2)	9,53E+04	2,74	0,0199	2,76	11,01	12,95	5,35	54,5	58,96	1	142,67	14,27
Guinea	GM14-13(3)	8,52E+04	0,78	0,0057	0,78	12,03	13,91	3,61	74	73,83	1	186,39	18,64
Guinea	GM14-13(4)	1,77E+05	1,54	0,0112	1,55	21,79	12,20	6,67	43	53,36	1	212,91	21,29
Guinea	GM14-13(5)	1,42E+05	6,78	0,0492	6,83	18,95	14,13	11,28	55	56,42	1	101,82	10,18
Guinea	GM14-13(6)	1,12E+05	1,01	0,0073	1,02	8,67	7,87	3,05	100,5	98,60	0	291,70	29,17

Guinea	GM14-13(7)	2,03E+05	7,99	0,0580	8,05	18,97	15,79	12,51	54	61,65	1	131,11	13,11
Guinea	GM14-13(8)	2,02E+05	10,09	0,0732	10,17	28,56	20,86	16,88	46	53,52	1	97,23	9,72
Guinea	GM14-13(9)	7,13E+04	1,52	0,0110	1,53	7,68	8,08	3,34	109	115,07	1	170,92	17,09
Guinea	GM14-13(10)	2,16E+05	1,99	0,0144	2,00	25,43		7,98	65	72,35	1	220,73	22,07
Guinea	GM14-13(11)	8,90E+04	4,87	0,0354	4,91	11,89	12,13	7,70	70,5	81,10	1	93,53	9,35
Guinea	GM14-13(12)	5,54E+04	6,39	0,0464	6,44	19,73	10,94	11,07	57	59,98	1	40,77	4,08
Guinea	GM14-13(13)	1,06E+05	0,86	0,0062	0,86	10,82	8,91	3,41	100	103,42	1	247,92	24,79
Guinea	GM14-13(16)	1,64E+05	1,08	0,0078	1,09	18,28	10,21	5,38	38	45,48	1	243,75	24,37
Guinea	GM14-13(17)	7,25E+04	0,66	0,0048	0,67	8,57		2,68	67,5	73,07	2	219,87	21,99
Guinea	GM14-13(19)	1,02E+05	2,46	0,0178	2,47	13,35	11,20	5,61	46,5	54,41	1	145,20	14,52
Guinea	GM14-13(20)	2,15E+05	6,94	0,0503	6,99	14,94	15,62	10,50	71	69,07	1	165,18	16,52
											Mean	**168,77**	**16,88**
Guinea	GM14-14(7)	2,39E+05	8,17	0,0592	8,22	17,85		12,42	68,5	75,83	2	156,83	15,68
Guinea	GM14-14(9)	1,53E+05	1,39	0,0100	1,40	19,14		5,89	53,5	58,84	2	211,41	21,14
Guinea	GM14-14(13)	1,26E+05	1,58	0,0115	1,59	35,88		10,03	54	69,18	2	102,76	10,28
											Mean	**157,00**	**15,70**
Benin	BN2 (1)	4,01E+04	2,34	0,0170	2,36	7,26		4,07	71,5	75,23	1	80,78	8,08
Benin	BN2 (2)	5,08E+04	2,25	0,0163	2,26	7,48		4,02	72,5	75,27	1	103,53	10,35
Benin	BN2 (3)	3,59E+05	16,79	0,1218	16,91	25,87		22,99	51	56,70	1	127,58	12,76
Benin	BN2 (4)	3,78E+05	22,27	0,1615	22,43	26,67		28,70	47,5	59,52	2	107,90	10,79
Benin	BN2 (9)	8,87E+04	5,50	0,0399	5,54	15,22		9,11	42,5	52,62	2	79,82	7,98
											Mean	**99,92**	**9,99**
Benin	BN3 (1)	4,17E+04	3,06	0,0222	3,08	7,78		4,91	66,5	80,99	2	69,65	6,96
Benin	BN3 (2)	1,31E+05	5,50	0,0399	5,54	17,95	31,01	9,76	71,5	73,54	0	107,47	10,75
Benin	BN3 (4)	2,26E+05	14,54	0,1055	14,65	19,82		19,31	64	77,55	2	95,94	9,59
Benin	BN3 (5)	1,25E+05	8,31	0,0603	8,37	18,38	26,16	12,69	72	77,98	1	79,73	7,97
Benin	BN3 (6)	2,06E+05	11,44	0,0830	11,52	29,55	30,70	18,47	72	78,32	1	90,13	9,01
Benin	BN3 (7)	9,41E+04	5,90	0,0428	5,94	27,42	28,17	12,39	62	60,79	0	61,19	6,12

Benin	BN3 (8)	9,74E+04	5,20	0,0377	5,24	12,31	16,69	8,13	78	78,98	1	96,53	9,65
Benin	BN3 (9)	2,30E+05	10,59	0,0768	10,66	49,66	59,28	22,33	65,5	75,39	1	82,51	8,25
Benin	BN3 (10)	4,23E+04	3,55	0,0257	3,57	5,95	22,76	4,97	61	67,75	1	67,22	6,72
Benin	BN3 (11)	3,93E+05	12,60	0,0914	12,69	45,07	20,74	23,29	61,5	64,91	1	137,04	13,70
Benin	BN3 (12)	6,88E+04	8,66	0,0628	8,72	24,91		14,57	36,5	45,48	2	38,80	3,88
Benin	BN3 (13)	2,22E+05	10,07	0,0730	10,14	20,71	33,56	15,01	78	78,66	1	118,93	11,89
Benin	BN3 (14)	3,00E+05	10,41	0,0755	10,48	45,57	233,87	21,19	85,5	77,83	1	106,31	10,63
Benin	BN3 (15)	8,40E+04	2,77	0,0201	2,79	12,82	6,61	5,81	140	158,78	1	117,29	11,73
Benin	BN3 (16)	1,10E+05	5,34	0,0387	5,37	13,05	22,24	8,44	110	111,14	0	104,84	10,48
Benin	BN3 (17)	4,41E+04	2,35	0,0170	2,37	3,55	13,17	3,20	92,5	91,48	1	109,20	10,92
Benin	BN3 (18)	3,23E+05	9,06	0,0657	9,13	33,95	44,20	17,11	74,5	86,86	1	150,91	15,09
Benin	BN3 (19)	3,71E+05	20,25	0,1469	20,40	39,48	43,78	29,68	58,5	66,75	1	101,26	10,13
Benin	BN3 (20)	2,32E+05	12,17	0,0882	12,26	25,32	34,68	18,21	54,5	60,78	1	102,77	10,28
Benin	BN3 (21)	1,93E+05	13,86	0,1005	13,96	13,46		17,12	62	73,97	2	92,47	9,25
Benin	BN3 (22)	1,14E+05	4,93	0,0358	4,97	19,87	5,39	9,64	111,5	114,35	1	96,49	9,65
Benin	BN3 (23)	7,80E+04	4,30	0,0312	4,34	10,32	4,50	6,76	78	83,07	1	93,97	9,40
											Mean	**96,39**	**9,64**
Benin	BN4 (7)	7,68E+04	5,53	0,0401	5,57	7,35		7,30	50	58,70	2	86,35	8,63
Benin	BN4 (9)	1,72E+05	10,81	0,0784	10,89	10,66		13,39	61,5	71,04	2	105,27	10,53
Benin	BN4 (10)	9,24E+04	6,00	0,0435	6,05	4,43		7,09	93	115,61	2	106,85	10,69
											Mean	**99,49**	**9,95**
Benin	BN5 (3)	8,86E+04	4,81	0,0349	4,85	1,88		5,29	153,5	160,19	1	136,91	3,41
Benin	BN5 (6)	3,78E+05	22,98	0,1667	23,14	12,80		26,15	45,5	60,85	2	118,30	11,83
Benin	BN5 (8)	2,41E+05	7,99	0,0580	8,05	4,43		9,09	99,5	113,34	2	215,02	21,50
Benin	BN5 (9)	4,93E+04	2,80	0,0203	2,82	0,42		2,92	121	128,96	2	138,26	13,83
Benin	BN5 (10)	3,70E+04	2,49	0,0180	2,51	0,72		2,68	134	158,52	2	113,20	11,32
Benin	BN5 (11)	5,14E+04	3,22	0,0234	3,24	1,77		3,66	137,5	153,78	2	115,21	11,52
Benin	BN5 (13)	1,16E+05	5,74	0,0416	5,78	3,40		6,58	126	135,36	2	144,29	14,43

											Mean	**140,17**	**14,02**
Benin	BN7 (1)	7,65E+04	3,48	0,0253	3,51	5,37	0,82	4,77	55,5	57,93	1	130,64	13,06
Benin	BN7 (2)	8,28E+04	3,36	0,0244	3,39	2,38	1,36	3,95	72	64,07	1	170,07	17,01
Benin	BN7 (3)	2,50E+05	7,72	0,0560	7,78	6,14		9,22	59,5	67,35	2	220,42	22,04
Benin	BN7 (4)	2,94E+05	8,78	0,0636	8,84	8,46		10,83	34	40,09	2	220,43	22,04
Benin	BN7 (6)	5,65E+05	6,96	0,0504	7,01	6,32	1,72	8,49	52,5	58,83	1	524,85	52,48
Benin	BN7 (7)	9,36E+04	3,65	0,0264	3,67	5,54		4,97	57,5	59,51	2	153,53	15,35
Benin	BN7 (10)	2,37E+05	5,19	0,0377	5,23	31,54		12,64	97	97,00	1	153,18	15,32
Benin	BN7 (12)	1,71E+05	1,75	0,0127	1,77	8,89		3,86	39	44,24	1	356,28	35,63
Benin	BN7 (13)	1,29E+05	5,69	0,0412	5,73	7,28		7,44	36,5	41,65	1	141,61	14,16
Benin	BN7 (14)	1,06E+05	3,73	0,0270	3,75	4,86		4,90	65,5	70,81	2	175,76	17,58
Benin	BN7 (15)	4,06E+04	2,22	0,0161	2,24	2,43		2,81	45,5	50,04	2	117,90	11,79
Benin	BN7 (16)	7,14E+04	3,12	0,0226	3,14	3,38		3,94	46,5	51,78	2	147,69	14,77
Benin	BN7 (17)	2,51E+05	10,73	0,0778	10,80	14,03		14,10	33,5	42,10	2	145,45	14,55
Benin	BN7 (18)	1,41E+05	6,08	0,0441	6,13	12,39		9,04	41,5	46,73	2	127,17	12,72
Benin	BN7 (19)	4,66E+04	2,00	0,0145	2,02	2,88		2,69	43	48,19	2	140,86	14,09
Benin	BN7 (20)	1,27E+05	4,47	0,0324	4,50	2,67		5,13	46,5	51,27	1	200,18	20,02
Benin	BN7 (21)	2,48E+05	7,75	0,0562	7,81	7,32		9,53	54	57,61	2	211,30	21,13
											Mean	**196,31**	**19,63**
Benin	BN9 (3)	2,56E+05	8,72	0,0632	8,78	0,58		8,91	66	78,32	2	232,65	23,27
Benin	BN9 (6)	1,93E+05	8,21	0,0596	8,27	1,15		8,55	65,5	68,53	1	184,00	79,17
Benin	BN9 (16)	6,03E+05	11,72	0,0850	11,80	1,00		12,04	51,5	64,88	2	399,74	39,97
											Mean	**272,13**	**27,21**
Benin	BN10 (5)	7,83E+05	18,03	0,1308	18,17	0,34		18,25	121	121,00	1	344,04	348,68
Benin	BN10 (6)	6,21E+05	17,62	0,1278	17,74	0,26		17,80	108	122,86	2	281,40	28,14
Benin	BN10 (8)	6,80E+05	18,77	0,1361	18,91	0,57		19,04	96,5	112,23	2	287,99	28,80
Benin	BN10 (11)	3,46E+05	12,89	0,0935	12,99	0,22		13,04	92,5	110,70	2	215,36	21,54

											Mean	**282,20**	**28,22**
Benin	BN11 (1)	1,99E+04	1,27	0,0092	1,28	1,40		1,61	101	107,40	1	101,31	10,13
Benin	BN11 (2)										2	225,15	22,51
Benin	BN11 (5)	3,64E+04	1,25	0,0091	1,26	8,05		3,15	108	118,04	2	94,78	9,48
Benin	BN11 (11)	5,48E+04	2,57	0,0187	2,59	7,59		4,37	120,5	137,23	2	102,72	10,27
Benin	BN11 (12)	1,12E+05	1,76	0,0128	1,77	2,26		2,30	128	149,70	2	391,22	39,12
Benin	BN11 (16)	7,64E+04	1,78	0,0129	1,79	5,02		2,97	59	67,10	2	208,89	20,89
Benin	BN11 (19)	2,76E+04	1,87	0,0136	1,88	2,82		2,55	89,5	103,40	2	89,04	8,90
Benin	BN11 (20)	1,95E+05	13,85	0,1004	13,95	22,09		19,14	57,5	71,42	2	83,49	8,35
											Mean	**162,07**	**16,21**
Benin	BN12 (1)	3,53E+05	16,52	0,1198	16,64	1,28		16,94	62,5	73,92	2	169,89	16,99
Benin	BN12 (8)	4,72E+05	22,15	0,1606	22,31	1,54		22,67	77,5	90,62	2	169,94	16,99
Benin	BN12 (10a)	6,30E+05	22,83	0,1656	23,00	2,73		23,64	69,5	58,25	2	216,31	21,63
Benin	BN12 (10b)	8,13E+05	27,60	0,2002	27,80	2,88		28,48	73	72,32	2	231,47	23,15
Benin	BN12 (14)	9,02E+05	31,86	0,2311	32,10	4,01		33,04	78,5	91,68	2	221,61	22,16
Benin	BN12 (16)	4,12E+05	14,88	0,1079	14,99	1,88		15,43	92	106,65	2	216,52	21,65
Benin	BN12 (18)	3,76E+04	2,38	0,0172	2,39	-0,14		2,36	64,5	76,12	2	130,43	13,04
											Mean	**193,74**	**19,37**
Benin	BN14 (1)	1,02E+06	38,60	0,2800	38,88	2,82		39,55	140	143,78	1	209,90	20,99
Benin	BN14 (4)	5,24E+05	23,70	0,1719	23,87	2,29		24,40	75	75,49	1	174,86	17,49
											Mean	**192,38**	**19,24**
Benin	BN17 (2)	1,06E+05	9,08	0,0659	9,15	0,63		9,30	64,5	76,39	2	93,75	9,38
Benin	BN17 (4)	9,18E+03	3,19	0,0231	3,21	0,48		3,32	93	99,21	2	22,83	2,28
Benin	BN17 (6)	2,51E+04	5,40	0,0392	5,44	0,43		5,54	71	82,11	2	37,45	3,74
Benin	BN17 (8)	2,48E+04	5,68	0,0412	5,72	0,69		5,88	45	51,34	2	34,79	3,48
Benin	BN17 (10)	1,28E+04	3,72	0,0270	3,75	1,30		4,05	49	56,59	2	26,00	2,60

Benin	BN17 (14)	1,17E+05	9,86	0,0715	9,93	0,79		10,11	56	66,83	2	95,35	9,54
											Mean	**51,69**	**5,17**
Benin	BN18 (1)	1,89E+05	15,44	0,1120	15,55	3,54		16,38	27	34,07	2	94,62	9,46
Benin	BN18 (2)	3,37E+05	6,00	0,0435	6,04	10,26		8,45	80	82,65	2	320,99	32,10
Benin	BN18 (6)	1,14E+06	30,10	0,2183	30,32	11,42		33,01	26	33,77	2	279,23	27,92
Benin	BN18 (7)	3,40E+04	2,44	0,0177	2,46	2,56		3,06	47,5	52,40	2	90,90	9,09
											Mean	**196,43**	**19,64**
Ivory Coast	SA-14 (7)	3,75E+05	15,27	0,1107	15,38	51,84		27,56	57,5	69,75	2	111,49	11,15
Ivory Coast	SA-14 (8)	1,62E+05	7,24	0,0525	7,29	25,26		13,23	60	70,36	2	100,54	10,05
Ivory Coast	SA-14 (11)	1,96E+05	9,48	0,0687	9,54	28,70		16,29	77,5	84,47	2	98,73	9,87
Ivory Coast	SA-14 (14)	2,93E+05	12,11	0,0878	12,20	41,56		21,97	56	63,55	2	109,06	10,91
											Mean	**104,95**	**10,50**
Ivory Coast	MK-64 (1)	7,94E+05	28,94	0,2099	29,14	30,43		36,30	55,5	68,32	2	178,19	17,82
Ivory Coast	MK-64 (5)	1,35E+06	30,42	0,2207	30,65	42,39		40,61	49,5	60,14	2	268,34	26,83
Ivory Coast	MK-64 (6)	6,56E+05	15,27	0,1107	15,38	47,44		26,53	119,5	138,87	2	201,36	20,14
Ivory Coast	MK-64 (7)	5,85E+05	16,45	0,1193	16,57	17,07		20,58	92,5	117,76	2	230,60	23,06
Ivory Coast	MK-64 (8)	5,02E+05	18,06	0,1310	18,19	21,99		23,36	81,5	90,47	2	175,13	17,51
Ivory Coast	MK-64 (11)	5,83E+05	16,66	0,1208	16,78	18,71		21,18	75	93,19	2	223,60	22,36
Ivory Coast	MK-64 (12)	4,10E+05	12,21	0,0886	12,30	12,89		15,33	96	119,49	2	217,28	21,73
Ivory Coast	MK-64 (15)	6,13E+05	1,24	0,0090	1,25	36,04		9,71	71	86,28	2	509,04	50,90
Ivory Coast	MK-64 (16)	8,80E+05	28,90	0,2096	29,11	33,54		36,99	50	63,39	2	193,59	19,36
Ivory Coast	MK-64 (18)	1,36E+06	34,21	0,2481	34,46	41,11		44,12	89,5	104,91	2	249,65	24,97
Ivory Coast	MK-64 (19)	7,69E+05	24,10	0,1748	24,28	27,35		30,71	64,5	82,84	2	203,62	20,36
											Mean	**240,95**	**24,09**

Appendix 8. Geological constraints used for samples of the Guinea transect

(Provided by Dominique Chardon)

Samp.	lat N	long E	Alt. (m)	Lithology	Geological constraints on the denudation/burial history
GM1	9,7164	-13,41813	4	Granitoid	– 4.2 km from a major mafic – ultramafic intrusion dated at c. 104 Ma: potential resetting effect? – Less than 1 km from the bounding cuesta of the Bové basin: must have undergone burial between at least the Ordovician and the Silurian (490 – 410 Ma) under series of at least 1500 m in thickness. Must have been exposed sometime in the Ordovician before burial. – The cuestas are capped by the bauxite (@ 400 m): the sample underwent at least 400 m of denudation since 45 Ma.
GM2	9,72433	-13,37092	27	Gneiss	– 5 km from a major mafic – ultramafic intrusion dated at ca. 88 Ma: potential resetting effect? – Right at the base of the Bové basin: must have undergone burial between at least the Ordovician and the Silurian (490 – 410 Ma) under series of at least 1500 m of thickness. – The cuestas are capped by the bauxite (@ 400 m): the sample underwent at least 400 m of denudation since 45 Ma.
GM3	9,83433	-13,14429	303	Sandstone	– Ordovician sandstone deposited (therefore exposed) in shore environment between ca. 490 and 445 Ma (duration of the Ordovician). – Dominated by bauxite plateau @ 570 m: has undergone 270 of denudation since 45 Ma. – Middle glacis province: Negligible denudation since 6 Ma.

					– Has been buried under later Ordovician and Silurian sediments (probably eroded here).
GM4	10,01673	-12,82185	324	Sandstone	– Ordovician sandstone deposited (therefore exposed) in shore environment between ca. 490 and 445 Ma (duration of the Ordovician). – Middle glacis surface: no denudation since 6 Ma. Bauxitic cuesta up to 1100 m: More than 700 m of denudation since 45 Ma. – Has been buried under later Ordovician and Silurian sediments (probably eroded here).
GM5	10,02741	-12,67767	255	Dolerite	– CAMP dolerite sill (ca. 203 Ma?). – Middle glacis surface: no denudation since 6 Ma.
GM6	10,1125	-12,55918	125	Sandstone	– Neoproterozoic sandstones deposited @1350 – 1000 Ma(?) (Madinakouta formation). Series containing limestones. – Dominated by bauxitic mesa @ 870 m: 700 m of denudation since 45 Ma. – Had been buried under Ordovician and Silurian series. – Numerous large CAMP sills in the environment of the sample.
GM7	10,71441	-12,24887	1247	Sandstone	– Ordovician sandstone deposited (therefore exposed) in shore environment between ca. 490 and 445 Ma (duration of the Ordovician). – Has been buried under later Ordovician and Silurian sediments (probably eroded here). – Numerous large CAMP sills in the environment of the sample. – Hilly bauxitic relief: no significant denudation since 45 Ma.

GM8	10,7017	12,25725	1228	Dolerite	– CAMP dolerite (ca. 203 Ma?). – Hilly bauxitic relief: no significant denudation since 45 Ma.
GM9	10,61369	-12,19874	980	Dolerite	– CAMP dolerite (ca. 203 Ma?). Large sill with equant texture and large crystals. – Hilly bauxitic relief: no significant denudation since 45 Ma.
GM10	10,6038	-11,85709	840	Dolerite	– CAMP dolerite (ca. 203 Ma?). Fresh corestone in weathering profile. – dominated by bauxitic plateau @ 920 m: 100 m of denudation since 45 Ma.
GM11	10,6364	-11,81488	784	Granitoid	– dominated by bauxitic plateau @ 910 m: 100 m of denudation since 45 Ma. – thick CAMP sill structurally under the sample.
GM12	10,73259	-11,57986	679	Granitoid	– dominated by bauxitic plateaux @ 920 m: 250 m of denudation since 45 Ma.
GM13	10,73559	-11,29056	656	Granitoid	– dominated by bauxitic plateaux @ 980 m: 300 m of denudation since 45 Ma. – middle glacis surface: no denudation since 6 Ma.
GM14	10,82268	-10,99629	438	Granitoid	– dominated by bauxitic plateaux @ 1100 m: 550 m of denudation since 45 Ma. – middle glacis surface: no denudation since 6 Ma. – structurally below a major CAMP sill.
GM15	10,91783	-10,74739	496	Granitoid	– dominated by bauxitic plateaux @ 1000 m: 500 m of denudation since 45 Ma. – middle glacis surface: no denudation since 6 Ma.

GM16	10,73857	-10,08871	415	Granitoid	– middle glacis surface: no denudation since 6 Ma.
GM17	12,347	-8,40856	430	Sandstone	– Basal term of the Neoproterozoic Taoudeni basin forming the regional escarpment. – Bauxites top the cuesta @ 700 m: 250 m of denudation since 45 Ma. – Must have been buried under later Neoproterozoic sediments (at least).
GM18	12,66357	-7,98985	438	Sandstone	– Neoproterozoic sandstones forming the upper part of the Taoudeni basin escarpment. – 75 under the bauxite: limited erosion since 45 Ma. – Must have been buried under later Neoproterozoic sediments (at least).
GM19	12,66337	-7,98911	408	Sandstone	– Neoproterozoic sandstones forming the lower part of the Taoudeni basin escarpment (same section as GM 18). – 90 under the bauxite: limited erosion since 45 Ma. – Must have been buried under later Neoproterozoic sediments (at least).
GM20	12,64776	-7,93109	324	Sandstone	– Neoproterozoic sandstones of the Taoudeni Basin under the escarpment outcropping in the Niger River course. – Must have been buried under later Neoproterozoic sediments (at least).

Appendix 9. Geological constraints used for samples of the Ivory Coast transect

(Provided by Dominique Chardon)

Sample	Lat N	Long W	Elev. (m)	Lithology	Geological constraints on the denudation/burial history
SA-14	4,93300	6,10583	15	granodiorite	– Coastal sample. At the margin of Neogene sediments of the coastal basin. May have undergone burial, at least in the Neogene.
SA-3	4.72695	6.6293	2	Tonalitic gneiss	– Coastal sample. May / must have undergone burial, at least in the Neogene.
SOK-1a	5,67650	6,64933	159	Tonalitic gneiss	– Middle glacis surface: no denudation since 6 Ma.
SOK-1b	5,67650	6,64933	159	Tonalitic gneiss	– Middle glacis surface: no denudation since 6 Ma. – ca. 100 km from the coast and the coastal basin: may have undergone burial under the coastal basin.
DLO3bis	6,49950	6,45933	201	Leucogranite	– High / Middle glacis province: no denudation since 11 Ma.
LOG-2	7,05867	7,52883	269	migmatitic gneiss	– Neighboring inselberg @ 470 m: minimum of 200 m of denudation since 45 Ma. Middle glacis: no denudation since 6 Ma.
VAA-1	7,41133	6,63650	270	Granodioritic gneiss	– Middle glacis country. No denudation since 6 Ma.
BEZ-1	7,45900	6,16400	266	Granodioritic gneiss	– Middle glacis country. No denudation since 6 Ma.

YOR-1	7,47733	7,39067	308	granodriorite	– Middle glacis surface: no denudation since 6 Ma. Site at the margin of a dissected high country bearing several inselberg above 710 m: at least 400 m of denudation since 45 Ma.
YOR-2	7,47733	7,39067	308	granodriorite	Same as YOR-1
YAL-1	7,77250	7,56183	511	Granulitic grey gneiss	– Piedmont of a massif with several summits @ 1100 m: minimum of 600 m of denudation since 45 Ma.
SEN-1	7,82833	6,53383	324	Granodioritic gneiss	– Middle glacis geomorphic province: No denudation since 6 Ma. Adjoining inselberg field culminating @ 480 m: minimum of 160 m of denudation since 45 Ma.
SEN-2	7,82833	6,53383	324	Granodioritic gneiss	– Middle glacis geomorphic province: No denudation since 6 Ma. Adjoining inselberg field culminating @ 470 m: minimum of 150 m of denudation since 45 Ma.
MK64	8,15900	6,36383	295	granodiorite	Western edge of Séguéla massif. Quartz, plagioclase, microline, hornblende & biotite.
KG32	9,07983	5,76900	407	migmatitic gneiss	– Middle glacis geomorphic province : No denudation since 6 Ma.
BD507	9,19900	6,95217	471	migmatitic gneiss	– Foot of an inselberg (middle glacis). W margin of a high, inselberg studded plateau, with bauxites up to 780 m high. Has undergone ca. 300 m of denudation since 45 Ma and negligible erosion since 6 Ma.
KG33a	9,46500	5,65417	393	migmatitic gneiss	– Collected on the Middle glacis surface : No denudation since 6 Ma.

Appendix 10. Geological constraints used for samples of the Benin transect

(Provided by Dominique Chardon)

Sample	lat N	long E	Elev. (m)	Lithology	Geological constraints on the denudation/burial history
BN 1	7.40153	2.08989	160	Granitoid	– Structurally and topographically "right" under the Coastal basin. Was therefore exposed near sea level sometime during the Maastrichtian; age of the shallow marine sediments immediately overlying the sample) and buried after that. – Collected from an extensive, slightly dissected middle glacis relict landscape. Has therefore undergone negligible denudation since 6 Ma.
BN 2	7.61572	2.19132	144	Granulitic gneiss	- Collected from an extensive, slightly dissected middle glacis relict landscape. Has therefore undergone negligible denudation since 6 Ma. – Located in an inselberg country culminating at 400 m. Has therefore undergone a minimum of 250 m of denudation between 45 and 6 Ma.
BN 3	8.04684	2.49882	197	Granitoid	- Collected from an extensive, slightly dissected middle glacis relict landscape. Has therefore undergone negligible denudation since 6 Ma. – Located in an inselberg country culminating at 400 m. Has therefore undergone a minimum of 250 m of denudation between 45 and 6 Ma.
BN 4	8.74617	2.60651	302	Granitoid	- Collected from an extensive, slightly dissected middle glacis relict landscape. Has therefore undergone negligible denudation since 6 Ma.

BN 5	9.19113	2.55006	374	Granitoid	- Collected from an extensive, slightly dissected middle glacis relict landscape. Has therefore undergone negligible denudation since 6 Ma.
BN 6	11.67882	3.19195	238	Sandstone	– The sample belongs to a fluvial / coastal formation of Ordovician – Silurian age (Kandi Formation). Was therefore exposed and near sea level sometime between ca. 490 and 420 Ma and could have been buried consequently. – Sample in the close vicinity (30 km) of the intracratonic Iullemmeden basin and “directly” underlies the Continental Terminal (CT) formation that was deposited from the Lutetian onward. The sample was therefore exposed 59 Ma ago. No significant burial since then (given the extent of the CT) – Underlying a relict of the Intermediate ferricrete. Has therefore undergone no denudation since 29 Ma. – Sample is located at the western margin of the Kandi basin, exposing a very thin (<100 m) Cretaceous continental formation (tree remains suggest a Lower Cretaceous age). The sample was therefore exposed at the surface sometime between ca. 140 and 100 Ma.
BN 7	11.13767	2.90475	298	Gneiss	– Sample is located at the western margin of the Kandi basin, exposing a very thin (<100 m) Cretaceous continental formation (tree remains suggest a Lower Cretaceous age). The sample was therefore exposed at the surface sometime between ca. 140 and 100 Ma.
BN 8	10.80048	2.80781	347	Sandstone	– The sample belongs to a fluvial / coastal formation of Ordovician – Silurian age (Kandi Formation). Was therefore exposed and near sea level sometime between ca. 490 and 420 Ma and could have been buried consequently. – Collected from an extensive, slightly dissected middle glacis relict landscape. Has therefore undergone negligible denudation since 6 Ma.

					– Sample lying along the western margin of the Kandi basin, exposing a thin (<100 m) Cretaceous continental formation (chronostratigraphic uncertainties on the tree remains does not allow asserting an age within the Cretaceous). The sample was therefore exposed at the surface before filling of the Kandi basin sometime between ca. 140 and 70 Ma.
BN 9	10.56113	2.73231	351	Gneiss	– Collected from an extensive, slightly dissected middle glacis relict landscape. Has therefore undergone negligible denudation since 6 Ma. – Sample is located at the western margin of the Kandi basin, exposing a very thin (<100 m) Cretaceous continental formation (tree remains suggest a Lower Cretaceous age). The sample was therefore exposed at the surface sometime between ca. 140 and 100 Ma.
BN 10	10.37225	2.72320	345	Gneiss	– Collected from an extensive, slightly dissected middle glacis relict landscape. Has therefore undergone negligible denudation since 6 Ma.
BN 11	9.77403	2.60340	346	Granitoid	– Collected from an extensive, slightly dissected middle glacis relict landscape. Has therefore undergone negligible denudation since 6 Ma.
BN 12	9.77020	2.30326	338	Metamorphic rock	– Collected from an extensive, slightly dissected middle glacis relict landscape. Has therefore undergone negligible denudation since 6 Ma.
BN 13	10.00532	1.50905	397	Granitoid	– Collected from an extensive, slightly dissected middle glacis relict landscape. Has therefore undergone negligible denudation since 6 Ma.
BN 14	10.75895	1.19141	247	Sandstone	– Lower slope of an inselberg dominating a middle-low glacis pediplain: negligible denudation since 6 Ma.

BN 15	10.61275	1.27637	268	Sandstone	– Sampled at the western exit of a gorge carved in the Atacora range (530 m elevation). Since the "top" of the range is a plateau relict of the "African (bauxitic) surface", the sample has undergone a minimum of 330 m of (local) denudation since 45 Ma.
BN 16	10.56254	1.32132	557	Sandstone	– Sample from the "African (bauxitic) surface". Negligible to no denudation since 45 Ma.
BN 17	8.36322	2.62905	262	Gneiss	- Collected from an extensive, slightly dissected middle glacis relict landscape. Has therefore undergone negligible denudation since 6 Ma. – Located in an inselberg country culminating at 400 m. Has therefore undergone a minimum of 250 m of denudation between 45 and 6 Ma.
BN 18	7.05832	1.81862	203	Sandstone	- The sample is a Maastrichtian sandstone from shallow marine environment. Was therefore exposed "on the shore" sometime between 94 and 86 Ma. Then burial history. – Exposed under the Intermediate ferricrete: no denudation since 29 Ma.

Appendix 11. Poster presented in EGU 2016, Vienna, Austria

MESOZOIC SOURCE-TO-SINK OF THE AFRICAN MARGIN OF THE EQUATORIAL ATLANTIC

J. Ye[1,2] (jing.ye@get.omp.eu), D. Chardon[1], D. Rouby[1], F. Guillocheau[3], D. Huyghe[1], C. Robin[3], M. Dall'Asta[2], R. Brown[4], M. Wildman[4], D.Webster[4]

(1) Géoscience Environnement Toulouse (CNRS/IRD/Université de Toulouse), France - (2) TOTAL E&P, CSTJF, Avenue Larribau, Pau, France - (3) Geosciences Rennes (CNRS), Université de Rennes 1, France - (4) School of Geographical and Earth Sciences, University of Glasgow, Scotland

Aim and Methods

The aim of this study is to discuss the erosion dynamics of the West African Craton (Source) and sediment export to the Equatorial Atlantic Ocean (Sink) during the Mesozoic, as well as their relationships.

Methods of investigation:

1. Paleogeographic and structural reconstruction
2. Mesozoic stratigraphic architecture of the Equatorial Atlantic margin from interpretation of reflecting seismic and well data
3. Denudation history along the margin form Apatite Fission Track and (U-Th)/He thermochronological dating

1. Paleogeograpic Reconstruction

We reconstructed the paleogeography and paleo-structures, showing the evolution of the Equatorial Atlantic margin, intracratonic basins, marginal upwarps and their relationships.

Maps show:

- Preserved deposits and their potential minimum extension;
- The propagation of rifting and intracontinental rift systems;
- Present-day intracratonic basins resulting from the uplift of the Hoggar Swell during the Eocene.

2. Equatorial Atlantic Margin

a) Narrow margin along transfrom segment:

- Narrow necking zone with rapide transition from continental to oceanic crust
- No post-rift deposits preserved on the shelf during the Late Cretaceous
- Remarkable stacking of Maastrichtian turbiditic chenal-levee complexes

b) Wide margin along divergent segment:

- Wide necking zone with extended oceanic-continental transition domain
- Late Cretaceous post-rift sediments preserved on the shelf

Different uplift or subsidence histories within the same basin!

3. Low-Temperature Thermochronology (AFTA +AHe dating)

Preliminary results show younger AFTA age toward marginal area and older age in the interior of the craton. The younger ages mark the erosion of rift-related relief of the Equatorial Atlantic margin during the Early Cretaceous. Marginal upwarp is probably related to the rifting.

Conclusion

(1) Marginal upwarp formed since the Early Cretaceous related probably to rifting of the Equatorial Atlantic margin

(2) Post-rift stratigraphy of the Equatorial Atlantic margin varies according to the structure of margin (necking zone width)

(3) Intracratonic basins must be taken into account for the evaluation of Source-to-Sink budget.